BrJAC

Brazilian Journal of Analytical Chemistry

an International Scientific Journal

cuqa 8

Congreso Uruguayo de Química Analítica-2024

Special Edition of BrJAC on the

8th Uruguayan Congress of Analytical Chemistry

(CUQA 8)

April – June 2026 Volume 13 Number 51

inscrições e informações:
82 98193.0529 / 98821.4091

REALIZAÇÃO

UNIVERSIDADE FEDERAL DE ALAGOAS

APOIO

IQB PPGQB Programa de Pós-Graduação em Química e Biotecnologia

FAPEAL FUNDAÇÃO DE AMPARO À PESQUISA DO ESTADO DE ALAGOAS

CNPq Conselho Nacional de Desenvolvimento Científico e Tecnológico

SECRETARIA EXECUTIVA

PRIME EVENTOS

BrJAC

Brazilian Journal of Analytical Chemistry

VISÃO FOKKA - COMMUNICATION AGENCY

Aims & Scope

BrJAC is a double-blind peer-reviewed research journal, dedicated to the diffusion of significant and original knowledge in all branches of Analytical Chemistry and Bioanalytical Chemistry. It is addressed to professionals involved in science, technology, and innovation projects at universities, research centers and in industry. The **BrJAC welcomes** the submission of research papers reporting studies devoted to new and significant analytical methodologies, putting in evidence the scientific novelty, impact of the research, and demonstrated analytical or bioanalytical applicability. BrJAC **strongly discourages** those simple applications of routine analytical methodologies, or the extension of these methods to new sample matrices, unless the proposal contains substantial novelty and unpublished data, clearly demonstrating advantages over existing ones.

BrJAC is a quarterly journal that publishes original, unpublished scientific articles, reviews and technical notes. In addition, it publishes interviews, points of view, letters, sponsor reports, and features related to analytical chemistry.

For complete information on ethics and policies on conflicts of interest, copyright, reproduction of already published material, preprints, use of AI by authors and reviewers and studies involving biological material, in addition to the manuscript submission and peer review system, please visit 'About us' and 'Author Guidelines' at www.brjac.com.br.

ISSN 2179-3425 printed

ISSN 2179-3433 electronic

Indexing Sources

Scopus

CiteScore$_{2024}$ 2.2
SJR$_{2024}$ 0.207
SNIP$_{2024}$ 0.305
CiteScoreTracker$_{2025}$ 1.9
Last updated on March 5, 2026
Access source details

CiteScore trend

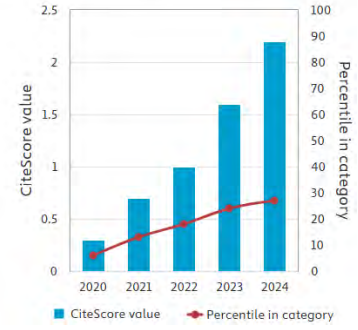

CLARIVATE ANALYTICS EMERGING SOURCES CITATION INDEX INDEXED

IF$_{2024}$ 1.1
JCI$_{2024}$ 0.19

CAPES
QUALIS

BrJAC is in the Qualis B1 stratum
Period 2021-2024

Google scholar

Cited by

	All	Since 2021
Citations	1263	1056
h-index	16	15
i10-index	35	29

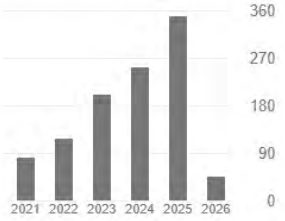

Last updated on March 4, 2026

ABEC BRASIL
BrJAC is associated to the
Brazilian Association of Scientific Editors

BrJAC is published quarterly by:
Visão Fokka Communication Agency
Av. Washington Luiz, 4300 - Bloco G - 43
13042-105 – Campinas, SP, Brazil
contato@visaofokka.com.br
www.visaofokka.com.br

EDITORIAL BOARD

EDITORIAL ADVISORY BOARD

EDITORIAL ADVISORY BOARD (Continued)

CONTENTS

CONTENTS

Sponsor Technical Applications and Instrumentation Updates

Sponsor Reports

Sponsor Releases

New Books & Upcoming Events & Trusted Sources for Analytical Chemistry

Brazilian Journal of Analytical Chemistry
2026, Volume 13, Issue 51, pp 1-2
doi: 10.30744/brjac.2179-3425.editorial.N51

BrJAC

EDITORIAL

Special Issue CUQA 8

Lucía Pareja[1]*, Ignacio Machado[2]*

*Guest Editors of this BrJAC Special Edition on the 8th Uruguayan Congress of Analytical Chemistry (CUQA 8)

[1]*Departamento de Química del Litoral, Cenur Litoral Norte, Universidad de la República, Uruguay*

[2]*Grupo de Bioanalítica y Especiación (BIOESP), Facultad de Química, Universidad de la República, Uruguay*

It is with great pleasure that we present this Special Issue of the Brazilian Journal of Analytical Chemistry (BrJAC), dedicated to the 8th Uruguayan Congress of Analytical Chemistry (CUQA 8), held in Montevideo, Uruguay, on October 13–15, 2024. This Special Issue celebrates the vitality, diversity, and scientific maturity of the Analytical Chemistry community in Uruguay and the Southern Cone.

This Special Issue opens with an engaging interview with Prof. Eduardo Dellacassa, who offers a rich and personal reflection on his scientific trajectory, from his rural childhood to becoming one of the most influential Latin American researchers in natural products, metabolomics, and analytical applications in food and pharmaceutical sciences. His reflections on the evolving landscape of analytical chemistry—particularly the need for "evolutionary analytics" as an open and flexible concept—provide a thought-provoking perspective for readers. Complementing this piece, the Point of View article by Prof. Eduardo Méndez addresses key conceptual and methodological aspects of nanometrology, underscoring its growing importance in ensuring measurement quality at the nanoscale. Additionally, the Letter authored by Prof. Ignacio Machado and Prof. Lucía Pareja, titled "Artificial Intelligence: A Transformative Ally in Analytical Chemistry," highlights the expanding role of AI-driven tools in method development, data treatment, and decision-making, and discusses how these technologies are reshaping analytical practice in academic and applied settings.

The research articles featured in this Special Issue represent the scientific breadth showcased during CUQA's 8th edition and illustrate the multidisciplinary character of contemporary analytical chemistry. These contributions include:

"Incidence study of two UV filters (octocrylene and octinoxate) and the synthetic fragrance galaxolide in commercial yellow clam (*Amarilladesma mactroides*)" – an environmental analytical study addressing contaminants of emerging concern in coastal ecosystems.

"Risk-Based Selection of Active Pharmaceutical Ingredients in the Development of HPLC and NIR Methods for Pediatric Preparations" – an applied pharmaco-analytical work integrating quality-by-design principles with spectroscopic and chromatographic method development.

"Development of methods for selenium determination in fish: tools for ecotoxicological studies" – a contribution that highlights the importance of trace-element analysis for environmental and toxicological monitoring.

"Low-cost particulate matter sensor in indoor and external classroom environments'' – an innovative approach that demonstrates the relevance of accessible analytical technologies for public health and educational settings.

"Evaluation of *Calendula officinalis* extract as a functionalization agent for gold nanoparticles" – a study at the interface of nanotechnology and bioanalytical chemistry, exploring sustainable routes for nanoparticle functionalization.

Cite: Pareja, L.; Machado, I. Editorial of the BrJAC Special Issue on CUQA 8. *Braz. J. Anal. Chem.* 2026, *13* (51), pp 1-2. http://dx.doi.org/10.30744/brjac.2179-3425.editorial.N51

This Editorial is part of the BrJAC Special Issue on the 8th Uruguayan Congress of Analytical Chemistry (CUQA 8 2024).

Together, these articles reflect the scientific rigor and creativity of researchers working in Uruguay and the region. They also underscore the commitment of CUQA to fostering high-quality research, methodological innovation, and meaningful applications across environmental, pharmaceutical, food, and bioanalytical chemistry.

We extend our sincere appreciation to all authors for their valuable contributions and to all reviewers for generously offering their time and expertise to ensure the scientific quality of this collection. We are also grateful to the CUQA 8 Organizing and Scientific Committees for their dedication, and to BrJAC for supporting this Special Issue devoted to strengthening regional analytical chemistry.

We wish all readers an inspiring and enriching reading experience.

Lucía Pareja is a pharmaceutical chemist and holds a PhD in Chemistry. She is a professor in the Department of Chemistry of Litoral at Cenur Litoral Norte, University of the Republic, Uruguay. As a researcher, her work focuses on assessing the presence of organic contaminants at trace levels to address the multiple problems their presence causes in food and the environment. To achieve this, she develops robust analytical methods based on mass spectrometry that allow for the determination of compounds at trace levels. The main objective of this work is the development of multi-class, miniaturized, and environmentally friendly analytical methodologies, following, as far as possible, the principles of green chemistry, for application to problems of national interest.

Ignacio Machado is Associate Professor of Analytical Chemistry at the Faculty of Chemistry, Universidad de la República, Montevideo, Uruguay. He works mainly on atomic spectrometry and mass spectrometry, with a focus on bioanalytical chemistry. He was a postdoc researcher at the Department of Trace Element Analysis, the Institute of Analytical Chemistry of the ASCR, Prague, Czech Republic, in 2017. He has been a member of the Academic Assembly of Faculty of Chemistry, Universidad de la República, since 2018, and the International Medical Geology Association (IMGA) since 2019. He has been a researcher for the National System of Researchers (SNI, Uruguay) since 2016, and of the Basic Sciences Development Program – Chemistry Area (PEDECIBA – Química, Uruguay) since 2017. He is responsible for the BIOESP Group

Brazilian Journal of Analytical Chemistry
2026, Volume 13, Issue 51, pp 3-5
doi: 10.30744/brjac.2179-3425.interview.N51

INTERVIEW

Professor Eduardo Dellacassa kindly granted an interview to BrJAC

Professor Eduardo Santiago Dellacassa Beltrame is widely recognized in Latin America for his contributions to phytochemistry, pharmacognosy, natural products chemistry, enology, and the study of aromatic and medicinal plants. His career is marked by strong international engagement, scientific leadership, and a consistent commitment to research, teaching, and technological development.

Throughout his academic career, Dellacassa received several prestigious international fellowships, including a scholarship from the Italian Government (IILA–Universidad de la República, 1989), a Research Grant from the Third World Academy of Sciences (TWAS), and multiple research stays at leading European institutions. He carried out scientific training and specialization programs in Italy, Spain, France, England, and Mexico, with notable periods at the Università degli Studi di Messina, the University of Barcelona, Rothamsted Experimental Station (UK), the Istituto Agrario di San Michele all'Adige, INRA Pech Rouge, and the Centro de Investigación y Asistencia en Tecnología y Diseño del Estado de Jalisco. These experiences helped shape a highly international and multidisciplinary academic profile.

Dellacassa is an active member of numerous scientific societies, including the Latin American Society of Phytochemistry, the American Chemical Society (ACS), the International Society for Horticultural Sciences, the Spanish Society of Phytotherapy (SEFIT), the Royal Spanish Society of Chemistry, and several national associations related to chemistry, food science, horticulture, natural products, and essential oils. His broad institutional engagement reflects his sustained contributions to scientific development across the region.

Professionally, he has served as a technical director for additives companies and for pharmacies, and has professional experience in the pharmaceutical sector, particularly in analytical control, production planning, and product development. This industrial background complements his strong academic foundation, enabling him to bridge fundamental science with practical applications.

Within the Universidad de la República (UdelaR), Uruguay, Dellacassa developed extensive teaching and academic activity over more than a decade. He has taken part in numerous Academic Merit Committees, evaluation boards, and selection processes in areas such as Pharmacognosy and Natural Products, Organic Chemistry, Pharmaceutical Chemistry, Enology, Food Science and Technology, and Mass Spectrometry. Over the years, he held positions as Assistant Professor, Associate Professor, and Senior Professor, and contributed to funded research projects supported by agencies such as CSIC, INIA, and PDT. His academic contributions span topics from natural product chemistry and sensory analysis of foods to phytochemical characterization and enological science.

With a career defined by academic excellence, international collaboration, and a commitment to scientific training, Eduardo Santiago Dellacassa Beltrame stands as a leading figure in the field of

Cite: Beltrame, E. S. D. Professor Eduardo Dellacassa kindly granted an interview to BrJAC**.** *Braz. J. Anal. Chem.* 2026, *13* (51), pp 3-5. http://dx.doi.org/10.30744/brjac.2179-3425.interview.N51

This Interview is part of the BrJAC Special Issue on the 8th Uruguayan Congress of Analytical Chemistry (CUQA 8 2024).

natural products, aromatics, medicinal plants, and analytical applications in food and pharmaceutical sciences. His trajectory represents a distinctive combination of scientific rigor, technical expertise, and long-standing contributions to the development of chemistry and natural sciences in Latin America.

BrJAC: How was your childhood?

Prof. Dellacassa: I spent my childhood in a low-income rural area where immigrant tradition dictated that my destiny was to work the land.

BrJAC: What early influences encouraged you to study chemistry? Did you have any influencers, such as a teacher?

Prof. Dellacassa: The benchmark for continuing my studies was always to have the option of other choices for my future. Curiously, my interest in studying never involved any aspiration for social advancement. The greatest influence on my decision about what to study—which was not easy—was a secondary school chemistry teacher who will always remain in my memory.

BrJAC: How was the beginning of your career in chemistry?

Prof. Dellacassa: The beginning of our time at university was difficult for my entire generation, as the university was under intervention and there were very limited opportunitiesfor decision-making. Personally, my salvation came from older generations who took me under their wing and helped me realize that university education encompasses far more than attending classes and taking examinations.

BrJAC: What has changed in your profile, ambitions, and performance since the time you started your career?

Prof. Dellacassa: My change in perspective since I began my research activities has been complete: I can no longer conceive of university education without considering the possibility that our students may develop the critical and human capacities to become our equals.

BrJAC: Could you comment briefly on the recent evolution of analytical chemistry, considering your contributions?

Prof. Dellacassa: In my opinion, analytical chemistry is undergoing a period of qualitative growth. Where stricter training in analytics inevitably leads to more sophisticated analytical instruments, we are not yet fully capable of interpreting results with the rigor that analytics, by definition, provides.
I wonder if we should not begin the journey of evolutionary analytics: as an open, flexible concept with multiple applications.

BrJAC: What are your lines of research? You have published many scientific papers. Would you highlight any?

Prof. Dellacassa: I am pleased to say that my current vocation is volatile and non-volatile metabolomics, mediated by the facilities offered by chromatography as a separation method and mass spectrometry as a means of interpreting the processes under evaluation.

BrJAC: What is your opinion about the current progress of chemistry research in word? What are the recent advances and challenges in scientific research?

Prof. Dellacassa: Technological and instrumental development is advancing so fast that it is very difficult for researchers to keep pace with it, and even more difficult to apply it without having to change their objectives to suit current trends. On the other hand, the rising cost of instrumentation is beginning to increasingly

discriminate between those who have access to these tools and those who do not. This situation may have a positive aspect if it leads to greater intergroup collaboration, even when such collaboration is not necessarily focused on the same research topics.

BrJAC: For you, what have been the most important recent achievements in analytical chemistry research? What are the landmarks?

Prof. Dellacassa: In my opinion, there is no doubt that advances in sample preparation systems are the most significant development currently taking place. If we add to this the increase in sensitivity and reproducibility of analytical tools, the situation is very close to what we all want, which is the application of more powerful and accessible statistical tools to respond to the problems we face.

BrJAC: There are, in Brazil and in the world, several conferences on chemistry. To you, how important are these meetings to the chemistry scientific community?

Prof. Dellacassa: Brazil truly represents a universe of meetings, seminars, courses, and congresses. The importance of these opportunities for staying up to date, establishing contacts, and receiving constructive criticism of our work is unparalleled in Latin America.

BrJAC: What is the importance of awards for the development of science and new technologies?

Prof. Dellacassa: Basic: it is a human necessity to receive minimal recognition for work well done and results well presented.

BrJAC: What advice would you give to a young scientist who wants to pursue a career in chemistry?

"...In my opinion, chemistry has ceased to be a discipline and has become a tool for communication among different disciplines. From this point of view, I believe that ..."

Prof. Dellacassa: In my opinion, chemistry has ceased to be a discipline and has become a tool for communication among different disciplines. From this point of view, I believe that the different options offered by chemistry education provide unique opportunities for understanding, communication, and collaboration with other areas of scientific knowledge and their applications.

BrJAC: For what would you like to be remembered?

Prof. Dellacassa: I would like to be remembered as someone who, having tried to achieve all the goals that an academic education aims for, continues to work to generate collaborations that allow us to overcome the individualism that is a hallmark of academic life.

Brazilian Journal of Analytical Chemistry
2026, Volume 13, Issue 51, pp 6-8
doi: 10.30744/brjac.2179-3425.point-of-view-N51

POINT OF VIEW

The Challenges of Nanometrology for Metallic Nanoparticles

Eduardo Méndez

Laboratorio de Biomateriales, Instituto de Química Biológica, Facultad de Ciencias, Universidad de la República. 11400 Montevideo, Uruguay

The emergence of nanotechnology as the new industrial revolution following biotechnology has brought new challenges, new learning opportunities, and also the repetition of old mistakes. The discovery of new physical properties at the nanoscale and the ability to measure them significantly accelerated the amount of research related to this area. Furthermore, the possibility of direct manipulation at the nanoscale opened the door to the design of specific applications, resulting in a flood of new products on the market. All these advances go hand in hand with the need for methods and tools to accurately measure the dimensions, shapes, composition, and other characteristics of nanomaterials and nanostructures, among which nanoparticles play a prominent role. Without reliable measurements, the production of nanoparticles would be impossible, with a clear impact on their quality, the necessary government oversight, and, importantly, the public's understanding of this new industrial revolution.[1]

What nanotechnology didn't learn from biotechnology?

Several decades ago, innovations in biotechnology followed a similar path. The market was flooded with biotechnological products, which simultaneously served as a "label" to distinguish and market them, and as a warning to those who distrusted them and their potential harm to health and the environment. This confrontation between the market and a segment of the population marked a learning point for the implementation of new developments.

Nanotechnology, as a new industrial revolution, had the opportunity to learn from this mistake, which could be summarized as empowering the public to take ownership of new advances. This implies information, education, but also extensive prior research, as well as disseminating this research to consumers and the general public.

Beyond the ethical obligation to keep the public informed, it is necessary to know what information is being shared. When dealing with new materials or structures, accurate measurements are necessary to establish precise toxicological studies and for proper quality control of commercial products containing them.

Analytical challenges

In analytical terms, measuring the concentration of a substance in a given matrix is the ultimate goal of any metrological analysis. With nanotechnology products, the equivalent situation is not so simple, since the properties of nanoparticles depend not only on the chemical nature of what is being measured but also on their size and shape. The matrix plays a fundamental role that must be considered when validating the measurement, but in the case of nanoparticles, reference materials must be designed for a specific size and shape, making the number of required reference materials virtually infinite. The proposed analytical methods

Cite: Méndez, E. The Challenges of Nanometrology for Metallic Nanoparticles. *Braz. J. Anal. Chem.* 2026, *13* (51), pp 6-8. http://dx.doi.org/10.30744/brjac.2179-3425.point-of-view-N51

This Point of View is part of the BrJAC Special Issue on the 8th Uruguayan Congress of Analytical Chemistry (CUQA 8 2024).

for discriminating the nature and size of nanoparticles include asymmetric flow field-flow fractionation (AF4), high-performance size-exclusion chromatography (HPSEC), and nanotracking analysis (NTA). These are complemented by specific characterization techniques, including UV/VIS spectroscopy (plasmonic properties), infrared/Raman spectroscopy (nature of the stabilizing agent), dynamic light scattering (DLS) (aggregate detection), Z-potential (colloidal stability), and transmission electron microscopy (TEM) (size and shape). In other words, a multiplicity of techniques is necessary to adequately describe the nanomaterial and the matrix in which it is embedded,[2] even allowing for the observation of changes resulting from interactions with the matrix.[3] Another layer of difficulty arises from the fact that there are no reference materials to validate the methodologies, so the techniques themselves do not have the metrological value to be used by official agencies in the control of products.

This is where analytical chemistry encounters its greatest challenges. Recent studies show that if UV/VIS spectroscopy and oxidation charge measurement analytical results are reported as a function of total atom concentration (mass or moles/L) instead of nanoparticles, it becomes possible to become independent of the size and chemical nature of the protecting agent. This greatly facilitates the generation of reference materials for technique validation. Future developments in analytical methodologies should aim to eliminate the influence of factors that alter analytical results, making them more general, so that more “universal” reference materials can be generated.

Analytical decentralization

As I mentioned initially, commercial products containing nanoparticles have flooded the market, making it necessary to have rapid and decentralizable analytical methodologies to implement effective, rigorous, and quick control of these products. Many portable devices are available for their eventual use in the rapid control of commercial products, primarily liquids. For example, a simple laser pointer can determine the colloidal nature of a solution, allowing for an initial positive/negative analysis. Based on UV/VIS spectra measurements, cell phones can be used for rapid color measurement of a solution and its correlation with the optical properties of plasmonic nanoparticles (gold, silver, and copper). Oxidation charge measurements can be performed using disposable screen-printed electrodes and portable potentiostats.

In short, nanometrology presents an exciting challenge for the analytical community. Developing rigorous methodologies independent of particle size and stabilizing agents is essential for creating reference materials, which are crucial for properly controlling commercial products. Only through such efforts can the public have confidence in products emerging from this new industrial revolution.

REFERENCES

(1) Chávez-Hernández, J. A.; Velarde-Salcedo, A. J.; Navarro-Tovar, G.; González, C. Safe nanomaterials: from their use, application, and disposal to regulations. *Nanoscale Adv*. **2024**, *6* (6), 1583-1610. https://doi.org/10.1039/d3na01097j

(2) Fagúndez, P.; Botasini, S.; Tosar, J. P.; Méndez, E. Systematic process evaluation of the conjugation of proteins to gold nanoparticles. *Heliyon* **2021**, *7* (6), e07392. https://doi.org/10.1016/j.heliyon.2021.e07392

(3) Botasini, S.; Heijo, G.; Méndez, E. Toward decentralized analysis of mercury (II) in real samples. A critical review on nanotechnology-based methodologies. *Anal. Chim. Acta* **2013**, *800*, 1-11. https://doi.org/10.1016/j.aca.2013.07.067

Eduardo Méndez has a Master (1993) and Doctoral (2001) degrees in Physical Chemistry and Electrochemistry from the Universidad de la República (Uruguay), with postdoctoral studies at Karlsruhe and Ulm Universities in Germany. He was former Head of the Biomaterials Laboratory at the Faculty of Science and is currently Director of the Chemical Biology Institute at the Faculty of Sciences in Uruguay. His main research interests are analytical decentralization, biomaterials and nanosystems, for which co-authored more than 60 papers and supervised several MSc and PhD theses.

Brazilian Journal of Analytical Chemistry
2026, Volume 13, Issue 51, pp 9-10
doi: 10.30744/brjac.2179-3425.letter-N51

BrJAC

LETTER

Artificial Intelligence: A Transformative Ally in Analytical Chemistry

Lucía Pareja[1], Ignacio Machado[2]

[1]Departamento de Química del Litoral, Cenur Litoral Norte, Universidad de la República, Uruguay

[2]Grupo de Bioanalítica y Especiación (BIOESP), Facultad de Química, Universidad de la República, Uruguay

The scientific landscape is undergoing a profound transformation driven by artificial intelligence (AI). While its influence is already evident in disciplines such as bioinformatics, materials science, and drug discovery, analytical chemistry has only now begun to fully embrace its potential.[1] Yet, few areas could benefit more from the structured, data-rich nature of AI than the analytical sciences themselves. Analytical chemistry has always been the discipline of signals, patterns, and interpretation. In that sense, analytical chemistry could be regarded as a conceptual precursor to machine learning thinking, long before the modern algorithms existed.

AI provides an unprecedented opportunity to enhance analytical workflows, at every stage, from experimental design and method development to data processing, interpretation and decision-making.[2] Machine learning models can optimize instrumental conditions, uncover hidden correlations between parameters, and automate complex calibration or validation procedures. For several years now, the trend has been toward the use of miniaturized and more environmentally friendly methodologies, and in this regard the development of AI can be of great help to improve existing greenness-assessment algorithms, providing smarter, more sustainable analytic protocols with lower sample and solvent consumption. In spectroscopic and chromatographic analyses, AI algorithms are increasingly capable of distinguishing genuine analytical signals from background noise or matrix interferences, enabling faster and more reliable quantification and identification.[2] Beyond improving performance, AI is redefining the very role of the analytical chemist—from manual operator to data curator and critical interpreter. AI may also facilitate structural elucidation of unknown compounds, possibly offering a cost-effective alternative to expensive commercial spectral libraries or extensive manual interpretation workflows.

However, this transformation brings certain challenges. AI systems must be transparent, explainable, and validated according to the same rigorous standards that govern traditional analytical methods.[3] The “black box” problem remains one of the greatest barriers to trust and acceptance. It is essential that machine-learned models complement, rather than replace, human expertise — that they become partners in analytical reasoning, not substitutes for it. This balance between automation and understanding is central to the spirit of analytical chemistry.

The adoption of AI also requires rethinking education and training. Future analytical chemists will need to navigate not only spectral lines and chromatograms but also fluency in algorithms, datasets, and validation metrics[1,3] Integrating AI literacy and data science skills into analytical chemistry curricula is no longer optional: it is a prerequisite for keeping the discipline relevant and forward-looking. Those who understand how to merge chemical intuition with computational power will lead the next generation of analytical breakthroughs.

Cite: Pareja, L.; Machado, I. Artificial Intelligence: A Transformative Ally in Analytical Chemistry. *Braz. J. Anal. Chem.* 2026, *13* (51), pp 9-10. http://dx.doi.org/10.30744/brjac.2179-3425.letter-N51

This Letter is part of the BrJAC Special Issue on the 8th Uruguayan Congress of Analytical Chemistry (CUQA 8 2024).

The essence of analytical chemistry has always been about transforming raw data into knowledge. In this new era, artificial intelligence emerges not just as a tool, but as a collaborator in that pursuit. The challenge —and opportunity— lies in ensuring that as machines learn to think, we do not lose our capacity to question. The analytical chemist of tomorrow will not merely measure, they will also design, model, predict, and interpret. Embracing AI is not the end of analytical chemistry as we know it—it is its most exciting reinvention.

REFERENCES

(1) Xue, X.; Sun, H.; Yang, M.; Liu, X.; Hu, H. Y.; Deng, Y.; Wang, X. Advances in the application of artificial intelligence-based spectral data interpretation: A Perspective. *Anal. Chem.* **2023**, *95* (37), 13733–13745. https://doi.org/10.1021/acs.analchem.3c02540

(2) Liu, X.; An, H.; Cai, W.; Shao, X. Deep learning in spectral analysis: Modeling and imaging. *TrAC, Trends Anal. Chem.* **2024**, *172*, 117612. https://doi.org/10.1016/j.trac.2024.117612

(3) Rial, R. C. AI in analytical chemistry: Advancements, challenges, and future directions. *Talanta* **2024**, *274*, 125949. https://doi.org/10.1016/j.talanta.2024.125949

Lucía Pareja is a pharmaceutical chemist and holds a PhD in Chemistry. She is a professor in the Department of Chemistry of Litoral at Cenur Litoral Norte, University of the Republic, Uruguay. As a researcher, her work focuses on assessing the presence of organic contaminants at trace levels to address the multiple problems their presence causes in food and the environment. To achieve this, she develops robust analytical methods based on mass spectrometry that allow for the determination of compounds at trace levels. The main objective of this work is the development of multi-class, miniaturized, and environmentally friendly analytical methodologies, following, as far as possible, the principles of green chemistry, for application to problems of national interest.

Ignacio Machado is Associate Professor of Analytical Chemistry at the Faculty of Chemistry, Universidad de la República, Montevideo, Uruguay. He works mainly on atomic spectrometry and mass spectrometry, with a focus on bioanalytical chemistry. He was a postdoc researcher at the Department of Trace Element Analysis, the Institute of Analytical Chemistry of the ASCR, Prague, Czech Republic, in 2017. He has been a member of the Academic Assembly of Faculty of Chemistry, Universidad de la República, since 2018, and the International Medical Geology Association (IMGA) since 2019. He has been a researcher for the National System of Researchers (SNI, Uruguay) since 2016, and of the Basic Sciences Development Program – Chemistry Area (PEDECIBA – Química, Uruguay) since 2017. He is responsible for the BIOESP Group

Brazilian Journal of Analytical Chemistry
2026, Volume 13, Issue 51, pp 11-24
doi: 10.30744/brjac.2179-3425.AR-55-2025

ARTICLE

Incidence Study of Two UV Filters (Octocrylene and Octinoxate) and the Synthetic Fragrance Galaxolide in Commercial Yellow Clam (*Amarilladesma mactroides*)

Belén Salvatierra*, **Andrés Perez-Parada**, **Julio Gómez**, **Germán Azcune**

Centro Universitario de la Región Este, Universidad de la República, Ruta Nacional Nº 9 intersección con ruta Nº 15, Rocha, Rocha, 27000, Uruguay

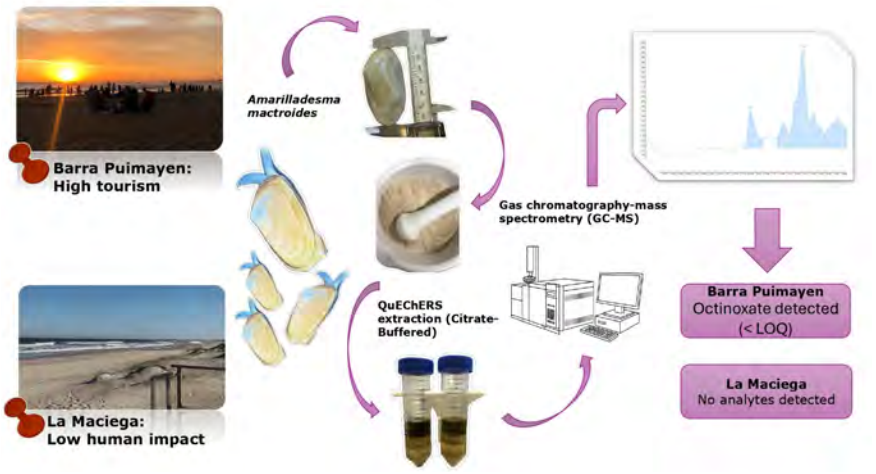

In this work, we study two UV filters (octocrylene and octinoxate) and the synthetic fragrance galaxolide in the yellow clam (*Amarilladesma mactroides*). Two beaches were strategically selected based on their contrasting population density, level of tourism and recreational activity. The clam samples used in this study originate from two distinct sub-populations. Samples from each beach were separated into 4 sizes (<54 mm, 55-56 mm, 57-58 mm and >59 mm); then, a modified citrate buffered QuEChERS method was used for subsequent evaluation in gas chromatography-mass spectrometry (GC-MS). The recoveries for all analytes were in the range between 70 to 102%, the RSD oscillated between 1 to 18%, and the limit of quantification was defined as the lowest recovery level with a value of 50 μg Kg^{-1} for all three analytes. As a result, the presence of the UV filter octinoxate was detected in the size of 55-56 mm on *Barra Puimayen* beach, being lower than the limit of quantification (50 μg Kg^{-1}). However, the evaluation indicated the absence of analytes from the individuals belonging to *La Maciega* beach, which presents a minimal anthropogenic impact.

Keywords: UV filters, synthetic fragrances, GC-MS, QuEChERS, bivalve mollusks

Cite: Salvatierra, B.; Perez-Parada, A.; Gómez, J.; Azcune, G. Incidence Study of Two UV Filters (Octocrylene and Octinoxate) and the Synthetic Fragrance Galaxolide in Commercial Yellow Clam (*Amarilladesma mactroides*). *Braz. J. Anal. Chem.* 2026, *13* (51), pp 11-24. http://dx.doi.org/10.30744/brjac.2179-3425.AR-55-2025

Received: June 26, 2025; **Revised:** August 30, 2025; September 25, 2025; **Accepted:** September 30, 2025; **Published online:** October 15, 2025.

This article is part of the BrJAC Special Issue on the 8th Uruguayan Congress of Analytical Chemistry (CUQA 8 2024).

INTRODUCTION

Pharmaceutical and personal care products (PPCPs) range from medicines used in humans and animals' health, to sunscreens, fragrances and cosmetics.[1] They enter aquatic and terrestrial environments through multiple pathways, including domestic and industrial wastewater, hospital effluents, agricultural runoff, and direct inputs from recreational coastal activities.[2] While some PPCPs can be degraded or transformed by physical, chemical, or biological processes, others are considered pseudo-persistent due to continuous discharge,[3] leading to long-term accumulation and potential adverse effects on both aquatic and terrestrial organisms,[4] as well as human health.[5,6]

Within the PPCPs there is the personal care products group, in which the two subgroups selected for this purpose are found: synthetic fragrance and UV filters.[7] These compounds reach the marine environment indirectly via wastewater discharges or directly through recreational activities.[8] Their lipophilic nature facilitates bioaccumulation in the muscle and adipose tissues of marine organisms,[9] and several studies have documented their potential for both bioaccumulation and biomagnification through marine food webs.[10] Bivalve mollusks, given their filter-feeding behavior and sedentary lifestyle, serve as effective bioindicators for monitoring these substances.[11] Previous studies have applied QuEChERS extraction followed by GC-MS analysis to detect UV filters and synthetic fragrances in marine bivalves, demonstrating the feasibility of this approach.[10,12] However, compound and matrix-specific validation data remain scarce, and the overall use of QuEChERS-GC-MS in aquatic organisms is still limited.

Building on these advances, the present study evaluates the performance of this methodology for the detection of selected UV filters and synthetic fragrances in marine bivalves, thereby contributing to the development of reliable analytical tools for environmental monitoring.

The *Amarilladesma mactroides* fishery in Uruguay opens their authorization during the summer season, under the co-management process among fishermen (39 clam farmers with permits) and the National Directorate of Aquatic Resources (*Dirección Nacional de Recursos Acuáticos*, DINARA, Uruguay) since 2009. In 2012 a "Fishing Counsil" for the yellow clam was formed, with the purpose of generating a consultative space for the management of this resource.[13,14] DINARA annually assesses its biomass for the opening of the fishery, establishing a "Total Extractable Commercial Biomass" which is distributed in equal quotas among the authorized fishermen.[15] The consumption of yellow clams has been highly valued over the years, becoming a coveted gastronomic product in the coastal area.[16] Therefore, the consumption of *Amarilladesma mactroides* contaminated by UV filters and fragrances might represent a threat to human health in the future. The objective of this study is to broaden the understanding of the yellow clam's behavior toward these contaminants, to guarantee a better management in the fishery and to provide safer consumption of *Amarilladesma mactroides* as a national resource.

To the best of our knowledge, the only studies to date specifically addressing *Amarilladesma mactroides* focus on the effects of the UV filter benzophenone-3 (BP3) on various biomarkers of the species.[17,18] Therefore, based on the available literature, this is the first study to investigate the occurrence of octocrylene, octinoxate and galaxolide in the yellow clam. This study expands the current understanding of the presence of personal care products in bivalve species by exploring compounds not previously evaluated in *Amarilladesma mactroides*. These findings contribute to the frontier of knowledge on the occurrence of emerging contaminants in commercially valuable marine resources, supporting both environmental monitoring and food safety initiatives.

MATERIALS AND METHODS

Chemicals

The compounds selected for this study were three organic pollutants belonging to two different categories: UV filters and fragrances. The UV filters were: octinoxate (EHMC) and octocrylene (OC). The fragrance was: galaxolide. Their structure and physicochemical properties are presented in Table I. Octocrylene and octinoxate were selected due to their widespread use as organic UV filters and their frequent detection in aquatic environments, which raises concerns about persistence and ecotoxicological impacts.[19] Notably,

octinoxate has been banned in Key West and Hawaii owing to its recognized toxic effects on marine ecosystems.[20] Additionally, galaxolide (a synthetic polycyclic musk commonly used in personal care products) was included due to its widespread presence in the environment, potential for bioaccumulation, and documented adverse effects on marine organisms.[21,22] Together, these compounds represent relevant targets for assessing contamination and ecological risk in coastal areas, as chemicals with Log Kow values between 3 and 5 are generally considered likely to bioaccumulate.[23] Notably, the three analytes examined in this study have log Kow values exceeding 5, indicating an even higher potential for bioaccumulation.

Table I. Physicochemical properties of the three standards

Substance	Structure	Molecular weight (g/mol)	CAS	Log Kow
Octocrylene	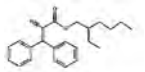	361.5	6197-30-4	6.88
Octinoxate	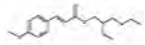	290.4	5466-77-3	5.2
Galaxolide	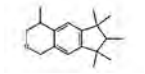	258.4	1222-05-5	5.90

Type I water was obtained using a Smart2Pure 3 UV ultrapurifier system (Thermo Scientific). Ethyl acetate (HPLC grade) was supplied by J.T. Baker (Avantor). Anhydrous sodium sulfate and sodium choride were purchased from Dorwil and Merck, respectively. Sodium citrate dihydrate and sodium hydrogen citrate trihydrate were obtained from Emsure and Sigma-Aldrich. The target compounds – octocrylene, octinoxate and galaxolide – were acquired from HPC Standards. ExtraBond C18 and PSA bulk adsorbent were provided by Scharlau.

Sample collection

The yellow clam fishery (*Amarilladesma mactroides*) in Uruguay is located between *La Coronilla* city and the *Barra del Chuy* city in the state of *Rocha*, covering a coastal strip of 20 km.[24] All the clams used for this work were purchased alive on the market in May 2023 from the artisanal fishing plant *Almejas Palmares*, authorized by DINARA.[25] All samples are considered part of the adult population, as they exhibit a shell length greater than 43 mm, which corresponds to the size at first sexual maturity;[26] whereas the commercial biomass consists of individuals with a shell length greater than 50 mm.[26] Belonging to two different subpopulations on the coasts of *Barra del Chuy* (*Rocha*), these beaches differ in the intensity of anthropogenic pressures and recreational activities conducted on them (Figure 1).

The sampling design of this study aims to determine whether there are significant differences in the impact of UV filters and fragrances on yellow clam populations located in areas with contrasting levels of anthropogenic influence. Two beaches were strategically selected that contrast due to their interaction with tourism and the recreational activities, with site selection agreed in consultation with the staff of the *Almejas Palmares* artisanal fishing plant, who have known the area for several generations.[25] The *Barra Puimayen* beach is in *Barra del Chuy* with a population of 370 inhabitants,[27] and an extension of 4.5 Km. The selection of this beach was based on its proximity to the *Barra del Chuy* city, and the attendance of tourists and locals for recreational use. The *Barra Puimayen* is mainly exposed to two major polluted discharges: the mouth of the *Chuy* stream (border between Uruguay and Brazil) which has had pollution problems for more than 20 years and the lack of wastewater treatment plant in the city of *Barra del Chuy*, which generates various sources of wastewater that reach the coast.[28] *La Maciega* beach is located in front of the small town of *Palmares de la Coronilla*, with a population of 10 inhabitants.[29] It is located approximately 6 km south of *Barra del Chuy* and 7 km north of the town of *La Coronilla*. *La Maciega* has an extension of 5 km and is

characterized by being a sport fishing area and low tourist attendance for different recreational activities due to its distance from both cities.

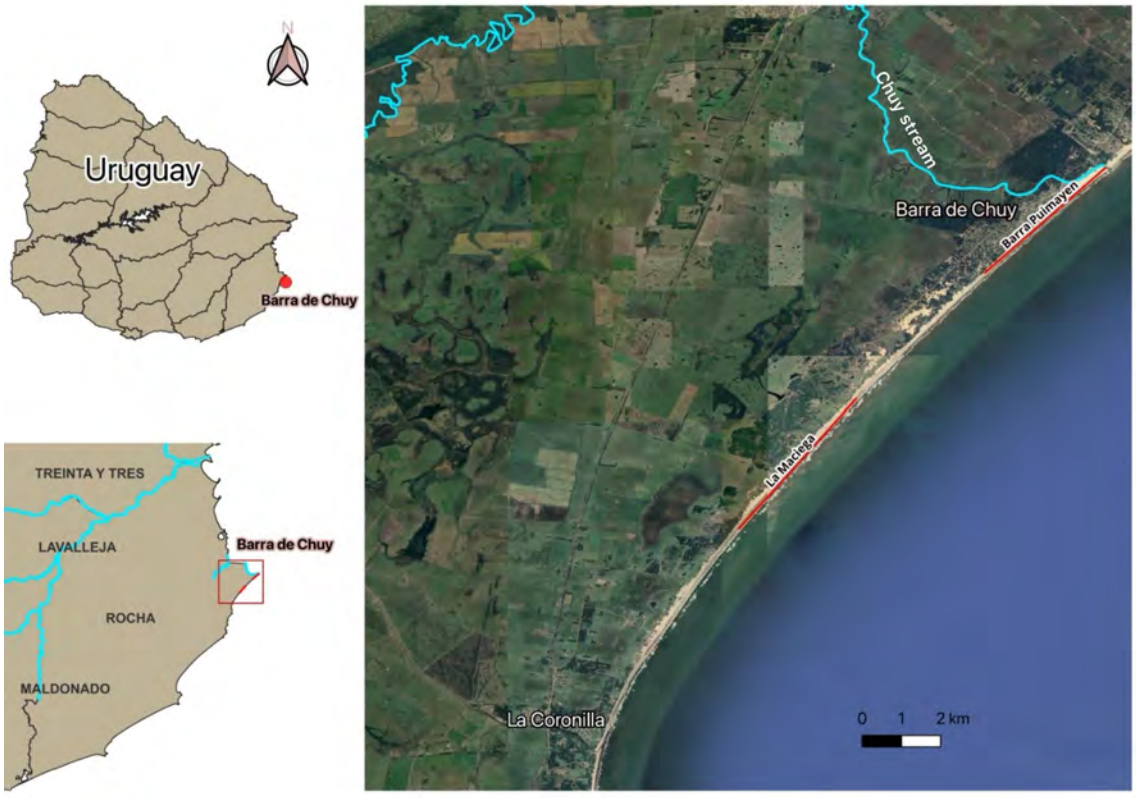

Figure 1. Sample zone of both subgroups of yellow clams (*Barra Puimayen* and *La Maciega*).

Sample preparation

The clams were subjected to: (a) 72-hour purification process, aerated, in 20 L containers at a salinity of 30 g L^{-1} and a temperature of 19 °C. (b) Both subpopulations were measured for total length (TL) with calliper and grouped by size in the following measurements: <54 mm, 55-56 mm, 57-58 mm, >59 mm. Each size group was composed of 15 individuals per beach, totalling 60 individuals evaluated at each beach and 120 individuals overall. The individuals were weighed to obtain the total body mass (including shell and muscle) (TBM) of each individual, then the valves were removed, and the wet muscle mass (WMM) was obtained. The samples were stored in zip-lock bags and taken to the freezer at -18 °C until they were freeze-dried. (c) The samples were frozen at -50 °C for 24 hours and then freeze-dried until constant mass. (d) The samples from both subgroups were weighed again to obtain the dry muscle mass (DMM) of each size group (4 groups defined before) and based on WMM and DMM the percentage of water lost (%WL) was calculated. The mean weight per individual (MWI) was calculated by dividing the total weight of each group by the number of individuals in that group (Table II). (e) The samples were then ground with a mortar. (f) The samples were stored in 50 mL centrifuge tubes (Figure 2).

Figure 2. Process for treating yellow clam samples. (a) Purchase and purification process, (b) length measurement and grouping, (c) freeze-drying, (d) weighing of the dry muscle mass, (e) dry muscle mass mortared and (f) storage.

Table II. Summed values of TBM, WMM, DMM, MWI and %WL for each size group (< 54 mm, 55-56 mm, 57-58 mm and > 59) from *Barra Puimayen* and *La Maciega* beaches

Barra Puimayen				
TL (mm)	**TBM**	**WMM (g)**	**DMM (g)**	**%WL**
< 54	192.2720	45.3863	12.6263	72.18
MWI	12.0170	2.8366	0.8417	
55-56	222.9812	55.6546	11.1230	80.01
MWI	13.9363	3.4784	0.7415	
57-58	253.8309	62.4515	13.1574	78.93
MWI	15.8644	3.9032	0.8771	
> 59	263.8631	67.0444	13.7003	79.56
MWI	17.5908	4.4696	2.0271	

(continued on next page)

Table II-cont. Summed values of TBM, WMM, DMM, MWI and %WL for each size group (< 54 mm, 55-56 mm, 57-58 mm and > 59) from *Barra Puimayen* and *La Maciega* beaches

La Maciega				
TL (mm)	**TBM**	**WMM (g)**	**DMM (g)**	**%WL**
< 54	183.6297	48.5177	8.9086	81.63
MWI	12.2419	3.2345	0.5939	
55-56	238.9608	64.4261	12.4050	80.74
MWI	14.9315	3.9787	0.8270	
57-58	251.2778	68.3873	13.0134	80.97
MWI	15,7401	4.2577	0.8955	
> 59	276.5727	76.8660	13.4333	82.52
MWI	17.3283	4.8283	1.8950	

For the determination of UV filters and fragrances in yellow clam, a modified citrate QuEChERS (quick, easy, cheap, effective, rugged and safe) extraction was performed,[30] adapted from Picot-Groz et al. 2014[31] and Martinez-Bueno et al. 2013.[32] Both studies were conducted on mussels (*Mytilus galloprovincialis*),[31,32] considering that they share the same feeding system as clams, as both species are non-selective filter feeders. Picot-Groz et al. (2014)[31] investigated the presence of the three analytes examined in the present work, among others, whereas Martinez-Bueno et al. (2013)[32] focused exclusively on two anticonvulsants. Nonetheless, both studies utilize the QuEChERS extraction method. In this study, the QuEChERS method was selected because octinoxate and octocrylene are ester-based UV filters that can undergo hydrolysis when exposed to strongly acidic or basic conditions. Such degradation would compromise their stability during sample preparation and potentially lead to an underestimation of their actual concentrations. The use of a buffered QuEChERS approach allows the maintenance of a stable pH throughout the extraction process, thereby preserving the chemical integrity of these analytes and ensuring reliable quantification.[33] Briefly, 2 g of freeze-dried sample from each size group of both subgroups of yellow clam were weighed in a 50 mL polypropylene centrifuge tube. 10 mL of Type 1 water was added, and the mixture was vortexed for 30 seconds. Then, 10 mL of ethyl acetate (AcOEt) was added, and the mixture was shaken manually for 2 minutes. After shaking, 4 g of anhydrous Na_2SO_4, 1 g of NaCl, 1 g of $Na_3Cit{:}2H_2O$ and 0.5 g of $Na_2HCit{:}3H_2O$ were added, and the mixture was shaken manually for 1 minute and centrifuged at 3500 rpm for 5 minutes. 2 mL of the upper layer was taken and transferred to a new 15 mL centrifuge tube for clean-up, with 750 mg Na_2SO_4, 125 mg ExtraBond C18 and 125 mg PSA bulk adsorbent. Subsequently, it was manually shaken for 1 minute and centrifuged for 5 minutes at 4000 rpm. 1 mL was filtered through a 0.45 µm PTFE syringe filter and transferred to a vial.

Recovery experiments were carried out by adding the analytes to the freeze-dried blank sample, followed by the extraction procedure, analogous to that applied to the real samples. For the matrix-matched calibration points, the blank sample was first extracted, and the analytes were then added directly into the vial at the indicated concentrations before analysis.

GC-MS Analysis

The above extracts were analyzed by GC-MS, using an Agilent Technologies 7890B GC coupled to an Agilent Technologies 5977B MS, and a Thermo Scientific GC TraceGOLD TG-5MS capillary column

(30 m × 0.25 mm and 0.25 µm). 1 µL was injected in splittles mode at 150 °C and helium was used as a carrier gas with a flow at 1 mL/min. The starting temperature was maintained at 150 °C for 2 minutes, increasing 10 °C per minute until reaching 310 °C, maintaining the temperature for 5 minutes, with a run time of 23 minutes. The mass detector was operated in electron impact ionization mode with an ionization energy of 70 eV. The GC-MS was used in "Selective Ion Monitoring" (SIM) mode. A source temperature of 250 °C and a quadrupole temperature of 150 °C were used for all analyses. The identification of compounds using GC-MS followed the SANTE guideline criteria for QA/QC. This required the use of three ions, with the ion ratio from sample extracts falling within ±30% (relative) of the average from calibration standards in the same sequence. Additionally, the analyte peaks for all three ions had to be fully overlapping.[34] The limit of quantification (LOQ) was defined as the lowest recovery level where recoveries ranged between 70% and 120%, with a maximum relative standard deviation (RSD%) of 20%.[34]

The quantification and qualification ions for all standards and the retention times for the peaks were defined (Table III).

Table III. Analytical parameters for the three standards

Substance	Quantification ion (*m/z*)	Qualification ion 1 (*m/z*)	Qualification ion 2 (*m/z*)	Retention time (min)	Window time (min)
Octocrylene	232	360	248	15.65	14.2–17.0
Octinoxate	178	161	290	12.84	12.0–14.2
Galaxolide	243	213	258	8.61	7.5–9.4

An external calibration curve of 50 µg Kg^{-1}, 100 µg Kg^{-1}, 200 µg Kg^{-1}, 300 µg Kg^{-1} and 500 µg Kg^{-1} was used for all standards. As quality control and quality assurance (QA/QC) criteria, a curve point was injected every 10 samples. Calibration curves were performed twice, once at the beginning and once at the end of the sequence. The second calibration confirmed the instrument´s repeatability over the course of the analysis.[35]

The matrix effect was evaluated according to the next three categories: weak < 25%, moderate 25-50% and strong > 50%. And it was calculated according to Equation (1).[36]

$$\%\ matrix\ effect = \frac{Slope_{matrix-solvent}}{Slope_{solvent}}\ x\ 100 \qquad \text{Equation (1)}$$

For QA/QC purposes, both procedural blanks and blank samples were analysed to assess potential contamination and background interferences. Recovery studies were conducted at two levels (50 and 100 µg Kg^{-1}) in triplicate, by spiking the target analytes into blank samples prior to the extraction procedure. These experiments were performed to evaluate the accuracy of the method and to ensure its reliability under the selected analytical conditions.

RESULTS AND DISCUSSION

The standardized sample preparation, including depuration, size classification, freeze-drying, and calculation of %WL and MWI, ensured comparability among individuals and minimized variability due to size and water content.

Quality Assurance and Quality Control

The comparison of the corresponding levels of both curves showed recoveries within 83% to 113%, meeting the criteria established by the SANTE guidelines.[34] For the samples' evaluation, calibration curves were made in matrix of both beaches as a single matrix, having been verified that they presented comparable matrix effect. External curves were performed for galaxolide, octocrylene and octinoxate at the following concentrations: 50 µg Kg^{-1}, 100 µg Kg^{-1}, 200 µg Kg^{-1}, 300 µg Kg^{-1}, 500 µg Kg^{-1} (Figure 3).

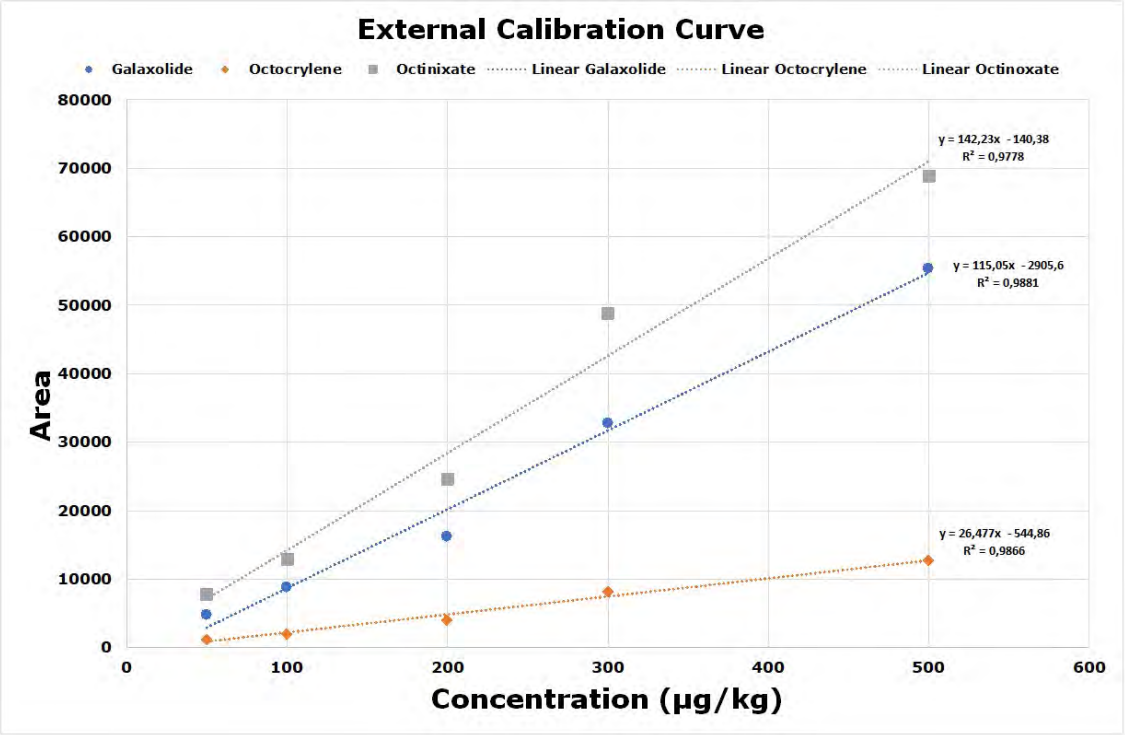

Figure 3. External calibration curves for galaxolide, octocrylene, and octinoxate at concentrations of 50, 100, 200, 300, and 500 µg Kg^{-1}.

All analytes were successfully recovered at the levels tested, with recoveries ranging from 72% to 102%, thereby meeting the acceptance criteria established by the SANTE guidelines (70–120%); the limit of quantification was defined as the lowest level with effective recovery. The relative standard deviation (%RSD) ranged from 1% to 18%, also in compliance with the SANTE criterion of ≤20%.[33] Full recovery data are presented in Table IV.

Our findings are consistent with previous studies on bivalve mollusks. Petrarca et al. (2022)[12] and Lestido-Cardama et al. (2023)[10] reported the bioaccumulation of galaxolide and octinoxate in mussels (*Mytilus galloprovincialis*) and clams (*Ruditapes philippinarum*), detecting both analytes with LODs between 0.5–50 µg Kg^{-1} dw and LOQs between 1–50 µg Kg^{-1} dw. Similarly, Picot-Groz et al. (2014)[31] evaluated octocrylene in mussels, reporting the highest concentrations among UV filters (up to 3992 µg Kg^{-1} dw) and LOQs ranging from 0.5–50 µg Kg^{-1}. Together, these works demonstrate the suitability of the QuEChERS method for assessing bioaccumulation of UV filters and synthetic fragrances in bivalves. The LOQ obtained in the present study (50 µg Kg^{-1}) is comparable to those previously reported, supporting the applicability of this approach for the determination of these compounds in clam samples.

It is important to note that studies combining QuEChERS extraction with GC-MS for the assessment of these contaminants in aquatic organisms remain limited, which hinders an in-depth comparative analysis across different works. Nevertheless, the available evidence consistently demonstrates that QuEChERS is a reliable and robust method for evaluating the presence of these compounds in marine bivalves.

To evaluate the matrix effect and compare the behavior of the analytes across different matrices, calibration curves were prepared both in solvent and in matrix-matched samples from both beaches (*Barra Puimayen* and *La Maciega*). As a result, octocrylene, octinoxate and galaxolide showed a positive matrix effect. Analytes showed comparable matrix effects on both beaches, showing a strong effect for octocrylene, a moderate effect for octinoxate and finally a weak effect for galaxolide (Table IV). Therefore, it was verified that the matrices of both beaches had comparable behaviors for the realization of the same matrix curve.

Table IV. Matrix effect of all standards and recoveries of the three standards performed for triplicate and the average of both concentrations for the three standards

Substance	Concentration (µg Kg^{-1})	Recovery (%)	% RSD	Matrix effect	
				La Maciega	*Barra Puimayen*
Octocrylene	50	85	7	Strong	
	100	72	18	60	57
Octinoxate	50	92	11	Moderate	
	100	102	7	49	36
Galaxolide	50	82	5	Weak	
	100	100	1	18	10

The three analytes were evaluated for the *Barra Puimayen* and *La Maciega* beaches for all clam sizes (<54 mm, 55-56 mm, 57-58 mm and >59 mm) in duplicate. No contaminants were detected in the clam samples collected from *La Maciega* beach. This could be attributed to the low number of houses that contribute to the wastewater discharges and the low number of inhabitants. Due to its difficult access, both because of the distance from *Barra Puimayen* and the absence of lifeguards, recreational activities by families are virtually absent. Only a few local residents use the area for activities such as sport fishing, according to information provided by the staff of "*Almejas Palmares*". The only analyte found in the clams was the UV filter octinoxate, from samples from *Barra Puimayen* beach measuring 55-56 mm (Figure 4). The concentration was detectable according to the detection parameters established by SANTE but was below the limit of quantification (LOQ) for this analyte (50 µg Kg^{-1}).

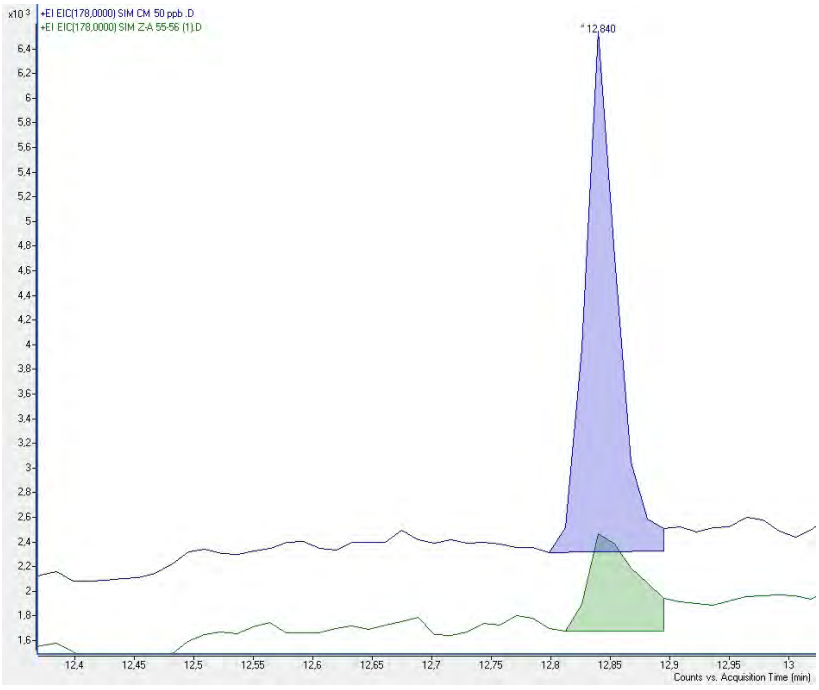

Figure 4. Extracted ion chromatogram (SIM, *m/z* 178) showing the detection of octinoxate in clam samples (55–56 mm) collected from *Barra Puimayen* beach.

The higher anthropogenic pressure at *Barra Puimayen* beach compared to *La Maciega* beach may explain the presence of octinoxate in the samples from this location, while no traces were detected in those from *La Maciega*. The presence of octinoxate in the samples collected in May, despite the reduced anthropogenic pressure compared to the summer season, suggests that *Amarilladesma mactroides* may bioaccumulate this UV filter. The detection of octinoxate in clams from *Barra Puimayen* beach is particularly relevant considering that this compound has already been banned in Hawaii and Key West due to its adverse effects on marine ecosystems.[21] Its presence in filter-feeding bivalves from Uruguay highlights the potential for bioaccumulation and raises concerns regarding ecological risks in coastal environments where no such regulatory measures are currently in place. The half-life of UV filters in the environment depends on various physical and chemical factors.[37] For octocrylene and octinoxate, among other UV filters, the reported half-lives suggest that their persistence in aquatic environments is typically less than one day.[37] This could tell us that the detection of octinoxate in the yellow clams in this study, represents the possibility that the contaminant had already accumulated in the individuals from the months prior to their purchase. In addition, there is a possibility that contaminants continue to enter the system during the low season.

The potential bioaccumulation of UV filters and fragrances detected in clams may not reflect the actual concentration levels to which individuals are exposed. In fact, the metabolic biotransformation and/or biodegradation processes occurring within the organism or in the marine environment should also be considered.[38] Furthermore, assessing emerging contaminants such as UV filters in combination with other stressors (e.g. elevated temperatures, salinity) is essential to gain a better understanding of both organismal responses and contaminant behavior.[39,40] Yellow clam present limited depuration capacity, retaining certain contaminants (e.g. microplastics) and pathogens even after standard depuration (48 hours).[41] To date, no studies have investigated the ability of the yellow clam to depurate the three analytes assessed in this study, nor any other similar compounds.

Regarding international regulatory restrictions, there is currently no legislation establishing maximum allowable concentrations of organic UV filters in marine waters or bivalves mollusks.[42] Worldwide there are different regulations concerning the UV filters allowed in Personal Care Products,[43,44,45] and all of them regulate the maximum amount of organic UV filters in personal care products and cosmetic products. Likewise, Uruguay is a member of the Southern Common Market (*Mercado Común del Sur*, MERCOSUR), and its current legislation on UV filters is governed by Decree No. 300/017.[47] This decree incorporates the provisions of MERCOSUR's Resolution No. 44/15, issued by the "Grupo Mercado Común", which approved the "MERCOSUR Technical Regulation on the List of Permitted Ultraviolet Filters for Personal Hygiene Products, Cosmetics, and Perfumes". As a result, Uruguay does not have specific regulations addressing the presence of pharmaceuticals and personal care products in bivalve mollusks.

In recent decades, yellow clam populations have suffered mass mortality, overfishing, and other anthropogenic pressures.[46]

The detection of the UV filter octinoxate in the present study suggests that current regulations on PPCPs may not adequately consider their potential effects on *Amarilladesma mactroides* and coastal ecosystems. The lack of previous studies in Uruguay on PPCPs in yellow clams prevents direct comparisons with our findings but highlights the need for future monitoring to support decision-making for the sustainable management of this fishery resource. Taken together, these results underscore the importance of incorporating emerging pollutants into monitoring programs and strengthening management strategies to ensure the conservation of this ecologically and socio-economically relevant species.

CONCLUSION

This study assessed the occurrence of octocrylene, octinoxate, and galaxolide in *Amarilladesma mactroides* from two Uruguayan beaches subject to contrasting anthropogenic pressures. The method, based on QuEChERS extraction followed by GC–MS, complied with SANTE guidelines and proved reliable for detecting UV filters and synthetic fragrances in bivalve mollusks. Octinoxate was detected in clams from *Barra Puimayen*, particularly in individuals above the commercial size threshold, suggesting a potential

accumulation trend related to size and seasonality. In contrast, no target analytes were found in samples from *La Maciega*, a site with minimal human activity, supporting the role of local anthropogenic inputs in determining contaminant occurrence. These results highlight the need to investigate temporal trends and sources of PPCPs in coastal environments, especially where fishery resources are exploited.

The study also demonstrates the applicability of the QuEChERS-GC-MS approach for environmental biomonitoring in aquatic organisms, where its use remains limited. Expanding future research to include additional bivalve species, broader spatial and temporal sampling, and a wider range of contaminants will strengthen its relevance for ecological risk assessment and regulatory decision-making.

Conflicts of interest

The authors declare that there are no financial conflicts of interest related to any of the affiliations of the authors of this article, nor with any other affiliations.

REFERENCES

(1) Kumar, M; Sridharan, S.; Sawarkar, A. D.; Shakeel, A.; Anerao, P.; Mannina, G.; Sharma, P.; Pandey, A. Current research trends on emerging contaminants pharmaceutical and personal care products (PPCPs): A comprehensive review. *Sci. Total Environ.* **2023**, *859* (1). https://doi.org/10.1016/j.scitotenv.2022.160031

(2) Keerthanan, S.; Jayasinghe, C.; Biswas, J. K.; Vithanage, M. Pharmaceutical and Personal Care Products (PPCPs) in the environment: Plant uptake, translocation, bioaccumulation, and human health risks. *Crit. Rev. Environ. Sci. Technol.* **2020**, *51* (12), 1221–1258. https://doi.org/10.1080/10643389.2020.1753634

(3) Sengar, A.; Vijayanandan, A. Human health and ecological risk assessment of 98 pharmaceuticals and personal care products (PPCPs) detected in Indian surface and wastewaters. *Sci. Total Environ*. **2022**, *807*. https://doi.org/10.1016/j.scitotenv.2021.150677

(4) Chakraborty, A.; Adhikary, S.; Bhattacharya, S.; Dutta, S.; Chatterjee, S.; Banerjee, D.; Ganguly, A.; Rajak, P. Pharmaceuticals and Personal Care Products as Emerging Environmental Contaminants: Prevalence, Toxicity, and Remedial Approaches. *ACS Chem. Health Saf.* **2023**, *30* (6), 362-388. https://doi.org/10.1021/acs.chas.3c00071

(5) Mo, J.; Guo, J.; Iwata, H.; Diamond, J.; Qu, C.; Xiong, J.; Han, J. What Approaches Should be Used to Prioritize Pharmaceuticals and Personal Care Products for Research on Environmental and Human Health Exposure and Effects? *Environ. Toxicol. Chem***. 2022**, *43* (3), 488-501. https://doi.org/10.1002/etc.5520

(6) Just-Sarobé, M. Sunscreens and Their Impact on Human Health and the Environment: A Review. *Int. J. Dermatol*. **2025**. https://doi.org/10.1111/ijd.17800

(7) Zhang, M.; Shen, J.; Zhong, Y.; Ding, T.; Dissanayake, P. D.; Yang, Y.; Tsang, Y. F.; Ok, Y. S. Sorption of pharmaceuticals and personal care products (PPCPs) from water and wastewater by carbonaceous materials: A review. *Crit. Rev. Environ. Sci. Technol*. **2020**, *52* (5), 727-766. https://doi.org/10.1080/10643389.2020.1835436

(8) Picot-Groz, M.; Fenet, H.; Martinez Bueno, M. J.; Rosain, D.; Gomez, E. Diurnal variations in personal care products in seawater and mussels at three Mediterranean coastal sites. *Environ. Sci. Pollut. Res*. **2018**, *25*, 9051-9059. https://doi.org/10.1007/s11356-017-1100-1

(9) Granados-Galvan, I. A.; Provencher, J. F.; Mallory, M. L.; De Silva, A.; Muir, D. C. G.; Kirk, J. L.; Wang, X.; Letcher, R. J.; Loseto, L. L.; Hamilton, B. M.; Lu, Z. Ultraviolet absorbents and industrial antioxidants in seabirds, mammals, and fish from the Canadian Arctic. *Sci. Total Environ*. **2024**, *951* (15). https://doi.org/10.1016/j.scitotenv.2024.175693

(10) Lestido-Cardama, A.; Petrarca, M.; Monteiro, C.; Ferreira, R.; Marmelo, I.; Maulvault, A. L; Anacleto, P.; Marques, A.; Fernandes, J. O.; Cunha, S. C. Seasonal occurrence and risk assessment of endocrine-disrupting compounds in Tagus estuary biota (NE Atlantic Ocean coast). *J. Hazard. Mater*. **2023**, *444*. https://doi.org/10.1016/j.jhazmat.2022.130387

(11) Vereycken, J. E.; Aldridge, D. C. Bivalve molluscs as biosensors of water quality: state of the art and future directions. *Hydrobiologia* **2023**, *850*, 231–256. https://doi.org/10.1007/s10750-022-05057-7
(12) Petrarca, M. H.; Fernandes, J. O.; Marmelo, I.; Marques, A.; Cunha, S. C. Multi-analyte gas chromatography-mass spectrometry method to monitor bisphenols, musk fragrances, ultraviolet filters, and pesticide residues in seafood. *J. Chromatogr. A* **2022**, *1663*. https://doi.org/10.1016/j.chroma.2021.462755
(13) D'Ambrosio, L.; Martínez, G.; González, V.; Keldjian, E.; Clavijo, I; Cuberos, V. Permanencias, transformaciones y desafíos en dos pesquerías artesanales de la Región Este de Uruguay. Tekoporá. *Revista Latinoamericana de Humanidades Ambientales y Estudios Territoriales* **2020**, *2* (1), 98-132. https://doi.org/10.36225/tekopora.v2i1.36
(14) D'Ambrosio, L.; Martínez, G.; Clavijo, I.; Cuberos, V. Articulaciones del conocimiento ecológico desarrollado en las prácticas de localidad con el conocimiento científico: una etnografía de una pesquería artesanal en Uruguay. Tekoporá. *Revista Latinoamericana de Humanidades Ambientales y Estudios Territoriales* **2020**, *2* (2), 90-111. https://doi.org/10.36225/tekopora.v2i2.92
(15) Ministerio de Ganadería, Agricultura y Pesca. Resolución No 10/2023 Dirección Nacional de Recursos Acuáticos. *Situación actual almeja amarilla*. Available at: https://www.gub.uy/ministerio-ganaderia-agricultura-pesca/institucional/normativa/resolucion-n-10023-dinara-situacion-actual-almeja-amarilla (accessed 2023/01/12).
(16) Proverbio, C.; Carnevia, D.; Jorge-Romero, G.; Lercari, D. Herramientas para el mantenimiento de la almeja amarilla *Mesodesma mactroides* en condiciones experimentales de cautiverio. *INNOTEC* **2019**, 124–141. https://doi.org/10.26461/18.02
(17) Chaves, F.; de Castro, M. R.; Toledo, G.; Guerreiro, A. S.; Barbosa, S. C.; Primel, E. G; Martins, C. M. G. Detoxification and effects of the UV filter Benzophenone-3 in the digestive gland and hemocytes of yellow clam (*Amarilladesma mactroides*) under a perspective of global warming scenario. *Mar. Pollut. Bull*. **2022**, *185*. https://doi.org/10.1016/j.marpolbul.2022.114188
(18) Lopes, F. C.; de Castro, M. R.; Barbosa, S. C.; Primel, E. G.; Martins, C. M. G. Effect of the UV filter, Benzophenone-3, on biomarkers of the yellow clam (*Amarilladesma mactroides*) under different pH conditions. *Mar. Pollut. Bull*. **2020**, *158*. https://doi.org/10.1016/j.marpolbul.2020.111401
(19) Carve, M.; Nugegoda, D.; Allinson, G.; Shimeta, J. A systematic review and ecological risk assessment for organic ultraviolet filters in aquatic environments. *Environ. Pollut*. **2020**. https://doi.org/10.1016/j.envpol.2020.115894
(20) Suh, S.; Pham, C.; Smith, J.; Mesinkovska, N. A. The banned sunscreen ingredients and their impact on human health: a systematic review. *Int. J. Dermatol*. **2020**, *59* (9), 1033-1042. https://doi.org/10.1111/ijd.14824
(21) Ehiguese, F. O.; González-Delgado, M. J.; Garrido-Perez, C.; Araújo, C. V. M.; Martin-Diaz, M. L. Effects and Risk Assessment of the Polycyclic Musk Compounds Galaxolide® and Tonalide® on Marine Microalgae, Invertebrates, and Fish. *Processes* **2021**, *9* (2), 371. https://doi.org/10.3390/pr9020371
(22) Ehiguese, F. O.; Alam, M. R.; Pintado-Herrera, M. G.; Araújo, C. V. M.; Martin-Diaz, M. L. Potential of environmental concentrations of the musks galaxolide and tonalide to induce oxidative stress and genotoxicity in the marine environment. *Mar. Environ. Res*. **2020**, *160*. https://doi.org/10.1016/j.marenvres.2020.105019
(23) Gimeo, S.; Allan, D.; Paul, K.; Remuzat, P.; Collard, M. Are current regulatory log K_{ow} cut-off values fit-for-purpose as a screening tool for bioaccumulation potential in aquatic organisms? *Regul. Toxicol. Pharmacol*. **2024,** *147*. https://doi.org/10.1016/j.yrtph.2023.105556
(24) Azambuja, F.; Egüez, R. Detección de microplásticos en almeja amarilla (*Amarilladesma mactroides)* en la costa rochense. Tesis de grado, Universidad de la República (Uruguay), Facultad de Veterinaria, 2020. https://hdl.handle.net/20.500.12008/27513

(25) Portal Oficial de Turismo en Rocha. https://turismorocha.gub.uy/destinos/la-coronilla/pesca-artesanal/almejas-palmares (accessed 2025/08/09).
(26) Lercari, D.; Celentano, E.; Jorge-Romero, G.; Bausero, S.; Licandro, J. Evaluación poblacional de la almeja amarilla (*Mesodesma mactroides*) en La Coronilla-Barra del Chuy, Rocha. Laboratorio de Ciencias del Mar, Facultad de Ciencias, Uruguay, 2021. Available at: https://www.gub.uy/ministerio-ganaderia-agricultura-pesca/comunicacion/publicaciones/evaluacion-poblacional-almeja-amarilla-mesodesma-mactroides-coronilla (accessed 2025/06/22).
(27) Municipios de Uruguay, Barra del Chuy. Available at: https://www.municipio.uy/localidad-barra-del-chuy-ro.html (accessed 2023/10/01).
(28) Hernández, D; Beretta, N. Calidad de agua del Arroyo del Chuy: percepción y monitoreo. Presented at the "II Congreso de Agua, Ambiente y Energía", Asociación de Universidades, Grupo Montevideo, Universidad de la República, Uruguay, 2019. Available at: https://www.fing.edu.uy/imfia/congresos/caae/assets/trabajos/new/Trabajos-Poster/121_Calidad_de_agua_del_Arroyo_del_Chuy:_percepci%C3%B3n_y_monitoreo.pdf (accessed 2025/06/22).
(29) Municipios de Uruguay, Coronilla. Localidad Palmares de la Coronilla. Available at: https://www.municipio.uy/localidad-palmares-de-la-coronilla-ro.html (accessed 2023/10/01).
(30) Pareja, L.; Pérez-Parada, A.; Azcune, G.; Muela, A; Colazzo, M. Determination of multiclass emerging contaminants using QuEChERS method. In: Sarma, H.; Dominguez, D. C.; Lee, W-Y. (Eds.). *Emerging Contaminants in the Environment, Challenges and Sustainable Practices*. Elsevier, 2022. Chapter 15, pp 335-380. https://doi.org/10.1016/B978-0-323-85160-2.00003-2
(31) Picot-Groz, M.; Bueno, M. J. M.; Rosain, D.; Fenet, H.; Casellas, C.; Pereira, C.; Maria, V.; Bebianno, M. J.; Gomez, E. Detection of emerging contaminants (UV filters, UV stabilizers and musks) in marine mussels from Portuguese coast by QuEChERS extraction and GC–MS/MS. *Sci. Total Environ*. **2014**, *493*, 162–169. https://doi.org/10.1016/j.scitotenv.2014.05.062
(32) Martinez-Bueno, M. J.; Boillot, C.; Fenet, H.; Chiron, S.; Casellas, C.; Gomez, E. Fast and easy combined QuEChERS extraction and high resolutionmass spectrometry methodology for residue analysis of two anticonvulsants and their transformation in marine mussels. *J. Chromatogr. A* **2013**, *1305*, 27–34. https://doi.org/10.1016/j.chroma.2013.06.071
(33) Álvarez-Ruiz, R.; Picó, Y.; Sadutto, D.; Campo, J. Development of multi-residue extraction procedures using QuEChERS and liquid chromatography tandem mass spectrometry for the determination of different types of organic pollutants in mussel. *Anal. Bioanal. Chem*. **2021**, *413*, 4063–4076. https://doi.org/10.1007/s00216-021-03363-y
(34) European Commission. Analytical quality control and method validation procedures for pesticides residues analysis in food and feed. SANTE 11312/2021, 2021, 1-55.
(35) Azcune, G.; del Puerto, L.; Blasi, A.; Castiñeira, C.; Pérez, L.; Inda, H.; Pérez Parada, A.; Fornaro, L. Paleoenvironmental characterization and historical trends of polycyclic aromatic hydrocarbons (PAHs) of Nutrias Lagoon, Uruguay. *Chemosphere* **2024**, *367*. https://doi.org/10.1016/j.chemosphere.2024.143617
(36) Cerqueira, M. B. R.; Guilherme, J. R.; Caldas, S. S.; Martins, M. L.; Zanella, R.; Primel, E. G. Evaluation of the QuEChERS method for the extraction of pharmaceuticals and personal care products from drinking-water treatment sludge with determination by UPLC-ESI-MS/MS. *Chemosphere* **2014**, *107*, 74–82. https://doi.org/10.1016/j.chemosphere.2014.03.026
(37) O'Malley, E.; McLachlan, M. S.; O'Brien, J. W.; Verhagen, R.; Mueller, J. F. The presence of selected UV filters in a freshwater recreational reservoir and fate in controlled experiments. *Sci. Total Environ*. **2021**, *754*. https://doi.org/10.1016/j.scitotenv.2020.142373
(38) Gómez, M. C.; Martín, L.; Cantarero, S.; Hidalgo, F.; Zafra, A. Ultra-high performance liquid chromatography tandem mass spectrometry analysis of UV filters in marine mussels (*Mytilus galloprovinciallis*) from the southern coast of Spain. *Microchem. J*. **2021**, *171*. https://doi.org/10.1016/j.microc.2021.106800

(39) Bordalo, D.; Cuccaro, A.; Meucci, V.; De Marchi, L.; Soares, A.; Pretti, C.; Freitas, R. Will warmer summers increase the impact of UV filters on marine bivalves? *Sci. Total Environ*. **2023**, *872*. https://doi.org/10.1016/j.scitotenv.2023.162108

(40) Santos, J. J. S.; Bernardes, J. P.; Ramírez, J. R. B.; De Miranda Gomes, C. H. A.; Romano, L. A. Effect of salinity on embryo-larval development of yellow clam *Mesodesma mactroides* (Reeve, 1854) in laboratory. *An. Acad. Bras. Ciênc*. **2020**, *92* (S1). https://doi.org/10.1590/0001-3765202020190169

(41) Azambuja, F.; Egüez, R. Detección de microplásticos en almeja amarilla (*Amarilladesma mactroides*) en la costa rochense. Tesis de grado, Universidad de la República (Uruguay), Facultad de Veterinaria, 2020. https://hdl.handle.net/20.500.12008/27513

(42) Carve, M.; Allinson, G.; Nugegoda, D.; Shimeta, J. Trends in environmental and toxicity research on organic ultraviolet filters: A scientometric review. *Sci. Total Environ*. **2021**, *773*. https://doi.org/10.1016/j.scitotenv.2021.145628

(43) Cadena, M. Evaluación e impacto de la presencia de filtros ultravioleta orgánicos por actividades antropogénicas en el medio marino costero. Tesis doctoral, Universidad de Las Palmas de Gran Canaria, España, 2022. https://accedacris.ulpgc.es/jspui/handle/10553/119572

(44) Nitulescu, G.; Lupuliasa, D.; Adam-Dima, I.; Nitulescu, G.M. Ultraviolet Filters for Cosmetic Applications. *Cosmetics* **2023**, *10* (101). https://doi.org/10.3390/cosmetics10040101

(45) Kroll, A.; Kienle, C.; Junghans, M. Organic UV-filters and freshwater organisms: data gaps impede a robust retrospective environmental risk assessment. *Environ. Sci. Eur.* **2025**, *37* (6). https://doi.org/10.1186/s12302-024-01046-w

(46) Gauthier, N. B; Goes, F. S.; Quaresma, L.; Pedrosa, V. F.; Roselet, F.; Romano, L. A.; Cavalli., R. O. Design and optimization of an experimental maintenance system for yellow clam broodstock *Amarilladesma mactroides* (Reeve, 1854). *Braz. J. Biol*. **2022**, *82*. https://doi.org/10.1590/1519-6984.243168

(47) IMPO Centro de Información Oficial. Normativa y Avisos Legales del Uruguay. Decreto No. 300/017. Aprobación de la Resolución GMC 44/15. Reglamento Técnico Mercosur sobre lista de filtros ultravioletas permitidos para productos de higiene personal, cosméticos y perfumes. Available at: https://www.impo.com.uy/bases/decretos/300-2017 (accessed 2025/10/11).

Brazilian Journal of Analytical Chemistry
2026, Volume 13, Issue 51, pp 25-35
doi: 10.30744/brjac.2179-3425.AR-58-2025

BrJAC

ARTICLE

Development of Methods for Selenium Determination in Fish: Tools for Ecotoxicological Studies

Lucía Falchi, Juan Gularte, Fiorella Iaquinta*

Grupo Química Analítica Ambiental, Facultad de Química, Universidad de la República
Av. Gral. Flores 2124, 11800 Montevideo, Uruguay

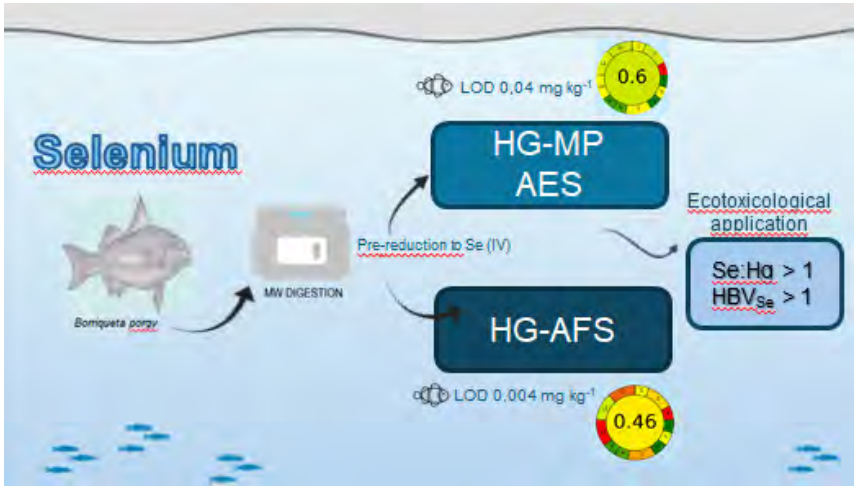

Selenium (Se) plays a significant role in many physiological processes. During the past years the role of Se has changed, from being considered toxic to the definition of being essential in almost every cell of our body. Furthermore, Se species play a role in mercury (Hg) detoxification suggesting that the protective effect of Se against Hg is related to the amount of Se available. In this work, two methods for Se determination in fish, by HG-AFS and HG-MP AES were developed. Moreover, a green analysis was applied to evaluate them. To both methods, optimization conditions were exhaustively evaluated and validated. Excellent figures of merit were obtained, with LOD of 0.04 mg kg^{-1} and 0.004 mg kg^{-1} to HG-MP AES and HG-AFS, respectively. The developed methods fit our purpose, being adequate for the determination of Se in fish and were compared in terms of accordance with the green analytical chemistry principles using AGREE metrics. The HG-MP AES method constitutes a greener alternative (0.60) than AFS (0.46). Borriqueta porgy (*Boridia grossidens*) fish samples from the Uruguayan coast were analyzed. The levels of Se in the samples were between 0.15 – 0.40 mg kg^{-1} determined by HG-MP AES and 0.13 – 0.35 mg kg^{-1} with HG-AFS, being the developed methods two alternatives for the Se monitoring. Finally, an ecotoxicological study was conducted to evaluate Se protection against Hg in fish tissue. All samples presented a Se:Hg molar ratio and the Selenium Health Benefit Value above 1, suggesting the protection of Se against mercury toxicity. This work presents two developed analytical methods suitable for the determination of Se in fish samples; in addition, this is the first evaluation that presents HG-MP AES for Se determination in fish. Furthermore, this work constitutes the first to determine Se in Uruguayan coast as well as the first to evaluate the Se protection against Hg in fish tissue.

Cite: Falchi, L.; Gularte, J.; Iaquinta, F. Development of Methods for Selenium Determination in Fish: Tools for Ecotoxicological Studies. *Braz. J. Anal. Chem.* 2026, *13* (51), pp 25-35. http://dx.doi.org/10.30744/brjac.2179-3425.AR-58-2025

Received: June 30, 2025; **Revised:** September 2, 2025; **Accepted:** September 30, 2025; **Published online:** October 16, 2025.

This article is part of the BrJAC Special Issue on the 8th Uruguayan Congress of Analytical Chemistry (CUQA 8 2024).

Keywords: selenium, fish, HG-MP AES, HG-AFS, ecotoxicology

INTRODUCTION

Selenium (Se) exists in both inorganic and organic forms. In its inorganic forms, Se is commonly found as selenate and selenite. Its organic forms include selenomethionine and selenocysteine. Geochemically, Se is primarily found in crustal rocks and phosphate-rich soils, and is introduced into aquatic ecosystems through both natural sources and human activities. Anthropogenic activities, such as mining, coal combustion, oil refining, and wastewater from agricultural drainage, are the main sources of Se contamination in aquatic systems, leading to elevated concentrations that are toxic to aquatic organisms.[1]

Selenium is a vital micronutrient that helps maintain physiological homeostasis in all vertebrates. However, these elements can become toxic when present in supraphysiological concentrations. It can move through aquatic food chains via bioconcentration and biomagnification. Given that, fish are top predators in most aquatic ecosystems and provide approximately 60% of the total animal protein consumed by humans, for this reason Se accumulation poses a significant food safety concern.[1,2] However, it seems that Se species play a role in mercury (Hg) detoxification.[3-6]

Mercury is a well-known toxic metal that has the capability of bioaccumulation, bioconcentration and biomagnification. Its main toxic form, methylmercury (II), causes severe damage to the nervous system, increases in severity of nephrotoxicity and blood pressure, among other effects. One of the main sources of Hg intoxication is throw diet, mainly to fish or seafood.[7]

It is suggested that the protective effect of Se against Hg is related to the amount of Se available. This occurs when the Se concentration is higher than Hg in tissues, and the Hg is sequestrated. A parameter that evaluates the protection of Se against Hg is the molar concentration ratio, where tissues need to exceed.[3,4]

Due to its capacity of volatile generation species, Se is commonly determined by hydride generation using borohydride as a reductant.[8] The hydride generation could be coupled to atomic fluorescence spectrometry (HG-AFS) or atomic absorption spectrometry (HG-AAS).[9,10] HG-AFS continues to be a widely used technique due to its high sensitivity and outstanding limits of detection.[11] Additionally, the Se determination could be performed using inductively coupled plasma mass spectrometry (ICP-MS).[12-14] Also, Se determination could be carried out by hydride generation coupled to Microwave Plasma Atomic Emission Spectrometry (HG-MP AES). The MP AES uses plasma generated by nitrogen gas obtained from an air compressor and a nitrogen generator.[15] MP AES “runs on air”, so the costs are reduced and the need for the supply of flammable or expensive gases is eliminated. Furthermore, ICP-OES limit of detection reported in complex matrix are in the same order of MP AES.[16,17] For this reason, it is a less expensive and more environmentally friendly offer than the ICP-OES.[15] The determination of Se by HG-MP AES has been developed for meat samples before.[16] However, to the best of our knowledge, this is the first work to determine Se in fish samples by HG-MP AES.

This work presents the development of two methods for the determination of Se in fish, by HG-AFS and HG-MP AES. A green analysis was applied to evaluate both methods. Then, fish samples were analyzed, as an application to ecotoxicological studies; Se protection against Hg was evaluated for the first time on the Uruguayan coast.

MATERIALS AND METHODS

Reagents

Standard solutions for calibration curves were prepared by serial dilution of commercial atomic absorption stock solutions (1000 mg L^{-1}) of Se and Hg (Merck, Darmstadt, Germany) in acidic media. Nitric acid (HNO_3) 70% w w^{-1} (Merck, Darmstadt, Germany) was used for microwave-assisted digestions. Ultrapure water (ASTM Type I) of 18.2 MΩ cm resistivity was obtained from a Millipore™ DirectQ3 UV water purification system (Bedford, Massachusetts, USA). Sodium tetrahydroborate ($NaBH_4$) solutions were prepared from the salt (Fluka, Hauppauge, USA) in 0.5% w v^{-1} NaOH (Merck, Darmstadt, Germany). Hydrochloric acid (HCl) (Merck, Darmstadt, Germany) was used to pre-reduce Se (VI) and as the carrier in the determination of Se employing AFS. All reagents were of analytical grade.

Samples

According to Muniz et al. (2004),[18] Montevideo harbour presented Hg levels that could be harmful to the ecosystem. For this reason, a representative coastal species of fish such as Borriqueta porgy (*Boridia grossidens*) was sampled from Montevideo, Uruguay harbour in winter from July to August 2024.

Fish samples were dissected using a stainless-steel knife, and muscle samples were crushed using a knife mill and preserved in polypropylene tubes at -4 ºC until analysis.

A certified reference material of Dogfish Liver (NRC-DOLT-5, National Research Council Canada, Canada) was used for the optimization and method validation.

Sample digestion

A microwave-assisted acid digestion was performed using CEM Mars6 microwave equipment (Matthews, NC, USA) provided with 12 Easy Prep Plus® Teflon vessels. For sample preparation, 0.25 g of sample was accurately weighed into each reaction vessel, and 10.0 mL of 4.8 mol L^{-1} HNO_3 was added. The program consisted of a 15-minute ramp to 200 °C, holding for 30 minutes, and then cooling to room temperature. Power varied between 400 and 1800 W, with a maximum pressure of 3.45 MPa. After mineralization, samples were filled up to 15.0 mL with ultrapure water. Samples and reagent blanks were run in duplicate. Reagent blanks were also run.

Sample pre-reduction

Since lower oxidation states can generate Se hydrides, firstly, it is necessary to reduce Se (VI) to Se (IV).[8] For this task, 5.0 mL of HCl 12 mol L^{-1} were added to 5.0 mL of the digested sample and heated at 100 °C for 50 minutes using a heating plate.[16] Calibration solutions were also run according to this procedure. Finally, the online reduction with $NaBH_4$ generates the selenium hydride (H_2Se).

Analytical determinations

Selenium determination by microwave-induced plasma optical emission spectrometry (MP AES) was performed with an Agilent 4210 spectrometer (Agilent Technologies, Santa Clara, USA). An online nitrogen generator, Agilent 4107 (Agilent Technologies, Santa Clara, USA), fed from environmental air through a KK70 TA-200 K compressor (Agilent Technologies, Santa Clara, USA) was used. The instrument was equipped with a multimode spray chamber (MSIS) for vapor generation and a standard torch (Agilent Technologies, Santa Clara, USA). The instrumental parameters are presented in Table I. Mercury determinations were also performed by MP AES coupled to cold vapor using $NaBH_4$ 2 % w v^{-1} as reductant according to Iaquinta et al. 2024.[19]

Table I. Instrumental parameters of HG-MP AES to determine Se

MP AES instrumental parameter	Optimized condition
Pump speed (rpm)	30 (0.90 mL min^{-1})
Nitrogen flow (L min^{-1})	1.0
Reading time (s)	10
Viewing position	-10
Stabilization time (s)	10
Wavelength (nm)	196.026
Background correction	Automatic

Meanwhile, Se determination by atomic fluorescence spectroscopy (AFS) was performed with a Persee PF7 Spectrophotometer (Persee Analytics, Beijing, China). Equipped with an integrated continuous flow hydride system, quartz atomization system, and high-intensity hollow cathode lamp (HCL) used as the radiation source (Persee Analytics, Beijing, China). Argon 99.998% (Praxair, Montevideo, Uruguay) was used as a gas carrier. Instrumental conditions were optimized, achieving the following parameters: argon flow of 200 L min^{-1}, sample injection of 1.5 mL, lamp main current of 40 mA, atomizer temperature of 200 °C, and 30 s for the lecture time.

Method validation

Validation was performed according to the recommendations of the Eurachem Guide.[20] The figures of merit evaluated were linear range, limit of detection (LOD), limit of quantification (LOQ), precision, and trueness. Precision and trueness were evaluated using dogfish liver CRMs.

RESULTS AND DISCUSSION

Optimization of HG-MP AES conditions

A previously validated method was used to determine Se in beef samples through HG-MP AES.[16] Based on these conditions, some parameters were optimized to fit our purpose. Pump speed, nitrogen flow, view position, and $NaBH_4$ concentration were evaluated.

Three different concentrations of $NaBH_4$ dissolved in NaOH 0.5% w v^{-1} were used to determine the optimal concentration to generate the hydride. For this task, certified reference material was used, and the evaluation was the percentage of signal recovery in duplicate. Table II presents the results and conditions evaluated. Since experiments 2 and 3 presented similar recoveries, it was decided to continue with $NaBH_4$ 2.0% w v^{-1} (Experiment 2). This selection was made to seek the lower amount of $NaBH_4$ to achieve a quantitative reduction of Se. Then, the analytical optimization was performed using this concentration.

Table II. Optimization results in using the HG-MP AES method

Experiment	$NaBH_4$ (% w v^{-1})	% Signal Recovery*
1	1.5	86 ± 1
2	2.0	100 ± 1
3	3.0	101 ± 1

*Signal recovery (%) = [intensity of CRM signal * 100] / [intensity of CRM signal obtained on calibration curve conditions (Experiment 2)].

Once the hydride conditions were optimized, the view position and the nebulizer flow were evaluated using a standard of 20 µg L^{-1}. The nebulizer flow optimization was evaluated between 0.30 and 1.00 L min^{-1}, obtaining the highest signal at 1.00 L min^{-1}. On the other hand, the viewing position was optimized, obtaining a result of -10, in a range from steps -120 to 120. Results are presented in Figure 1.

Finally, the pump speed was evaluated between 15 (0.45 mL min^{-1}) and 45 rpm (1,35 mL min^{-1}). The best condition was 30 rpm (0.9 mL min^{-1}). For this task, sensibility (slope of the calibration curve) was evaluated, resulting on highest sensibility at 30 rpm (0.9 mL min^{-1}) with a value of 18.4736 L $µg^{-1}$.

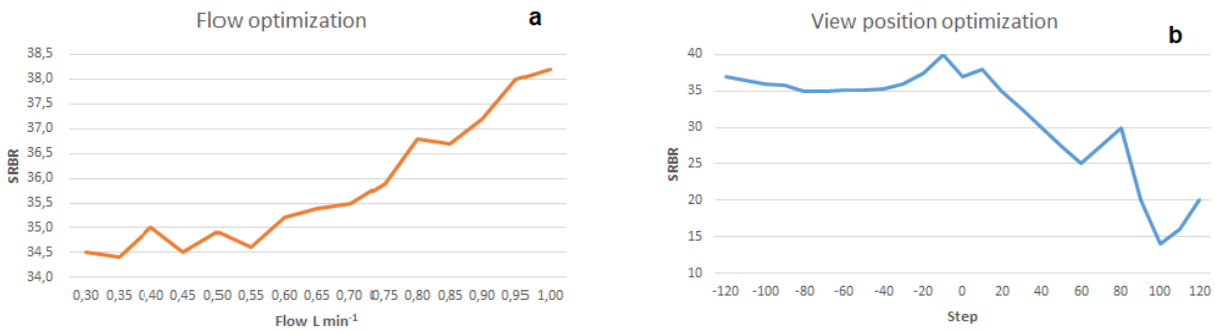

Figure 1. Flow (a) and view position (b) optimization for Se determination by HG-MP AES.

Optimization of HG-AFS conditions

For Se determination by HG–AFS, the recommended conditions of the Operational Persee Manual (Persee Analytics, Beijing, China) were considered. Based on them, some parameters were optimized to fit our requirements. The evaluated parameters were carrier and reductor ($NaBH_4$) concentrations, gas carrier flow, and sample injection volume, for the proper hydride generation.

A solution of HCl was employed as a carrier for Se determination. Three different acid concentrations (2.5, 5, and 7.5% v v^{-1}) were evaluated for the optimal hydride generation. Using the higher signal (area) for the dogfish liver CRM solution as a criterion, the optimal condition obtained was 5% v v^{-1}.

Under those carrier optimized conditions, the reductor concentration ($NaBH_4$), injection volume, and gas flow were evaluated using a composite-central experimental design of three variables in three levels.[21] The reductor concentrations studied were between 0.4 and 2.5% w v^{-1} in 0.5% w v^{-1} NaOH solution, the gas flow range was 200-400 mL min^{-1}, and the injection volume between 1.0 and 2.0 mL. All the experiments were done using the dogfish liver CRM solutions. The signals (area) obtained from the experimental design were analyzed in STATISTICA 8.0 software (StatSoft Inc, USA), gathering a graphic shown on Figure 2. Since 1.5 mL presents the highest area (550 IF), showing significant differences between 1 and 2 mL, the response surface was plotted with reductor concentration (Y), gas flow (X) and area (Z).

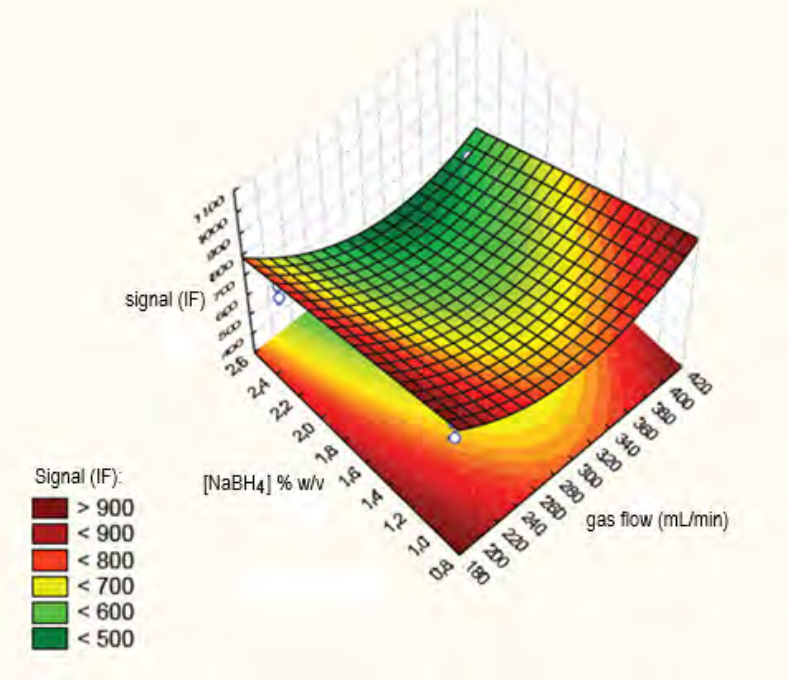

Figure 2. Results of the composite-central experimental design.

Finally, the optimal conditions for the proper hydride generation and detection of Se were under an HCl carrier concentration of 5% v v^{-1}, with an injection of 1.5 mL, flow gas of 200 mL min^{-1} and $NaBH_4$ reducer of 0.8% w v^{-1} in a 0.5% w v^{-1} NaOH solution.

Method validation

Once the critical parameters for hydride generation and the instrumental conditions were optimized, both methods were validated. The figures of merit evaluated, and their results are presented in Table III.

Table III. Performance parameters obtained for the proposed methods

Figure of merit	HG-MP AES	HG-AFS
Linear range (µg L^{-1}, n=6)	2.45 - 20.00	0.21 - 20.00
LOD (instrumental limits / method limits)	0.73 µg L^{-1} / 0.04 mg kg^{-1}	0.065 µg L^{-1} / 0.004 mg kg^{-1}
LOQ (instrumental limits / method limits)	2.45 µg L^{-1} / 0.15 mg kg^{-1}	0.210 µg L^{-1} / 0.013 mg kg^{-1}
Precision (RSD%, n=6)	5.8	3.8
Trueness (R%, n=6)	92 ± 5	86 ± 3
t-experimental	-2.54	1.68
t (0.05; 5)	2.57	

Linearity was evaluated by visual inspection and determinant coefficients after the evaluation of six points of calibration in triplicate. In all cases, the coefficient presented R^2>0.99, proper visual adjustment, and proper randomness study of the residuals. Figure 3 presents the calibration curve with the respective residuals, showing its randomness. Limits of detection and quantification were evaluated by 3*s*/b and 10*s*/b criteria. Where b is the slope of the calibration curve, and *s* is the standard deviation of 10 blanks previously pre-reduced. It is highlighted by the ten-times lower limits in the HG-AFS compared with HG-MP AES. HG-AFS limits allow the detection with reliability of lower levels of Se, being a strength of the technique. The obtained results are, in the same order or lower than the reported by recent works for HG-AFS.[22-24] Moreover, HG-AFS limits are in the same order as ICP-MS.[12-14] However, the results obtained with both methods were adequate for our purpose due to the Se content in fish samples previously reported in Atlantic Ocean.[5] Precision was estimated as repeatability and expressed as a percentage relative standard deviation (%RSD) after the analysis of the CRM (n=6). In both methods, it was below 6% which is suitable for our purpose since Horwitz theory about variability at trace levels has been proposed in 15% RSD.[25] For trueness evaluation, recoveries of the CRM were evaluated with results of 85-100%. Also, a student's *t*-test was performed to compare the obtained values with the certified values of the CRM. Table III presents the results obtained after the statistical analysis. Experimental *t*-values obtained were below the theoretical *t* (0.05, 5) = 2.57, indicating that at the 95% confidence level, the experimental concentrations did not differ significantly from the certified ones.[26]

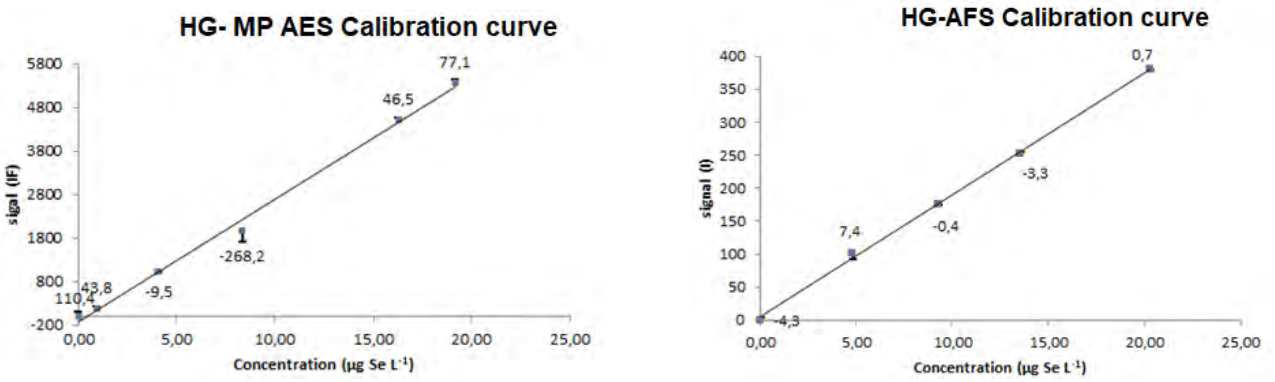

Figure 3. Calibration curve and residuals for Se determination by means of HG -MP AES (left) an HG-AFS (right).

The performance of the analysis between the developed methods was also evaluated by comparing the obtained Se levels in fish. For this task, a *t*-student test of mean values was applied. The result is presented in Table IV, where the means obtained by both methods were comparable since they did not differ significantly at a significance level of 95%.

Both methods fit our purpose, being adequate for the determination of Se in fish. It is worth noting that to the best of our knowledge, this is the first work that presents HG-MP AES for Se determination in fish.

Table IV. Comparison of methods by Student´s *t*-test

	HG-MP AES	HG-AFS
Average	0.303	0.254
t experimental	0.45	
t (0.05; 6)	2.23	

Greenness analysis

Both methods were compared in terms of accordance with the green analytical chemistry (GAC) principles.[27] There are many tools that allow the greenness assessment, Green Analytical Procedure Index (GAPI), AGREEPrep, Eco-scale.[28,29] For this task, the Analytical GREEnnes (AGREE) metric tool was applied.[26] This metric evaluates the 12 principles of green analytical chemistry individually, having each principle its type of evaluation. Finally, the result is a figure with colors and numbers, where the green color and the number 1 represent a complete approximation to green analytical chemistry principles.[30] Since sample preparation is the same for both methods, this tool provides more information than the AGREEPrep. Also, the AGREE pictograms are more friendly and easier to compare than GAPI pictograms or Eco-scale categories. Figure 4 presents the results of the AGREE evaluation. As can be observed, HG-MP AES method is more aligned with the green analytical chemistry principles, with a total score of 0.60. The main problems for both methods are that they are offline methods (Principle 3) and require a sample treatment (Principle 1). However, HG-MP AES presents advantages compared to the HG-AFS since it uses lower amounts of reagents, with lower toxicity and safer conditions, which is better for the environment and operator´s safety (Principles 2 and 12). Also, it generates a higher volume of waste (Principle 7). But the main difference is presented in principle 10, which involves renewable sources, and HG-MP AES uses air as a consumable, meanwhile HG-AFS uses argon. Thus, the HG-MP AES method constitutes a greener alternative than AFS.

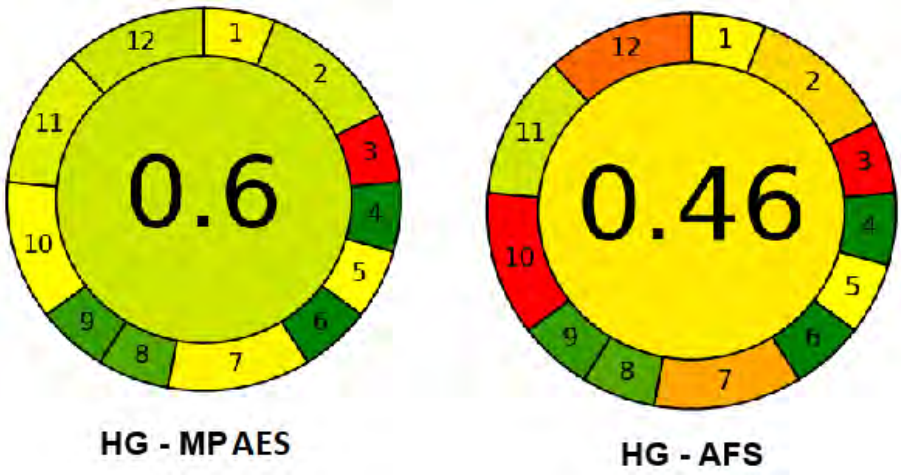

Figure 4. Results of AGREE metrics for the methods used.

Application to fish samples

Borriqueta porgy is a common fish from the southwest Atlantic Ocean, which is found in Uruguay, Brazil, and Argentina. However, there is no evidence of Se determination in fish of the Uruguayan coast. In this work, six fish samples were analyzed in duplicate using both methods for Se determination. The levels of Se in the samples were between 0.15 – 0.40 mg kg^{-1}, determined by HG-MP AES, and 0.13 – 0.35 mg kg^{-1} with HG-AFS.

The Se levels found in this work are in the same range as previous studies of fish in the Atlantic Ocean,[5] and also in the Mediterranean Sea.[31] Since fish is a good model for detecting toxic and nutritional chemicals in aquatic ecosystems,[32] the developed methods are two alternatives for the Se monitoring.

Selenium:mercury evaluation

In this work an ecotoxicological application was studied: the evaluation of Se protection against Hg. Selenium has an important role in the sequestration and reduction of bioavailability of methylmercury, suggesting its relevance in the reduction of mercury toxicity.[4,5] There are many studies in which the evaluation of the selenium:mercury molar ratio is presented in fish muscle. This ratio provides information about the protection against mercury toxicity. When the ratio is above 1 suggests that it is protecting against Hg.[4-6] Also, a Health Benefit Value (HBV) has been proposed as an indicator of sufficient selenium in fish in comparison to mercury. A positive Se-HBV suggests that Se could protect against Hg toxicity.[4,33]

The selenium:mercury (Se:Hg) molar ratio was evaluated using Equation (1):[6]

$$Se{:}\,Hg = \frac{Se\ concentration\ \left(\frac{g}{kg}\right) \Big/ 78.9}{Hg\ concentration\ \left(\frac{g}{kg}\right) \Big/ 200.59} \qquad \text{Equation (1)}$$

Meanwhile, Selenium Health Benefit Value was evaluated using Equation (2):[33]

$$HBV\ (Se) = \frac{(Se - Hg)}{Se\ \times\ (Se + Hg)} \qquad \text{Equation (2)}$$

Table V presents the results for the six samples evaluated.

Table V. Total selenium and mercury content, molar ratios, and HBV_{Se}

Selenium (mg kg^{-1})	Mercury (mg kg^{-1})	Se:Hg ratio	HBV_{Se}
0.345 ± 0.011	0.108 ± 0.017	8.14	4.31
0.256 ± 0.021	0.088 ± 0.013	7.41	3.19
0.250 ± 0.020	0.211 ± 0.087	3.01	2.81
0.294 ± 0.027	0.251 ± 0.019	2.98	3.31
0.197 ± 0.044	0.162 ± 0.022	3.09	2.23
0.305 ± 0.016	0.108 ± 0.014	7.18	3.79

Mean concentration ± standard deviation.

As we can observe, all samples presented a Se:Hg molar ratio above 1, suggesting the protection of Se against the mercury toxicity. As we can notice, even when the samples are from the same fish species, the ratio may vary; this could be related to the few samples evaluated. Nevertheless, this constitutes the first work that evaluates this relationship in Uruguayan samples. Also, the HBV_{Se} is positive in all cases, reinforcing the Se protection in the evaluated samples.

CONCLUSIONS

Two analytical methods were developed and validated for the determination of Se in fish muscle tissue. Both methods were adequate for the purpose proposed, HG-MP AES being more aligned with the Green Analytical Chemistry principles. To the best of our knowledge, this constitutes the first work assessing Se in fish through HG-MP AES.

The methods proposed were used for the determination of Se in Borriqueta porgy samples from Montevideo, Uruguay. An ecotoxicological application for a preliminary evaluation of Se protection against mercury was conducted in each sample, showing that it has a protective role in fish samples from Montevideo bay. However, more samples should be analyzed to confirm this protective activity.

Finally, these methods, HG-AFS and HG-MP AES could be used for the Se determination in ecotoxicological studies.

Conflicts of interest

The authors declare that there is no conflict of interest regarding the publication of this article.

Acknowledgements

The authors thank “Agencia Nacional de Investigación e Innovación” (ANII) and the “Programa de Desarrollo de las Ciencias Básicas” PEDECIBA-Química.

REFERENCES

(1) Uddin, M. H.; Ritu, J. R.; Putnala, S. K.; Rachamalla, M.; Chivers, D. P.; Niyogi, S. Selenium Toxicity in Fishes: A Current Perspective. *Chemosphere* **2024**, *364*, 143214. https://doi.org/10.1016/j.chemosphere.2024.143214

(2) Tóth, R. J.; Csapó, J. The Role of Selenium in Nutrition – A Review. *Acta Universitatis Sapientiae, Alimentaria* **2018**, *11* (1), 128–144. https://doi.org/10.2478/ausal-2018-0008

(3) Ribeiro, M.; Zephyr, N.; Silva, J. A. L.; Danion, M.; Guérin, T.; Castanheira, I.; Leufroy, A.; Jitaru, P. Assessment of the Mercury-Selenium Antagonism in Rainbow Trout Fish. *Chemosphere* **2022**, *286*, 131749. https://doi.org/10.1016/j.chemosphere.2021.131749
(4) Looi, L. J.; Aris, A. Z.; Haris, H.; Yusoff, F. M.; Hashim, Z. The Levels of Mercury, Methylmercury and Selenium and the Selenium Health Benefit Value in Grey-Eel Catfish (*Plotosus canius*) and Giant Mudskipper (*Periophthalmodon schlosseri*) from the Strait of Malacca. *Chemosphere* **2016**, *152*, 265–273. https://doi.org/10.1016/j.chemosphere.2016.02.126
(5) Burger, J.; Gochfeld, M. Mercury and Selenium Levels in 19 Species of Saltwater Fish from New Jersey as a Function of Species, Size, and Season. *Sci. Total Environ.* **2011**, *409* (8), 1418–1429. https://doi.org/10.1016/j.scitotenv.2010.12.034
(6) Burger, J.; Jeitner, C.; Donio, M.; Pittfield, T.; Gochfeld, M. Mercury and Selenium Levels, and Selenium:Mercury Molar Ratios of Brain, Muscle and Other Tissues in Bluefish (*Pomatomus saltatrix*) from New Jersey, USA. *Sci. Total Environ.* **2013**, *443*, 278–286. https://doi.org/10.1016/j.scitotenv.2012.10.040
(7) Agency for Toxic Substances and Disease Registry (ATSDR). *Toxicological Profile for Mercury,* 1999. https://www.atsdr.cdc.gov/toxprofiles/tp46.pdf (accessed 2025-02-04).
(8) Dedina, J.; Tsalev, D. L. *Hydride Generation Atomic Absorption Spectrometry*. Wiley, 1995.
(9) Cabañero, A. I.; Carvalho, C.; Madrid, Y.; Batoréu, C.; Cámara, C. Quantification and Speciation of Mercury and Selenium in Fish Samples of High Consumption in Spain and Portugal. *Biol. Trace Elem. Res.* **2005**, *103* (1), 017–036. https://doi.org/10.1385/BTER:103:1:017
(10) Robinson, J.; Shroff, J. Observations on the Levels of Total Mercury (Hg) and Selenium (Se) in Species Common to the Artisanal Fisheries of Seychelles. *Neurotoxicology* **2020**, *81*, 277–281. https://doi.org/10.1016/j.neuro.2020.09.017
(11) Zou, X.; Shen, K.; Wang, C.; Wang, J. Molecular Recognition and Quantitative Analysis of Free and Combinative Selenium Speciation in Selenium-Enriched Millets Using HPLC-ESI-MS/MS. *J. Food Compos. Anal.* **2022**, *106*, 104333. https://doi.org/10.1016/j.jfca.2021.104333
(12) Ohki, A.; Nakajima, T.; Hirakawa, S.; Hayashi, K.; Takanashi, H. A Simple Method of the Recovery of Selenium from Food Samples for the Determination by ICP-MS. *Microchem. J.* **2016**, *124*, 693–698. https://doi.org/10.1016/j.microc.2015.10.012
(13) Grotto, D.; Batista, B. L.; Carneiro, M. F. H.; Barbosa Jr., F. Evaluation by ICP-MS of Essential, Nonessential and Toxic Elements in Brazilian Fish and Seafood Samples. *Food Nutr. Sci.* **2012**, *03* (09), 1252–1260. https://doi.org/10.4236/fns.2012.39165
(14) Okati, N.; Moghadam, M. S.; Einollahipeer, F. Mercury, Arsenic and Selenium Concentrations in Marine Fish Species from the Oman Sea, Iran, and Health Risk Assessment. *Toxicol. Environ. Health Sci.* **2021**, *13* (1), 25–36. https://doi.org/10.1007/s13530-020-00062-6
(15) Agilent Technologies. *Microwave Plasma Atomic Emission Spectroscopy (MP-AES). Application eHandbook*. https://www.agilent.com/ (accessed 2025-06-22).
(16) Pistón, M.; Silva, J.; Suárez, A.; Belluzzi, M.; Iaquinta, F.; Panizzolo, L.; Méndez, C.; Cerminara, M. Estudio Del Contenido de Selenio En Carne Vacuna Luego Del Proceso de Cocción. *INNOTEC* **2020***, 19*. https://doi.org/10.26461/19.05
(17) Khan, N.; Jeong, I. S.; Hwang, I. M.; Kim, J. S.; Choi, S. H.; Nho, E. Y.; Choi, J. Y.; Kwak, B.-M.; Ahn, J.-H.; Yoon, T.; Kim, K. S. Method validation for simultaneous determination of chromium, molybdenum and selenium in infant formulas by ICP-OES and ICP-MS. *Food Chem.* **2013***, 141* (4)*,* 3566–3570. https://doi.org/10.1016/j.foodchem.2013.06.034
(18) Muniz, P.; Danulat, E.; Yannicelli, B.; Garcıa-Alonso, J.; Medina, G.; Bicego, M. C. Assessment of contamination by heavy metals and petroleum hydrocarbons in sediments of Montevideo Harbour (Uruguay). *Environ. Int.* **2004***, 29* (8)*,* 1019–1028. https://doi.org/10.1016/S0160-4120(03)00096-5
(19) Iaquinta, F.; Mollo, A.; Machado, I.; Vögler, R.; Banhos, S. G.; Nogueira, A. R. A. Microwave-induced plasma optical emission spectrometry coupled to vapor generation (VG-MIP OES) as an alternative technique for As and Hg determination for seafood surveillance. *Spectrochim. Acta, Part B* **2025**, *232*, 107281. https://doi.org/10.1016/j.sab.2025.107281

(20) Magnusson, B.; Örnemark, U. *Eurachem Guide: The Fitness for Purpose of Analytical Methods – A Laboratory Guide to Method Validation and Related Topics*, 2nd Ed., Eurachem, 2014.
(21) Massart, D.; Vandeginste, B.; Buydens, L.; De Jong, S.; Lewi, P.; Smeyers-Verbeke J. *Handbook of Chemometrics and Qualimetrics: Part A, Data Handling*, 1997.
(22) Schmitz, C.; Grambusch, I. M.; Lehn, D. N.; Hoehne, L.; de Souza, C. F. V. A Systematic Review and Meta-Analysis of Validated Analytical Techniques for the Determination of Total Selenium in Foods and Beverages. *Food Chem.* **2023**, *429*, 136974. https://doi.org/10.1016/j.foodchem.2023.136974
(23) LeBlanc, K. L.; Kumkrong, P.; Mercier, P. H. J.; Mester, Z. Selenium Analysis in Waters. Part 2: Speciation Methods. *Sci. Total Environ.* **2018**, *640–641*, 1635–1651. https://doi.org/10.1016/j.scitotenv.2018.05.394
(24) Skok, A.; Manousi, N.; Anthemidis, A.; Bazel, Y. Automated Systems with Fluorescence Detection for Metal Determination: A Review. *Molecules* **2024**, *29* (23), 5720. https://doi.org/10.3390/molecules29235720
(25) Horwitz, W.; Albert, R. The Horwitz Ratio (HorRat): A Useful Index of Method Performance with Respect to Precision. *J. AOAC Int.* **2006**, *89* (4), 1095–1109. https://doi.org/10.1093/jaoac/89.4.1095
(26) Miller, J. N.; Miller, J. C. *Statistics and Chemometrics for Analytical Chemistry* (6th Ed.). Prentice Hall, Harlow, 2010, Vol. 2010.
(27) Gałuszka, A.; Migaszewski, Z.; Namieśnik, J. The 12 Principles of Green Analytical Chemistry and the SIGNIFICANCE Mnemonic of Green Analytical Practices. *TrAC, Trends Anal. Chem.* **2013**, *50*, 78–84. https://doi.org/10.1016/j.trac.2013.04.010
(28) Nowak, P. M.; Wietecha-Posłuszny, R.; Pawliszyn, J. White Analytical Chemistry: An approach to reconcile the principles of Green Analytical Chemistry and functionality. *TrAC, Trends Anal. Chem.* **2021**, *138,* 116223. https://doi.org/10.1016/j.trac.2021.116223
(29) Falchi, L.; Pistón, M.; Casarotto, G.; Carro, S.; Cajarville, C.; Iaquinta, F. Development of a Green Methodology for the Determination of Artisanal Danbo Cheese Quality Parameters. *Braz. J. Anal. Chem*. **2023**, *10* (41), 30-41. https://doi.org/10.30744/brjac.2179-3425.AR-21-2023
(30) Pena-Pereira, F.; Wojnowski, W.; Tobiszewski, M. AGREE—Analytical GREEnness Metric Approach and Software. *Anal. Chem.* **2020**, *92* (14), 10076–10082. https://doi.org/10.1021/acs.analchem.0c01887
(31) Barone, G.; Storelli, A.; Meleleo, D.; Dambrosio, A.; Garofalo, R.; Busco, A.; Storelli, M. M. Levels of Mercury, Methylmercury and Selenium in Fish: Insights into Children Food Safety. *Toxics* **2021**, *9* (2), 39. https://doi.org/10.3390/toxics9020039
(32) Sumana, S. L.; Chen, H.; Shui, Y.; Zhang, C.; Yu, F.; Zhu, J.; Su, S. Effect of Dietary Selenium on the Growth and Immune Systems of Fish. *Animals* **2023**, *13* (18), 2978. https://doi.org/10.3390/ani13182978
(33) Ralston, N.; Raymond, L. Selenium Status and Intake Influences Mercury Exposure Risk Assessments. In: Banuelos, G. S.; Yin, X.; Lin, Z-Q. (Eds.). *Selenium in the Environment and Human Health*. Taylor & Francis Group, London, 2014.

Brazilian Journal of Analytical Chemistry
2026, Volume 13, Issue 51, pp 36-53
doi: 10.30744/brjac.2179-3425.AR-59-2025

BrJAC

ARTICLE

Low-Cost Particulate Matter Sensor in Indoor and External Classroom Environments

José Henrique De Souza Fernandes[1]*, Leonardo Marques Alves Ribeiro[2], Iêda Aparecida Pastre[3], Cristina Maria Roque Ramiro de Oliveira[4], Fernando Luís Fertonani[3]

[1]*Departamento de Metrologia, Pontifícia Universidade Católica do Rio de Janeiro (PUC-Rio). Rua Marquês de São Vicente, 225, Gávea, Rio de Janeiro, RJ 22451-900, Brazil*

[2]*Instituto de Química, Universidade de São Paulo (IQ-USP), Laboratório de Sensores Eletroquímicos e Métodos Eletroanalíticos (LSEME). Avenida Professor Lineu Prestes, 748, Cidade Universitária, São Paulo, SP 05508-000, Brazil*

[3]*Departamento de Química e Ciências Ambientais, Universidade Estadual Paulista (UNESP), Instituto de Biociências, Letras e Ciências Exatas (Ibilce). Rua Cristóvão Colombo, 2265, Jardim Nazareth, São José do Rio Preto, SP 15054-000, Brazil*

[4]*Departamento de Química e Bioquímica, Faculdade de Ciências, Universidade de Lisboa (FCUL). Campo Grande, 1749-016, Lisboa, Portugal*

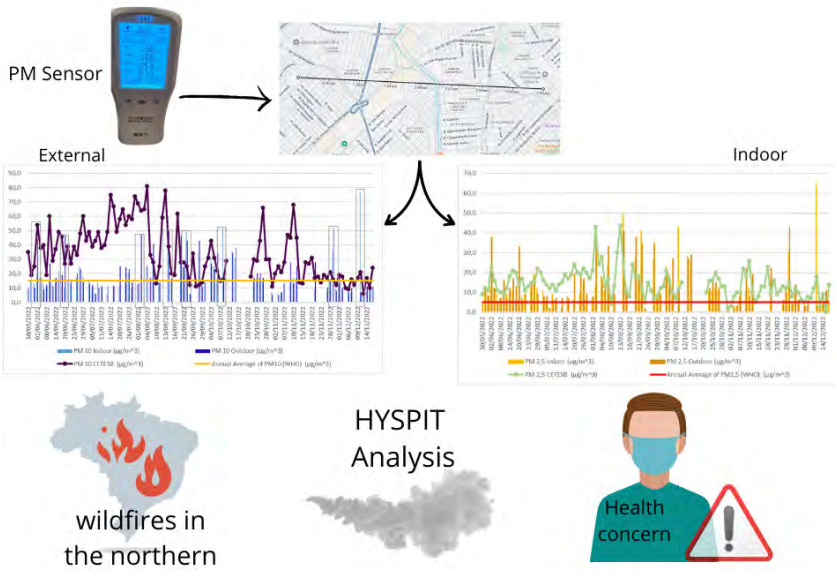

This study evaluates the concentrations of particulate matter (PM_{10} and $PM_{2.5}$) in indoor and outdoor university classrooms using a low-cost particulate matter sensor. Measurements were conducted hourly, daily, and annually in a closed, air-conditioned classroom at the Institute of Biosciences, Letters and Exact Sciences (Ibilce) of São Paulo State University (UNESP) throughout 2022. Results revealed that PM_{10} levels consistently exceeded the World Health Organization's (WHO) annual guideline of 15 μg m^{-3}, aligning with local CETESB data. Meanwhile, average indoor $PM_{2.5}$ concentrations (12.5 ± 11.2 μg m^{-3}) were almost three times the annual WHO limit of 5 μg m^{-3}. Peak values reached 43.75 μg m^{-3}, nearly 900% above the guideline, raising significant health concerns, and the calculated hazard quotient (HQ) approached the reference threshold. Outdoor $PM_{2.5}$ concentrations showed similar trends, with multiple peaks surpassing recommended thresholds. The Hybrid Single-Particle Lagrangian Integrated Trajectory (HYSPLIT) analysis linked high

Cite: Fernandes, J. H. S.; Ribeiro, L. M. A.; Pastre, I. A.; de Oliveira, C. M. R. R.; Fertonani, F. L. Low-Cost Particulate Matter Sensor in Indoor and External Classroom Environments. *Braz. J. Anal. Chem.* 2026, *13* (51), pp 36-53. http://dx.doi.org/10.30744/brjac.2179-3425.AR-59-2025

Received: July 7, 2025; **Revised:** October 4, 2025; November 6, 2025; November 19, 2025; **Accepted:** November 28, 2025; **Published online:** February 23, 2026.

This article is part of the BrJAC Special Issue on the 8th Uruguayan Congress of Analytical Chemistry (CUQA 8 2024).

PM levels to wildfires in central and northern Brazil and localized factors, including vehicle traffic and classroom maintenance. Statistical analysis revealed no significant difference between indoor and outdoor $PM_{2.5}$ levels, emphasizing the influence of external pollution on indoor air quality. These findings show the urgency of implementing targeted interventions, such as regular cleaning of classrooms, curtains, and air conditioning systems, to mitigate PM exposure. The study highlights the need for improved air quality management to ensure a safe learning environment for students and faculty.

Keywords: environmental chemistry, HYSPLIT, indoor air quality, low-cost sensor, $PM_{2.5}$ concentration

INTRODUCTION

Air quality is directly linked to the concentration and size of particulate matter (PM) in the atmosphere. According to the World Health Organization (WHO), in 2019, almost seven million premature deaths worldwide (accounting for almost 12% of all deaths)[1] were partially attributed to poor air quality, compromised by high levels of atmospheric PM.[2]

The term “aerosol” was introduced by Schmauss in 1920 to describe particles that remain suspended in the air with high stability, particularly those smaller than 100 μm in diameter.[3] Aerosols can exist in both solid and liquid states. For many years, the atmospheric particle standards of numerous countries were based on the measurement of the mass concentration of “Total Suspended Particles” (TSP). However, since TSP often includes non-inhalable particles that have a lesser impact on respiratory and cardiovascular diseases, there was no clear correlation between TSP levels and health effects.[4]

PM is categorized by size into coarse particles (PM_{10}), fine particles ($PM_{2.5}$), and ultrafine particles (less than 0.1 μm). PM is further classified by its emission sources, categorized as primary (natural sources such as volcanic activity, forest fires, sea spray) or secondary (anthropogenic sources, including particles formed through nucleation, condensation of gaseous components, and chemical and photochemical reactions in the atmosphere). Secondary aerosols are divided into four major groups: sulphate aerosols, nitrate aerosols, Cl-aerosols and secondary organic aerosols, with secondary anthropogenic fine particles having a significant impact on human health.[5]

In indoor environments, concerns about air quality became prominent in the 1970s with the trend of constructing sealed buildings for acoustic insulation, climate control, aesthetics, and security. This led to an increase in health issues related to indoor air quality.[6] Poor indoor air quality is mainly caused by inadequate cleaning of air conditioning systems, recirculation of air, and a lack of periodic control over potential sources of contamination.[7] The fine fraction of indoor air typically contains a mixture of particles from combustion processes and secondary particles generated by atmospheric chemical reactions, including acid condensates, sulphates, and nitrates.[8] $PM_{2.5}$ particles, in particular, can adsorb and carry high concentrations of mutagenic substances, such as polycyclic aromatic hydrocarbons (PAHs), which are predominantly concentrated in $PM_{2.5}$.[9]

Beyond direct health effects, aerosols have significant economic impacts,[10] and exposure to these particles is associated with cardiovascular diseases,[11,12] pulmonary inflammation,[13] bronchitis, asthma, and other respiratory conditions,[14] lung cancer,[15] and an increased risk of diabetes due to exposure to $PM_{2.5\text{-}0.1}$.[16,17] Additionally, these particles can impair cognitive function in individuals exposed to them in closed, climate-controlled environments,[18] with increased carbon dioxide (CO_2) levels further reducing concentration and cognitive abilities. This study aims to assess the concentration of PM_{10} and $PM_{2.5}$ in both indoor (closed and air-conditioned classrooms) and outdoor university environments, with a focus on the impact of exposure over time.

While indoor air quality has been extensively studied in residential and commercial buildings,[19,20] university classrooms remain underrepresented in the literature. Despite advances in understanding PM dynamics, the complexity of factors influencing indoor pollutant concentrations such as outdoor PM infiltration[21] and human activity-driven particle resuspension[22] remains poorly characterized in educational environments. This gap is particularly critical in classrooms, where prolonged student occupancy and climate-controlled conditions

may amplify exposure risks. By investigating the emission of these PMs on closed indoor classrooms, this study seeks to contribute to assess the exposure of students to PM in these settings.

MATERIALS AND METHODS

Sensor configuration

The sensor used in this study was a commercially available portable multiparameter air quality sensor (version 2.03) equipped with a PMS5003 sensor, suitable for measuring PM with diameters up to 10 μm. The measurements were divided between coarse (10 μm to 2.5 μm) and fine particles (2.5 μm to greater or equal than 1.0 μm). Although the sensor is sensitive to particles with diameters below 1.0 μm, the ultrafine particle fraction was not explicitly reported by the air quality sensor. According to the manufacturer, the reported maximum errors are ±10 μg m^{-3} in the concentration range 0–100 μg m^{-3} range, and ±10 % in the range of 100–500 μg m^{-3}. The device was factory-calibrated following the manufacturer's specifications. This sensor employs a light-scattering approach to measure $PM_{2.5}$, and PM_{10} mass concentrations in real-time with a total response time of about 10 seconds.

Additionally, it was equipped with a DHT11 module to monitor temperature and humidity. The DHT11 is a digital sensor capable of measuring temperature in the range of -40 to 80 °C with an accuracy of ±0.5 °C and relative humidity from 0 to 100% with an accuracy of ±2-5%. This combination allows the sensor to provide comprehensive environmental data, offering insights into both PM and ambient conditions, crucial for assessing air quality in indoor and external environments.

The PM values displayed on the sensor screen were manually transcribed during classes and subsequently digitized into an Excel spreadsheet to enable systematic analysis and comparison with reference data.

Sensor sampling

Measurements were conducted with a single sensor on each weekday when classes were held, with a minimum of eight indoor measurements per day. Additionally, outdoor measurements were taken every two hours to map the concentration of PM on days when the spaces were in use, as is shown in Table I. This systematic monitoring primarily focused on the C block at the Institute of Biosciences, Letters and Exact Sciences of São Paulo State University (UNESP-Ibilce), which was selected because it hosted most of the chemistry, mathematics, and physics classes (Lat: -20.785402, Long: -49.360823), providing a detailed assessment of PM concentrations in both indoor and outdoor environments during active periods.

Table I. Sampling plan for 2022

	1st Semester of 2022					2nd Semester of 2022				
Schedule	**Mon**	**Tue**	**Wed**	**Thu**	**Fri**	**Mon**	**Tue**	**Wed**	**Thu**	**Fri**
8 a.m.	ID	ID	ID	ID		ID	ID	ID	ID	
9 a.m.	ID	ID	ID	ID		ID	ID	ID	ID	
10 a.m.	OD	OD	OD	OD		OD	OD	OD	OD	
10:10 a.m.	ID	ID	ID	ID		ID	ID	ID	ID	
11 a.m.	ID	ID		ID		ID	ID		ID	
12 p.m.	OD	OD	OD	OD		OD	OD	OD	OD	
12:10 p.m.	ID	ID	ID	ID		ID	ID	ID	ID	
1 p.m.										
2 p.m.	OD	OD	OD	OD		OD	OD	OD	OD	

(continued on next page)

Table I. Sampling plan for 2022 (continued)

	1st Semester of 2022					2nd Semester of 2022				
Schedule	**Mon**	**Tue**	**Wed**	**Thu**	**Fri**	**Mon**	**Tue**	**Wed**	**Thu**	**Fri**
2:10 p.m.	ID	ID	ID			ID	ID	ID		
3 p.m.	ID	ID	ID			ID	ID	ID		
4 p.m.	OD	OD	OD	OD		OD	OD	OD	OD	
4:10 p.m.	ID	ID	ID			ID	ID	ID		
5 p.m.		ID	ID				ID	ID		
6 p.m.		ID	ID				ID	ID		
6:10 p.m.	OD	OD	OD			OD	OD	OD		
7 p.m.		ID	ID				ID	ID		

ID: Indoor sampling; OD: outdoor sampling.

All measurements were conducted at a height of 120 cm from the ground, approximately at the average seated nose height, and positioned at the center of the classroom. During measurements, the door was kept closed, and the air conditioner was operating to maintain consistent indoor conditions. The data collection aimed to capture the presence and behavior of PM across three different temporal scales: hourly, daily, and annually. This was achieved by calculating the mean PM concentration for each day, providing a comprehensive analysis of PM variations over time.

The measurements were taken during class sessions because the primary objective was to assess the actual exposure of students to PM. By measuring in the occupied classroom, we capture the effects of human activity and occupancy on indoor air quality, which directly reflects the environment that students experience.

Environmental Company of the State of São Paulo (CETESB) comparison

To benchmark classroom PM measurements against the ambient urban air, we incorporated data from a nearby CETESB monitoring station. The specific sensor model used by CETESB is not disclosed. The station is operated by the state government environmental agency and is located at Lat: -20.784862, Long: -49.398324. The station continuously records hourly PM concentrations and serves as a proxy for the city's overall air quality. In our methodology, we aligned the temporal resolution of our classroom measurements with CETESB's hourly data, ensuring consistency in comparison. This approach allows us to assess student exposure within the classroom relative to the broader urban environment. Figure 1 displays a Google Maps view depicting the spatial relationship between the UNESP campus and the CETESB station. Notably, the map shows that the CETESB station is located at a significant distance from UNESP and is situated in an area surrounded by several high-pollution sources, such as major roads and industrial zones. This geographical context suggests that the higher average PM levels recorded by CETESB may be influenced by these external sources, thereby providing a meaningful benchmark for comparing indoor and urban air quality.

Figure 1. Distance between C-block-UNESP and CETESB station.

Retro-trajectory HYSPLIT

HYSPLIT (Hybrid Single-Particle Lagrangian Integrated Trajectory) is a widely used atmospheric modeling tool developed by the National Oceanic and Atmospheric Administration (NOAA) Air Resources Laboratory.[23-26] NOAA is the primary U.S. federal agency for monitoring and researching atmospheric and oceanic processes, and its models are internationally recognized for applications in air quality and climate studies. HYSPLIT simulates the dispersion and trajectory of particles in the atmosphere using a Lagrangian framework, where an air parcel is tracked as it moves through space. This approach calculates advection and diffusion separately, driven by meteorological data from numerical weather prediction models such as the Global Forecast System (GFS).

In this study, twelve days of retro-trajectories were simulated throughout 2022 over the C block of UNESP, resulting in a total of 36 retro-trajectories at three different altitudes: 500 m, 1000 m, and 1500 m.

Health risk assessment

To estimate the potential health impacts associated with exposure to particulate matter (PM), a quantitative health risk assessment was conducted based on the mean concentrations obtained for both $PM_{2.5}$ and PM_{10}. The calculation considered the following parameters: inhalation rate (IR) ($m^3 \times day^{-1}$), exposure time (ET) ($hours \times day^{-1}$), exposure frequency (EF) ($\text{days} \times year^{-1}$), exposure duration (ED) ($year$), body weight (BW) (kg), and averaging time (AT) (days). These parameters were integrated to determine the Average Daily Dose (ADD) ($\text{mg} \times \text{kg}^{-1} \times \text{day}^{-1}$), according to Equation (1).[27]

$$ADD = {C_{air}\ x\ IRx\ ETx\ EFx\ ED}/{BW\ x\ AT} \qquad \text{Equation (1)}$$

Where C_{air} is the mean particulate concentration in the air ($mg \times m^{-3}$).The values adopted for IR and BW were obtained from the Environmental Protection Agency (EPA)[28] (21 to <31 years old) and Centers for Disease Control and Prevention (CDC),[29] respectively.

Subsequently, the Lifetime Excess Cancer Risk (ELCR) was calculated to evaluate potential carcinogenic effects during the period of university attendance, assumed to be four years. The ELCR was derived from the ADD and the slope factor (SF), as described in Equation (2).[30]

$$\mathrm{ELCR} = \mathrm{ADD} \times \mathrm{SF}$$ Equation (2)

In this context, the slope carcinogenic potency factor (SF) was obtained from the literature.[31] It is important to note that, given the well-established evidence that PM_{10} exhibits less detrimental health effects compared to $PM_{2.5}$, only $PM_{2.5}$ concentrations were considered for the carcinogenic risk assessment.

In addition, the Hazard Quotient (HQ) was calculated for both $PM_{2.5}$ and PM_{10} to estimate potential non-carcinogenic risks, as expressed in Equation (3).[32]

$$\mathrm{HQ\ (hazard\ quotient)} = {}^{\mathrm{ADD}}/_{\mathrm{RfD}}$$ Equation (3)

Where ADD corresponds to the average daily dose and RfD is the reference dose. The RfD was estimated from the inhalation reference concentrations (RfC) established by the WHO, with values of 5 μg m^{-3} for $PM_{2.5}$ and 15 μg m^{-3} for PM_{10}, as shown in Equation (4):

$$\mathrm{RfD} = {}^{\mathrm{RfC} \times \mathrm{IR}}/_{\mathrm{BW}}$$ Equation (4)

According to international guidelines, HQ values greater than 1 indicate potential non-carcinogenic risks of concern, requiring preventive or corrective actions. Conversely, HQ values below 1 are generally considered within acceptable limits of exposure.[33]

RESULTS AND DISCUSSION

The following represent the complete sampling/measurement periods in a broader context. The measurement values, specifically the daily averages of PM_{10} and $PM_{2.5}$, were compared against the WHO limits and the data provided by the local CETESB station for the same period.

Hourly behavior of PM inside classrooms

During the afternoon of August 2, 2022, measurements of PM_{10} and $PM_{2.5}$ were conducted inside active classrooms to assess PM levels and their behavior. Figures 2 and 3 present the results of these measurements over a 60-minute period, with data sampled approximately every 5 minutes. Both PM_{10} and $PM_{2.5}$ concentrations displayed similar trends throughout the 60-minute period, with PM_{10} values consistently higher than those of $PM_{2.5}$.

The average concentration of $PM_{2.5}$ measured indoors was approximately 6.92 ± 0.92 μg m^{-3} (or 6.92 ± 13.6%), remaining below the 24-hour limit of 15 μg m^{-3} recommended by the WHO.[2] However, if this average is extrapolated for the hole year compared to the annual limit of 5 μg m^{-3}, it exceeds the threshold, indicating a potential long-term exposure risk. Conversely, the average PM_{10} concentration indoors was 11.42 ± 1.49 μg m^{-3} (or 11.42 ± 13.0%), staying below both the WHO's 24-hour limit of 45 μg m^{-3} and the annual limit of 15 μg m^{-3} if the value is extrapolated, suggesting compliance with air quality standards for this pollutant.

A key observation from these data is the relative consistency in individual measurements, with variations close to 10%, which indicates a stable indoor air quality environment during the period of observation. Based on this finding, the monitoring strategy was adjusted to be conducted on an hourly basis. The rationale for this decision is that preliminary comparisons among different measurement intervals (every 10 minutes, every 30 minutes, and every hour) did not reveal substantial short-term fluctuations that would justify higher-frequency sampling. Thus, adopting hourly measurements still capture representative variations in PM concentrations throughout the observation period. This approach allowed the data to consistently reflect the ongoing indoor conditions without unnecessary redundancy in sampling.

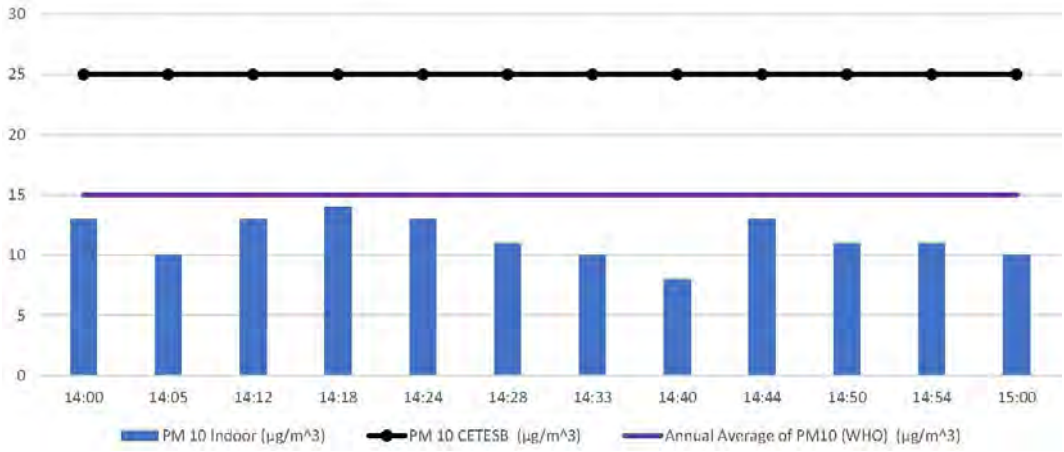

Figure 2. PM_{10} concentration in an active classroom environment, measured every 5 minutes, compared to CETESB data.

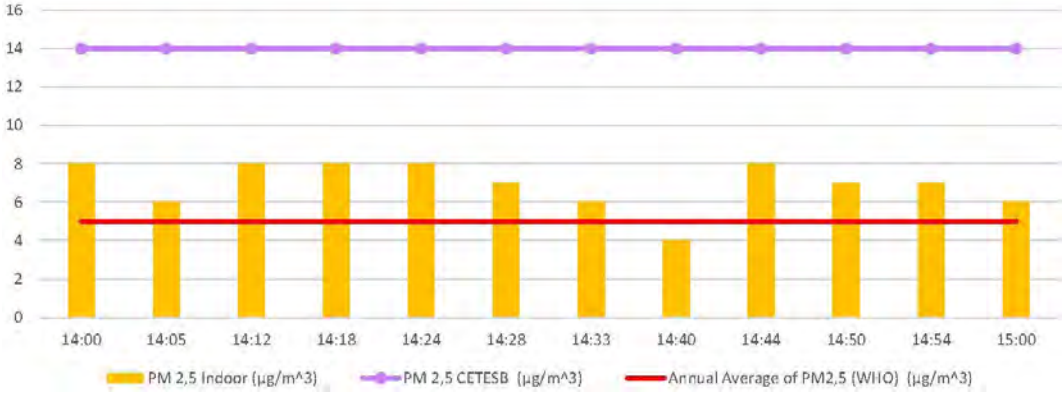

Figure 3. $PM_{2.5}$ concentration in an active classroom environment, measured every 5 minutes, compared to CETESB data.

Daily behavior of PM inside classrooms

On May 31, 2022, PM_{10} and $PM_{2.5}$ sampling and measurements were conducted at consistent 60-minute intervals, as illustrated in Figures 4 and 5, excluding the period allocated for lunch. These measurements aimed to evaluate the behavior of PM throughout a day of academic activities.

Analysis of Figure 5 reveals a significant trend at the commencement of classes, where $PM_{2.5}$ concentrations approached the WHO recommended limit for 24 hours. This increase is likely attributable to the influx of individuals into the classrooms, the movement of curtains, and the activation of fans in conjunction with the air conditioning systems. Subsequently, $PM_{2.5}$ levels decrease as students remain stationary during instructional periods. A minimum concentration was observed at 10:00 a.m., corresponding with the recess period, after which $PM_{2.5}$ levels rise again due to the re-entry of students into the classrooms.

This pattern is consistently observed during the afternoon session, external classroom measurements exhibit similar trends to the internal measurements, with internal values remaining near the WHO recommended limits for 24 hours, which may adversely affect teaching activities. Internal PM_{10} concentrations, as shown in Figure 4, follow a pattern analogous to $PM_{2.5}$, with concentrations decreasing between 6:00 a.m. and 11:00 a.m., reaching a minimum at 9:00 a.m., and decreasing again after 5:00 p.m. External $PM_{2.5}$ measurements occasionally exceeded CETESB values between 8:00 a.m. and 3:00 p.m.

This observed behavior is likely a consequence of vehicular traffic both within the campus (parking lot) and on adjacent public roads, as well as intra-campus activities performed by general services. However, $PM_{2.5}$ concentrations decrease relative to CETESB data from 4:00 p.m. to 6:00 p.m., coinciding with the cessation of general services activities. In contrast, external PM_{10} concentrations generally parallel CETESB data, except during the period from 12:00 p.m. to 2:00 p.m., when local measurements exceed CETESB values due to increased traffic of cars and motorcycles in the parking area and public roads.

Overall, the data indicate that PM levels inside and outside the classrooms are influenced by both internal campus activities and external traffic patterns. The proximity of internal $PM_{2.5}$ measurements to WHO limits underscores the necessity for effective air quality management strategies to maintain a conducive learning environment.

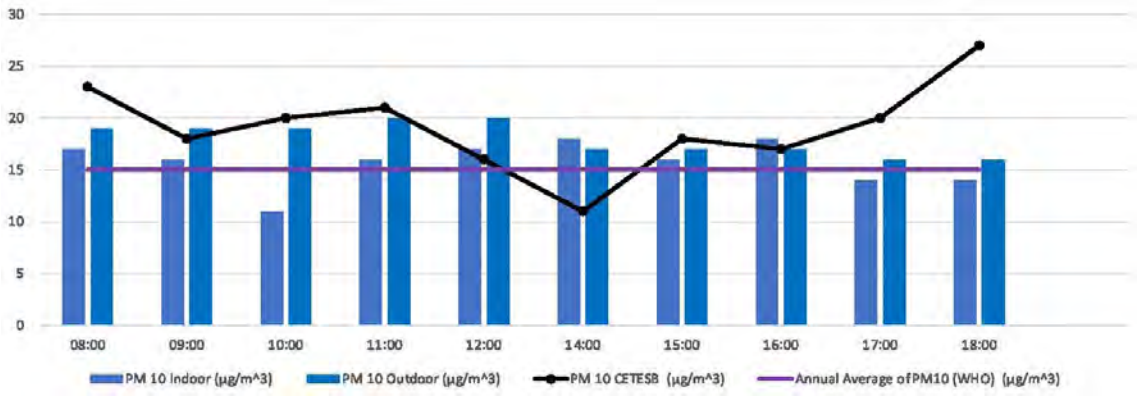

Figure 4. Concentration of PM_{10} measurements (Indoor/Outdoor) obtained at 60-minute intervals, compared with CETESB values on 2022-05-31.

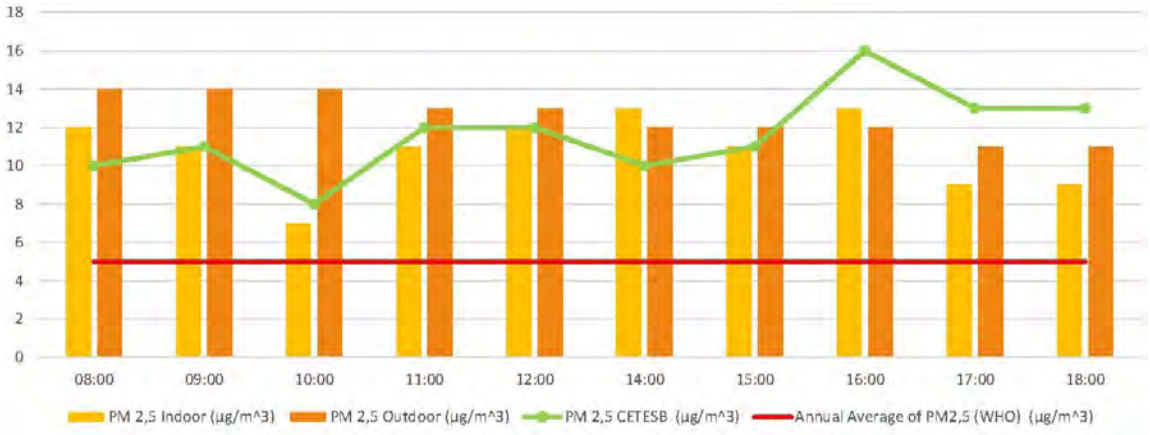

Figure 5. Concentration of $PM_{2.5}$ measurements (Indoor/Outdoor) obtained at 60-minute intervals, compared with CETESB values on 2022-05-31.

Yearly behavior of PM inside classrooms

Throughout 2022, systematic sampling and measurements of PM_{10} and $PM_{2.5}$ concentrations were conducted both inside and outside the classrooms. The results over the course of the year are presented in Figures 6 and 7, which illustrate the temporal evolution of PM concentrations during 2022. The data show that, for the most part, PM_{10} and $PM_{2.5}$ concentrations, both indoors and outdoors, remained well above the WHO's recommended thresholds of 15 µg m^{-3} and 5 µg m^{-3}, respectively. Furthermore, it is evident that the data from CETESB and the measurements taken inside the classrooms follow a similar pattern.

Exceptions to this trend are highlighted in orange rectangles in Figures 6 and 7. These anomalies are likely due to sporadic rainfall during the second semester, which led to periods of higher humidity and warmer conditions, resulting in atypical concentration levels during the study period.

The outliers observed at the end of the year, specifically on 2022-11-28 and 2022-12-12, were traced back to specific events. These included maintenance activities near the classrooms, such as grass cutting and sweeping with specialized equipment and manual blowers, as well as the release of chalk dust from careless eraser cleaning within the classroom environment.

Regarding CETESB's monitoring during the same period, several intense peaks in PM_{10} and $PM_{2.5}$ were recorded, all exceeding WHO guidelines. These discrepancies between the study's findings and CETESB's data can be explained by the geographical location of the CETESB station, which is near a busy highway. The increased vehicular traffic and lack of adequate tree cover likely contributed to these peaks.

Notably, during the first semester, the PM_{10} and $PM_{2.5}$ concentrations recorded by CETESB were significantly higher than those observed in the classrooms. Conversely, in the second semester, this trend reversed. This inversion may be attributed to temperature variations, as May to July are characterized by colder temperatures, with chilly mornings and evenings. The presence of trees, as previously mentioned, helps reduce temperature and acts as a barrier to PM, contributing to lower PM concentrations in the atmosphere.

As observed in Figures 6 and 7, there are some data gaps in CETESB's records. These gaps are due to maintenance issues in CETESB's data collection and measurement systems, which prevented the availability of PM_{10} and $PM_{2.5}$ data for certain days.

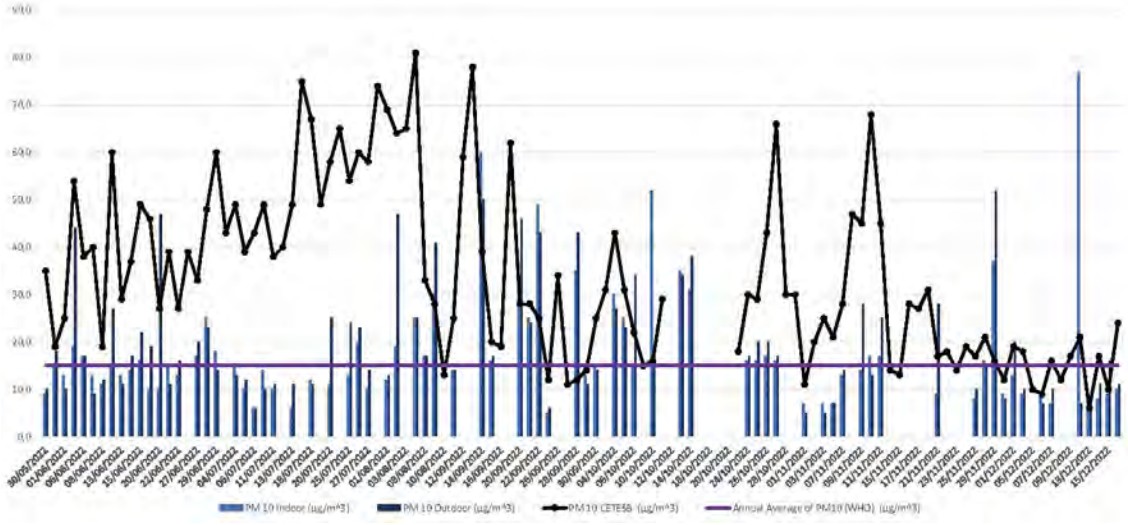

Figure 6. Average concentrations of PM_{10} for the year 2022, both outside and inside classrooms, compared with CETESB data.

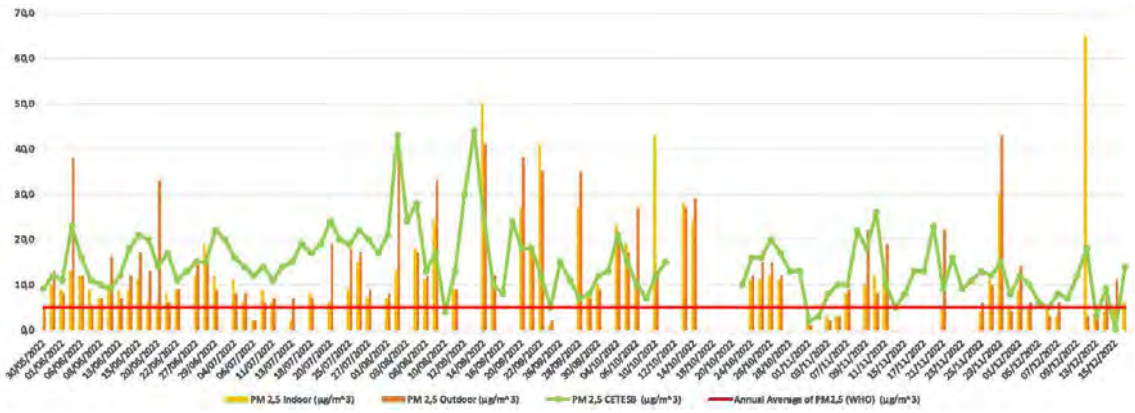

Figure 7. Average concentrations of $PM_{2.5}$ for the year 2022, both outside and inside classrooms, compared with CETESB data.

The annual data collected in this study, along with the measurements provided by CETESB's monitoring station, analyzed using a paired-sample *t*-test (df = 72, α = 0.05, two-tailed; *t* critical = ±1.99) to assess statistical differences in $PM_{2.5}$ and PM_{10} concentrations, the summarized results are in Table II.

The results indicate that $PM_{2.5}$ levels measured indoors were slightly lower than those recorded by CETESB, but this difference did not exceed the critical threshold and was therefore not statistically significant. Similarly, outdoor $PM_{2.5}$ concentrations were comparable to those reported by CETESB, with no significant differences observed. Furthermore, a direct comparison between indoor and outdoor $PM_{2.5}$ concentrations revealed no significant differences, suggesting that the levels in both environments were statistically similar, which can be explained because most of the indoor pollution in a classroom can be attributed to outdoor pollution that was brought inside by the students. Pearson correlation analysis showed moderate positive correlations for $PM_{2.5}$ between CETESB and UNESP Outdoor (r = 0.44) and between Indoor and Outdoor concentrations (r = 0.49), while the correlation between CETESB and Indoor was weaker (r = 0.29). This indicates that outdoor levels were more strongly associated with both CETESB measurements and indoor classroom concentrations, reinforcing the role of outdoor air as the main source of indoor $PM_{2.5}$ pollution.

In contrast, the analysis of PM_{10} concentrations revealed a more pronounced disparity. Indoor PM_{10} levels were significantly lower than those measured by CETESB. Likewise, outdoor PM_{10} concentrations were also significantly lower than CETESB's reported values, with very small *p*-values ($p < 0.001$), confirming that the differences were statistically significant. However, the comparison between indoor and outdoor PM_{10} levels showed no significant differences, indicating that the distribution of PM_{10} was similar in both environments. Pearson correlation analysis for PM_{10} showed weak or no correlation between CETESB and UNESP measurements ($r \approx 0$), but a moderate positive correlation was observed between Indoor and Outdoor levels (r = 0.48). This suggests that, while CETESB's PM_{10} dynamics were influenced by localized sources near the monitoring station, indoor and outdoor conditions at UNESP followed a more similar pattern.

These findings underscore a clear discrepancy in PM_{10} levels between the UNESP-Ibilce site and CETESB's monitoring station. The significantly higher PM_{10} levels reported by CETESB are likely attributable to its proximity to a major highway, which contributes to elevated emissions of PM in the 2.5–4 µm range.[34] This contrasts with the conditions at UNESP-Ibilce, where the absence of such localized sources of pollution results in significantly lower PM_{10} concentrations.

Table II. *t*-test (one-way factor) and Pearson test for PM from CETESB compared with annual indoor and outdoor PM measurements

Parameter	$PM_{2.5}$	PM_{10}
UNESP Indoor mean (μg m^{-3})	12.11	17.20
UNESP Outdoor mean (μg m^{-3})	13.77	19.22
CETESB mean (μg m^{-3})	14.34	34.22
t-Statistic CETESB-UNESP Indoor	-1.70	-6.69
t-Statistic CETESB-UNESP Outdoor	-0.51	-6.46
t-Statistic UNESP Outdoor-Indoor	-1.30	-1.38
Two-tailed *p*-value CETESB-UNESP Indoor	0.09	
Two-tailed *p*-value CETESB-UNESP Outdoor	0.61	
Two-tailed *p*-value UNESP Outdoor-Indoor	0.20	0.17
Pearson Test CETESB-UNESP Indoor	0.29	0.14
Pearson Test CETESB-UNESP Outdoor	0.44	-0.01
Pearson Test UNESP Outdoor-Indoor	0.49	0.48

All tests used a paired design with df = 72 (*t* Critical two-tail = ±1.99).

HYSPLIT of the dispersion on three different heights

HYSPLIT simulations were conducted on days with observed peaks in PM_{10} and/or $PM_{2.5}$ concentrations, as well as on days with minimal concentrations. Figures 8A through 8G capture the air masses that reached UNESP-Ibilce during peak moments at three different altitudes: 500 m, 1500 m, and 3000 m above sea level. All of these days were characterized by air masses passing through the states of Tocantins, Pará, Mato Grosso, Goiás, or a combination of these regions, where significant wildfires occurred (as shown in Figure 9). This allows us to infer those wildfires in central and northern Brazil led to a substantial increase in PM_{10} and $PM_{2.5}$ concentrations in the classrooms.

In Figure 8H, a PM peak was observed even in the absence of air masses from polluted areas, which can likely be attributed to local issues. During this period, leaf blowers were used in front of the classrooms. Conversely, in Figure 8I, from December 12, 2022, the peak of PM concentration was caused by classroom activities, in this case was the cleaning of an eraser inside the classroom.

Figures 8J through 8L illustrate the days with minimal particulate concentrations. No air masses passed through polluted or fire-affected areas during these times, and the classrooms had been cleaned in the preceding days.

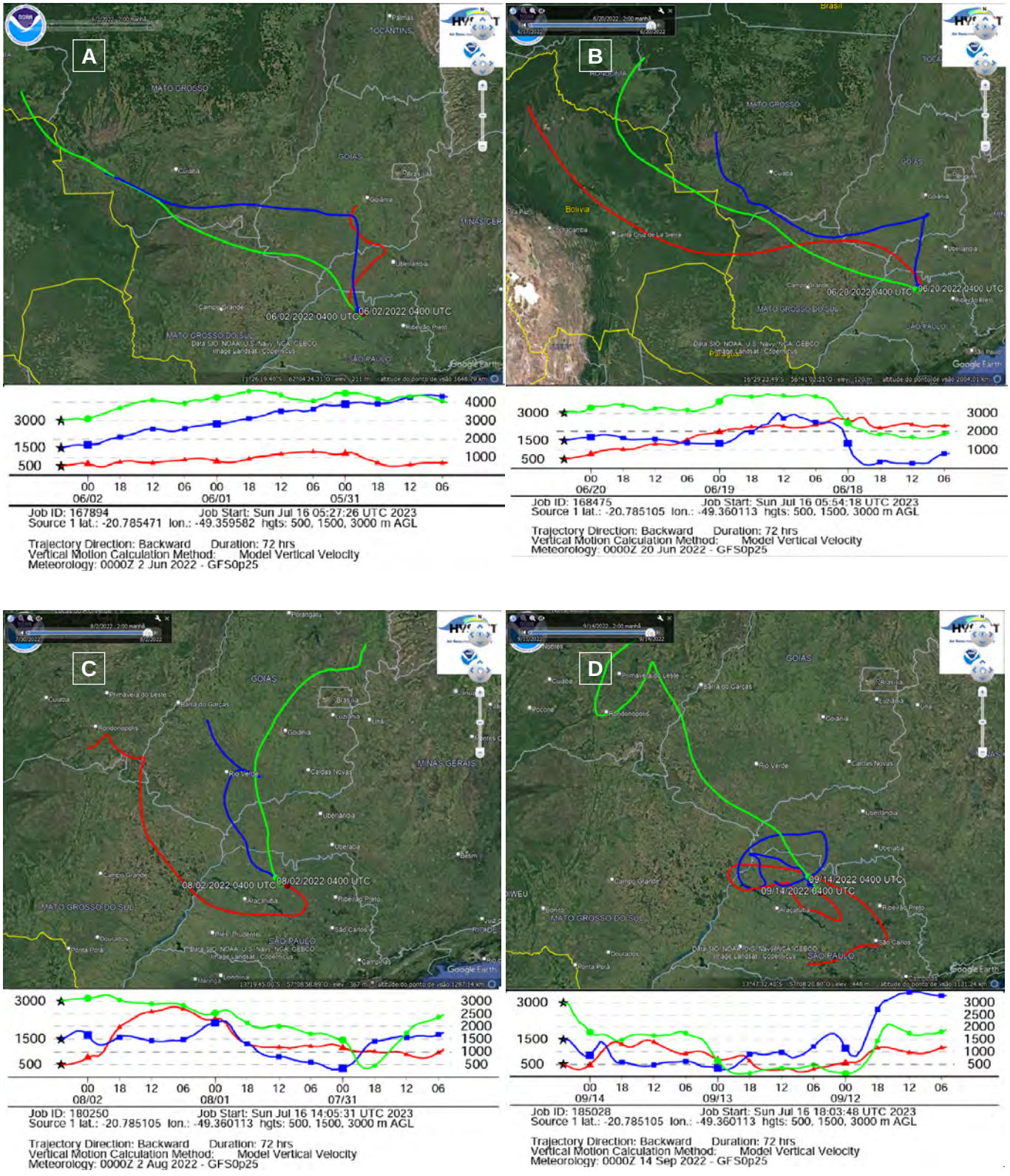

Figure 8. (A) Hysplit air dispersion on 2022-06-02 peak of PM_{10} and $PM_{2.5}$. (B) Hysplit air dispersion on 2022-06-20 peak of PM_{10} and $PM_{2.5}$. (C) Hysplit air dispersion on 2022-08-02 peak of PM_{10} and $PM_{2.5}$. (D) Hysplit air dispersion on 2022-09-14 peak of PM_{10} and $PM_{2.5}$. (continued on next page)

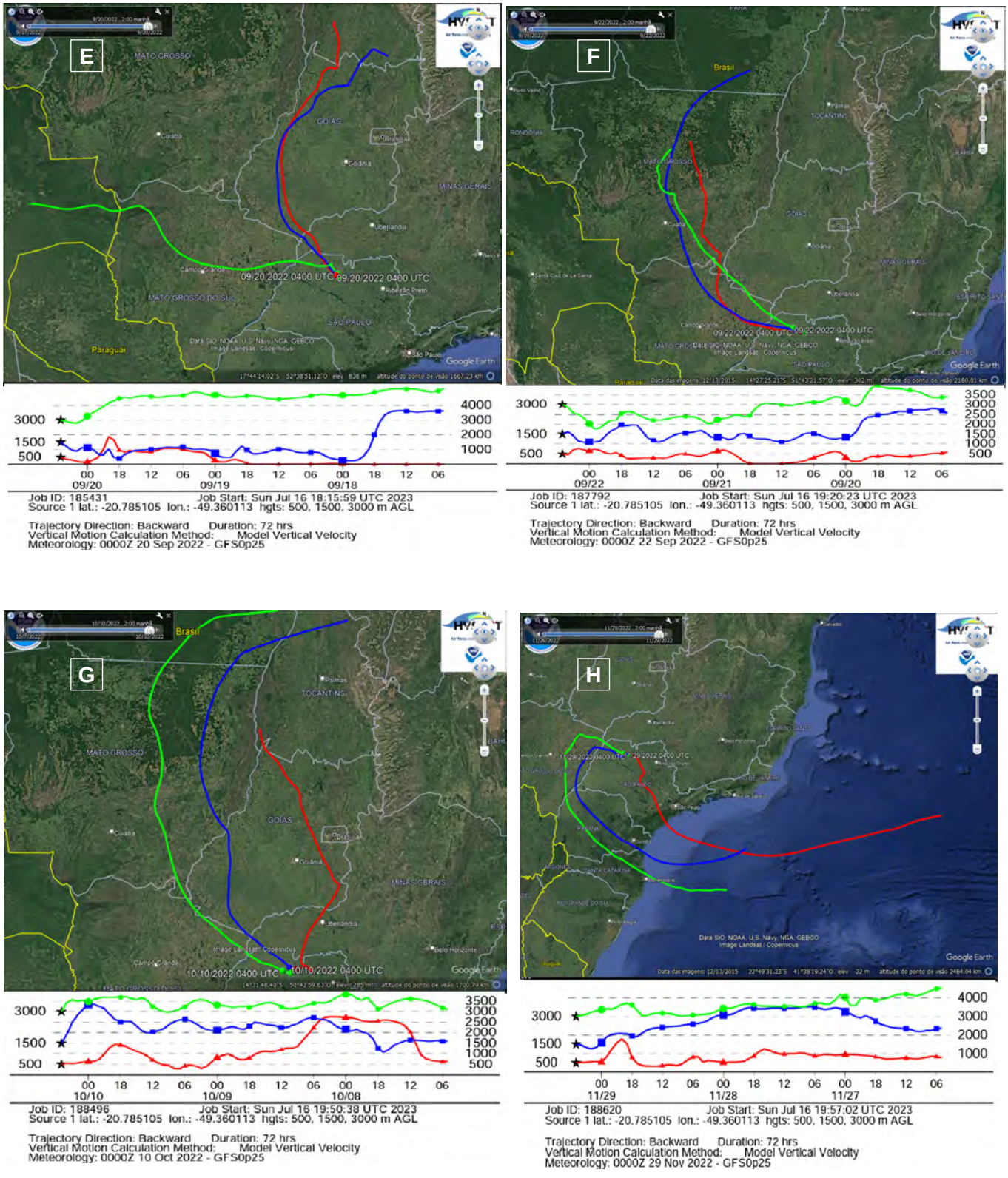

Figure 8 cont. (E) Hysplit air dispersion on 2022-09-20 peak of PM_{10} and $PM_{2.5}$. (F) Hysplit air dispersion on 2022-09-22 peak of PM_{10} and $PM_{2.5}$. (G) Hysplit air dispersion on 2022-10-10 peak of PM_{10} and $PM_{2.5}$. (H) Hysplit air dispersion on 2022-11-29 peak of PM_{10} and $PM_{2.5}$ indoors due to local factors. (continued on next page)

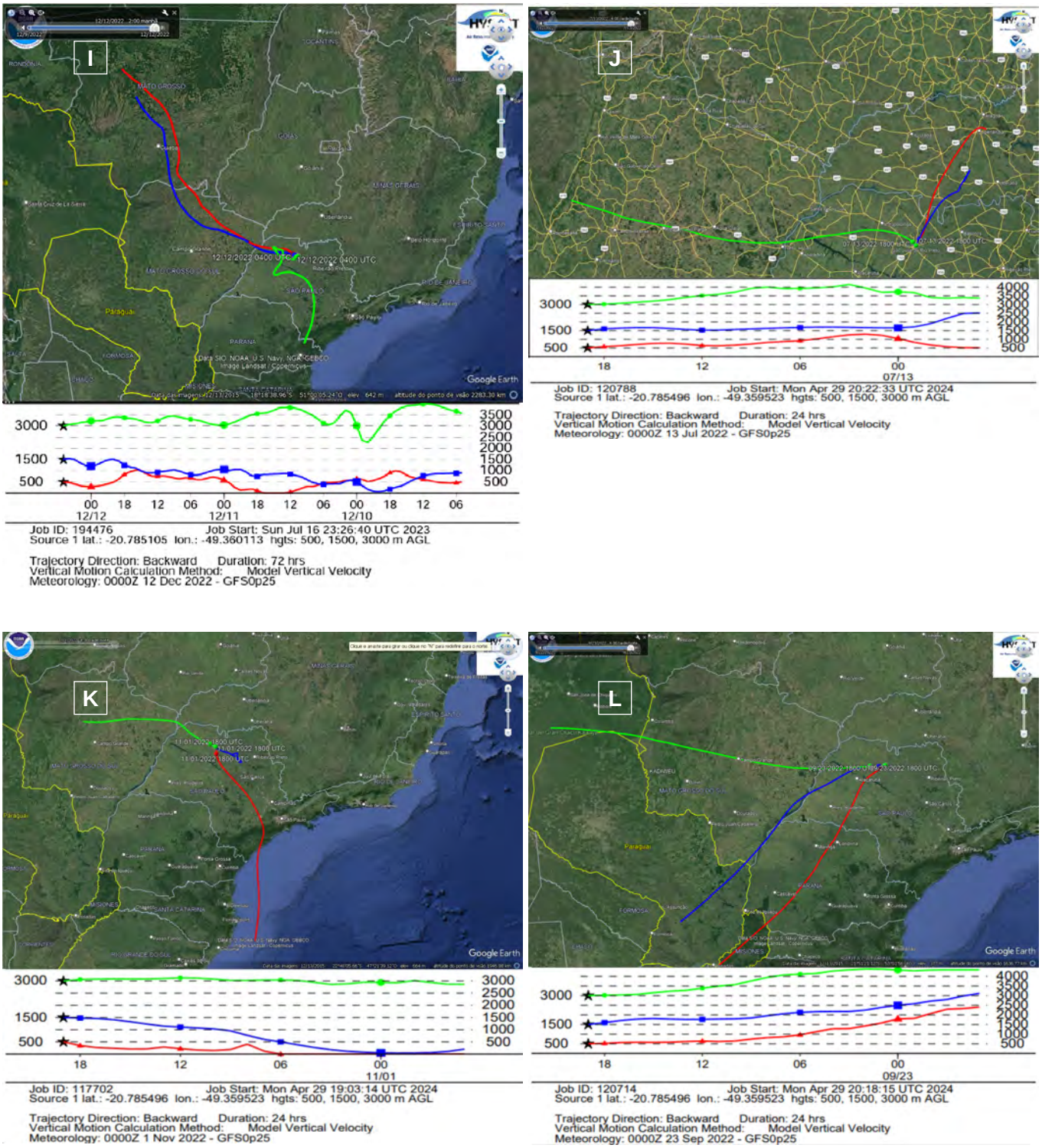

Figure 8 cont. (I) Hysplit air dispersion on 2022-12-12 peak of PM_{10} and $PM_{2.5}$ indoors due to local factors. (J) Hysplit air dispersion on2022-07-13 minimum of PM_{10} and $PM_{2.5}$. (K) Hysplit air dispersion on 2022-11-01 minimum of PM_{10} and $PM_{2.5}$. (L) Hysplit air dispersion on 2022-11-23 minimum of PM_{10} and $PM_{2.5}$.

Figure 9. Map of Central Brazil with fire locations represented by dots from "Projeto MapBiomas – Coleção monitor do fogo" (2022).

All products, methods and tools of the MapBiomas Project are open access, transparent and publicly available in the internet (https://mapbiomas.org/) for non-commercial use.

Toxicological analysis

The health risk assessment indicated that the average daily dose (ADD) associated with a four-year exposure period only in the university environment is as in Table III when considering a mean $PM_{2.5}$ concentration of 12.5 μg m^{-3} and a PM_{10} concentration of 17.2 μg m^{-3} respectively.

Based on these values, the hazard quotient (HQ) was almost exceeding the reference threshold of 1 with only the 8 hours at the university. This finding suggests that continuous exposure to $PM_{2.5}$ at this level is when looking at the hole day could associate with potential non-carcinogenic health effects, such as respiratory and cardiovascular impairments, consistent with the health risk criteria established by the WHO and the EPA.

Regarding carcinogenic risk, the excess lifetime cancer risk (ELCR) calculated using PM_{10} literature SF value for both PM_{10} and $PM_{2.5}$ resulted in values of much lower than the commonly accepted risk range (10^{-6} to 10^{-4}), it is important to highlight that no specific slope factor for $PM_{2.5}$ has been established in official databases such as the EPA or WHO. Consequently, these results should be interpreted with caution, serving as an indicative rather than definitive estimate of carcinogenic risk.

Table III. Average daily dose for the exposed time for man and woman in the classroom

	ADD $PM_{2.5}$ $mg \times kg^{-1} \times day^{-1}$	ADD PM_{10} $mg \times kg^{-1} \times day^{-1}$	$HQ_{2.5}$	HQ_{10}	$ELCR_{2.5}$	$ELCR_{10}$
Male	0.0001730	0.0002353	0.593607	0.269102	3.46	4.71
Female	0.0001708	0.0002322	0.593607	0.269102	3.42	4.64

CONCLUSIONS

Upon evaluating the Figures 6 and 7 for the year 2022, it was evident that the presence of PM_{10}, both indoors and outdoors, consistently remained above the maximum value recommended by the WHO, 15 μg m^{-3}, throughout the monitoring period. These values generally aligned with the data monitored by the local CETESB station. This assessment is crucial for ensuring air quality in the indoor working environment of classrooms.

Moreover, for $PM_{2.5}$, which is significantly more harmful to human health and more resistant to physical deposition, the average value was found to be 12.5 ± 11.2 μg m^{-3} (12.5 ± 90% μg m^{-3}) inside the classrooms. This average is more than doble to the WHO's maximum recommended value of 5 μg m^{-3}. However, with a standard deviation of 90%, the levels often exceed the WHO guideline by almost 5 times the maximum, posing a potential health risk to students and faculty. Specifically, peak values for $PM_{2.5}$ were recorded at 43 μg m^{-3}, which is almost 900% higher than the WHO limit (5 μg m^{-3}). For outdoor areas, long sampling periods also revealed several intense peaks with values exceeding the WHO standard.

Therefore, even at average concentrations of 12.5 μg m^{-3} for $PM_{2.5}$ and 17.2 μg m^{-3} for PM_{10}, representative of typical university classroom conditions, prolonged exposure may pose significant health risks. The persistence of HQ values near 1 reinforces the necessity for mitigation strategies, including enhanced natural or mechanical ventilation, installation of air filtration systems, and institutional policies for continuous indoor air quality monitoring.

These findings underscore the importance of implementing policy measures, such as regular cleaning of classrooms between sessions and continual cleaning of curtains and air conditioning filters, to improve indoor air quality. This study did not monitor CO_2 levels, which can have a synergistic effect with particulates on cognitive performance in classrooms.

In conclusion, the presence of $PM_{2.5}$ and PM_{10}, both inside and outside the classroom environment, should be regarded as a significant concern. Students and faculty spend extended hours in classrooms and corridors, making air quality a critical factor for their health and well-being.

Conflicts of interest

The authors declare that they have no financial or management relationships that could be construed as a potential conflict of interest. No affiliations or funding sources, other than those explicitly acknowledged below, influenced the study design, data collection and analysis, interpretation of data, writing of the manuscript, or decision to publish.

Acknowledgements

This work was supported by "Agência UNESP de Inovação" (AUIN) – UNESP [02-2022].

REFERENCES

(1) Global Change Data Lab (England). *Our World in Data*. Number of deaths per year. 1 Jan 2025. Available at: https://ourworldindata.org/grapher/number-of-deaths-per-year (accessed July 7, 2025).

(2) World Health Organization. Ambient (outdoor) air pollution. WHO, 2022. Available at: https://www.who.int/news-room/fact-sheets/detail/ambient-(outdoor)-air-quality-and-health (accessed July 7, 2025).

(3) Alves, C. Aerossóis atmosféricos: Perspectiva histórica, fontes, processos químicos de formação e composição orgânica. *Quim. Nova* **2005**, *28* (5), 859–870. https://doi.org/10.1590/S0100-40422005000500025

(4) Querol, X.; Alastuey, A.; Viana, M.; Dall'Osto, M.; Moreno, T.; Gilardoni, S.; Pey, J.; Rodríguez, S.; Artíñano, B.; Sánchez de la Campa, A. Monitoring of PM_{10} and $PM_{2.5}$ around primary particulate anthropogenic emission sources. *Atmos. Environ.* **2001**, *35*, 845–858. https://doi.org/10.1016/S1352-2310(00)00387-3

(5) Wilson, R.; Spengler, J. D. *Particles in Our Air: Concentrations and Health Effects*. Harvard School of Public Health: Cambridge, MA, Harvard University Press, 1996.
(6) Gioda, A. Poluição Atmosférica e de Interiores: Influência Mútua e Seus Reflexos na Saúde. Doctoral thesis, Universidade Federal do Rio de Janeiro, Rio de Janeiro, Brazil, 2003.
(7) World Health Organization. Indoor air quality: biological contaminants. Rautavaara, 1998.
(8) Ormtstad, H.; Gaarder, P. I.; Johansen, B. V. Quantification and characterisation of suspended particulate matter in indoor air. *Sci. Total Environ.* **1997**, *193* (3), 185–196. https://doi.org/10.1016/S0048-9697(96)05337-5
(9) Sun, C. J.; Jia, H.; Zhao, J.; Zhang, W.; Duan, F.; Zhang, R. Study on size distribution of eight polycyclic aromatic hydrocarbons in airborne suspended particulates indoor and outdoor. *J. West China Univ. Med. Sci.* **1994**, *25* (4), 442–446.
(10) Vormittag, E. M. P. A.; Rodrigues, C. G.; de André, P. A.; Saldiva, P. H. N. Assessment and Valuation of Public Health Impacts from Gradual Biodiesel Implementation in the Transport Energy Matrix in Brazil. *Aerosol Air Qual. Res.* **2018**, *18*, 2375–2382. https://doi.org/10.4209/aaqr.2017.11.0449
(11) Pope, III, C. A.; Burnett, R. T.; Thurston, G. D.; Thun, M. J.; Calle, E. E.; Krewski, D.; Godleski, J. J. Cardiovascular mortality and longterm exposure to particulate air pollution: Epidemiological evidence of general pathophysiological pathways of disease. *Circulation* **2004**, *109*, 71–77. https://doi.org/10.1161/01.CIR.0000108927.80044.7F
(12) Miller, K. A.; Siscovick, D. S.; Sheppard, L.; Shepherd, K.; Sullivan, J. H.; Anderson, G. L.; Kaufman, J. D. Long-term exposure to air pollution and incidence of cardiovascular events in women. *N. Engl. J. Med.* **2007**, *356*, 447–458. https://doi.org/10.1056/NEJMoa054409
(13) Wang, J.; Li, R.; Li, G.; Meng, L.; Wu, D.; Wang, C.; Li, Z.; Yuan, Z.; Zhao, X.; Hou, Y. Urban particulate matter triggers lung inflammation via the ROS-MAPK-NF-κB signaling pathway. *J. Thorac. Dis.* **2017**, *9* (11), 4398–4412. https://doi.org/10.21037/jtd.2017.09.135
(14) Cançado, J. E. D.; Saldiva, P. H. N.; Pereira, L. A. A.; Lara, L. B. L. S.; Artaxo, P.; Martinelli, L. A.; Arbex, M. A.; Zanobetti, A.; Braga, A. L. F. The impact of sugar cane-burning emissions on the respiratory system of children and the elderly. *Environ. Health Perspect.* **2006**, *114* (5), 725–729.
(15) Hamra, G. B.; Guha, N.; Cohen, A.; Laden, F.; Raaschou-Nielsen, O.; Samet, J. M.; Vineis, P.; Forastiere, F.; Saldiva, P.; Yorifuji, T.; Loomis, D. Outdoor Particulate Matter Exposure and Lung Cancer: A Systematic Review and Meta-Analysis. *Environ. Health Perspect.* **2014**, *122* (9), 906–912.
(16) Bowe, B.; Xie, Y.; Li, T.; Yan, Y.; Xian, H.; Al-Aly, Z. The 2016 global and national burden of diabetes mellitus attributable to $PM_{2.5}$ air pollution. *Lancet Planet Health* **2018**, *2* (7), E301–E312.
(17) Riant, M.; Meirhaeghe, A.; Giovannelli, J.; Occelli, F.; Havet, A.; Cuny, D.; Amouyel, P.; Dauchet, L. Associations between long-term exposure to air pollution, glycosylated hemoglobin, fasting blood glucose and diabetes mellitus in northern France. *Environ. Int.* **2018**, *120*, 121–129. https://doi.org/10.1016/j.envint.2018.07.034
(18) Zhang, X.; Chen, X.; Zhang, X. The impact of exposure to air pollution on cognitive performance. *Proc. Natl. Acad. Sci. U.S.A.* **2019**, *115* (37), 9193–9197. https://doi.org/10.1073/pnas.1809474115
(19) Romero, M. T. B.; Dudzinska, M. R.; Torkmahalleh, M. A.; Barros, N.; Coggins, A. M.; Ruzgar, D. G.; Kildsgaard, I.; Naseri, M.; Rong, L.; Saffell, J.; et al. A review of critical residential buildings parameters and activities when investigating indoor air quality and pollutants. *Indoor Air* **2022**, *32* (11), e13144. https://doi.org/10.1111/ina.13144
(20) Cheng, Z.; Lei, N.; Bu, Z.; Sun, H.; Li, B.; Lin, B. Investigations of indoor air quality for office buildings in different climate zones of China by subjective survey and field measurement. *Build. Environ.* **2022**, *214*, 108899. https://doi.org/10.1016/j.buildenv.2022.108899
(21) Committee on Health Risks of Indoor Exposures to Fine Particulate Matter and Practical Mitigation Solutions. *Health Risks of Indoor Exposure to Fine Particulate Matter and Practical Mitigation Solutions*. National Academies Press, Washington, DC, 2024.

(22) Yuan, F.; Yao, R.; Yu, W.; Sadrizadeh, S.; Awbi, H.; Kumar, P. Dynamic characteristics of particulate matter resuspension due to human activities in indoor environments: A comprehensive review. *J. Build. Eng.* **2023**, *79*, 107914. https://doi.org/10.1016/j.jobe.2023.107914
(23) Stein, A. F.; Draxler, R. R; Rolph, G. D.; Stunder, B. J. B.; Cohen, M. D.; Ngan, F. NOAA's HYSPLIT atmospheric transport and dispersion modeling system. *Bull. Amer. Meteor. Soc*. **2015**, *96*, 2059-2077, http://dx.doi.org/10.1175/BAMS-D-14-00110.1
(24) Draxler, R. R. HYSPLIT User's Guide. NOAA Tech. Memo. ERL ARL-230, NOAA Air Resources Laboratory, Silver Spring, MD, 1999.
(25) Draxler, R. R.; Hess, G. D. An overview of the HYSPLIT_4 modeling system of trajectories, dispersion, and deposition. *Aust. Met. Mag*. **1998**, *47*, 295-308.
(26) Draxler, R. R.; Hess, G. D. Description of the HYSPLIT_4 modeling system. NOAA Tech. Memo. ERL ARL-224, NOAA Air Resources Laboratory, Silver Spring, MD, 1997.
(27) U.S. Environmental Protection Agency. *Exposure Assessment Tools by Routes – Inhalation*. Available at: https://www.epa.gov/expobox/exposure-assessment-tools-routes-inhalation (accessed July 7, 2025).
(28) U.S. Environmental Protection Agency. *Exposure Factors Handbook, Chapter 6: Inhalation Rates*. Washington, DC, 2011. Available at: https://www.epa.gov/sites/default/files/2015-09/documents/efh-chapter06.pdf (accessed July 7, 2025).
(29) Centers for Disease Control and Prevention. National Center for Health Statistics. *Body Measurements*. Atlanta, GA. Last reviewed June 26, 2025. Available at: https://www.cdc.gov/nchs/fastats/body-measurements.htm (accessed July 7, 2025).
(30) Almamun, M.; Fallica, J.; Irwin, M.; Wier, E.; Wurcel, K.; Valerio Jr., L. G.; Yucesoy, B.; Rosenfeldt, H. Calculating Excess Lifetime Cancer Risk in ENDS Premarket Tobacco Product Applications; Division of Nonclinical Science, Center for Tobacco Products, U.S. Food and Drug Administration: Silver Spring, MD, June 3, 2024. Available at: https://www.fda.gov/media/180610/download (accessed July 7, 2025).
(31) Sekhavati, E.; Yengejeh, R. J. Particulate matter exposure in construction sites is associated with health effects in workers. *Frontiers in Public Health* **2023**, *11*. https://doi.org/10.3389/fpubh.2023.1130620
(32) Benson, R. W. Hazards of Food Contact Material: Phthalates. In: Motarjemi, Y. (Ed.). *Encyclopedia of Food Safety*. Academic Press: Amsterdam, Netherlands, 2014, Vol. 2, pp 438–443. https://doi.org/10.1016/B978-0-12-378612-8.00219-5
(33) U.S. Environmental Protection Agency. Reference concentration for chronic inhalation exposure (RfC). IRIS Summary. Integrated Risk Information System, 2007.
(34) Beji, A.; Deboudt, K.; Khardi, S.; Muresan, B.; Flament, P.; Fourmentin, M.; Lumière, L. Non-exhaust particle emissions under various driving conditions: Implications for sustainable mobility. *Transportation Research Part D: Transport and Environment* **2020**, *81*, 102290. https://doi.org/10.1016/j.trd.2020.102290

Brazilian Journal of Analytical Chemistry
2026, Volume 13, Issue 51, pp 54-78
doi: 10.30744/brjac.2179-3425.AR-70-2025

BrJAC

ARTICLE

Evaluation of *Calendula officinalis* Extract as a Functionalization Agent for Gold Nanoparticles

Comprehensive Multi-Technique Analytical Characterization and its use as a Dye-Sensitized Solar Cell Sensitizer

Mauricio Ávila[1]*, Hiroyuki Kinoshita[1], Pablo Fagúndez[2], María Fernanda Cerdá[1]

[1]Laboratorio de Biomateriales, Instituto de Química Biológica, Facultad de Ciencias, Universidad de la República. Iguá 4225, Anexo Norte, Piso 2, Laboratorio 205, Zip Code 11400, Montevideo, Uruguay

[2]Unidad de Bioquímica Analítica, Centro de Investigaciones Nucleares, Universidad de la República. Mataojo 2055, Zip Code 11400, Montevideo, Uruguay

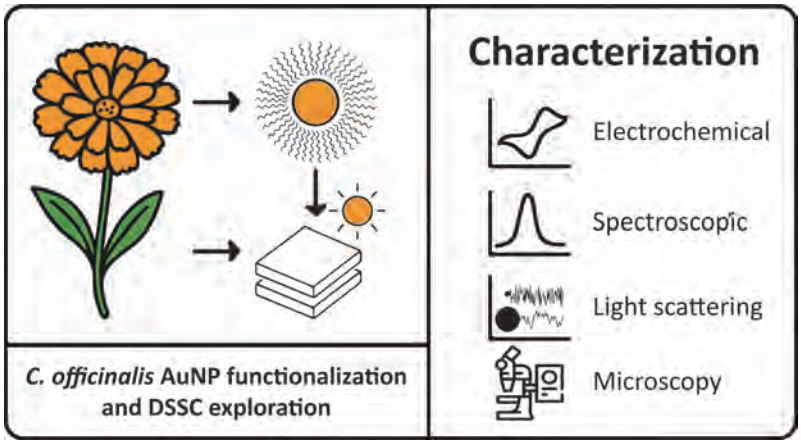

Calendula officinalis extract was evaluated as a functionalization agent for gold nanoparticles (AuNPs). The resulting nanoconjugate (AuNP-Cale) was thoroughly characterized, and explored as a sensitizer for dye-sensitized solar cells (DSSC). As a starting point, citrate-reduced AuNPs (AuNP-Cit) were synthesized and fully characterized. Comprehensive characterization for both AuNP-Cit and AuNP-Cale included dynamic light scattering (DLS), electrophoretic light scattering (ELS), colloidal and stability assay. Successful functionalization included increased hydrodynamic diameter, reduced zeta potential, and improved colloidal stability. DSSC evaluation demonstrated that while pre-formed AuNP-Cale did not enhance efficiency, improved performance was achieved when AuNP-Cit was added sequentially after the extract on the TiO_2 electrode, likely due to better electrode coverage. This result correlated with enhanced light absorption (FORS) and favorable electrochemical impedance spectroscopy parameters.

Keywords: gold nanoparticles, functionalization, spectroscopy, voltammetry, dye-sensitized solar cells

Cite: Ávila, M.; Kinoshita, H.; Fagúndez, P.; Cerdá, M. F. Evaluation of *Calendula officinalis* Extract as a Functionalization Agent for Gold Nanoparticles – *Comprehensive Multi-Technique Analytical Characterization and its use as a Dye-Sensitized Solar Cell Sensitizer*. *Braz. J. Anal. Chem.* 2026, *13* (51), pp 54-78. http://dx.doi.org/10.30744/brjac.2179-3425.AR-70-2025

Received: July 29, 2025; **Revised:** September 22, 2025; November 3, 2025; **Accepted:** November 30, 2025; **Published online:** January 2026.

This article is part of the BrJAC Special Issue on the 8th Uruguayan Congress of Analytical Chemistry (CUQA 8 2024).

INTRODUCTION

The XXI century is the time for nanotechnologies. The term “nanotechnology” was first used by the eminency of Richard P. Feynman in 1960.[1] Nanotechnology is the scientific discipline that studies, designs and applies materials, devices and systems at the nanometric scale, including particulate substances, which have at least one dimension less than 100 nm.[2] In the continued search for better and smaller devices, properties related to the use and applications of nanoparticles became relevant. Examples of nanoparticle applications are everywhere, comprising pharmaceutical,[3-5] properties modification for manufacturing materials,[6-8] environment,[9-10] electronics,[11-14] energy,[15-20] and informatics[21-23] just to name a few.

Gold nanoparticles (AuNPs) exhibit unique optical properties among the metallic nanoparticles due to localized surface plasmon resonance (LSPR), which can enhance light absorption and energy transfer in dye-sensitized solar cells (DSSC).[20,24-29]

Metallic nanoparticles, particularly AuNPs, have experienced a significant boom in scientific research since the 1990s, although their use dates back to ancient times in the coloration of glasses and ceramics.[30] Interest in AuNPs has intensified due to advances in characterization and synthesis techniques and their consequent improvement in the ability to control size, shape and surface properties.[31] In addition, the diverse applications of AuNPs are due to their exceptional optical, electronic and catalytic properties.[32]

In the field of energy and optoelectronics, they stand out for their ability to improve solar cell efficiency through the plasmonic effect,[33] which allows for increased light absorption and energy transfer. Their unique properties derive mainly from localized surface plasmon resonance (LSPR), a phenomenon resulting from the collective oscillation of free electrons at the nanoparticle surface in response to incident electromagnetic radiation.[34,35] This feature gives AuNPs their distinctive colors and makes them especially valuable in applications requiring efficient interaction with light, such as optical sensors and photovoltaic devices.[36]

Functionalizing AuNPs with different ligands can modify their surface properties, stability and interactions with other molecules in the system under evaluation.[37] In this context, the present study explores using *Calendula officinalis* extract for AuNPs derivatization.

Calendula officinalis is an annual perennial flowering plant in the family Asteraceae, native to southern Europe and cultivated worldwide for medicinal, ornamental, and culinary purposes.[38] This plant has vibrant orange-yellow daisy-like flowers with multiple layers of overlapping petals and aromatic leaves.[39] *Calendula officinalis* extracts have around 7.71% (w/w) carotenoids (mainly flavoxanthin, luteoxanthin, and lycopene, Figure 1),[39] 0.21-0.68% (w/w) of flavonoids (mainly rutin, isorhamnetin and isoquercitrin),[39-42] and xanthophylls.[43] Many of these compounds have functional groups as hydroxyl moieties, making them an attractive option for nanoparticle functionalization.

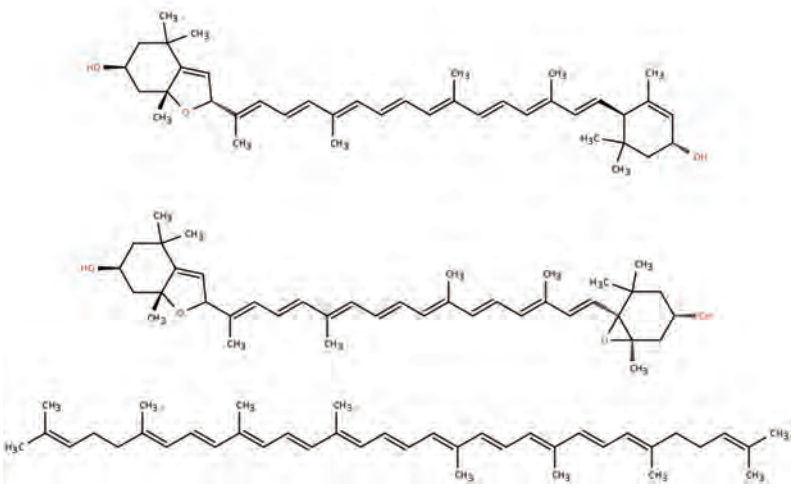

Figure 1. The three main carotenoids present in *Calendula officinalis.* From top to bottom: flavoxanthin, luteoxanthin and lycopene.

Normally, the synthesis of biogenic AuNPs is performed using the natural extract as both a reducing and capping agent. However, it is often difficult to control the shape and size of the obtained nanoparticles, since the concentration and type of reducing agent are not known with certainty, and the amount of this agent can vary from one extract to another.[44-46] In this regard, we approached the initial synthesis of AuNPs using classical, more controlled methods, which allow precise control of the Au/reducing agent molar ratio, and then proceeded with post-synthesis functionalization using calendula extract following the standard adsorption procedure described in the literature. No previous reports were found on post-synthesis functionalization of AuNPs with calendula's extract. However, there are reports of direct synthesis of gold, silver, and titanium nanoparticles from calendula extract, where stable nanoparticles are obtained, confirming the extract's ability not only to provide a reducing agent but also to contribute stabilizing molecules to the colloidal system.[47-50]

In this work we derivatize AuNPs with *Calendula officinalis* extract and exhaustively characterize the nanoconjugate AuNP-Cale. The research encompasses synthesizing and characterizing functionalized AuNPs, including comprehensive analysis through UV-Vis spectrophotometry, dynamic light scattering (DLS), electrophoretic light scattering (ELS), colloidal stability assay, transmission electron microscopy (TEM), and cyclic voltammetry studies.

To essay on a possible technological application, dye-sensitized solar cells (DSSC) performance is evaluated by incorporating AuNPs functionalized with *Calendula officinalis* extract, since the use of metal nanoparticles has been reported to increase the performance of dye-sensitized solar cells.[51] In this case, the performance of the DSSC was evaluated by measuring the current-voltage (J-V) profiles under both illumination and dark conditions, complemented by electrochemical impedance spectroscopy (EIS). To understand the performance of the assembled DSSC, spectroscopic characterization of the sensitizers was performed using reflectance spectrophotometry and Fourier transform infrared (FTIR) analyses (before and after adsorption to the semiconductor of the photoanode). This comparative study involves cells with functionalized AuNP-Cale, AuNP-Cit, and calendula's extract without nanoparticles, providing an insight into the capability of *Calendula officinalis* extract as a dye for DSSC purposes.

MATERIALS AND METHODS

Materials and chemicals

Chloroauric acid ($HAuCl_4.3H_2O$ ≥ 99.9%, CAS No. 16961-25-4), trisodium citrate dihydrate ($Na_3C_6H_5O_7.2H_2O$ ≥ 98%, CAS No. 6132-04-3), sodium chloride (NaCl ≥ 99%, CAS No. 7647-14-5), and sodium perchlorate ($NaClO_4$ ≥ 98%, CAS No. 7601-89-0), were purchased from Sigma-Aldrich. Potassium bromide (KBr, FTIR grade, CAS No. 7758-02-3) was purchased from Pike Technologies. Absolute ethanol (≥ 99.8%, CAS No. 64-17-5) and heptane (≥ 99%, CAS No. 142-82-5) were obtained from Dorwil, Química Analítica. Ultrapure water (resistivity > 18.2 MΩ·cm, Millipore Milli-Q®) was used throughout. DSSC components (FTO/TiO_2 electrodes, Pt counter electrodes, Iodolyte AN-50 electrolyte) were purchased from Solaronix. All chemicals were used as received without further purification.

Calendula officinalis dyes extraction

The *Calendula officinalis* flowers were collected from the "Universidad de la República, Facultad de Ciencias", orchard at the beginning of October 2024 (southern hemisphere's spring).

Petals from 20 flowers were collected, chopped, and mortared with absolute ethanol. Samples were ultrasounded for 15 minutes, vortexed, and centrifuged for 15 minutes at 5000 rpm, preserving the supernatant. After extracting the supernatant, the same procedure was done from the pellet. Two extractions were obtained; the first (denoted 1E) was the extraction without resuspension, and the second (denoted 2E) was the extraction plus the resuspension.

Samples were withdrawn, and heptane-ethanol phase separation was performed to eliminate chlorophyll. The remaining ethanolic phase did not significantly differ from the fraction before the phase separation, so for practical purposes, extraction 2E without heptane purification was used.

AuNP-Cit synthesis

The glassware used in the synthesis and storage of AuNPs was previously treated with an aqua regia solution (HCl:HNO_3 3:1 (v/v)) for 30 min, subsequently rinsed with abundant ultrapure water (resistivity > 18.2 MΩ.cm) and dried in an oven at 60 °C prior to use. The synthesis of AuNPs was carried out according to the traditional Turkevich method with modifications. Briefly, 50 mL of ultrapure water and 1 mL of a 20 g L^{-1} chloroauric acid solution (≈ 50 µmol) were placed in a two-neck round-bottom flask, and the system was completed with a water condenser. The solution was heated to boiling and 5 mL of 38.8 mM sodium citrate solution was immediately added. The solution was continued to be heated under reflux until the appearance of an intense red-burgundy color and maintained for an additional 10 min. The AuNP-cit solution was allowed to cool for 24 h in the dark before characterization.[52-55]

AuNP-Calendula officinalis extract derivatization

For derivatization, the citrate-reduced gold nanoparticles (AuNP-Cit) were obtained by the Turkevich method.[56] After that, the AuNP-Cit were incubated overnight in the presence of the *Calendula officinalis* extract using a 9:1 (v:v) AuNP-Cit:Cale proportion.

UV-Vis absorption spectrophotometry

The UV-Vis spectra were acquired with an Analytic-Jena SPECORD 200 Plus spectrophotometer only in the range from 350 to 700 nm, using the optical path b = 1 cm. Spectrometer increments were set at 0.05 nm.

Dynamic light scattering

Dynamic light scattering was performed to determine the average hydrodynamic diameter (d_h) of both AuNP-Cit and AuNP-Cale using the Brookhaven ZetaPlus 90 instrument equipped with a 659 nm laser and a correlator. DLS measurements were conducted at a fixed angle of 90 degrees in 1 cm polystyrene cuvettes following ISO 22412 guidelines.[57]

Transmission electron microscopy

AuNP-Cit's diluted colloidal solutions (10 µL, 1:10 in water) were drop-casted to a carbon-coated copper grid and air-dried at room temperature. TEM images were captured using a JEOL JEM 1010 microscope at an acceleration voltage of 80 kV. The diameters (d_{TEM}) of over 200 individual AuNPs were determined from 10 micrographs using FIJI software,[58] following the previously established guidelines.[59,60]

Electrophoretic light scattering

Electrophoretic light scattering was performed to determine the zeta potential (ζ-potential) of the AuNPs with the same equipment and configuration as DLS. Additionally, a fixed angle of 15° was used with a surface zeta potential (SZP) electrode system consisting of two parallel palladium electrodes. All measurements were performed at 25 °C using a 1 nM AuNP solution in 1 mM NaCl. The data (n = 6) was analyzed using Particle Solution v. 2.5 software, applying CONTIN and Smoluchowski algorithms for hydrodynamic diameter and ζ-potential calculations, respectively.

Colloidal stability assay

Colloidal stability was determined using a simplified, rapid screening version of the colloidal stability titration assay with a Tekan Infinite F50 microplate reader adapted from the methodology described in the literature[61] and detailed in our previous work.[56]

In a 96-well microplate, 100 µL of the AuNP-Cit or AuNP-Cale was added. To each well, 100 µL of a 20 to 300 mM sodium chloride (NaCl) solution (NaCl final concentration 10 to 150 mM) was added. After mixing, absorbance was measured at 520 nm and 650 nm.[56] All measurements were duplicated. The Boltzmann sigmoidal equation's inflexion point on the curve determined the critical concentration. Boltzmann sigmoidal fitting was performed using the Levenberg-Marquart iteration algorithm.

Infrared spectroscopy

Infrared spectra were collected in the 400-3000 cm^{-1} range at ambient temperature using a Shimadzu IR-Prestige 21 spectrometer. Each spectrum represented an average of 10 scans with 2 cm^{-1} resolution. Sample preparation involved thoroughly mixing dried samples with KBr powder in an agate mortar, followed by forming 13-mm discs using a Pike Crush IR press at 10 tons of pressure. For comparative purposes, the following samples were analyzed: Cale, AuNP-Cit, AuNP-Cale, and these three samples after being deposited onto TiO_2 electrodes (TiO_2:Cale, TiO_2:AuNP-Cit, and TiO_2:AuNP-Cale). For the TiO_2-deposited samples, the same procedure was followed as previously described, where the electrode surface was scraped off after the adsorption period, mixed with KBr, and pressed into discs.

Cyclic voltammetry

All reagents were used as received from commercial sources without further purification. The voltammetric profiles were conducted using a Metrohm μStat-i 400 s Potentiostat in a one-compartment conic cell three-electrode system. Since EtOH was the extraction media, samples were measured in mixtures EtOH:supporting electrolyte (0.1 M sodium perchlorate $NaClO_4$ in high-purity MilliQ® water 18.2 MΩ.cm) in a proportion 1:1 (v:v). Evaluations were then performed using 1 mM of the analyte in the described mixture of solvents. The working electrode (W) was FTO/TiO_2 (FTO = Fluorine-doped Tin Oxide; TiO_2 = mesoporous titanium dioxide), and the auxiliary electrode (A) was made of Pt-*pc* (*pc* = polycrystalline). The reference electrode (R) was the silver/silver chloride (Ag/AgCl; E = 0.2586 V *vs.* NHE). All measurements were performed at a scan rate of 50 mV s^{-1}.

Dye sensitized solar-cell built-up and evaluation

Photoanodes were prepared by immersion of the FTO/TiO_2 (SOLARONIX test kit, active area of mesoporous TiO_2 0.36 cm^2) electrodes overnight into the dye's containing solution and then rinsed thoroughly with ethanol. Before use, the FTO/TiO_2 electrode was heated at 500 ºC for 30 minutes. A sandwich configuration was used, with the FTO/TiO_2 photoanode placed parallel to the FTO/Pt counter (20 mm x 20 mm sized, screen printed with SOLARONIX's Pt Platinum Catalyst). The cell was then completed by the addition of a liquid electrolyte (SOLARONIX Iodolyte AN-50). Different sensitizers were applied: Cale, AuNP-Cit, AuNP-Cale and Cale co-sensitized with AuNP following a sequential path.

To characterize the DSSC, the current density *vs.* voltage (J-V) profiles were measured using a CHI 604E potentiostat at a potential scan rate (*v*) of 0.05 V s^{-1} at room temperature, in the dark and using a solar simulator from ABET Technologies (100 mW cm^{-2}, 1.5 AM). Complementary data were assessed from the electrochemical impedance spectroscopy (EIS) results, performed between 0 and 0.5 V and within the frequency range of 0.1 Hz to 3 MHz (in the dark).

Fiber optic reflectance spectroscopy

Fiber optic reflectance spectroscopy (FORS) was employed to verify the incorporation of AuNP-Cale, AuNP-Cit and Cale within the TiO_2 matrix. Average reflectance measurements of 500 spectra were conducted using a UV-Vis SPELEC (200-900 nm) instrument (DROPSENS) equipped with a fiber optic probe. FTO/TiO_2 electrodes were immersed overnight with the corresponding solution. Prior to spectroscopic analysis in the 350–850 nm wavelength range, the electrodes were thoroughly rinsed with ethanol to remove any unbound components. This technique allowed for non-destructive confirmation of the adsorption onto the TiO_2 surface.

RESULTS AND DISCUSSION

Synthesis and characterization of functionalized gold nanoparticles

Calendula officinalis dyes extraction

After the extraction of *C. officinalis*, UV-Vis spectra were performed, and serial dilutions were performed until the absorbances measured were above 1 UA to calculate carotenoid concentration in the extract, according to the extinction coefficient estimation by Britton et al. 2004 (Figure 2).[62]

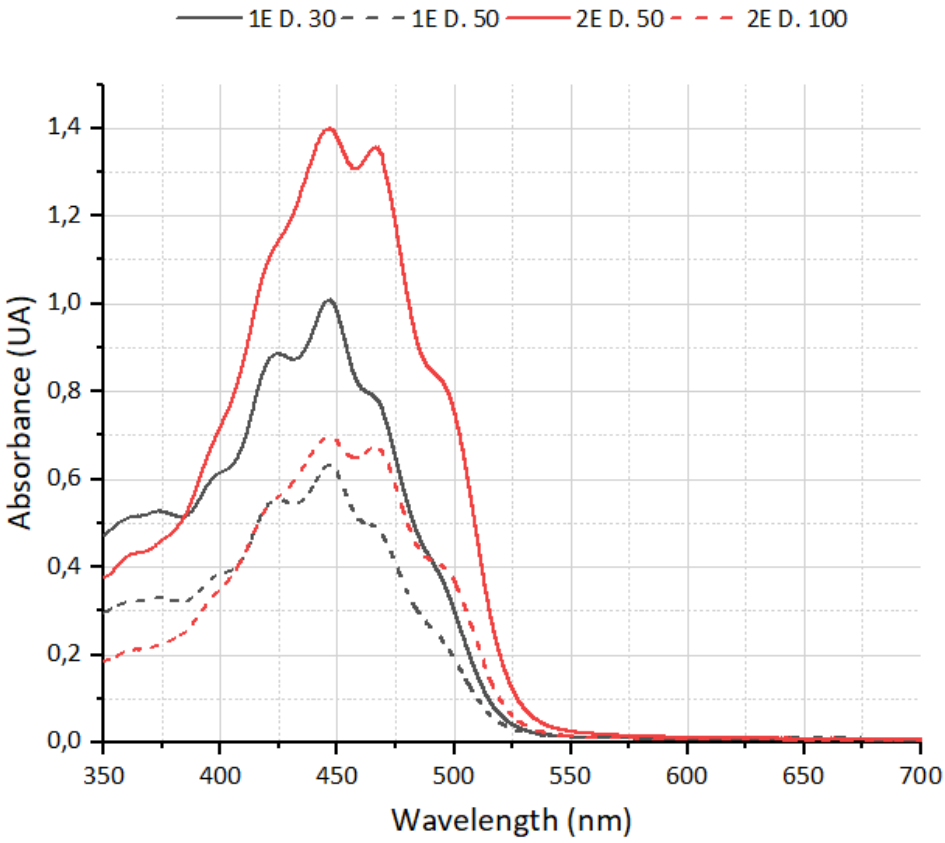

Figure 2. UV-Vis spectra of solutions containing the extracts from *Calendula officinalis*. Black lines correspond to the first extraction (in legend denoted 1E), while red lines correspond to the second extraction (in legend denoted 2E). The dilution factor for each spectrum is shown in the legend above. Being the most diluted fraction drawn in dashed lines.

Based on the extinction coefficients calculated following Britton et al. (2004)[62] and absorbance measurements at the characteristic carotenoid maximum (447 nm), the total carotenoid concentrations were determined to be 0.196 ± 0.006 mM for the first extraction (1E) and 0.442 ± 0.002 mM for the second extraction (2E). Due to its higher concentration and comparable spectral profile, extraction 2E was selected for all subsequent functionalization experiments (see calculations in the Supplementary Material).

Citrate-reduced gold nanoparticles characterization

Prior to functionalization with *Calendula officinalis* extract, the citrate-stabilized gold nanoparticles (AuNP-Cit) were thoroughly characterized. UV-Vis spectroscopy revealed a characteristic localized surface plasmon resonance (LSPR) peak at 520 nm (Figure SM-1). Transmission electron microscopy (TEM) analysis demonstrated that the synthesized AuNP-Cit exhibited a predominantly spherical morphology with an average diameter of d_{TEM} = (16 ± 3) nm (Figure 7). Dynamic light scattering (DLS) measurements indicated a hydrodynamic diameter of d_h = (19 ± 3) nm with a polydispersity index (PDI) of 0.23 ± 0.03 (Figure SM-2). The zeta potential value of (-52 ± 2) mV confirmed the presence of negatively charged citrate ions on the nanoparticle surface, providing electrostatic stabilization and preventing aggregation in aqueous solution. These baseline characteristics of AuNP-Cit serve as a reference point for evaluating the subsequent modifications introduced by *Calendula officinalis* extract functionalization. Similar results were obtained by Méndez et al.[55] and Fagúndez et al.[56]

AuNP-Cit:EtOH ratio optimization

As stated, *Calendula officinalis* dyes were extracted using ethanol. Since EtOH is less polar than water, it alters the colloidal stability of AuNP-Cit by shielding the charge between citrate molecules. Also, the presence of EtOH reduces the dielectric constant in the media, which, in turn, lowers the repulsion between AuNP-Cit. In sum, these effects tend to aggregate AuNP-Cit particles, so prior to the AuNP-Cale derivatization, the AuNP-Cit aqueous solution to EtOH relation was optimized by diluting AuNP-Cit in EtOH, and UV-Vis spectra were recorded (Figure SM-3).

It is clear from Figure SM-3 that AuNPs aggregate when the proportion of AuNP-Cit to EtOH is greater than 1:4. This is concluded based on the position of the localized surface plasmon resonance (LSPR), which has its maxima near 520 nm when AuNPs are not aggregated, and bathochromic shifts due to plasmonic coupling towards 620 nm when AuNPs aggregate. That is, higher AuNP-Cit to EtOH proportions diminish its absorbance at 520 nm and increase the absorbance at 620 nm, suggesting a shift of AuNPs from a non-aggregated to an aggregated state. In the case of 1:4 proportion, this mixture was borderline aggregation, so for conservative reasons 1:9 was the proportion against EtOH chosen for further analysis.

UV-Vis absorption spectrophotometry and LSPR position

Once the optimal AuNP-Cit with *Calendula officinalis* extract relation was determined, a fast procedure for AuNP-Cit derivatization with calendula extract confirmation was established as follows: Firstly, AuNP-Cit UV-Vis spectra were taken in serial dilutions. The LSPR position was determined by taking the point where the derivative of $d_{Abs}/d\lambda = 0$ (λ_{LSPR} = 519 nm) and at the mentioned wavelength absorbance was measured for every dilution, generating the calibration curve in Figure 3.

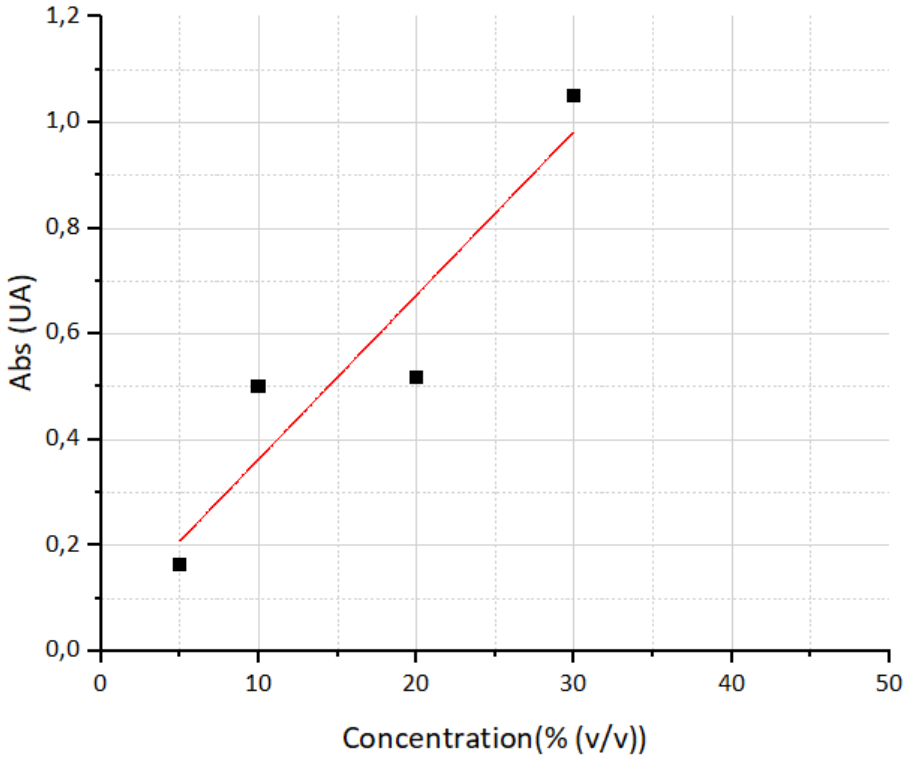

Figure 3. The absorbance at the LSPR wavelength (λ = 519 nm) was plotted as a function of AuNP-Cit concentration (% v/v), where 100% is the Turkevich synthesis product ([AuNP] ≈ 10 nM). The linear relationship y = (0.036 ± 0.002)x – (0.03 ± 0.03), R^2 = 0.993, followed by ANOVA analysis demonstrates that absorbance is an additive property within the measured range (0 – 30% v/v), following the Beer-Lambert law.

Lastly, the same procedure was followed with AuNP-Cale (calendula extract to AuNP-Cit 1:9 v/v proportion) and water dilutions as shown in Figure SM-4. From the mentioned figure, UV-Vis spectra were taken, derivatives were calculated, and the point where $d_{Abs}/d\lambda = 0$ was measured only for the peak corresponding to AuNP LSPR signal. By so doing, the LSPR position turned out to be λ_{LSPR} = 510 nm, showing a clear hypsochromic shift from the AuNP-Cit. Usually, the λ_{LSPR} shifts towards a greater wavelength since it is proportional to the media dielectric (ε). So, functionalizing with greater molecules augments ε concomitant to λ_{LSPR} bathochromic shifts. On the contrary, a hypsochromic shift was observed. Two hypotheses are proposed: (*i*) the extract's carotenoids could interact with the conjugated π electrons, which could be "extracting" electronic density from the plasmon surface, leading to a hypsochromic shift; and (*ii*) it's not possible to confirm derivatization by the LSPR shifting since the *Calendula officinalis* extract's spectra have a clear "shoulder" at λ = 495 nm, and it could be overlapping with the LSPR "unshifted" at 520 nm. In this case, the convolute peak is expected to be at 510 nm. From the abovementioned, there is little evidence yet to confirm an effective conjugation of AuNP with the carotenoids contained in the *Calendula officinalis*.

To confirm the functionalization, DLS and ELS measurements were also performed.

Dynamic light scattering

Through DLS analysis, the hydrodynamic diameter (d_h) of a particulate system dispersed in a continuous phase can be determined.[63] In this case, this refers to the AuNP-Cit and AuNP-Cale colloids in aqueous solution.

It is important to note that this technique is based on light scattering physics described by the "Tyndall Effect", so it is highly sensitive to nanoparticle diameter ($I \alpha d^6$).[64-66] Consequently, the intensity distribution plot $I = f(d)$ oversize the presence of larger AuNPs due to the sixth-power dependence of intensity. In addition, even a small minority of simple aggregates will be disproportionately represented in this graph (Figure 4, left). Taking the previous in mind, one could argue that there are two groups of AuNP-Cale synthesized with hydrodynamic diameters of d_h = (26 ± 3) nm and d_h = (122 ± 13) nm, which, as stated above is an overrepresentation of the fraction of AuNP-Cale aggregates.

For this reason, the number distribution plot $N = f(d)$ is also generated, as it indicates the majority population based on corrections applied to the autocorrelation function using known optical parameters theoretically derived from Mie equation.[67,68] (Figure 4, right).

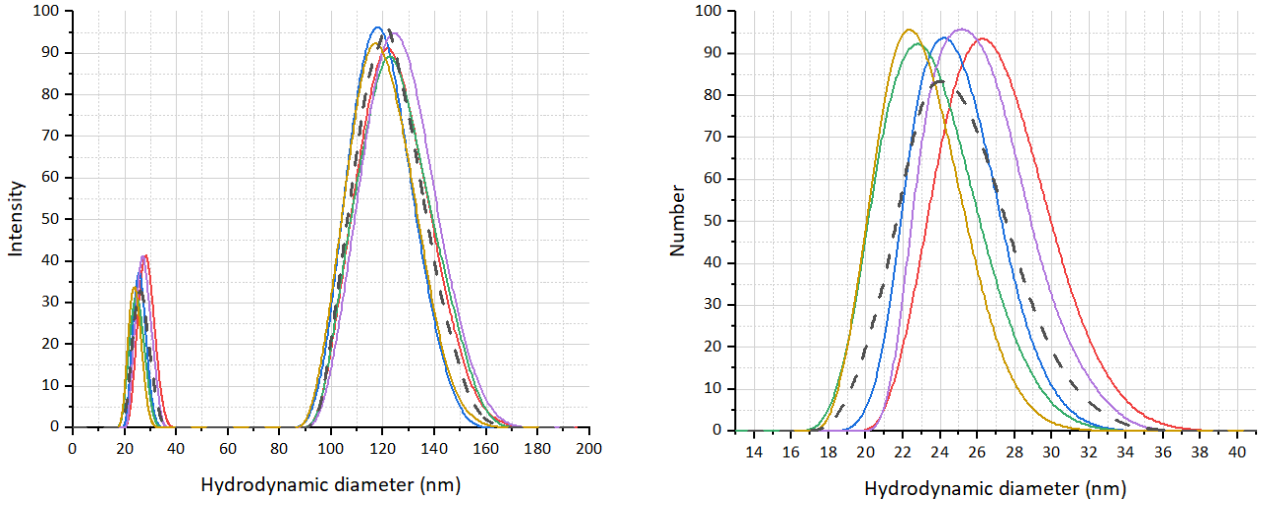

Figure 4. Intensity (left) and number (right) distribution as a function of hydrodynamic diameter of particles in suspension. Solid lines represent individual measurements (n = 6) and the dashed line corresponds to the average curve of all measurements.

Altogether, from the $N = f(d)$ graph, a hydrodynamic diameter of d_h = (25 ± 3) nm, with a PDI of 0.29 ± 0.01 was determined, in accordance with the d_h obtained for the small diameter group in the $I = f(d)$ graph in Figure 4, left. The same procedure was followed for AuNP-Cit, obtaining from $N = f(d)$ to d_h = (19 ± 3) nm (Figure SM-2).

These results show an increment by approximately 10 nm in the AuNP-Cit hydrodynamic diameter after derivatization procedure. DLS is highly sensitive to the presence of aggregates and changes in the hydration layer, so it cannot be assured that this increase is solely attributable to successful derivatization. If we were to consider this increase solely due to calendula adsorption, this growth was predicted by the following analysis: if it is assumed that the length of the functionalizing carotenoids is determined by lycopene, which is the longest carotenoid from the main three, involving 40 carbon atoms, of which 32 are sp^2 conjugated single and double bonds; that the average bond length is approximately 1.4 Å and that the molecule has its longer axis perpendicular to the AuNP surface; then it is expected the final diameter to grow d = 1.4 × 32 = 44.8 Å, each side of the sphere, so a total of roughly 89.6 Å ≈ 9 nm. Since citrate is such a small molecule, following the same reasoning, it is presumable that it provides only 1 nm per side to the AuNP core. In sum, the difference in d_h observed between AuNP-Cit and AuNP-Cale could be attributable to AuNP-Cit derivatization but need confirmation by other techniques.

Furthermore, the expected diameters of both AuNP-Cit and AuNP-Cale by transmission electron microscopy (TEM), should be in the range of 15 nm ≤ $d_{expected}$ ≤ 16 nm since this is the diameter of the AuNP core ($d_{expected} = d_h - 2.r_{ligand}$, where r_{ligand} is ligand longest axis length). To confirm these results AuNPs core diameter was measured by TEM.

Transmission electron microscopy

TEM measurements confirmed the AuNPs core diameter predicted by calculations based on the hydrodynamic diameter (d_h) determined by DLS.

For AuNP-Cit, TEM diameters (d_{TEM}) were determined for n = 372 individual AuNPs from 10 micrographs using FIJI software (Figure 5).

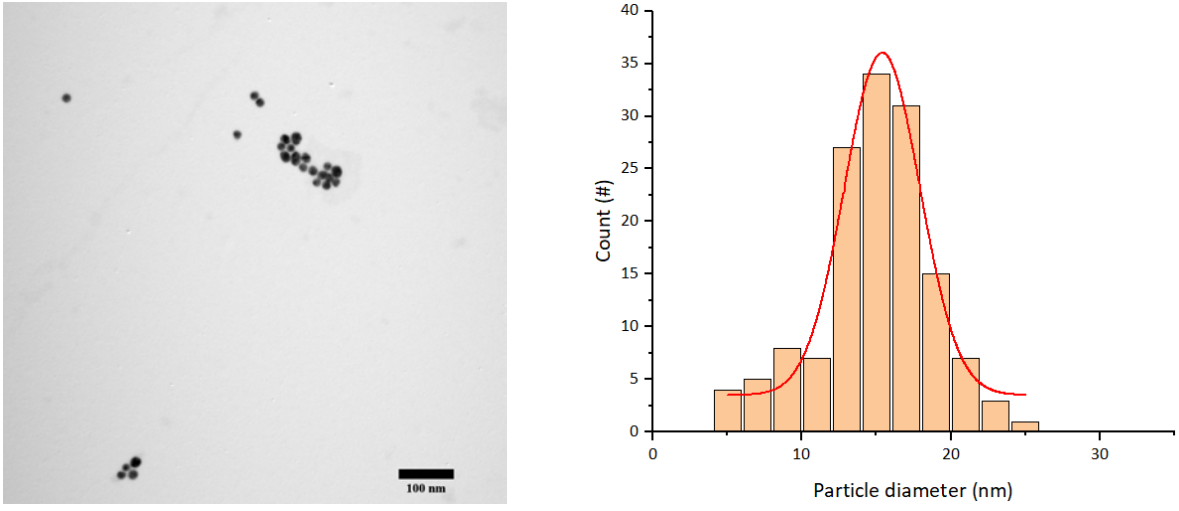

Figure 5. Left: TEM micrograph of citrate-reduced gold nanoparticles (AuNP-Cit) synthesized via the Turkevich method. The image shows spherical nanoparticles with varying degrees of aggregation. The scale bar indicates 100 nm. Right: Size distribution histogram of AuNP-Cit as a function of particle diameter. The synthesis resulted in particles with a diameter d_{TEM} = (16 ± 3). The discrete particles and small aggregates suggest successful formation of the desired colloidal gold system.

Random noise was manually diminished by outruling individuals AuNPs of areas less than A = 11 nm^2 (d_{TEM} < 4 nm) since they could be software artefacts from B&W noise in the picture. The presence of aggregates in some micrographs made individual nanoparticle measurement difficult, so they were excluded by applying a circularity threshold higher than 0.8 and restricting the area to less than 3000 nm^2. On doing so, a population of n = 253 individuals with the distribution presented in Figure 5 (right) was obtained.

The TEM size distribution analysis revealed a unimodal population distribution, with the majority of particles centered at approximately 16 nm and a minor subpopulation observed around 35 nm. These observations are consistent with the high polydispersity index obtained from dynamic light scattering (DLS) measurements, indicating significant heterogeneity in the sample's size distribution. From the gaussian fitting of the count graph for majority population, a diameter of d_{TEM} = (16 ± 3) nm was obtained. In accordance with $d_{expected}$, predicted from the d_h measured by DLS for both AuNP-Cit and AuNP-Cale.

Electrophoretic light scattering

The ζ-potential of a NP solution (diffuse layer potential) gives an idea of the surface charge of the NP and, therefore, of its stability (in terms of the interactions that keep the solid species dispersed in a homogeneous medium).[69]

It is considered that surface charges ζ-potential > 30 mV or ζ-potential < 30 mV are sufficient to overcome the weak attractive interactions between the dispersed particles in the homogeneous phase, so that NP whose ζ-potential meet the previous requirement are considered a stable NP colloidal suspension.

Considering the above, 12 ELS tests were carried out, obtaining a ζ-potential = (-52 ± 2) mV, indicating that the AuNP-Cit are stable under the working conditions (pH = 5 and T = 25 ºC).

In comparison, the ζ-potential obtained for the AuNP-Cale was ζ-potential = (-2 ± 6) mV, suggesting that the carotenoids of the *C. officinalis* extract displaced the citrates on the AuNP surface. Since those carotenoids are not charged, compared to citrate groups at pH 5—where two of three citrate carboxylic acid groups are ionized—if the derivatization is successful, it is expected to be a diminishment to round zero ζ-potential, from citrate to carotenoids, just as our results show.

Previously, ζ-potential was associated with the electrostatic repulsion forces needed for stable NP colloidal suspension. So, it is clear that AuNP-Cale does not fulfil this requirement. Thus, assessing a colloidal stability assay is mandatory to analyze how this diminishment in ζ-potential affected NP stability.

Colloidal stability assay

Colloidal stability was followed by spectrophotometry in the visible range at wavelengths of 520 nm (LSPR maxima), 650 nm plasmonic coupling's bathochromic shifts and 455 nm (maximum absorption of carotenoids, Figure 2). No changes were observed at 455 nm regarding increasing NaCl concentration (data not shown).

It was detected an increase in the critical concentration of NaCl (the concentration at which half of the NPs are aggregated) from $[NaCl]_c$ = (22 ± 2) mM for AuNP-Cit to $[NaCl]_c$ = (61 ± 1) mM for AuNP-Cale (Figure 6).

From this result, it is confirmed that, apart from having successfully achieved the functionalization of AuNP with carotenoids from *C. officinalis*, the same improves their stability, in contrast of what was expect by ELS measurements.

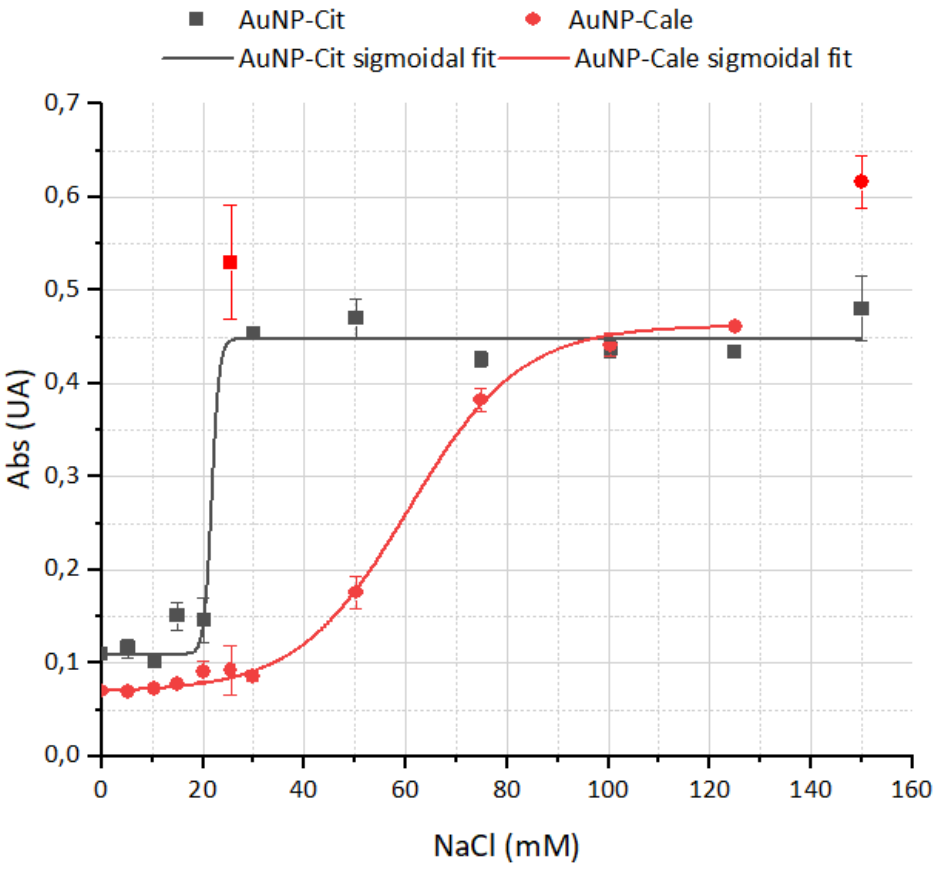

Figure 6. AuNP-Cit and AuNP-Cale colloidal stability assay, followed by UV-Vis spectrophotometry at 650 nm.

This apparent contradiction can be explained since the structure of carotenoids could provide extra steric stabilization that prevents nanoparticles from approaching each other, even when electrostatic repulsion is minimal. Also, carotenoids possess hydrophobic regions (polyene chains) and polar groups (hydroxyl groups in flavoxanthin and lutein). In this sense, interaction between hydrophobic groups of carotenoids (mainly Van der Walls interactions), and hydrophilic interactions between carotenoids and the solvent (hydrogen bonds and dipole mediated interactions) allow them to organize on the surface of NPs forming an effective protective layer.

In summary, Table I presents the key physicochemical parameters obtained for AuNP-Cit and AuNP-Cale, and the combined evidence from multiple characterization techniques demonstrates successful functionalization.

Table I. Comparative physicochemical characterization of AuNP-Cit and AuNP-Cale

Parameter	AuNP-Cit	AuNP-Cale	Change
λ_{LSPR} (nm)	519	510	- 9 nm
d_h (nm)	19 ± 3	25 ± 3	+ 6 nm
d_{TEM} (nm)	16 ± 3	16 ± 3	No change observed
ζ-potential (mV)	- 52 ± 2	- 2 ± 6	+ 50 mV
Colloidal stability against [NaCl] (mM)	22 ± 2	61 ± 1	+ 39 mM

Then, to further evaluate the nature of the functionalization, cyclic voltammetry studies were conducted.

Cyclic voltammetry

Voltammetric profiles for FTO/TiO_2 electrodes were recorded for the solutions containing AuNP-Cit, Cale, or AuNP-Cale in the supporting electrolyte. Distinct differences were observed, highlighting interesting variations in the redox behavior of the analyzed species (Figure 7).

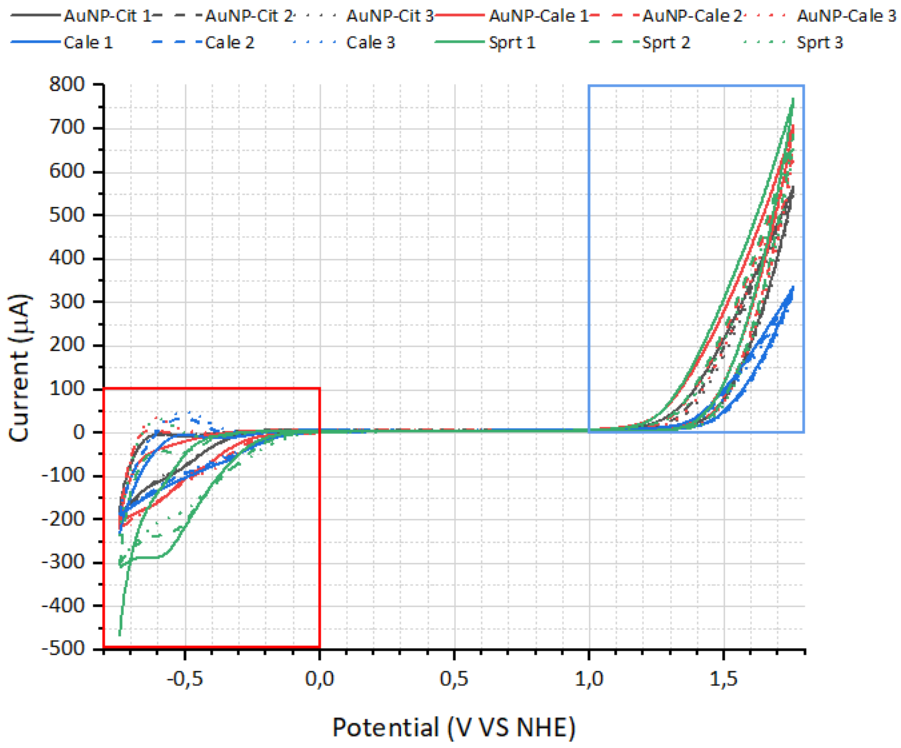

Figure 7. Voltammetric profiles recorded using FTO/TiO_2 electrodes for different analytes in the supporting electrolyte 0.1 M $NaClO_4$:EtOH (1:1) (Sprt, green lines), citrate reduced gold nanoparticles (AuNP-Cit, black lines), gold nanoparticles functionalized with *C. officinalis* extract (AuNP-Cale, red lines) and *C. officinalis* extract (Cale, blue lines). Scan rate: 50 mVs^{-1}. Straight, dashed and dotted lines correspond to the first, second and third voltammetric scans respectively.

As deduced from the voltammetric profiles, two main redox processes were detected for all the evaluated samples: an anodic contribution at ca. 1.5 V and a redox species at ca. -0.6 V (a cathodic contribution and, after cycling, a related anodic peak appeared). The oxidation peak at ca. 1.5 V could be ascribed to the -OH oxidation. Regarding the species at ca. -0.6 V, the cathodic and anodic peaks are ascribed to a process involving allylic oxygen, found in the carotenoids from AuNP-Cale and Cale, but not present in AuNP-Cit, as reported.[70,71]

To further analyze this voltammogram, Figure 8 zooms in on the red and blue windows in Figure 7.

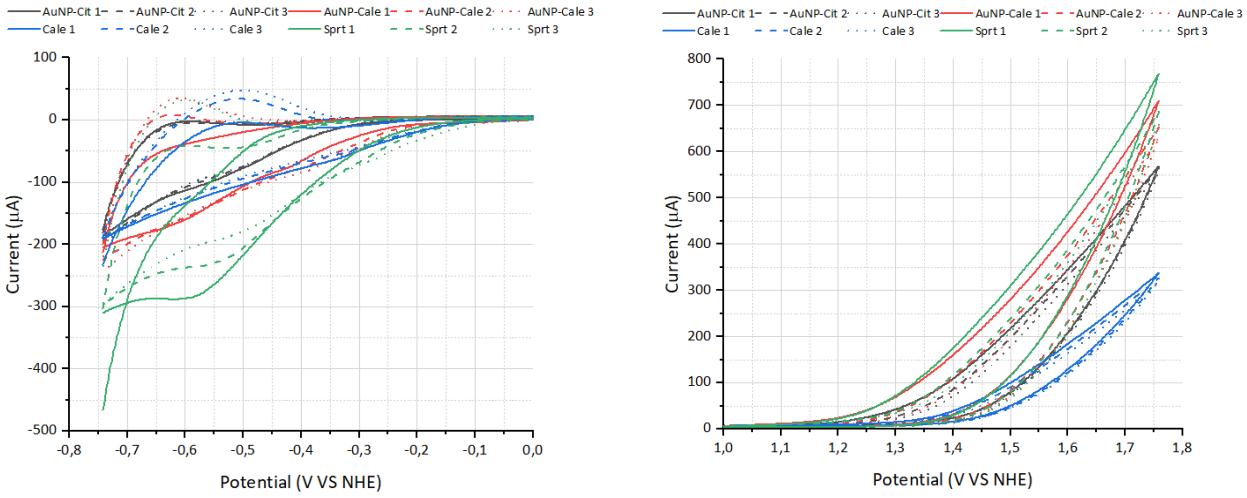

Figure 8. Voltammetric profiles recorded using FTO/TiO_2 electrodes for different analytes in the supporting electrolyte 0.1 M $NaClO_4$:EtOH (1:1). Zoomed from red window (left) and blue window (right) in Figure 7, colors and lines are as in the figure mentioned.

From Figure 8 (left), it is observed that profiles recorded within the -0.75 to 0.0 V range in the presence of AuNP-Cit show no discernible differences, i.e., the area, potential and shape are the same for the three potential scans. On the contrary, voltammetric profiles recorded from Cale solutions showed progressively increasing areas in every cycle. This behavior can be attributed to the electrochemical activity of carotenoids present in *Calendula officinalis* extract.[70] During the first cycle, electroactive carotenoids undergo redox reactions at the electrode surface allowing the adsorption of the involved species, which leads to a partial passivation of the electrode surface. This passivation subsequently increases the capacitive current in the following cycles, resulting in larger areas for the intensity current peaks. The progressive increase in area with each cycle suggests that this passivation process continues incrementally as more carotenoids interact and adsorb onto the electrode surface. The same behaviour is observed in the presence of AuNP-Cale conjugate, suggesting that the derivatization was successful and that the gold nanoparticles are, at least, partially covered with *Calendula officinalis* extract.

In addition, the anodic intensity current peaks were found at -0.65 V for AuNP-Cale, whereas are detected at -0.50 V for Cale alone. It could be argued, that besides the AuNP-Cit peaks have very small currents, their dI/dV = 0 values are closest to AuNP-Cale that to Cale alone. In this sense, it is suggested that the voltammogram corresponds to a different entity than both above-mentioned.

Thus, AuNP-Cale is a well-functionalized AuNP with *Calendula officinalis* extract, according to these voltammetric results. This conclusion is supported by both panels of Figure 8.

Following all the observations arising from the voltammetric measurements, it can be highlighted that: (1) profiles and features related to the redox behaviour coming from Cale extracts differ significantly from those observed when linked to the AuNP; (2) redox behaviour recorded in the presence of AuNP-Cit is different from that observed for AuNP-Cale; and (3) when AuNP-Cale solutions are evaluated, the voltammetric profiles significantly differs from those arose using pure Cale solutions. Then, conjugation between AuNP-Cit and Cale could be confirmed. The stability of the AuNP-Cale is good enough to support the application of different potential routines.

Technological evaluation of AuNP-Cale

AuNP-Cale as a dye-sensitized solar cell sensitizer

Having confirmed the successful functionalization of gold nanoparticles with *Calendula officinalis* extract through comprehensive physicochemical and electrochemical characterization, we next explored the potential technological application of this nanoconjugate as a sensitizer for DSSC.

To evaluate AuNP-Cale as a sensitizer, cells containing Cale, AuNP-Cit and AuNP-Cale were assembled. Cale was also used in a co-adsorption procedure, and AuNP-Cit was added in a sequential step. Measurements using citrate as sensitizer were taken as a blank experiment.

The performance of each configuration was evaluated through current-voltage measurements under simulated solar illumination (Table II) and electrochemical impedance spectroscopy in darkness (Table III).

Table II. Photovoltaic properties of cells assembled with different sensitizers. All measurements were performed under one sun light intensity of 100 mW cm^{-2}, AM 1.5 G and the active areas were 0.36 cm^2 for all the cells. J_{SC} is the short-circuit current density, V_{OC} the open circuit potential, FF is the fill factor and η is the power conversion efficiency (PCE). Average values coming from at least three independent assembled cells.

Dye	η (%)	FF	V_{oc} (V)	J_{sc} (A cm^{-2})
Cale	0.020	0.36	0.24	2.2 10^{-4}
AuNP-Cale	0.012	0.35	0.20	1.7 10^{-4}
AuNP-Cit	0.019	0.33	0.30	1.8 10^{-4}
Cale + AuNP	0.040	0.39	0.28	7.2 10^{-4}
Citrate	0.027	0.45	0.42	1.4 10^{-4}

Some facts can be deduced from the measured results. Firstly, when applied as a sensitizer, the conjugated AuNP-Cale did not improve the DSSC performance. The reason is that the conjugate split in the components, also considering that the photoanode prior to the cell's assembly is pink-coloured and became colourless after 60 min inside the DSSC (i.e., in contact with the electrolyte solution). This makes sense since the carotenoids and xanthophylls of the cell extract possess only a few OH groups that can interact with the AuNP or the TiO_2. Then, when conjugated AuNP-cale are added to the FTO/TiO_2 photoanode, cale is adsorbed onto the semiconductor involving the same functional groups bonded to the AuNP. Nevertheless, the efficiency improvement was measured when adding the AuNP-Cit to the FTO/TiO_2/Cale electrode. In this case, the cell's performance is probably related to a better electrode surface coverage. When compounds of the cale extract adsorbed to the semiconductor, some surface patches remained uncovered. Then, those areas could be covered by the added AuNP-Cit, improving the electrode transference between dyes and the semiconductor and, therefore, increasing the cell's efficiency.

From the electrochemical impedance spectroscopy measurements, characteristic times of the cell were determined (Table III). As previously reported, transmission line-based model was employed to fit the measured profiles.

Table III. Values obtained from fitting the experimental data measured at V = 0.45 V, in darkness, using a transmission line-based model. Γt is the time constant for the transport of the injected electrons that diffuse through the nanoparticle network (calculated as Γt = Rt × Cμ, with Cμ, the chemical capacitance at the TiO_2/dye/electrolyte interface associated with the variation in the electron density and the displacement of the Fermi level); Γrec, the recombination time that reflects the lifetime of an electron in the photoanode (calculated as Γrec = Rct × Cμ).

	AuNP-Cit	Cale + AuNP-Cit sequential	Cale
Γrec = Rct x Cμ / s	0.057	0.0200	0.0120
Γt = Rt x Cμ / s	0.011	0.0007	0.0002

The performances of the DSSCs have to be explained by the differences in the time-constant values. For this reason, DSSCs sensitized with AuNP-Cit are among the worst measured, because of their high Γt. In addition, DSSCs showed high Γrec values, which is essential to ensure an acceptable cell's efficiency.

As expected, more efficient cells are those with lower Γt times and higher Γrec ones. For the evaluated cells, these facts are shown for DSSC sensitized with a mixture of the extracted dye followed by the addition of AuNP. This is in agreement with our previous studies, where we reported the application of silver nanoparticles as co-adsorbents improves DSSC performance, highlighting the importance of achieving greater surface coverage to reduce direct electron transfer between the TiO_2 and the redox couple of the electrolyte.[72]

Infrared spectroscopy

IR spectra were taken to determine if conjugation was achieved by covalent bonding or by Van der Walls interactions. Also, to determine if the DSSCs were sensitized with the dye and/or with the AuNP-Cale conjugate.

Figure 9 shows the spectra of AuNP-Cit, AuNP-Cale and Cale alone, before sensitization. In parallel, Figure 10 shows AuNP-Cit, AuNP-Cale and Cale with and without TiO_2.

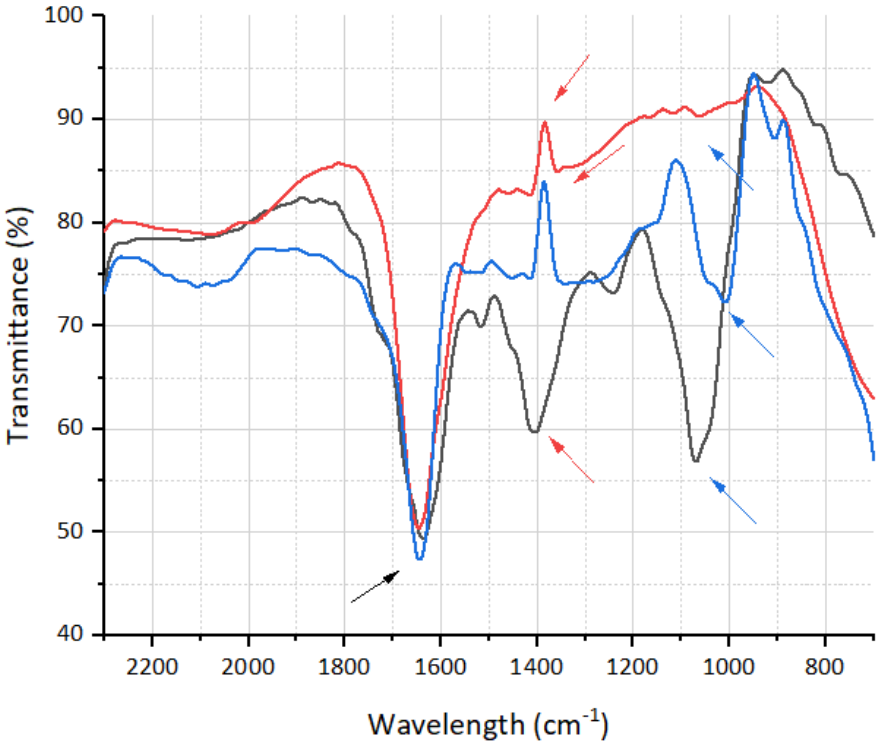

Figure 9. FTIR spectra of AuNP-Cit (black line), AuNP-Cale (red line), and Cale (blue line) in the 700-2300 cm^{-1} region. Black arrow indicates COO^- asymmetric stretching, red arrows indicate COO^- symmetric stretching, and blue arrows indicate C-OH stretching.

From Figure 9, the main absorption band appreciated has its minimum centered in $\tilde{\upsilon}$ = 1645 cm^{-1} (black arrow), which corresponds to both COO^- asymmetric stretching (from the citrate of AuNP-Cit). It is well established that the asymmetric COO^- stretching occurs at $\tilde{\upsilon}$ = 1715 cm^{-1} and the inductive effect on the stretching environment provokes shifting towards lower energies,[73] as seen in the spectra. Also, the C=C stretching energy from polyenes (like those from the main carotenoids presented in Figure 1) occurs at the abovementioned wavenumber. The next evident peak, which minimum is centered at $\tilde{\upsilon}$ = 1405 cm^{-1} (red

arrows), corresponds to the symmetric stretching of COO^-, which was observed only in the AuNP-Cit as expected. The last distinctive peak observed, which occurs at $\tilde{\upsilon}$ = 1070 cm^{-1} (blue arrows), corresponds to the C-O stretching of alcohols (as those from the citrate in AuNP-Cit). In the case of Cale, the C-O from the carotenoids shown in Figure 1 (except lycopene) have a different environment than those from the citrate. In addition, the extensive network of conjugated double bonds may affect the whole structure's electronic distribution, consequently lowering the vibration energy towards a wavenumber of $\tilde{\upsilon}$ = 1000 cm^{-1}. Here, it is proposed that the C-O that were forming C-OH bonds are now involved in the coordination with the gold nanoparticle surface (C-O-Au), which may lower the energies out of the spectra, diminishing its intensity until it is undetectable.

Some significant differences are observed when AuNP-Cit is compared with TiO_2/AuNP-Cit (AuNP-Cit after derivatization, Figure 10-a). The main difference is that AuNP-Cit shows deeper minima in the regions of approximately $\tilde{\upsilon}$ = 1400 cm^{-1} (Figure 9, red arrows) and $\tilde{\upsilon}$ = 1070 cm^{-1} (Figure 9, blue arrows). In parallel, TiO_2/AuNP-Cit presents a flatter profile in the mentioned region. Regarding the region of $\tilde{\upsilon}$ = 1645 cm^{-1} (corresponding to COO^- asymmetric stretching Figure 9, black arrow), it could be argued that this vibrational mode wasn't affected by TiO_2 sensibilization. On the other hand, symmetric stretching of COO^-, which is observed around $\tilde{\upsilon}$ = 1400 cm^{-1} was appreciably diminished after derivatization, suggesting coordination of COO^- with both TiO_2 and Au, causing the restriction of that particular vibration. Finally, the practically disappearing of the $\tilde{\upsilon}$ = 1070 cm^{-1} minima (corresponding to C-OH stretching of the citrate) suggests the place for bonding formation between AuNP-Cit and TiO_2, probably Au-$O_{(COOH)}$-C-$O_{(COH)}$-Ti, where $O_{(COOH)}$ corresponds to carboxylate oxygen, and $O_{(COH)}$ corresponds to the alcohol oxygen.

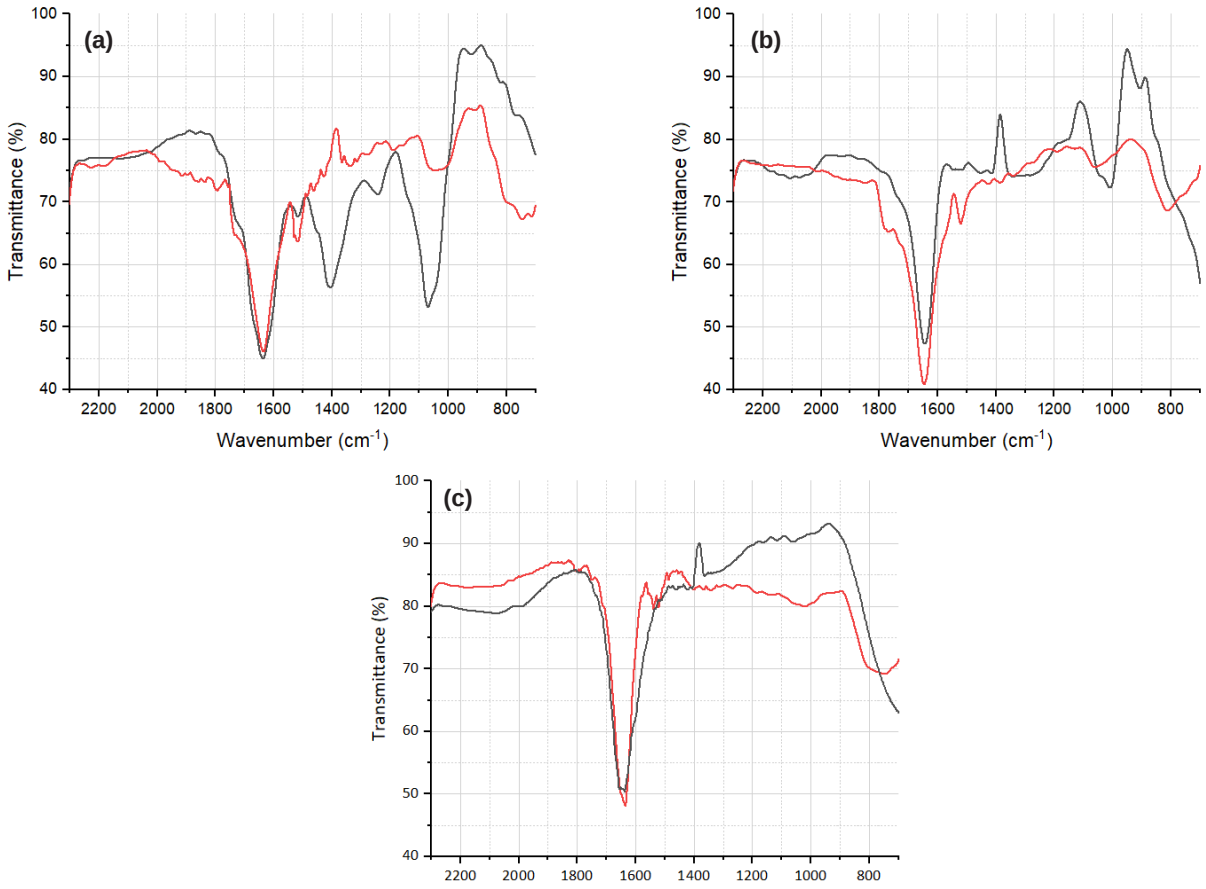

Figure 10. FTIR spectra of AuNP-Cit (a), Cale (b) and AuNP-Cale (c) alone (black lines) and adsorbed onto TiO_2 (red lines).

When Cale is compared with TiO_2/Cale (Cale after derivatization, Figure 10-b), the differences observed are comparable to those between Cale and AuNP-Cale. It is proposed that the hydroxyl and carbonyl groups of carotenoids appear to form coordination bonds with the TiO_2 surface, as they did with the gold nanoparticles, as evidenced by a general flattening of the spectrum and a decrease in the intensity of characteristic OH and C-O-C peaks.

No significant changes are observed when AuNP-Cale is compared with TiO_2/AuNP-Cale (AuNP-Cale after derivatization, Figure 10-c). Following the above reasoning, carotenoids from *Calendula officinalis* are now bonded to the gold nanoparticle, to the TiO_2 or both, being FTIR spectroscopy insufficient to conclude in this sense firmly. Because of this reason, FORS was performed as follows.

Fiber optic reflectance spectroscopy

FORS was performed for dyes adsorbed onto the TiO_2 before and after the DSSC was assembled, specifically before and after immersion in the iodine-based electrolyte used in the assembled cells (Figure 11). In all evaluated cases, absorbance profiles were improved after contacting the iodine-based solutions, probably due to the desorption of molecules attached to the TiO_2 surface through weak bondings. For samples measured before the DSSC built-up, it is appreciable that AuNP-Cale spectra are the sum of both AuNP-Cit and Cale spectra. AuNP-Cit and AuNP-Cale have their maxima of 520 and 540 nm, respectively, as expected from the LSPR position.

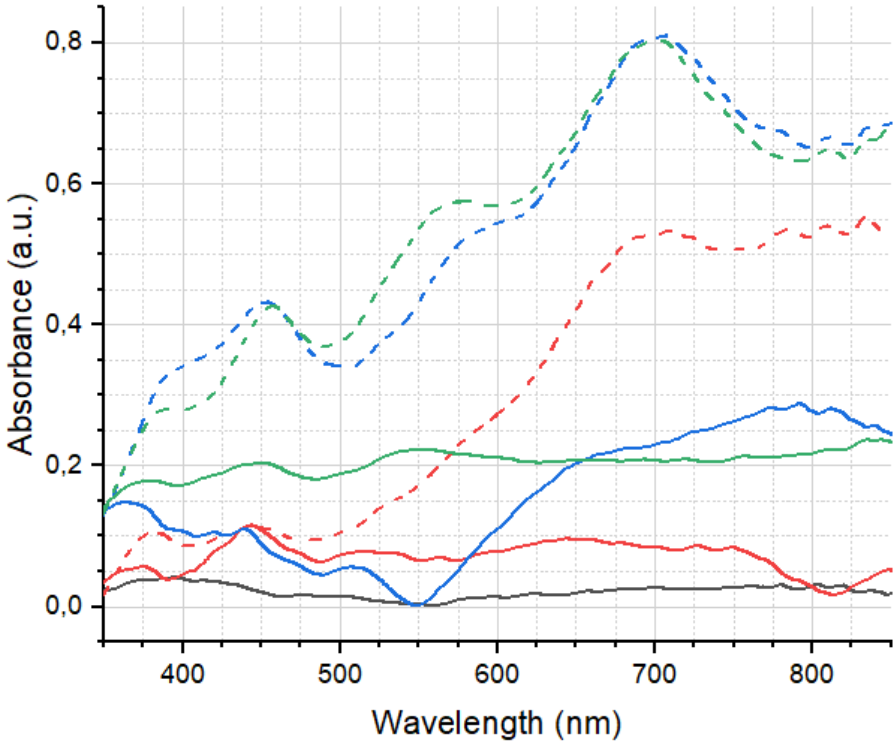

Figure 11. UV-Vis reflectance spectra of AuNP-Cit (red line), Cale (blue line) and AuNP-Cale (green line) before and after DSSC assembly (straight and dashed lines respectively) in the visible 350-850 nm range.

However, some features changed after the DSSC assembly and getting in contact with the iodine-based solutions. Spectra for Cale and AuNP-Cale are almost identical.

This is in line with what was observed when evaluating the DSSC: cells sensitized with the conjugate AuNP-Cale showed a similar power conversion efficiency to those sensitized with the components separated. Figure 11 shows that in all cases studied, absorbance profiles were improved after getting in contact with

the iodine-based solutions, probably to desorption of molecules attached to the TiO_2 surface through weak bonding. When attached to the TiO_2, carotenoids involved the same functional groups that bond the AuNP. Therefore, the conjugate is split into the elements, as confirmed by the reflectance spectra measured after the cell's evaluation.

CONCLUSIONS

Calendula officinalis extract was evaluated as a functionalization agent for gold nanoparticles (AuNPs), using citrate-reduced AuNPs (AuNP-Cit) as a reference. The resulting nanoconjugate, AuNP-Cale, underwent comprehensive characterization using DLS, ELS, colloidal stability assay, TEM, and spectroscopy.

Functionalization was confirmed by increased hydrodynamic diameter and reduced zeta potential of AuNP-Cale compared to AuNP-Cit. Despite the reduced zeta potential, the AuNP-Cale showed improved colloidal stability, which was attributed to the potential steric stabilization provided by the carotenoids in the extract. Voltammetry, FTIR and FORS analyses further supported the successful derivatization and possible interactions with the AuNP and TiO_2 surfaces.

AuNP-Cale was then explored as a sensitizer for DSSCs. While pre-formed AuNP-Cale did not enhance DSSC efficiency when applied directly, improved performance was achieved when AuNP-Cit was added sequentially after the *C. officinalis* extract on the TiO_2 electrode. This enhanced performance correlated with improved light absorption (FORS) and favorable EIS parameters, likely resulting from better electrode coverage achieved by the sequential deposition method.

Conflicts of interest

The authors have no known competing financial interests or personal relationships that could have appeared to influence the work reported in this paper.

Acknowledgements

Pablo Fagúndez and María Fernanda Cerdá are SNI-ANII (Agencia Nacional de Investigación e Innovación) and PEDECIBA (Programa de Desarrollo de las Ciencias Básicas) researchers.

REFERENCES

(1) Feynman, R. P. There's Plenty of Room at the Bottom. *Eng. Sci.* **1959**, *5* (23), 22–36.
(2) Laurent, S.; Forge, D.; Port, M.; Roch, A.; Robic, C.; Vander Elst, L.; Muller, R. N. Magnetic Iron Oxide Nanoparticles: Synthesis, Stabilization, Vectorization, Physicochemical Characterizations, and Biological Applications. *Chem. Rev.* **2010**, *110* (4), 2574–2574. https://doi.org/10.1021/cr900197g
(3) Loureiro, A.; Azoia, N. G.; Gomes, A. C.; Cavaco-Paulo, A. Albumin-Based Nanodevices as Drug Carriers. *Curr. Pharm. Des.* **2016**, *22* (10), 1371–1390. https://doi.org/10.2174/1381612822666160125114900
(4) Martis, E.; Badve, R.; Degwekar, M. Nanotechnology Based Devices and Applications in Medicine: An Overview. *Chron. Young Sci.* **2012**, *3* (1), 68. https://doi.org/10.4103/2229-5186.94320
(5) Nikalje, A. P. Nanotechnology and Its Applications in Medicine. *Med. Chem.* **2015**, *5* (2). DOI: 10.4172/2161-0444.1000247
(6) Todescato, F.; Fortunati, I.; Minotto, A.; Signorini, R.; Jasieniak, J.; Bozio, R. Engineering of Semiconductor Nanocrystals for Light Emitting Applications. *Materials* **2016**, *9* (8), 672. https://doi.org/10.3390/ma9080672
(7) Dong, H.; Wen, B.; Melnik, R. Relative Importance of Grain Boundaries and Size Effects in Thermal Conductivity of Nanocrystalline Materials. *Sci. Rep.* **2014**, *4* (1), 7037. https://doi.org/10.1038/srep07037
(8) Ma, E. Controlling Plastic Instability. *Nat. Mater.* **2003**, *2* (1), 7–8. https://doi.org/10.1038/nmat797
(9) Ripp, S.; Henry, T. B. (Eds.) *Biotechnology and Nanotechnology Risk Assessment: Minding and Managing the Potential Threats around Us*. American Chemical Society Publications, Washington, DC, 2011, Vol. 1079. https://doi.org/10.1021/bk-2011-1079

(10) Golobič, M.; Jemec, A.; Drobne, D.; Romih, T.; Kasemets, K.; Kahru, A. Upon Exposure to Cu Nanoparticles, Accumulation of Copper in the Isopod *Porcellio Scaber* Is Due to the Dissolved Cu Ions Inside the Digestive Tract. *Environ. Sci. Technol.* **2012**, *46* (21), 12112–12119. https://doi.org/10.1021/es3022182
(11) Kosmala, A.; Wright, R.; Zhang, Q.; Kirby, P. Synthesis of Silver Nano Particles and Fabrication of Aqueous Ag Inks for Inkjet Printing. *Mater. Chem. Phys.* **2011**, *129* (3), 1075–1080. https://doi.org/10.1016/j.matchemphys.2011.05.064
(12) Holzinger, M.; Le Goff, A.; Cosnier, S. Nanomaterials for Biosensing Applications: A Review. *Front. Chem.* **2014**, *2*. https://doi.org/10.3389/fchem.2014.00063
(13) Millstone, J. E.; Kavulak, D. F. J.; Woo, C. H.; Holcombe, T. W.; Westling, E. J.; Briseno, A. L.; Toney, M. F.; Fréchet, J. M. J. Synthesis, Properties, and Electronic Applications of Size-Controlled Poly(3-Hexylthiophene) Nanoparticles. *Langmuir* **2010**, *26* (16), 13056–13061. https://doi.org/10.1021/la1022938
(14) Shaalan, M.; Saleh, M.; El-Mahdy, M.; El-Matbouli, M. Recent Progress in Applications of Nanoparticles in Fish Medicine: A Review. *Nanomedicine: Nanotechnology, Biology and Medicine* **2016**, *12* (3), 701–710. https://doi.org/10.1016/j.nano.2015.11.005
(15) Avasare, V.; Zhang, Z.; Avasare, D.; Khan, I.; Qurashi, A. Room-Temperature Synthesis of TiO_2 Nanospheres and Their Solar Driven Photoelectrochemical Hydrogen Production: Metal Organic Mediated Room Temperature Synthesis of TiO_2 Nanospheres. *Int. J. Energy Res.* **2015**, *39* (12), 1714–1719. https://doi.org/10.1002/er.3372
(16) Mueller, N. C.; Nowack, B. Exposure Modeling of Engineered Nanoparticles in the Environment. *Environ. Sci. Technol.* **2008**, *42* (12), 4447–4453. https://doi.org/10.1021/es7029637
(17) Ning, F.; Shao, M.; Xu, S.; Fu, Y.; Zhang, R.; Wei, M.; Evans, D. G.; Duan, X. TiO_2 /Graphene/NiFe-Layered Double Hydroxide Nanorod Array Photoanodes for Efficient Photoelectrochemical Water Splitting. *Energy Environ. Sci.* **2016**, *9* (8), 2633–2643. https://doi.org/10.1039/C6EE01092J
(18) Fang, X.-Q.; Liu, J.-X.; Gupta, V. Fundamental Formulations and Recent Achievements in Piezoelectric Nano-Structures: A Review. *Nanoscale* **2013**, *5* (5), 1716. https://doi.org/10.1039/c2nr33531j
(19) Gawande, M. B.; Goswami, A.; Felpin, F.-X.; Asefa, T.; Huang, X.; Silva, R.; Zou, X.; Zboril, R.; Varma, R. S. Cu and Cu-Based Nanoparticles: Synthesis and Applications in Catalysis. *Chem. Rev.* **2016**, *116* (6), 3722–3811. https://doi.org/10.1021/acs.chemrev.5b00482
(20) Li, Y.; Wang, H.; Feng, Q.; Zhou, G.; Wang, Z.-S. Gold Nanoparticles Inlaid TiO2 Photoanodes: A Superior Candidate for High-Efficiency Dye-Sensitized Solar Cells. *Energy Environ. Sci.* **2013**, *6* (7), 2156-2165. https://doi.org/10.1039/c3ee23971c
(21) Maojo, V.; García-Remesal, M.; De La Iglesia, D.; Crespo, J.; Pérez-Rey, D.; Chiesa, S.; Fritts, M.; Kulikowski, C. A. Nanoinformatics: Developing Advanced Informatics Applications for Nanomedicine. In: Prokop, A. (Ed.). *Intracellular Delivery – Fundamentals and Applications*. Springer, Netherlands, Dordrecht, 2011, Vol. 5, pp 847–860. https://doi.org/10.1007/978-94-007-1248-5_26
(22) Maojo, V.; Fritts, M.; Martin-Sanchez, F.; De La Iglesia, D.; Cachau, R. E.; Garcia-Remesal, M.; Crespo, J.; Mitchell, J. A.; Anguita, A.; Baker, N.; et al. Nanoinformatics: Developing New Computing Applications for Nanomedicine. *Computing* **2012**, *94* (6), 521–539. https://doi.org/10.1007/s00607-012-0191-2
(23) Panneerselvam, S.; Choi, S. Nanoinformatics: Emerging Databases and Available Tools. *Int. J. Mol. Sci.* **2014**, *15* (5), 7158–7182. https://doi.org/10.3390/ijms15057158
(24) Brown, M. D.; Suteewong, T.; Kumar, R. S. S.; D'Innocenzo, V.; Petrozza, A.; Lee, M. M.; Wiesner, U.; Snaith, H. J. Plasmonic Dye-Sensitized Solar Cells Using Core−Shell Metal−Insulator Nanoparticles. *Nano Lett.* **2011**, *11* (2), 438–445. https://doi.org/10.1021/nl1031106
(25) Qi, J.; Dang, X.; Hammond, P. T.; Belcher, A. M. Highly Efficient Plasmon-Enhanced Dye-Sensitized Solar Cells through Metal@Oxide Core–Shell Nanostructure. *ACS Nano* **2011**, *5* (9), 7108–7116. https://doi.org/10.1021/nn201808g

(26) Jeong, N. C.; Prasittichai, C.; Hupp, J. T. Photocurrent Enhancement by Surface Plasmon Resonance of Silver Nanoparticles in Highly Porous Dye-Sensitized Solar Cells. *Langmuir* **2011**, *27* (23), 14609–14614. https://doi.org/10.1021/la203557f

(27) Nahm, C.; Choi, H.; Kim, J.; Jung, D.-R.; Kim, C.; Moon, J.; Lee, B.; Park, B. The Effects of 100 nm-Diameter Au Nanoparticles on Dye-Sensitized Solar Cells. *Appl. Phys. Lett.* **2011**, *99* (25), 253107. https://doi.org/10.1063/1.3671087

(28) Deepa, K. G.; Lekha, P.; Sindhu, S. Efficiency Enhancement in DSSC Using Metal Nanoparticles: A Size Dependent Study. *Sol. Energy* **2012**, *86* (1), 326–330. https://doi.org/10.1016/j.solener.2011.10.007

(29) Kawawaki, T.; Takahashi, Y.; Tatsuma, T. Enhancement of Dye-Sensitized Photocurrents by Gold Nanoparticles: Effects of Plasmon Coupling. *J. Phys. Chem. C* **2013**, *117* (11), 5901–5907. https://doi.org/10.1021/jp3120836

(30) Jeevanandam, J.; Barhoum, A.; Chan, Y. S.; Dufresne, A.; Danquah, M. K. Review on Nanoparticles and Nanostructured Materials: History, Sources, Toxicity and Regulations. *Beilstein J. Nanotechnol.* **2018**, *9*, 1050–1074. https://doi.org/10.3762/bjnano.9.98

(31) Yi, Z.; Zeng, Y.; Wu, H.; Chen, X.; Fan, Y.; Yang, H.; Tang, Y.; Yi, Y.; Wang, J.; Wu, P. Synthesis, Surface Properties, Crystal Structure and Dye-Sensitized Solar Cell Performance of TiO2 Nanotube Arrays Anodized under Different Parameters. *Results in Phys.* **2019**, *15*, 102609. https://doi.org/10.1016/j.rinp.2019.102609

(32) Korir, B. K.; Kibet, J. K.; Ngari, S. M. A Review on the Current Status of Dye-sensitized Solar Cells: Toward Sustainable Energy. *Energy Sci. Eng.* **2024**, *12* (8), 3188–3226. https://doi.org/10.1002/ese3.1815

(33) Javed, H. M. A.; Sarfaraz, M.; Nisar, M. Z.; Qureshi, A. A.; E Alam, M. F.; Que, W.; Yin, X.; Abd-Rabboh, H. S. M.; Shahid, A.; Ahmad, M. I.; Ullah, S. Plasmonic Dye-Sensitized Solar Cells: Fundamentals, Recent Developments, and Future Perspectives. *ChemistrySelect* **2021**, *6* (34), 9337–9350. https://doi.org/10.1002/slct.202102177

(34) Bohren, C. F.; Huffman, D. R. *Absorption and Scattering of Light by Small Particles*; A Wiley-Interscience publication. Wiley-CH Verlag GmbH & Co KGaA, New York, 2004. https://doi.org/10.1002/9783527618156

(35) Sepúlveda, B.; Angelomé, P. C.; Lechuga, L. M.; Liz-Marzán, L. M. LSPR-Based Nanobiosensors. *Nano Today* **2009**, *4* (3), 244–251. https://doi.org/10.1016/j.nantod.2009.04.001

(36) Jang, Y. H.; Jang, Y. J.; Kim, S.; Quan, L. N.; Chung, K.; Kim, D. H. Plasmonic Solar Cells: From Rational Design to Mechanism Overview. *Chem. Rev.* **2016**, *116* (24), 14982–15034. https://doi.org/10.1021/acs.chemrev.6b00302

(37) Zhou, J.; Ralston, J.; Sedev, R.; Beattie, D. A. Functionalized Gold Nanoparticles: Synthesis, Structure and Colloid Stability. *J. Colloid Interface Sci.* **2009**, *331* (2), 251–262. https://doi.org/10.1016/j.jcis.2008.12.002

(38) Vella, F. M.; Pignone, D.; Laratta, B. The Mediterranean Species *Calendula officinalis* and *Foeniculum vulgare* as Valuable Source of Bioactive Compounds. *Molecules* **2024**, *29* (15), 3594. https://doi.org/10.3390/molecules29153594

(39) Khalid, K.; da Silva, J. T. Biology of *Calendula officinalis* Linn.: Focus on Pharmacology, Biological Activities and Agronomic Practices. *Medicinal and Aromatic Plant Science and Biotechnology* **2012**, *6*, 12–27.

(40) Kurkin, V. A.; Sharova, O. V. Flavonoids from Calendula Officinalis Flowers. *Chem. Nat. Compd.* **2007**, *43* (2), 216–217. https://doi.org/10.1007/s10600-007-0084-3

(41) Komissarenko, N. F.; Chernobai, V. T.; Derkach, A. I. Flavonoids of Inflorescences of *Calendula officinalis*. *Chem. Nat. Compd.* **1988**, *24* (6), 675–680. https://doi.org/10.1007/BF00598181

(42) Muley, B.; Khadabadi, S.; Banarase, N. Phytochemical Constituents and Pharmacological Activities of Calendula Officinalis Linn (Asteraceae): A Review. *Trop. J. Pharm Res.* **2009**, *8* (5). https://doi.org/10.4314/tjpr.v8i5.48090

(43) Kishimoto, S.; Maoka, T.; Sumitomo, K.; Ohmiya, A. Analysis of Carotenoid Composition in Petals of Calendula (*Calendula officinalis* L.). *Biosci., Biotechnol., Biochem.* **2005**, *69* (11), 2122–2128. https://doi.org/10.1271/bbb.69.2122
(44) Hulkoti, N. I.; Taranath, T. C. Biosynthesis of Nanoparticles Using Microbes—A Review. *Colloids Surf., B* **2014**, *121*, 474–483. https://doi.org/10.1016/j.colsurfb.2014.05.027
(45) Durán, N.; Nakazato, G.; Seabra, A. B. Antimicrobial Activity of Biogenic Silver Nanoparticles, and Silver Chloride Nanoparticles: An Overview and Comments. *Appl. Microbiol. Biotechnol.* **2016**, *100* (15), 6555–6570. https://doi.org/10.1007/s00253-016-7657-7
(46) Tasic, L.; Stanisic, D.; Martins, L. G.; Cruz, G. C. F.; Savu, R. Insights of Green and Biosynthesis of Nanoparticles. In: Koduru, J. R.; Karri, R. R.; Mubarak, N. M.; Bandala, E. R. (Eds.). *Sustainable Nanotechnology for Environmental Remediation*, *Micro and Nano Technologies.* Elsevier, 2022. Chapter 3, pp 61–90. https://doi.org/10.1016/B978-0-12-824547-7.00020-5
(47) Baghizadeh, A.; Ranjbar, S.; Gupta, V. K.; Asif, M.; Pourseyedi, S.; Karimi, M. J.; Mohammadinejad, R. Green Synthesis of Silver Nanoparticles Using Seed Extract of *Calendula officinalis* in Liquid Phase. *J. Mol. Liq.* **2015**, *207*, 159–163. https://doi.org/10.1016/j.molliq.2015.03.029
(48) Wei, X.; Liu, Y.; El-kott, A.; Ahmed, A. E.; Khames, A. *Calendula officinalis*-based green synthesis of titanium nanoparticle: Fabrication, characterization, and evaluation of human colorectal carcinoma. *J. Saudi Chem. Soc.* **2021**, *25* (11), 101343. https://doi.org/10.1016/j.jscs.2021.101343
(49) Hao, W.; Jia, Y.; Wang, C.; Wang, X. Preparation, Chemical Characterization and Determination of the Antioxidant, Cytotoxicity and Therapeutic Effects of Gold Nanoparticles Green-Synthesized by *Calendula officinalis* Flower Extract in Diabetes-Induced Cardiac Dysfunction in Rat. *Inorg. Chem. Commun.* **2022**, *144*, 109931. https://doi.org/10.1016/j.inoche.2022.109931
(50) Santos, A. P.; Gonçalves, M. M.; Justus, B.; Fardin, D. P. D. S.; Toledo, A. C. O.; Budel, J. M.; Paula, J. P. D. *Calendula officinalis* L. flower extract-mediated green synthesis of silver nanoparticles under LED light. *Braz. J. Pharm. Sci.* **2022**, *58*, e19519. https://doi.org/10.1590/s2175-97902022e19519
(51) Fricano, A.; Tavormina, F.; Pignataro, B.; Vetri, V.; Ferrara, V. Progress and Prospects of Biomolecular Materials in Solar Photovoltaic Applications. *Molecules* **2025**, *30* (15), 3236. https://doi.org/10.3390/molecules30153236
(52) Turkevich, J. Colloidal Gold. Part II: Colour, Coagulation, Adhesion, Alloying and Catalytic Properties. *Gold Bull* **1985**, *18* (4), 125–131. https://doi.org/10.1007/BF03214694
(53) Turkevich, J.; Stevenson, P. C.; Hillier, J. A Study of the Nucleation and Growth Processes in the Synthesis of Colloidal Gold. *Discuss. Faraday Soc.* **1951**, *11*, 55. https://doi.org/10.1039/df9511100055
(54) Kimling, J.; Maier, M.; Okenve, B.; Kotaidis, V.; Ballot, H.; Plech, A. Turkevich Method for Gold Nanoparticle Synthesis Revisited. *J. Phys. Chem. B* **2006**, *110* (32), 15700–15707. https://doi.org/10.1021/jp061667w
(55) Méndez, E.; Fagúndez, P.; Sosa, P.; Gutiérrez, M. V.; Botasini, S. Experimental Evidences Support the Existence of an Aggregation/Disaggregation Step in the Turkevich Synthesis of Gold Nanoparticles. *Nanotechnology* **2021**, *32* (4), 045603. https://doi.org/10.1088/1361-6528/abbfd5
(56) Fagúndez, P.; Botasini, S.; Tosar, J. P.; Méndez, E. Systematic Process Evaluation of the Conjugation of Proteins to Gold Nanoparticles. *Heliyon* **2021**, *7* (6), e07392. https://doi.org/10.1016/j.heliyon.2021.e07392
(57) International Organization for Standardization (ISO). *Particle Size Analysis — Dynamic Light Scattering (DLS)*. ISO-22412:2017.
(58) Schindelin, J.; Arganda-Carreras, I.; Frise, E.; Kaynig, V.; Longair, M.; Pietzsch, T.; Preibisch, S.; Rueden, C.; Saalfeld, S.; Schmid, B.; et al. Fiji: An Open-Source Platform for Biological-Image Analysis. *Nat. Methods* **2012**, *9* (7), 676–682. https://doi.org/10.1038/nmeth.2019
(59) Botasini, S. Comparación del Tamaño de Nanopartículas de Oro Empleando Diferentes Técnicas y Protocolos de Medición. *INNOTEC* **2020**, No. 21, 10–24. https://doi.org/10.26461/21.02

(60) National Institute of Standards and Technology (NIST). Bonevich, J.; Haller, W. *Measuring the Size of Nanoparticles Using Transmission Electron Microscopy (TEM)*. NIST–Nanotechnology Characterization Laboratory (NCL) Joint Assay Protocol, PCC-X, Version 1.1, 2010. Gaithersburg, MD. Available at: https://tsapps.nist.gov/publication/get_pdf.cfm?pub_id=854083 (accessed: 10/2024)
(61) Abarca, C.; Ali, M. M.; Yang, S.; Dong, X.; Pelton, R. H. A Colloidal Stability Assay Suitable for High-Throughput Screening. *Anal. Chem.* **2016**, *88* (5), 2929–2936. https://doi.org/10.1021/acs.analchem.5b04915
(62) Britton, G.; Liaeen-Jensen, S.; Pfander, H. *Carotenoids: Handbook*. Birkhäuser Basel: Basel, 2004. https://doi.org/10.1007/978-3-0348-7836-4
(63) Stetefeld, J.; McKenna, S. A.; Patel, T. R. Dynamic light scattering: a practical guide and applications in biomedical sciences. *Biophys. Rev.* **2016**, *8* (4), 409–427. https://doi.org/10.1007/s12551-016-0218-6
(64) Tyndall, J. IV. On the blue colour of the sky, the polarization of skylight, and on the polarization of light by cloudy matter generally. *Proc. R. Soc. London* **1869**, *17*, 223–233. https://doi.org/10.1098/rspl.1868.0033
(65) Kerker, M.; Loebl, E. M. *The Scattering of Light and other Electromagnetic Radiation*. Elsevier Science, Saint Louis, 2016.
(66) Humzah, M. D. Tyndall, Rayleigh, Mei, and Raman scattering: Understanding their role in aesthetics. *Journal of Cosmetic Dermatology* **2024**, *23* (11), 3493–3496. https://doi.org/10.1111/jocd.16470
(67) Mie, G. “Beiträge zur Optik trüber Medien, speziell kolloidaler Metallösungen”. *Annalen der Physik* **1908**, *330* (3), 377–445. https://doi.org/10.1002/andp.19083300302
(68) Mishchenko, M. I. Gustav Mie and the fundamental concept of electromagnetic scattering by particles: A perspective. *J. Quant. Spectrosc. Radiat. Transfer* **2009**, *110* (14–16), 1210–1222. https://doi.org/10.1016/j.jqsrt.2009.02.002
(69) Xu, R. Electrophoretic Light Scattering / Zeta Potential Measurement. In: Scarlett, B. (Ed.). *Particle Characterization: Light Scattering Methods*. Springer Netherlands: Dordrecht, 2002, Chapter 6, pp 289–343. https://doi.org/10.1007/0-306-47124-8_6
(70) Čižmek, L.; Komorsky-Lovrić, Š. Study of Electrochemical Behaviour of Carotenoids in Aqueous Media. *Electroanalysis* **2019**, *31* (1), 83–90. https://doi.org/10.1002/elan.201800531
(71) Komorsky-Lovrić, Š. Voltammetry of Azobenzene Microcrystals. *J. Solid State Electrochem.* **1997**, *1* (1), 94–99. https://doi.org/10.1007/s100080050028
(72) Montagni, T.; Chialanza, M. R.; Cerdá, M. F. Blueberries as a Source of Energy: Physical Chemistry Characterization of their Anthocyanins as Dye-Sensitized Solar Cells’ Sensitizers. *Solar* **2023**, *3* (2), 283–297. https://doi.org/10.3390/solar3020017
(73) Silverstein, R. M.; Webster, F. X.; Kiemle, D. J. *Spectrometric Identification of Organic Compounds*, 7th ed. John Wiley & Sons: Hoboken, NJ, 2005.

SUPPLEMENTARY MATERIAL

Carotenoid concentration calculation

According to Britton, G. et al. 2004 (reference No. 62 in the article), the molar absorption coefficient of carotenoids can be estimated using Equation (1):

$$\varepsilon = \left(A^{1\%} \times molecular\ weight\right)/10 \qquad \text{Equation (1)}$$

Where $A^{1\%}$ is defined as the theoretical absorbance of a solution of 1% (w/v) concentration in a cuvette with a path length of b = 1 cm.

According to Kishimoto, S. et al. 2005 (reference No. 43 in the article), the main carotenoids present in *Calendula officinalis* are flavoxanthin (28.5 %), luteoxanthin (11.0 %) and lycopene (8.7 %). Taking these carotenoids as the only components in the sample (normalized to 100%), these percentages become 59.1%, 22.8%, and 18.1% for flavoxanthin, luteoxanthin, and lycopene, respectively. From the handbook previously mentioned (reference No. 62 in the article), $A^{1\%}$ at the absorption maxima of these carotenoids were found to be:

$$A^{1\%}_{Lycopene} = 3450,\ A^{1\%}_{Flavoxanthin} = 2570,\ \text{and}\ A^{1\%}_{Luteoxanthin} = 2940$$

The molecular weights of these carotenoids are:
$MW_{Lycopene}$ = 536 g mol^{-1}, $MW_{Flavoxanthin}$ = 568 g mol^{-1} and $MW_{Luteoxanthin}$ = 568 g mol^{-1}

Applying Equation (1), the absorption coefficients are:

$\varepsilon_{Lycopene}$ = (3450 × 536)/10 = 184,920 L mol^{-1} cm^{-1}
$\varepsilon_{Flavoxanthin}$ = (2570 × 568)/10 = 145,976 L mol^{-1} cm^{-1}
$\varepsilon_{Luteoxanthin}$ = (2940 × 568)/10 = 166,992 L mol^{-1} cm^{-1}

Meanwhile, applying the additivity property of absorptivity, the mixture coefficient is:

$\varepsilon_{mix} = \sum(xi \times \varepsilon_i)$.

So, for *C. officinalis* it is:

ε_{cale} = (0.591×145,976) + (0.228 × 166,992) + (0.181 × 184,920) = 157,817 L mol^{-1} cm^{-1}

Once the ε_{cale} was determined, carotenoids concentration in *Calendula officinalis* determination is trivial, by the *Bouguer-Lambert-Beer's Law*, in this sense:

For 1E extraction:

A_1 = 0.6311 × 50 = 31.555, [Carotenoid] = 31.555 / (157,817 × 1) = 0,000199947 M

A_2 = 1.0074 × 30 = 30.222, [Carotenoid] = 30.222 / (157,817 × 1) = 0,0001915 M

The, 1E extraction concentration is [Carotenoid] = (0,196 ± 0,006) mM

Analogously, for 2E extraction:

A_1 = 0.6951 × 100 = 69.51, [Carotenoid] = 69.510 / (157,817 × 1) = 0,000440447 M

A_2 = 1.3395 × 50 = 69.975, [Carotenoid] = 69.975 / (157,817 × 1) = 0,000443393 M

The, 2E extraction concentration is [Carotenoid] = (0,442 ± 0,002) mM

AuNP-Cit UV-Vis spectra

AuNP-Cit UV-Vis spectra were taken in serial dilutions. The LSPR position was determined by taking the point where the derivative of $d_{Abs}/d\lambda = 0$ (curve maxima).

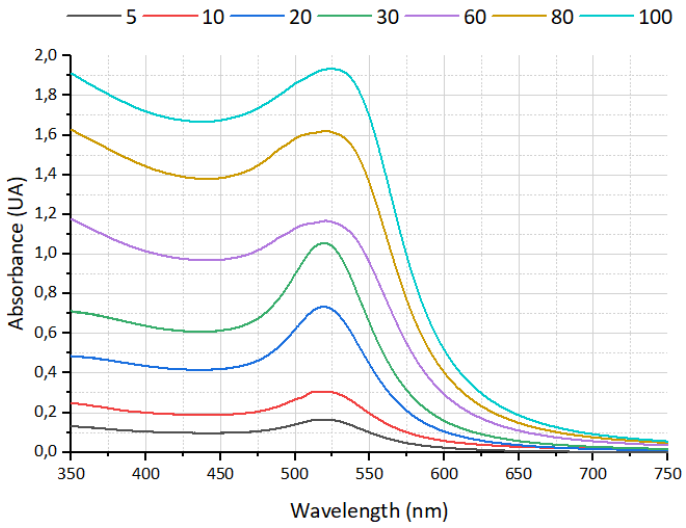

Figure SM-1. AuNP-Cit absorbance spectra in serial dilutions. The legend refers to % v/v, where 100% is the Turkevich synthesis product ([AuNP] ≈ 10 nM).

AuNP-Cit DLS

To determine the hydrodynamic diameter of AuNP-Cit particles, DLS measurements were performed.

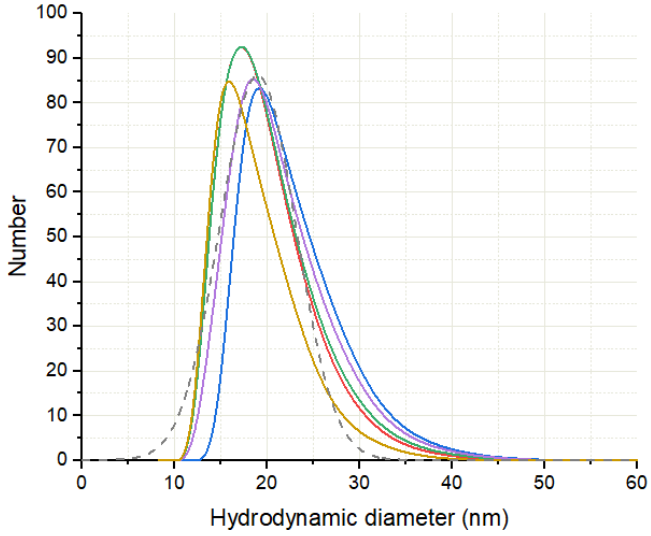

Figure SM-2. Number distribution as a function of hydrodynamic diameter of AuNP-Cit particles in suspension. Solid lines represent individual measurements () and the dashed line corresponds to the gaussian fitting of the average curve of all measurements (average curve not shown). Hydrodynamic diameter obtained: d_h = 19 ± 3 nm.

AuNP-Cit VS Ethanol proportion optimization

To determine the optimal AuNP-Cit VS Ethanol proportion, UV-Vis spectra were recorded at increasing proportion of EtOH, from (1:9) to (1:1) against AuNP.

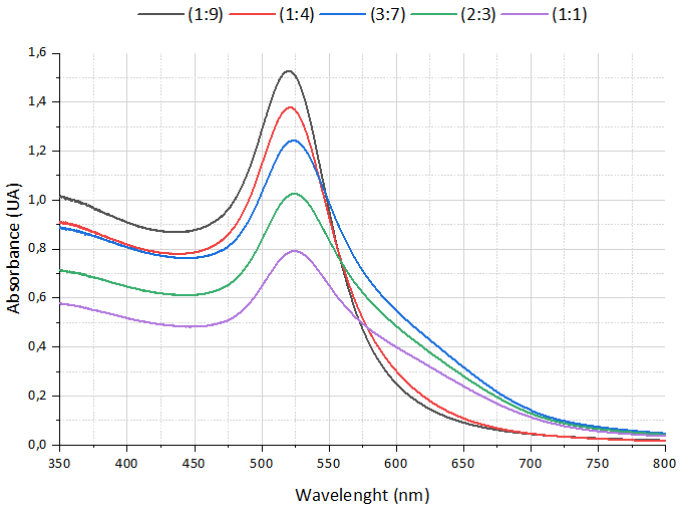

Figure SM-3. Visible spectra of AuNP-Cit with increasing proportion of EtOH (legend above graph).

AuNP-Cale UV-Vis and LSPR shift

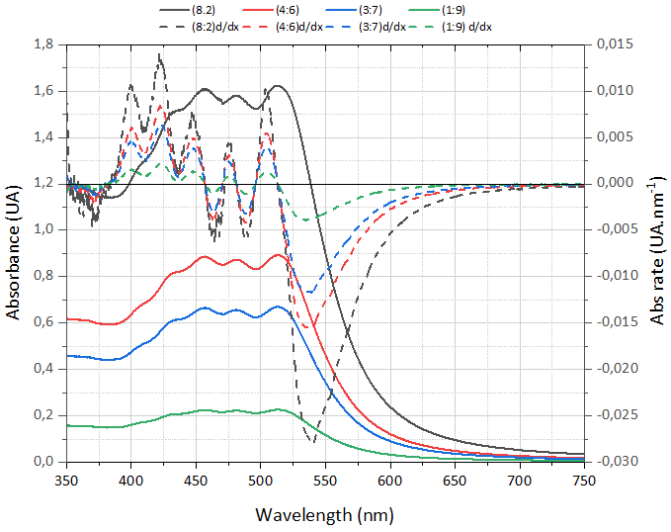

Figure SM-4. UV-Vis spectra of AuNP-Cale and it's first derivatives (denoted absorbance rates) with increasing dilution in water. Straight lines represent the UV-Vis spectra, while dashed lines represent the absorbance rates (legend above graph). An auxiliar axis at $d_{Abs}/d\lambda = 0$ was added to facilitate maxima's reading.

Brazilian Journal of Analytical Chemistry
2026, Volume 13, Issue 51, pp 79-93
doi: 10.30744/brjac.2179-3425.TN-56-2025

BrJAC

TECHNICAL NOTE

Risk-Based Selection of Active Pharmaceutical Ingredients in the Development of HPLC and NIR Methods for Pediatric Preparations

Juan Barbagelata*[1,2], Ana Vidarte[2], Ana Ochoa[2], Mariela Pistón*[3]

[1]*Graduate Program in Chemistry, Facultad de Química, Universidad de la República, Avda. Gral. Flores 2124, Montevideo 11800, Uruguay*

[2]*Área de Tecnología Farmacéutica y Control de Calidad de Medicamentos, CIENFAR, Facultad de Química, Universidad de la República, Avda. Gral. Flores 2124, Montevideo 11800, Uruguay*

[3]*Grupo de Análisis de Elementos Traza y Desarrollo de Estrategias Simples para Preparación de Muestras (GATPREM), Química Analítica (DEC), Facultad de Química, Universidad de la República, Montevideo 11800, Uruguay*

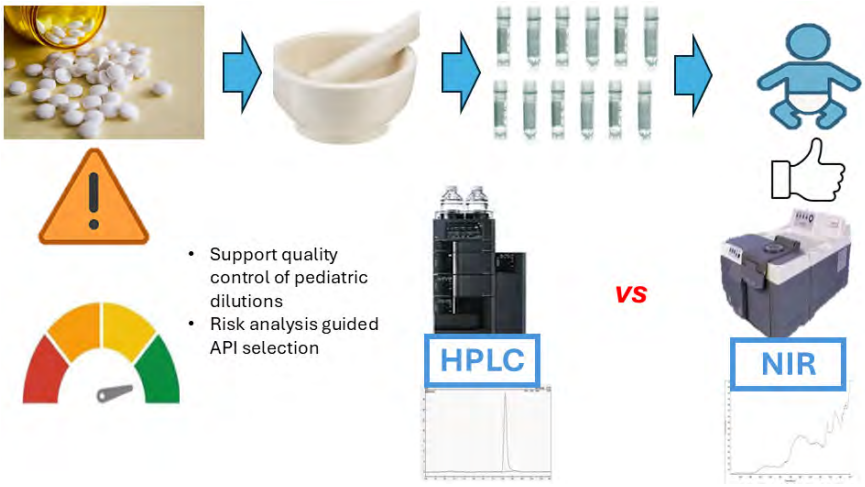

The lack of appropriate formulations for the pediatric population often requires the manipulation of adult dosage forms in hospital settings, a practice that can lead to errors that impact patient safety. This study aimed to support the quality control of pediatric preparations by developing and validating analytical methods for the quantification of active pharmaceutical ingredients (APIs) in the tablets used for their elaboration. Folic acid and phenobarbital were selected based on a risk analysis as the priority APIs to work with. High-performance liquid chromatography (HPLC) and Near-infrared (NIR) spectroscopy methods for the quantification of these APIs in commercially available products were developed and validated. NIR methods are presented as a rapid and non-destructive alternative that offers the possibility of determining the content of the same tablets that will be used to prepare the pediatric dilution. This could be considered as a promising analytical tool for drug quality control during the elaboration process of these preparations.

Keywords: Near-infrared spectroscopy, pediatric preparations, folic acid, phenobarbital, drug quality control

Cite: Barbagelata, J.; Vidarte, A.; Ochoa, A.; Pistón, M. Risk-Based Selection of Active Pharmaceutical Ingredients in the Development of HPLC and NIR Methods for Pediatric Preparations. *Braz. J. Anal. Chem.* 2026, *13* (51), pp 79-93. http://dx.doi.org/10.30744/brjac.2179-3425.TN-56-2025

Received: June 26, 2025; **Revised:** August 21, 2025; September 11, 2025; **Accepted:** September 30, 2025; **Published online:** October 16, 2025.

This Technical Note is part of the BrJAC Special Issue on the 8th Uruguayan Congress of Analytical Chemistry (CUQA 8 2024).

INTRODUCTION

There is a global shortage of medicines suitable for the pediatric population, as the pharmaceutical industry has conducted limited research in this area due to technical, economic, and ethical reasons.[1-3] As a result, there are relatively few formulations appropriate for children,[1] often leading to use of medications formulated for adults outside their approved indications (off-label) or their manipulation (e.g., splitting or crushing tablets) to obtain suitable pediatric doses.[4]

Off-label use is widespread, with reported prevalence ranging from 3.3% to 94%, with the highest rates commonly observed in neonatal clinical care settings.[3] A common practice in hospital settings is the preparation of solid dilutions from adult medications. At the Pharmacy Department of the *Hospital de Clínicas* (University Hospital, Montevideo, Uruguay), for instance, pediatric dilutions are routinely prepared to treat preterm and neonatal patients at the institution. These dilutions are made by grinding tablets in a mortar and mixing them with an excipient, such as lactose, before being divided into vials. Errors in this process—such as improper mixing or segregation of the blend during portioning—can lead to dose non-uniformity and result in inadequate treatment. This risk is heightened by the absence of standardized guidelines or procedures for these preparations.[5]

These circumstances highlight the need to study and standardize the processes of elaboration to ensure the safety and efficacy of pediatric treatments. The objective, therefore, is to ensure the quality and assess the uniformity of the prepared pediatric dilutions, as well as to determine their shelf life. Achieving this goal requires suitable analytical methods for quantifying the active pharmaceutical ingredient in the initial dosage form and its dilution.

Near-infrared spectroscopy (NIR) is proposed as a rapid and non-destructive technique with various applications in the pharmaceutical industry reported, including identification tests, quantification, and process monitoring.[6] NIR can be applied to analyze both the source tablets and the corresponding dilutions once prepared. Analyzing the source tablets will ensure the selection of the most suitable for pediatric preparation. This is particularly relevant considering that, according to the acceptance criteria for the Uniformity of Dosage Units test, tablet content may vary approximately between 75% to 125% of the labeled amount,[7] potentially impacting the accuracy of the prepared doses.

MATERIALS AND METHODS

Instruments

High-performance liquid chromatography (HPLC) analyses were conducted using an Agilent 1100 HPLC system equipped with a variable wavelength UV detector. Near-infrared (NIR) spectroscopy was performed using a Thermo Scientific Antaris II DR analyzer, operated with Result 4.5.159 and TQ Analyst 9.12.116 software for data acquisition and analysis.

Reagents and chemicals

For HPLC method development, folic acid (90.54%, Sigma, Germany), phenobarbital (99.7%, Fármaco Uruguayo, Uruguay) secondary standards were used. Other reagents were of analytical grade, and methanol was of HPLC gradient grade. Type II purified water was obtained by distillation in the laboratory. For NIR analysis, no additional reagents were required, as measurements were performed on intact tablets.

Four products from different suppliers of folic acid tablets available on the Uruguayan market (two containing 1 mg and two containing 0.8 mg of folic acid) were analyzed, along with the only available local product containing 100 mg of phenobarbital, which is used by the *Hospital de Clínicas* Pharmacy Service.

Survey for pediatric dilutions

A survey at the *Hospital de Clínicas* Pharmacy Service to obtain records of the prepared pediatric solid dilutions from the period between 2012 and 2022 was conducted. Folic acid and phenobarbital emerged as the most frequently used APIs.

Telephone consultations with hospital pharmacies across Uruguay revealed varied practices. Many hospitals, lacking pediatric units, did not prepare dilutions, while others outsourced to a particular laboratory, where hydrocortisone, captopril, and clonidine were prevalent.

The survey revealed distinct API needs, *Hospital de Clínicas* prioritizing folic acid and phenobarbital, while in other institutions hydrocortisone and other APIs prevailed.

Risk analysis

To select the active ingredients to be studied, a risk analysis was conducted to prioritize those active ingredients whose study could have the greatest impact. The analysis was restricted to data from the *Hospital de Clínicas*, as data from this service apply to a small subgroup of the high-risk pediatric population, such as newborn and preterm patients.

To prioritize APIs for method development, a risk analysis was carried out, based on the principles of failure mode and effects analysis (FMEA).[8,9] This kind of analysis is based on prior knowledge, the probability of failures occurring in a manufacturing process that is the same for all active ingredients, the severity of the lack of quality in solid dilutions according to the active ingredient, and the ability to detect failures if they occur. The risk factors associated with each API were identified to determine the parameters.

Probability of failure

Probability of failure was assessed based on three factors:

1. **Preparation frequency:** APIs prepared more frequently (e.g., daily vs. monthly) were assigned higher scores due to increased opportunities for errors. In this way, a value was assigned to each API according to Table I.

Table I. Scores associated with preparation frequencies

Preparation frequency	Score
Monthly or less	10
Between monthly and annual	5
Annual or higher	1

2. **Dilution level:** higher dilutions increased the risk of non-uniform mixing, increasing the probability of failure. Based on the highest dilution level possible for each API, a score was assigned according to Table II.

Table II. Scores associated with dilution level

Dilution level	Score
Higher than 1:200	10
1:100 – 1:200	7
1:50 – 1:100	5
1:10 – 1:50	3
1:1 – 1:10	1

3. **API environmental sensitivity:** during the compounding process, APIs will be exposed to environmental conditions. These conditions can affect the API differently, depending on its sensitivity. The more sensitive the API, the greater the likelihood of failure. Storage conditions recommended by recognized suppliers were considered to assess whether an active ingredient is sensitive to temperature, humidity, and light in each case. Each condition was assessed independently by assigning a score of 2 if the API is sensitive to the environmental condition and 1 otherwise. Finally, the sensitivity to the environmental conditions was calculated as the product of the scores for each condition.

Each factor was scored independently, averaged, and normalized to a 1–10 scale.

Severity of failure

Severity was evaluated using two pharmacological parameters:

1. **Minimum daily dose:** APIs with lower minimum doses indicates that a dosage error is likely to have an adverse effect on the patient. Thus, a score was assigned to each API according to Table III.

Table III. Scores associated with minimum daily dose

Minimum daily dose	Score
(1 – 10) mg	10
(10 – 100) mg	5
Higher than 100 mg	1

2. **Lethal dose (LD50):** to assess the toxicity of each API, data on the lethal dose 50 in rats is evaluated. In cases where this information is unavailable, the values obtained for mice are considered. The use of the values obtained in mice is considered not to affect the evaluation, thus the wide ranges used to assign scores. Considering that substances are more toxic at lower lethal doses 50, scores were assigned for the different active ingredients according to Table IV.

Table IV. Scores associated with lethal dose 50

LD50	Score
Less than 200 mg kg^{-1}	10
(20 – 2000) mg kg^{-1}	5
More than 200 mg kg^{-1}	1

These parameters were averaged and normalized to a 1–10 scale.

Detectability of failure

As no analytical controls were routinely applied during dilution preparation, all APIs received the maximum score of 10, reflecting the absence of methods to detect errors during the elaboration process.

From the values obtained, the risk priority number (RPN) is calculated as the product of probability, severity and detectability.

The values obtained will allow professionals to reach a decision on which active ingredients are prioritized for work. The results were classified as presented in Table V.

Table V. Classification of priorities according to RPN values

RPN	Score
Less than 100	Low priority
100 – 200	Medium priority
Higher than 200	High priority

HPLC method development

Folic acid

The HPLC method for folic acid quantification in tablets was developed with a UV detector set at 280 nm. Chromatographic conditions were optimized through a central composite design. Based on prior knowledge, critical methods attributes (CMAs), proportion of organic solvent (8%–12% v/v methanol), column temperature (20 ºC–40 °C), and mobile phase pH (5.6–7.2), were selected to evaluate their impact on the critical quality attributes (CQAs) defined for the method: retention time, resolution between folic acid and leucovorin, and peak symmetry. The effects of the studied factors on the defined CQAs were first evaluated using the regression coefficients and their statistical significance (p-values <0,05) (Table VI), together with the standardized effect estimates with their 95% confidence intervals, as shown in Figure 1.

Table VI. Regression coefficients and their p-value in folic acid HPLC method development

	Peak Symmetry		Resolution		Retention Time	
	Coefficient	p-value	Coefficient	p-value	Coefficient	p-value
Buffer pH (pH)	0,0303	0,0442	-0,1554	<0,0001	-1,5490	<0,0001
Methanol Content (%MeOH)	0,0498	0,0050	-0,1509	<0,0001	-1,2513	<0,0001
Temperature (T)	0,0750	0,0005	-0,1839	<0,0001	-0,3413	0,0003
pH*pH	-0,0124	0,6188	0,0716	<0,0001	0,3577	0,0084
%MeOH*%MeOH	0,0211	0,4076	0,0164	<0,0001	0,1742	0,1205
T*T	0,0131	0,6019	0,0224	<0,0001	-0,1488	0,1750
pH*%MeOH	0,0143	0,3373	0,0252	<0,0001	0,4224	0,0001
pH*T	0,0278	0,0849	0,0150	<0,0001	-0,1821	0,0152
%MeOH*T	0,0275	0,0872	0,0269	<0,0001	-0,0074	0,9008

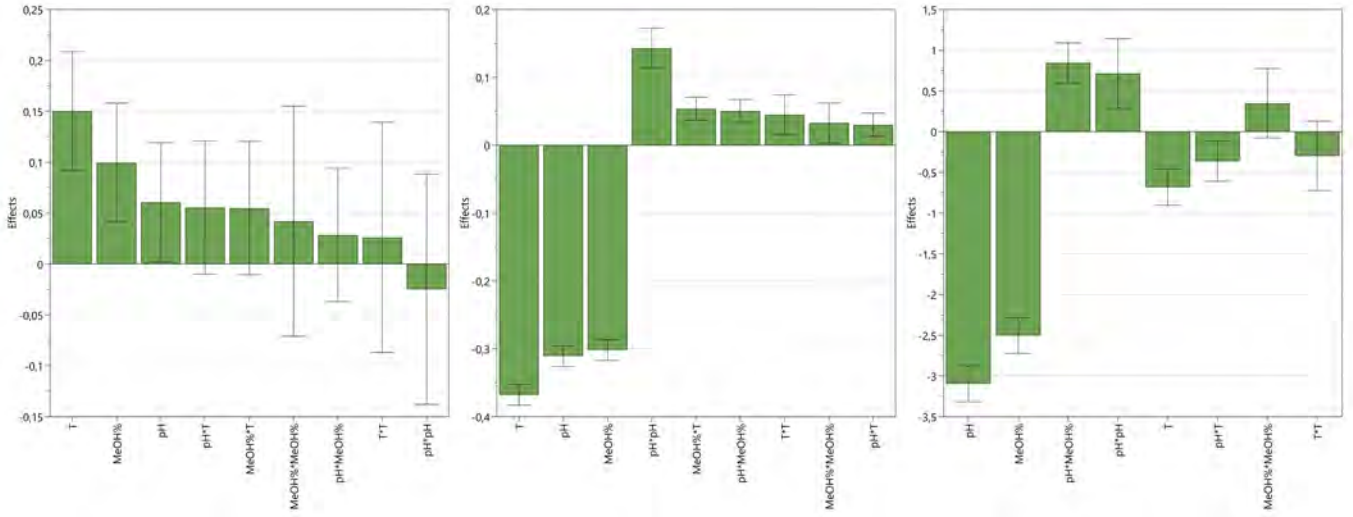

Figure 1. Standardized effects plots obtained for CQAs in folic acid HPLC method development.

A predictive model was then constructed using Multiple Lineal Regression (MLR), excluding non-significant factors (p-values <0,05). Model was assessed through the determination coefficients (R^2) and predictive ability (Q^2) presented in Table VII. The model presents good correlation and strong predictive ability for retention time and number of theoretical plates, while peak symmetry showed moderate correlation and acceptable predictive power.

Table VII. Regression model parameters for the CQAs in folic acid HPLC method development

CQA	R^2	Q^2
Peak Symmetry (Tailing)	0.769	0.560
Resolution	0.999	0.984
Retention time	0.993	0.977

Finally, response contour plots were generated to visualize the effect of the most influential factors and their interactions on the chromatographic performance (Figure 2). The analysis showed that retention time was affected by methanol content, pH and temperature, while resolution was strongly dependent on methanol content and pH. Peak symmetry proved relatively robust with only minor contributions from temperature and methanol content.

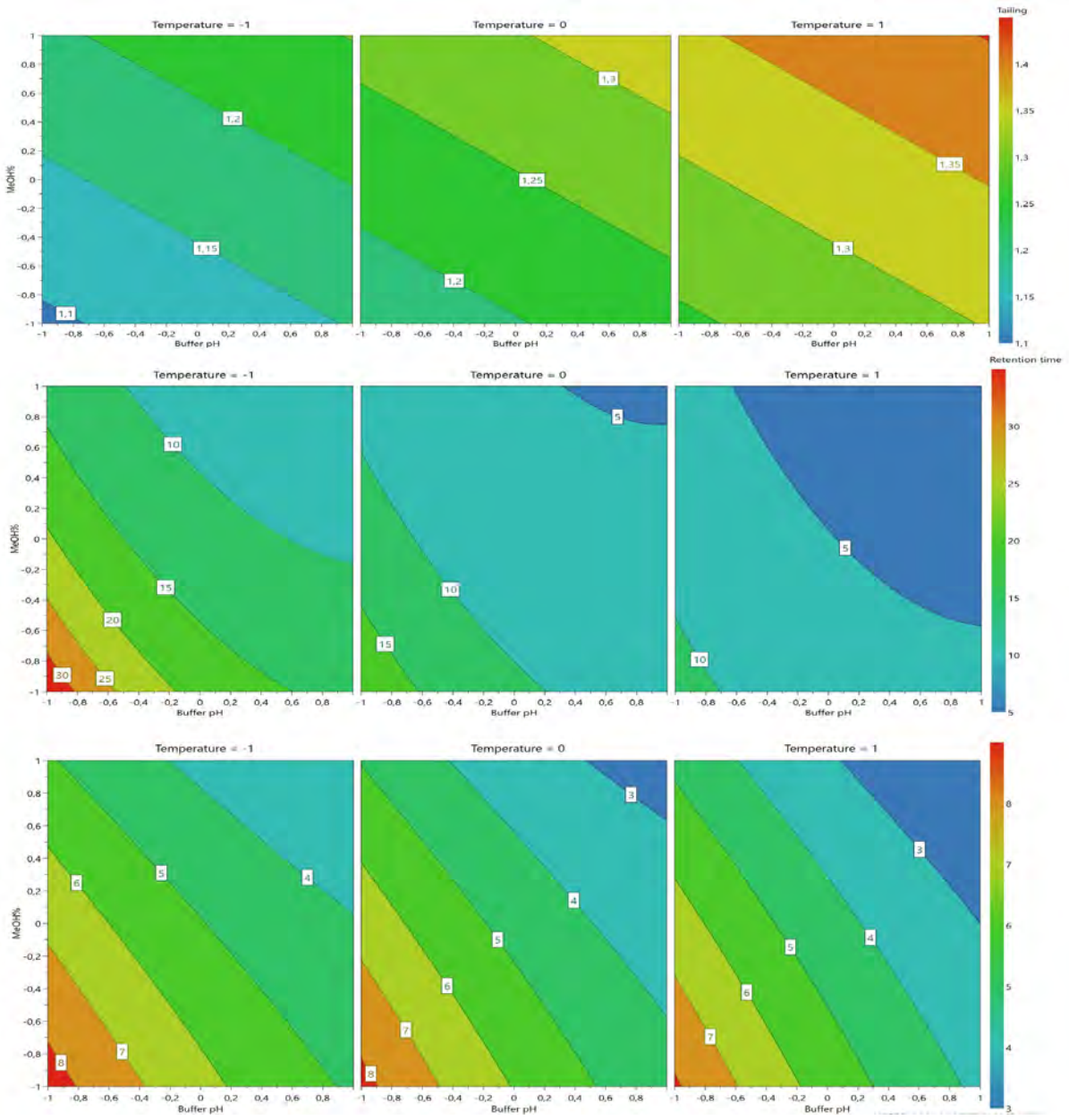

Figure 2. Response contour plots of the factor on the CQAs in folic acid method development.

The optimized conditions were: Zorbax Eclipse XDB C18 column (250 mm × 4.6 mm, 5 µm), mobile phase of phosphate buffer (pH 6.4):methanol (90:10), column temperature of 30 °C, flow rate of 1.0 mL min^{-1}, and injection volume of 25 µL.

Sample preparation involved placing one tablet in a 100.00 mL volumetric flask, adding 2.5 mL of sodium carbonate solution (28 g L^{-1}) and 50.0 mL of purified water, and agitation for 20 minutes using an orbital shaker. The solution was brought to volume with purified water, homogenized in an ultrasonic bath, allowed to settle, and filtered through 0.45 µm cellulose filters. A 10 mg L^{-1} standard solution of folic acid was prepared in purified water with the same volume of sodium carbonate solution added to aid dissolution.

Phenobarbital

The HPLC method for phenobarbital quantification was developed with a UV detector set at 254 nm. A fractional factorial screening design of resolution IV, to evaluate the impact of potentials CMAs like pH (3.8–5.0) and ionic strength (50 mM–200 mM) of the buffer component of the mobile phase, as well as methanol percentage (30%–70%), column temperature (25 ºC–35 °C), flow rate (0.6 mL min^{-1}–1.2 mL min^{-1}), and injection volume (10 µL–50 µL), on CQAs defined for the method: retention time, number of theoretical plates, and peak symmetry. As for phenobarbital, the influence of the studied factors on the selected CQAs was initially assessed by examining the regression coefficients and their statistical significance (p-values <0,05) (Table VIII), together with the standardized effect estimates with their 95% confidence intervals, as shown in Figure 3.

Table VIII. Regression coefficients and their p-value in phenobarbital HPLC method development

	Peak Symmetry		Number of Theoretical Plates		Retention Time	
	Coefficient	**p-value**	**Coefficient**	**p-value**	**Coefficient**	**p-value**
pH Buffer	-0,0019	0,8884	-360,69	0,3881	-0,8085	0,6963
MeOH%	0,0779	0,0001	-2583,44	<0,0001	-15,3244	<0,0001
Temperature	-0,0091	0,5003	1590,81	0,0019	-1,4254	0,4943
Ionic Strength	-0,0075	0,5785	3,5639	0,9931	-0,9416	0,6497
Flow	0,0066	0,6231	-2767,44	<0,0001	-6,1285	0,0104
Injection Volume	-0,0070	0,6038	642,81	0,1364	0,0916	0,9646

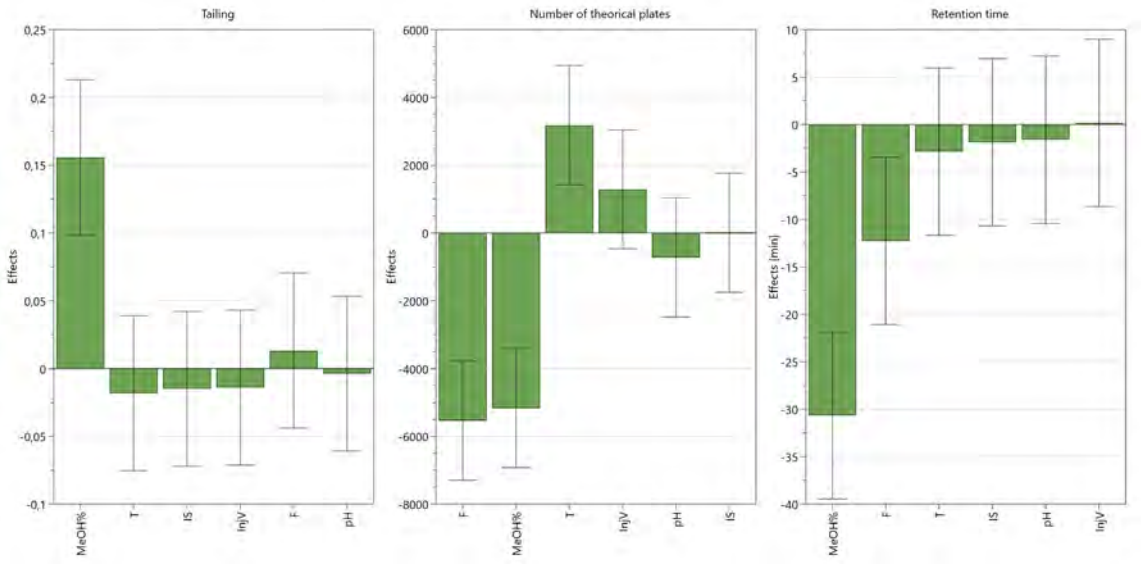

Figure 3. Standardized effects plots obtained for CQAs in phenobarbital HPLC method development.

A MLR model was built, excluding non-significant factors. As shown in Table IX, the model achieved good correlation and predictive ability for retention time and number of theoretical plates, while peak symmetry displayed moderate correlation and predictive power.

Table IX. Regression model parameters for the CQAs in phenobarbital method development

CQA	R2	Q2
Peak Symmetry (Tailing)	0.725	0.656
Number of Theoretical Plates	0.925	0.850
Retention time	0.909	0.879

Contour plots were generated to offer a graphical interpretation of the influence of the key factors and their interactions on the CQAs (Figure 4). The methanol proportion was identified as the most influential factor, simultaneously reducing retention time, decreasing efficiency, and increasing peak tailing. Flow rate also had a marked effect on retention time, while higher temperatures improved efficiency. Buffer pH and ionic strength contributed mainly to column efficiency, whereas peak symmetry proved relatively robust, showing only minor sensitivity to column temperature and injection volume.

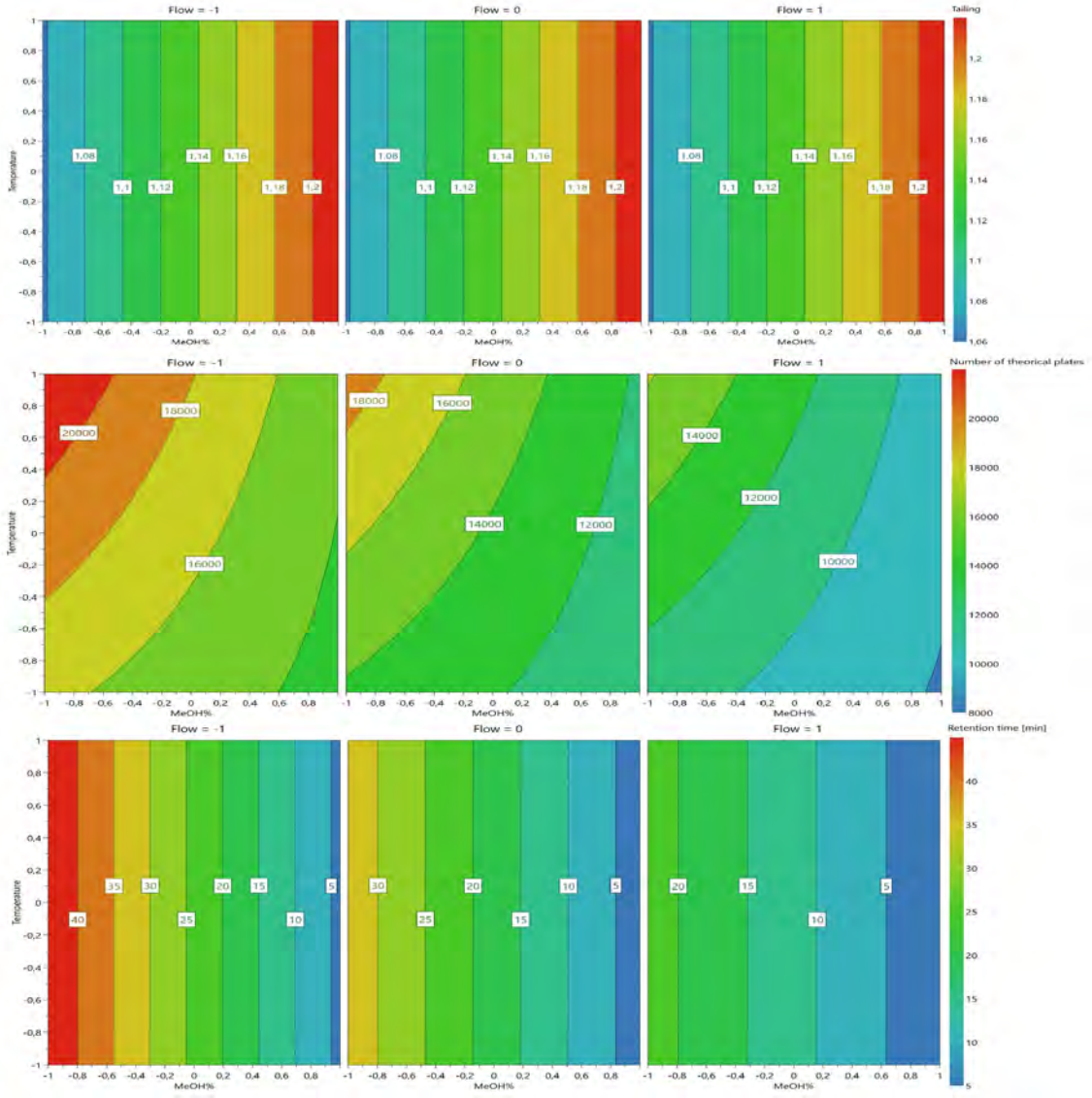

Figure 4. Response surface contour plots of the factor on the CQAs in phenobarbital method development.

The final method conditions were: Waters Symmetry C18 column (250 mm × 4.6 mm, 5 µm), mobile phase of 200 mM acetate buffer (pH 3.8): methanol (60:40), column temperature of 35 °C, flow rate of 1.0 mL min^{-1}, and injection volume of 35 µL.

Sample preparation involved placing one tablet in a 100.00 mL volumetric flask, adding 50.0 mL of purified water, and agitation for 20 minutes on an orbital shaker. The solution was brought to volume with purified water, homogenized in an ultrasonic bath, and allowed to settle. A 5.00 mL aliquot was diluted to 50.00 mL with purified water and filtered through 0.45 µm cellulose filters. A 10 mg L^{-1} standard solution of phenobarbital prepared in purified water.

NIR method development

Calibration sets consisted of 30 tablets per product, analyzed by both HPLC (as the reference method) and NIR. Tablets were scanned in diffuse reflectance mode over the 4000–10000 cm^{-1} range, with 32 scans averaged per spectrum at a resolution of 8 cm^{-1}. A calibration model was built using Partial Least Squares (PLS) regression to correlate NIR spectra with API concentrations determined by HPLC, optimizing the number of PLS factors to minimize the root mean square error of calibration (RMSEC).[10] Pre-processing techniques, including standard normal variate (SNV) transformation and first-derivative smoothing, were applied to reduce baseline shifts and enhance spectral features.[11] Figure 5 shows a NIR spectrum of folic acid tablets from Product 1, while Figure 6 presents the corresponding spectrum for phenobarbital tablets.

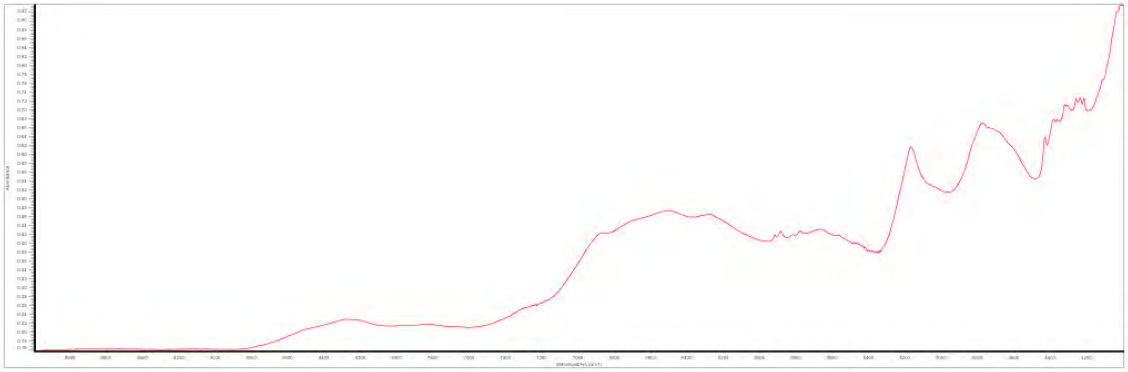

Figure 5. NIR spectrum of folic acid tablets from Product 1.

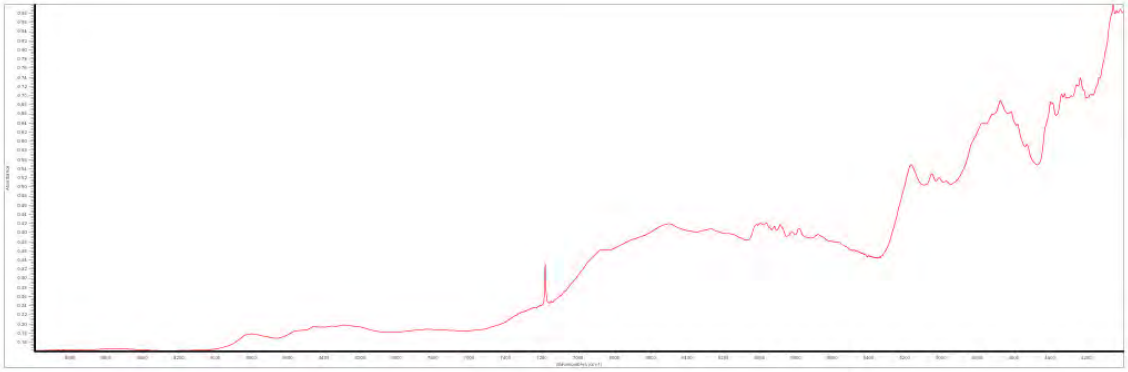

Figure 6. NIR spectrum of phenobarbital tablets.

Method validation

The analytical procedure validation was performed following the recommendations of the International Council for Harmonization of Technical Requirements for Pharmaceuticals for Human Use (ICH) Q2 guidelines.[12] The performance characteristics evaluated for both HPLC methods were accuracy, repeatability, linear response and specificity.

Validation of the novel proposed methodology using NIR was conducted with an independent set of 10 tablets per API, scanned under the same conditions as the calibration set. The performance characteristics evaluated were accuracy and repeatability.

RESULTS AND DISCUSSION

Survey and risk analysis

The survey identified folic acid and phenobarbital as the most frequently used APIs at the *Hospital de Clínicas*, primarily for neonates and preterm infants, with lactose as the diluent excipient. Other institutions reported hydrocortisone, captopril, and others, reflecting different pediatric subgroups. The FMEA results (Table X) confirmed folic acid and phenobarbital as critical APIs. Folic acid's high RPN resulted from frequent preparation, low therapeutic dose, and poor detectability, while phenobarbital's RPN reflected frequent use, high dilution levels, and a narrower therapeutic window. The risk-based approach ensured that method development targeted APIs with the greatest potential impact on patient safety, particularly for vulnerable neonates.

Based on the risk factors considered in this analysis, the control strategy prioritized the development of analytical methods to enhance the detectability of potential quality deviations.

Table X. Risk Analysis Summary for Selected APIs at Hospital de Clínicas

API	Probability	Severity	Risk	Detectability	RPN
Amiodarone	2	1	2	10	20
Captopril	6	3	17	10	165
Chlorpromazine	4	8	30	10	300
Ciprofloxacin	2	3	6	10	60
Fluconazole	2	3	6	10	60
Folic Acid	8	6	41	10	413
Furosemide	2	3	6	10	60
Hydrochlorothiazide	2	3	6	10	60
Hydrocortisone	3	3	9	10	90
Levetiracetam	1	1	1	10	10
Levothyroxine	1	10	10	10	100
Leucovorin	1	3	3	10	30
Nelfinavir	2	1	2	10	20
Nevirapine	2	1	2	10	20
Phenobarbital	5	8	38	10	375
Phenytoin	2	3	6	10	60

(continued on next page)

Table X-cont. Risk Analysis Summary for Selected APIs at Hospital de Clínicas

API	Probability	Severity	Risk	Detectability	RPN
Pyridostigmine	2	6	11	10	110
Pyrimethamine	2	5	10	10	100
Propranolol	3	3	9	10	90
Sildenafil	2	5	10	10	100
Spironolactone	2	5	10	10	100
Sucralfate	3	1	3	10	30
Sulfadiazine	2	1	2	10	20
Ursodeoxycholic Acid	2	1	2	10	20
Valganciclovir	2	1	2	10	20
Vigabatrin	2	1	2	10	20
Vitamin B1	2	3	6	10	60

HPLC method

The HPLC methods for folic acid and phenobarbital were validated according to the ICH guidelines.[12] Evaluation of linear response included visual inspection of the calibration curves, assessment of the determination coefficient (R^2), and confirmation of homoscedasticity and linearity of residuals. Linear response was achieved over 25–150 mg L^{-1} for phenobarbital and over 2.5–15 mg L^{-1} for folic acid. The calibration functions were $y = 9.00\times10^{7}\cdot x + 801$ ($R^2 = 0.9997$) for folic acid and $y = 1.11\times10^{7}\cdot x + 4.35\times10^{3}$ ($R^2 = 0.9998$) for phenobarbital where *y* was the peak area and *x* was the analyte concentration in mg mL^{-1}.

Specificity was verified through forced degradation studies. For folic acid, 5.0 mL of a 1.0 mg mL^{-1} solution were exposed to the conditions presented in Table XI, while for phenobarbital, 5.0 mL of a 0.5 mg mL^{-1} solution were exposed to the conditions presented in Table XII. The percentage of degradation observed under each condition is summarized in Tables XI and XII. This percentage was calculated as the difference in API content measured in the stressed solution compared to an unstressed reference solution. Folic acid exhibited significant degradation to oxidative and photolytic stress highlighting the need for light protection during handling and storage. In contrast, phenobarbital proved generally stable, showing significant degradation only under basic hydrolytic conditions, while no relevant degradation was observed under the other stress conditions. In all conditions studied, a resolution greater than 2 was obtained for both analytes in relation to the main degradation products, demonstrating that both methods are stability-indicating. For folic acid, specificity was further confirmed by evaluating structurally related compounds such as p-aminobenzoic acid and leucovorin.

Table XI. Forced degradation studies of folic acid

Degradation condition	Stress details	% Degradation observed
Acidic	5 mL HCl 1 M, 1-week, room temperature	3.6
Basic	5 mL NaOH 1 M, 1-week, room temperature	5.5
Oxidative	5 mL H_2O_2 3%, 1-week, room temperature	24.6
Photolytic	Natural light, 1-week, room temperature	28.0

Table XII. Forced degradation studies of phenobarbital

Degradation condition	Stress details	% Degradation observed
Acidic	5 mL HCl 5 M, 3 h, 70 ºC	0.5
Basic	5 mL NaOH 1 M, 15 min, 70 ºC	25.1
Oxidative	5 mL H_2O_2 3% w/v, 24 h, room temperature	3.3
Photolytic	UV lamp (254 nm 15 W), 3 h, room temperature	0

Accuracy was assessed through the analysis of spiked samples, since reconstruction of the original matrix was not possible due to the lack of information on its composition.[12] Repeatability was expressed as the relative standard deviation (n=6, RSD%). Detailed results are presented in Table XIII.

Table XIII. HPLC method validation results for four products of folic acid and phenobarbital

Pharmaceutical Product	API	Content (mg)	Repeatability (RSD %, n=6)	Accuracy (% Mean Recovery)
Product 1	Folic Acid	1	0.57	99.5
Product 2	Folic Acid	0.8	0.82	99.2
Product 3	Folic Acid	1	1.3	101.4
Product 4	Folic Acid	0.8	1.6	100.8
Product 5	Phenobarbital	100	0.72	100.4

These results were considered suitable for the intended purpose.

NIR method development

Accuracy and repeatability were assessed for NIR methods. Accuracy was verified as the average value (n=10) of the difference between the NIR and HPLC value results, using tablets that were not included in the calibration set. Repeatability was expressed as the relative standard deviation (n=10, RSD%) of 10 determinations of the same tablet. Detailed validation results are presented in Table XIV.

Table XIV. NIR method validation results for four suppliers of folic acid and one of phenobarbital

Pharmaceutical Product	API	Content (mg)	R^2	RMSEC	PLS factors	Repeatability (RSD %, n=6)	Deviation from HPLC results (%)
Product 1	Folic Acid	1	0.9988	0.0627	6	1.7	0.44
Product 2	Folic Acid	0.8	0.9996	0.0538	4	1.4	0.65
Product 3	Folic Acid	1	0.9960	0.243	4	2.7	1.9
Product 4	Folic Acid	0.8	0.9994	0.224	10	2.2	1.0
Product 5	Phenobarbital	100	0.9677	1.12	7	0.74	1.8

Based on these results, the methods provided a rapid, non-destructive alternative to HPLC, with potential for improved calibration through additional samples.

CONCLUSIONS

Through a risk analysis approach the priority for developing analytical methods for folic acid and phenobarbital was demonstrated.

A novel and rapid, non-destructive NIR analytical method was developed to determine the concentration of the active ingredients of interest in those tablets that will be used to prepare pediatric dilutions. Results showed that NIR can provide reliable results. This approach provided an effective control strategy for improving the detectability of quality deviations. Future work will focus on validating HPLC and NIR methods for the quantification of these APIs directly in the pediatric dilutions prepared at the Pharmacy Department and on evaluating their stability.

This research addresses a real problem that still has no solution for the on-demand production of a product aimed at a vulnerable population that is currently prepared by hand without enough guarantee regarding the final dose of the active ingredient.

Conflicts of interest

Authors declare no conflicts of interest.

Acknowledgments

The authors would like to thank the staff of the Pharmacy Department of *Hospital de Clínicas* Dr. Manuel Quintela (Montevideo, Uruguay) for their collaboration during this study.

REFERENCES

(1) Schrier, L.; Hadjipanayis, A.; Stiris, T.; Ross-Russell, R. I.; Valiulis, A.; Turner, M. A.; Zhao, W.; De Cock, P.; de Wildt, S. N.; Allegaert, K.; van den Anker, J. Off-Label Use of Medicines in Neonates, Infants, Children, and Adolescents: A Joint Policy Statement by the European Academy of Paediatrics and the European Society for Developmental Perinatal and Pediatric Pharmacology. *Eur. J. Pediatr.* **2020**, *179* (5), 839–847. https://doi.org/10.1007/s00431-019-03556-9

(2) Suwa, M.; Miyake, S.; Urushihara, H. Comparison of Regulations and Status of Promoting Drug Development and Authorization of Pediatric Indications among Japan, the United States and the United Kingdom. *Jpn. J. Clin. Pharmacol. Ther.* **2022**, *53* (6), 225–234. https://doi.org/10.3999/jscpt.53.6_225

(3) Petkova, V.; Georgieva, D.; Dimitrov, M.; Nikolova, I. Off-Label Prescribing in Pediatric Population—Literature Review for 2012–2022. *Pharmaceutics* **2023**, *15* (12) 2652. https://doi.org/10.3390/pharmaceutics15122652

(4) Litalien, C.; Bérubé, S.; Tuleu, C.; Gilpin, A.; Landry, É. K.; Valentin, M.; Strickley, R.; Turner, M. A. From Paediatric Formulations Development to Access: Advances Made and Remaining Challenges. *Br. J. Clin. Pharmacol.* **2022**, *88* (10), 4349–4383. https://doi.org/10.1111/bcp.15293

(5) Noguera, C.; Barbagelata, J.; Braga, M.; Guarinoni, G.; Vidarte, A.; Vaamonde, L.; Blasina, F.; Ferrando, V.; De los Santos, G.; Boronat, A. Preparaciones Magistrales Para Pacientes Pediátricos En El Hospital de Clínicas. Poster presented at the *Semana Académica del Hospital de Clínicas*, 2021. Available at: https://www.semanacademica.hc.edu.uy/index.php/galeria-eposters-2021/311-preparaciones-magistrales-para-pacientes-pediatricos-en-el-hospital-de-clinicas (accessed June 2025).

(6) Zhang, C.; Liu, Y.; Tang, Z.; Chen, X.; Zhang, H.; Liu, N.; Huo, C.; Wang, Z.; Zheng, A. Recent Applications of Near Infrared to Pharmaceutical Process Monitoring and Quality Control. *Anal. Sci.* **2025**, *41*, 923–944. https://doi.org/10.1007/S44211-025-00794-W

(7) United States Pharmacopoeia Convention. ⟨905⟩ Uniformity of Dosage Units. *United States Pharmacopoeia* **2025**, *2025* (1). https://doi.org/10.31003/USPNF_M99694_03_01

(8) Anjalee, J. A. L.; Rutter, V.; Samaranayake, N. R. Application of Failure Mode and Effect Analysis (FMEA) to Improve Medication Safety: A Systematic Review. *Postgrad. Med. J.* **2021**, *97* (1145), 168–174. https://doi.org/10.1136/postgradmedj-2019-137484

(9) The International Council for Harmonisation. *ICH Harmonized Tripartite Guideline - Quality Risk Management Q9*; 2005.
(10) Wold, S.; Sjöström, M.; Eriksson, L. PLS-Regression: A Basic Tool of Chemometrics. *Chemom. Intell. Lab. Syst.* **2001**, *58* (2), 109–130. https://doi.org/10.1016/S0169-7439(01)00155-1
(11) Wang, H. P.; Chen, P.; Dai, J. W.; Liu, D.; Li, J. Y.; Xu, Y. P.; Chu, X. L. Recent Advances of Chemometric Calibration Methods in Modern Spectroscopy: Algorithms, Strategy, and Related Issues. *TrAC, Trends Anal. Chem.* **2022**, *153*, 116648. https://doi.org/10.1016/J.TRAC.2022.116648
(12) The International Council for Harmonisation. *ICH Harmonized Tripartite Guideline - Validation of Analytical Procedures Q2(R2)*; 2023.

Brazilian Journal of Analytical Chemistry
2026, Volume 13, Issue 51, pp 94-95

FEATURE

8th Uruguayan Congress of Analytical Chemistry (CUQA 8)

Lucía Pareja[1], Ignacio Machado[2]

[1]Departamento de Química del Litoral, Cenur Litoral Norte, Universidad de la República, Uruguay
[2]Grupo de Bioanalítica y Especiación (BIOESP), Faculty of Chemistry, Universidad de la República, Uruguay

The Uruguayan Congress of Analytical Chemistry (CUQA) held its 8th edition from October 13–15, 2024, in Montevideo, Uruguay. The event was organized by researchers from the Faculty of Chemistry and the Faculty of Sciences of the Universidad de la República (UdelaR), together with the National Institute for Agricultural Research (INIA, Uruguay). Since its first edition in 2009, CUQA has traditionally taken place every two years. Notably, the 2012 edition was jointly organized with the 5th Ibero-American Congress of Analytical Chemistry (CIAQA). All editions have been hosted in Montevideo, a key destination in Latin America that offers visitors a rich cultural and recreational agenda, high-quality services, and beautiful urban and coastal landscapes. The city is widely recognized as an ideal venue for international scientific meetings.

Members of the Organizing Committee at the welcome ceremony of 8th CUQA.

The main goal of CUQA is to present and discuss the latest advances in Analytical Chemistry developed in Uruguay and across the region. The 8th edition featured a broad range of topics, including Automation in Analytical Chemistry, Bioanalytical Chemistry, Education in Analytical Chemistry, Analytical Nanosystems, Environmental Analytical Chemistry, Food Analytical Chemistry, Pharmaceutical Analytical Chemistry, Toxicological Analytical Chemistry, and Electroanalytical Chemistry. This year's meeting brought together approximately 200 participants from across the country, along with 20 international attendees from Argentina, Brazil, and Chile.

The scientific program comprised 10 sessions, including one pre-congress course, seven invited lectures, 11 oral presentations, 12 “shotgun” presentations, 75 poster contributions, and several social and networking activities. A highlight of the program was the panel discussion titled “Toward the Frontiers of Bioanalysis: The State of the Art of Omics Disciplines in Uruguay”, which gathered leading experts to address emerging trends and challenges in the field. The congress also offered a two-day exhibition for companies operating in the Analytical Chemistry sector in Uruguay. This provided a valuable opportunity for participants to interact with industry representatives and explore the latest technological developments and laboratory instrumentation. During the closing ceremony, six poster awards were presented to recognize outstanding scientific contributions.

The Organizing Committee expresses its sincere gratitude to all sponsors, whose support was essential for the successful organization of the event. Special thanks are extended to the Brazilian Journal of Analytical Chemistry (BrJAC) for offering a Special Issue dedicated to the 8th CUQA. This Special Issue features selected works presented at the 8th CUQA. The Guest Editors, Dr. Ignacio Machado and Dr. Lucía Pareja, thank all authors for submitting their contributions and all reviewers for generously sharing their time and expertise to ensure the high quality of this collection. Finally, the Committee acknowledges the valuable support of the Scientific Committee, the staff of the “José Luis Massera” Auditorium, and all participants who contributed to another successful edition of CUQA.

Closing ceremony of 8th CUQA.

Brazilian Journal of Analytical Chemistry
2026, Volume 13, Issue 51, pp 96-99

FEATURE

8th EspeQBrasil and 17th RSAS Bring Together Researchers in São Pedro (SP)

The 8th Brazilian Meeting on Chemical Speciation (8th EspeQBrasil) and the 17th Rio Symposium on Atomic Spectrometry (17th RSAS), both biennial events, brought together experts in chemical speciation and atomic spectrometry to discuss recent scientific advances, technological innovation, and strengthened collaboration between academia and the private sector.

The 8th EspeQBrasil and the 17th RSAS were held jointly. Photo: Fabio Castro

The events took place jointly at the Hotel Fazenda Fonte Colina Verde in São Pedro (SP) from November 16 to 21, 2025. Well established in their respective fields, the two meetings are held biennially to bring together researchers, professionals, students, and industry representatives to share scientific advances, discuss contemporary challenges, and strengthen collaboration networks.

The last joint edition took place in 2023 in the city of Bento Gonçalves (RS), marking the resumption of in-person activities after the interruption caused by the COVID-19 pandemic between 2020 and 2022.

Tradition and Scientific Relevance

The RSAS was conceived in 1988 by Professors Adilson J. Curtius and Bernhard Welz with the aim of promoting interaction between Latin American students and scientists and internationally recognized researchers. Since then, the symposium has been held in Brazil, Venezuela, Argentina, Mexico, and Chile, establishing itself as one of the leading forums in the field of atomic spectroscopy.

The event typically brings together approximately 300 to 350 participants, including internationally renowned researchers and representatives from leading companies in the analytical instrumentation sector.

EspeQBrasil and RSAS are recognized as important forums for scientific discussion in the field of Analytical Chemistry. Photo: Fabio Castro

EspeQBrasil was conceived by Professor Marco A. Z. Arruda in response to the growth of the field of chemical speciation and the need for a forum dedicated to disseminating advances related to the biological and environmental functions of chemical species. The meeting has been hosted in the states of Rio Grande do Sul, Bahia, Paraná, and São Paulo, consolidating itself as a strategic platform for scientific integration and the development of business opportunities.

EspeQBrasil Scientific Program

During the 8th edition of EspeQBrasil, the session “Speciation and Fractionation in the Environment” stood out, featuring national and international lectures and oral presentations that fostered high-level technical discussions.

The event also included “Lightning Talk” sessions, allowing students and researchers to present their results in a dynamic format.

Other sessions addressed:

- Advances in analytical techniques and sample preparation for chemical speciation and fractionation
- Speciation and fractionation in nutrition and food sciences
- Emerging topics in chemical speciation and isotopic analysis

The final day was marked by in-depth discussions and interaction among researchers from different fields. Emerging topics included studies involving nanomaterials, microplastics, emerging contaminants, climate change, renewable energy applications, and the use of synchrotron light.

Opening Ceremony and Initial Activities of the 17th RSAS

The opening ceremony of RSAS was marked by noteworthy institutional and scientific highlights. During the ceremony, three researchers and one representative from the private sector were honored for their scientific and institutional contributions. The event was also attended by representatives from São Paulo State University (Unesp) and the University of Campinas (Unicamp), reinforcing the commitment of academic institutions to the initiative.

Cultural presentation of *samba de gafieira*. Photo: Fabio Castro

The inaugural program included a cultural presentation of *samba de gafieira*, celebrating Brazilian art and diversity, followed by the opening lecture delivered by Dr. Ryszard Lobinski (CNRS, France), who reflected on the role of scientific research in an international context.

Discussion session on poster presentations. Photo: Fabio Castro

The scientific activities included keynote lectures, oral presentations, and poster sessions. One day was entirely devoted to X-ray, Raman, Mössbauer, Secondary Ion Mass Spectrometry (SIMS), and synchrotron-based techniques, followed by discussions on multimodal approaches and methodological innovations.

Scientific Integration and Institutional Opportunities

In addition to their academic relevance, the events provided a strategic environment for networking, strengthening institutional partnerships, and fostering closer ties with the private sector. The presence of sponsoring companies was considered essential to maintaining these spaces for scientific exchange and to exploring new business opportunities.

The events also received support from companies in the analytical sector. Photo: Fabio Castro

Among the participating companies were Agilent, Analítica, Analytik Jena, Anton Paar, Metrohm, PerkinElmer, SENS, Thermo Fisher Scientific, and Vert.

Text: Lilian Freitas – BrJAC Publisher
Source: 8th EspeQBrasil and 17th RSAS

SPONSOR REPORT

Trace analysis of epichlorohydrin in drinking water using GC-MS coupled with purge and trap

Authors

Adam Ladak[1], Terry Jeffers[2], and Amy Nutter[3]

[1]Thermo Fisher Scientific, UK
[2]Thermo Fisher Scientific, USA
[3]Teledyne LABS, Mason, OH, USA

Keywords

Epichlorohydrin, volatile organic compounds (VOCs), drinking water, U.S. EPA, Purge and Trap (P&T), GC-MS, Helium Saver

Goal

Demonstration of an analytical method for the analysis of epichlorohydrin in drinking water down to 30 ppt using the Teledyne LABS Tekmar Lumin purge and trap (P&T) concentrator combined with the AQUATek LVA autosampler and the Thermo Scientific™ ISQ™ 7610 GC-MS for the analysis. Method linearity, method detection limit (MDL), precision, and mid-point calibration check were assessed to evaluate method performance.

Introduction

Epichlorohydrin (ECH) is a versatile starting material in the production of drugs and polymers and is also used as an insect fumigant and solvent for organic synthesis reactions. ECH-based polymer pipes are commonly used in the production of drinking water due to their durability and resistance to corrosion. However, ECH is known for its high reactivity and toxicity, which poses significant health risks if it contaminates drinking water. Exposure to ECH can cause respiratory issues, skin irritation, and has been classified as a probable human carcinogen.[1] Due to these risks, many countries have imposed strict limits on the amount of ECH allowed in drinking water. Recently, Europe set a minimum detection limit (MDL) of 30 parts per trillion (ppt) for ECH in drinking water.[2] Whereas typically required detection limits for most compounds mandated for analysis in Europe can be achieved using methods based on static headspace, the stringent MDL required for ECH requires preconcentration, for example using purge and trap (P&T) technology.[3,4] This technology involves purging the water sample with an inert gas to release volatile organic compounds (VOCs), which are then trapped and concentrated for analysis, ensuring reliable detection at very low concentrations. In the United States, the analysis of VOCs in drinking water is mandated by the Environmental Protection Agency (EPA). The EPA requires the use of P&T technology for drinking water analysis to ensure that even trace amounts of harmful compounds like ECH are detected and managed appropriately.
The following evaluation describes the use of the ISQ 7610 Single Quadrupole MS system coupled with the Thermo Scientific™ TRACE™ 1610 GC with the Thermo Scientific™ HeSaver-H_2Safer™ split/splitless injector and Teledyne LABS Tekmar Lumin P&T concentrator combined with the AQUATek LVA autosampler for the analysis of ECH in drinking water.

Experimental

Sample preparation

Three working calibration standards were prepared in methanol at concentrations of 100 parts per billion (ppb), 500 ppb, and 5 parts per million (ppm) from the following Restek™ standard: Epichlorohydrin Standard (P/N 30679).

A five-point linear (r^2) calibration curve was used from 30 to 5,000 ppt for all compounds utilizing Thermo Scientific™ vials (P/N C4013-2W) and cap and septum (P/N C4013-60A). The relative response factor (RRF) was calculated for ECH using the internal standard fluorobenzene. The internal standard was prepared in methanol from the fluorobenzene Restek standard (P/N 30030) at a concentration of 5 ppb, after which 5 µL was mixed with each 25 mL sample for a resulting concentration of 1,000 ppt.

Seven 30 ppt standards were prepared to calculate the MDL. Also, seven 1,000 ppt standards were prepared for the accuracy and precision calculations of the mid-point calibration check. All calibration, MDL, and mid-point calibration check standards were analyzed with the Tekmar Lumin P&T and AQUATek LVA conditions in Table 1.

Table 1. Tekmar Lumin P&T and AQUATek LVA water method conditions

Standby	Variable
Valve oven temp.	150 °C
Transfer line temp.	150 °C
Sample mount temp.	90 °C
Standby flow	10 mL/min
Purge ready temp.	35 °C
MCS purge temp.	20 °C
Purge	**Variable**
Purge temp.	20 °C
Purge time	11.00 min
Purge flow	100 mL/min
Dry purge temp.	20 °C
Dry purge time	0.00 min
Dry purge flow	100 mL/min
Sample heater enable	Off
Desorb	**Variable**
Desorb preheat temp.	175 °C
Desorb temp.	185 °C
Desorb time	2.00 min
Drain flow	300 mL/min
GC start signal	Begin Desorb
Bake	**Variable**
Bake time	2.00 min
Bake temp.	230 °C
MCS bake temp.	180 °C
Bake flow	200 mL/min
AQUATek LVA	**Variable**
Sample loop time	0.85 min
Sample transfer time	1.25 min

(continued)

Table 1 contd. Tekmar Lumin P&T and AQUATek LVA water method conditions

AQUATek LVA	Variable
Rinse loop time	0.85 min
Sweep needle time	0.30 min
Presweep time	0.35 min
Water temp.	90 °C
Bake rinse cycles	1
Trap	1A
Chiller tray	On, 10 °C

GC-MS parameters

A TRACE 1610 GC was coupled to the ISQ 7610 MS equipped with the Thermo Scientific™ NeverVent ™ vacuum probe interlock (VPI) and an ExtractaBrite ion source. A Thermo Scientific™ TraceGOLD™ TG-VMS column, 30 m × 0.25 mm, 1.4 µm film (P/N 26080-3320) was used for compound separation. The HeSaver-H_2Safer SSL injector was utilized to reduce the carrier gas consumption by decoupling the gas used for the chromatographic separation from the gas used to pressurize the inlet and maintain split and purge flows. The critical separations were maintained with a run time of under 15 minutes. For this analysis, the ISQ 7610 MS was operated in Selected Ion Monitoring (SIM) mode for increased selectivity, as required for this application. Extended method parameters for the ISQ 7610 MS are shown in Table 2.

Table 2. GC-MS conditions

TRACE 1610 GC conditions	
Column	TraceGOLD TG-VMS, 30 m x 0.25 mm, 1.4 µm film; Helium carrier gas, 1.5 mL/min column flow
Oven profile	35 °C, 3 min 15 °C /min to 100 °C 25 °C/min to 240 °C 2 min hold Run time, 14.9 min
Inlet	HeSaver-H_2Safer SSL 200 °C, 20:1 split Purge flow, 5.0 mL/min 0.40 min helium delay
ISQ 7610 MS conditions	
Temp	Transfer line, 230 °C; Ion source, 280 °C
Mode	Timed-SIM
Scan	Fluorobenzene ions, *m/z* 96 Epichlorohydrin ions, *m/z* 57, *m/z* 49, *m/z* 62

Instrument control and data processing

Data was acquired, processed, and reported using the Thermo Scientific™ Chromeleon™ Chromatography Data System (CDS). This software can control both the GC-MS system and the Tekmar Lumin P&T with the AQUATek LVA. This allows a single software to be utilized for the full workflow, simplifying the instrument operation. This application note is available for download via the Thermo Scientific™ AppsLab Library, which contains all the parameters needed to acquire, process, and report the analytical data for analysis of ECH.[5]

Results and discussion

Linearity and sensitivity

Using the parameters described in Table 2, excellent chromatography was achieved. The Tekmar Lumin P&T has an innovative Moisture Control System (MCS) that improves water vapor removal, thereby reducing peak interference and increasing GC column lifespan. Figure 1 displays consistent peak shape of a 30 ppt epichlorohydrin standard with minimal water interference.

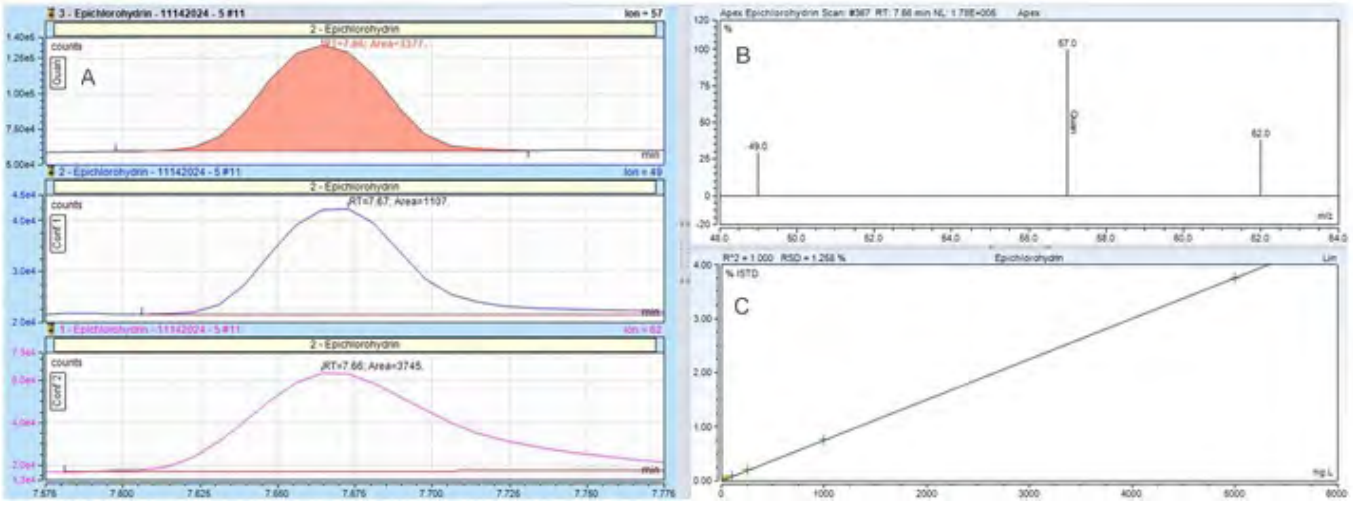

Figure 1. Chromeleon CDS results browser showing extracted ion chromatograms for ECH in the 30 ppt water standard, quantitation ion (*m/z* = 57) and two confirming ions (*m/z* = 49, *m/z* = 62) (A); a measured spectrum of ECH (B); and a linear calibration over a concentration range of 30 ppt to 5,000 ppt (C)

A calibration range of 30–5,000 ppt was evaluated. The calibration curve was used to calculate the response factor's average and relative standard deviation (%RSD), aiming for a %RSD of <20 to meet EPA criteria. The XLXR detection system of the ISQ 7610 MS, with its extended linear dynamic range and lifespan, enabled extended calibration curves and reduced replacement needs. The MDL was assessed using seven replicates of the 30 ppt standard. This data is shown in Table 3.

Method robustness

For use as a routine testing method, it is extremely important that the analytical method is stable and reproducible. To demonstrate this, 1,000 ppt standards (n=20) in water were injected at intervals over a 124-sample injection sequence. The samples were acquired with no user intervention at all on the P&T, GC or MS system and their concentrations were plotted to demonstrate the stability of the results. Figure 2 shows the reproducibility of epichlorohydrin over 124 injections with excellent percentage RSDs.

Reduced helium consumption and cost savings

The HeSaver-H_2Safer technology significantly extends helium cylinder lifetimes and offers substantial gas savings during idle periods and sample injection/analysis. Users can estimate its impact on helium consumption, cost, and cylinder lifetime using the Thermo Scientific™ Gas Saver Calculator tool.[6] By using this technology for epichlorohydrin analysis, the helium cylinder lifespan can nearly quadruple compared to a standard SSL injector, making it a prime choice for helium conservation. Figure 3 shows the helium saver calculator.

Table 3. Linearity, method detection limits, and mid-point calibration check

Compound	Calibration (30–5,000 ppt)			Method detection limits (n=7, 30 ppt)			Mid-point calibration check (n=7, 1,000 ppt)	
	RT	Ion	Linear ($r^2 \geq 0.995$)	MDL (ppt)	Precision (≤20%)	Accuracy (±30%)	Precision (≤20%)	Accuracy (±20%)
Fluorobenzene (IS)	6.27	96						
Epichlorohydrin	7.66	57	1.00	5	4.1	128	4.2	115

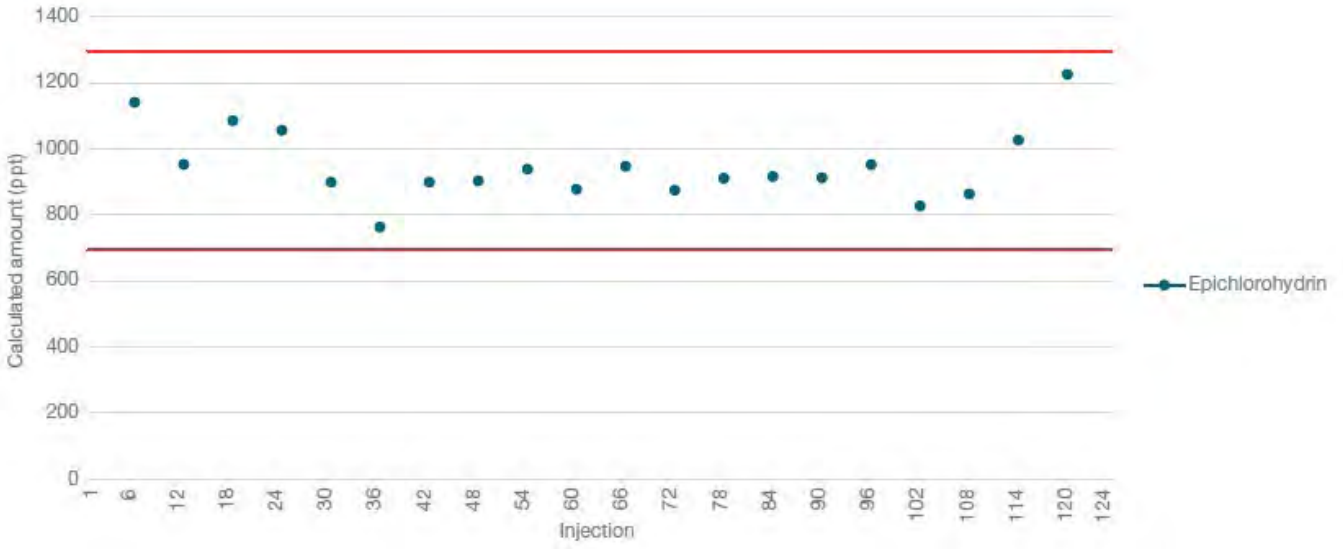

Figure 2. Reproducibility of epichlorohydrin at 1,000 ppt in water standards (n=20) over 124 injections

Figure 3. Helium saver calculator showing almost 4x savings of carrier gas

Conclusion

This study demonstrates the capability of the Tekmar Lumin P&T with the AQUATek LVA system connected to the ISQ 7610 Single Quadrupole GC-MS to detect and quantify low-level ECH in drinking water samples, in compliance with EPA requirements.

- Utilizing the Tekmar Lumin P&T's ability to purge with nitrogen, along with using the HeSaver-H_2Safer SSL injector, nearly four times less helium was consumed during the analysis without sacrificing system performance.
- The linearity of the calibration curve from 30 ppt to 5,000 ppt passed method requirements.
- The application proved robust during an extended study with 20 samples of a 1,000 ppt ECH standard injected over a series of 124 injections, obtaining 4.4% precision and 118% accuracy of the recovery.

References

1. Sram, R.J.; Landa, L.; Samkova, I. Effect of occupational exposure to epichlorohydrin on the frequency of chromosome aberrations in peripheral lymphocytes. *Mutat. Res.* 1983, *122,* 59.
2. Council Directive 98/83/EC of 3 November 1998: On the quality of water intended for human consumption, Official Journal of the European Communities 5 December 1998, No. 330/32.
3. Lucentini, L.; Ferretti, E.; Veschetti, E.; Sibio, V.; Citti, G.; Ottaviani, M. Static headspace and purge-and-trap gas chromatography for epichlorohydrin determination in drinking water. *Microchemical Journal* 2005, *80,* 89–98.
4. Mattioda, C. Low-level analysis of epichlorohydrin in drinking water by headspace trap-GC/MS. PerkinElmer Field Application Report: Gas Chromatography/Mass Spectrometry, 2008.
5. Thermo Scientific AppsLab Library: https://appslab.thermofisher.com/
6. Thermo Scientific Helium Saver Calculator: https://www.thermofisher.com/it/en/home/industrial/chromatography/chromatography-learning-center/chromatography-consumables-resources/chromatography-tools-calculators/helium-saver-calculator.html

Learn more at **thermofisher.com/gcms**

thermo scientific

Analysis of hydride-forming elements using ICP-OES

Authors

Tomoko Vincent and Bhagyesh Surekar

Thermo Fisher Scientific, Bremen, Germany

Keywords

Accuracy, high sensitivity, hydride, ICP-OES, robust, trace analysis

Goal

To demonstrate the performance of the Thermo Scientific™ iCAP™ PRO Series ICP-OES equipped with two different hydride generation sample introduction systems. These systems will improve sensitivity of hydride-forming elements, such as arsenic, bismuth, antimony, selenium, and mercury, over that provided by a standard sample introduction system.

Introduction

The analysis of antimony, arsenic, bismuth, mercury, and selenium in environmental, biological, and food samples is routine and is typically driven by regulations that require low limits of detection, ensuring that contamination by toxic substances is kept to a minimum. For example, the United States Environmental Protection Agency (EPA) regulates the maximum contamination levels allowed in drinking water to protect public health (Table 1).[1] These specified elements can cause negative health effects with long exposure, it is important to monitor them with accurate analysis techniques.

Table 1. Maximum contaminant level (µg·L^{-1}) and the main impact on health as detailed in the national primary drinking water regulations by the EPA

Element	Maximum contaminant level	Health effect from long term exposure
Antimony	6	Increase in blood cholesterol
Arsenic	10	Skin damage
Mercury	2	Kidney damage
Selenium	50	Hair or fingernail loss

Inductively coupled plasma atomic or optical emission spectroscopy (ICP-OES) is a common technique for trace element analysis. The analytical performance required for some elements is challenging to achieve using an ICP-OES with a standard sample introduction configuration (nebulizer, spray chamber, etc.). One such group of elements is the hydride-forming elements, which tend to emit towards the UV end of the spectrum; these wavelengths suffer a higher degree of transmission loss through absorption, further reducing sensitivity. The use of a hydride generation sample introduction system has been shown to improve sensitivity when analyzing hydride-forming elements by ICP-OES.[2] This is due to the chemical properties of these elements, which enable the formation of volatile gaseous hydrides when reacted with reducing agents such as sodium borohydride.

An example of the hydride generation reaction is given below. In this case, arsenic is the hydride-forming element:

$$6(BH)_{4\,(aq)} + As^{3+}{}_{(aq)} + 3H^{+}{}_{(aq)} \rightarrow 3(B_2H_6)_{(aq)} + 3H_{2\,(aq)} + AsH_{3\,(g}$$

[Equation 1]

For the hydride-forming reaction to take place, the hydride-forming element must be present in the test solution in the correct oxidation state (Table 2). If this is not the case, then a pre-reduction reaction will have to be carried out.

Table 2. Common oxidation states of the hydride-forming elements and oxidation states required for the hydride reaction to take place

Element	Most common oxidation state	Oxidation state needed for the reaction
Arsenic	As (V)	As (III)
Antimony	Sb (V)	Sb (III)
Bismuth	Bi (III)	Bi (III)
Mercury	Hg (II)	Hg (II)
Selenium	Se (VI)	Se (IV)

Experimental

For the analysis of the hydride-forming elements, two hydride-forming sample introduction systems were used—the basic and integrated hydride generator kits were coupled with the iCAP PRO Series ICP-OES instruments.
The details of the sample introduction kits and the instrument parameters used are listed in Table 3.

Table 3. iCAP PRO Series ICP-OES Duo instrument parameters

Parameter	Integrated hydride generation accessary (iCAP PRO XP ICP-OES and iCAP PRO XPS ICP-OES)	Basic hydride kit (iCAP PRO ICP-OES and iCAP PRO X ICP-OES)
Spray chamber	-	Cyclonic spray chamber
Nebulizer	-	Glass concentric nebulizer
Pump tubing	Sample: Tygon™ green/green i.d., 1.85 mm	Sample: Tygon™ orange/yellow i.d., 0.51 mm
	Drain: Tygon™ black/white i.d., 3.17 mm	Drain: Tygon™ green i.d., 1.85 mm
	Reagent: Tygon™ black/black i.d., 0.76 mm	Reagent: Tygon™ orange/yellow i.d., 0.51 mm
	Acid: Tygon™ orange/yellow i.d., 0.51 mm	-
Pump speed	40 rpm	
Nebulizer gas flow	0.45 L·min^{-1}	
Auxiliary gas flow	0.5 L·min^{-1}	
Coolant gas flow	12.5 L·min^{-1}	
RF power	1,350 W	

(continued)

Table 3 contd. iCAP PRO Series ICP-OES Duo instrument parameters

Center tube	2.0 mm	
Exposure time	eUV 10 s, iFR 10 s	
Total analysis time	120 s, including uptake and wash	
Sample volume	12 mL	5 mL

The basic hydride generation kit simply introduces a reducing solution and acidified sample solutions containing 3.6 w/w % HCl via a T-piece connector using three channels of the peristaltic pump of the Thermo Scientific™ iCAP PRO ICP-OES or the iCAP PRO X ICP-OES to the nebulizer. This system has the advantage of allowing additional non-hydride-forming elements to be analyzed simultaneously along with the hydride-forming elements.
The integrated hydride generation kit uses four channels of the peristaltic pump of the iCAP PRO XP ICP-OES or the iCAP PRO XPS ICP-OES. The hydride-forming reaction takes pace in a dedicated gas liquid separator. This allows the gaseous product from the hydride- forming reaction [Equation 1] to be separated and introduced into the ICP-OES system directly using argon carrier gas (nebulizer gas) (Figures 1 and 2).

Figure 1. iCAP PRO XP ICP-OES or iCAP PRO XPS ICP-OES coupled with an integrated hydride generation kit

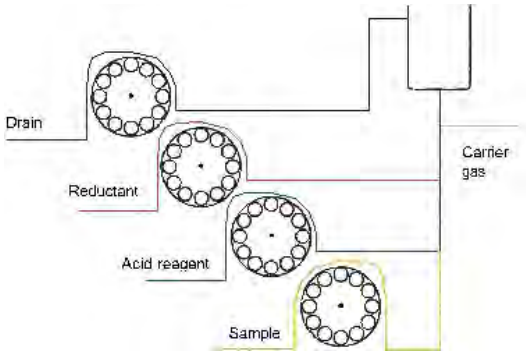

Figure 2. Schematic of pump tube allocation of integrated hydride generation kit

For automation of the sample introduction process, a Teledyne™ CETAC™ ASX-560 autosampler (Omaha, NE, USA) was used.

Data acquisition and data processing

The Thermo Scientific™ Qtegra™ Intelligent Scientific Data Solution™ (ISDS) Software was used to create LabBooks for sample analysis, data acquisition, processing, and reporting. The intuitive wavelength selection tool of the Qtegra ISDS Software, along with inspection of subarray plots and full frame images, was used to select interference-free wavelengths in standard solutions. In addition, the flexibility of the Qtegra ISDS Software allowed for a customized analysis method to be created by selecting the eUV mode for the ultraviolet wavelength range for the sample analysis.

Sample preparation

Pre-reduction techniques used during sample preparation are summarized in Table 4, and the preparation of the calibration standards is detailed in Table 5. Intermediate standards were prepared from single element solutions (1,000 mg·L^{-1}, SPEX™ CertiPrep™, Metuchen, NJ, USA).

The individual solutions were prepared using a mixture of 3.6 w/w % hydrochloric acid (TraceMetal™ grade, 32-36%, Fisher Chemical™), 1 w/v % potassium iodide (>99.5%, Merck) and 1 w/v % ascorbic acid (ACS grade, Merck). Acid reagent used in the study is 3.6 w/w % hydrochloric acid (HCl) and reducing agent used is 0.5 w/v % sodium borohydride ($NaBH_4$) stabilized in the 0.5 w/v % sodium hydroxide (NaOH) solution.

Table 4. Pre-reduction techniques used for sample preparation

Element	Reagents	Preparation condition
Arsenic/ Antimony	1 w/v % potassium iodide and ascorbic acid in 3.6 w/w % HCl	5 hours at room temperature
Bismuth/ Mercury	No pre-reduction required	N/A
Selenium	18 w/w % HCl	Boiled for 15 minutes

Table 5. Detail of standard preparation methods

Element	Intermediate standard (mg·L^{-1})	Calibration standard matrix solutions
Arsenic	100 µL of 1,000 mg·L^{-1} As in 100 mL of 1% potassium iodide and ascorbic acid in 3.6 w/w % HCl and left for 5 hours at room temperature	Intermediate standard diluted to the required concentrations with 1 w/v % potassium iodide and ascorbic acid in 3.6 w/w % HCl
Antimony	100 µL of 1,000 mg·L^{-1} Sb in 100 mL of 1% potassium iodide and ascorbic acid in 3.6 w/w % HCl and left for 5 hours at room temperature	
Bismuth	100 µL of 1,000 mg·L^{-1} Bi in 100 mL of 3.6 w/w % HCl	Intermediate standard diluted to the required concentrations with 3.6 w/w % HCl
Mercury	100 µL of 1,000 mg·L^{-1} Hg in 100 mL of 3.6 w/w % HCl	
Selenium	100 µL of 1,000 mg·L^{-1} Se boiled for 10 minutes in 18 w/w % HCl and made up to 100 mL	

The calibration standard matrix solutions (Table 5) were used to prepare the standards to final concentrations ranging from 0 to 10 µg·L^{-1} (Table 6).

Table 6. Detail of calibration standard concentration

	Basic hydride generation kit (µg·L^{-1})	Integrated hydride generation kit (µg·L^{-1})
Blank	0	0
Standard-1	2.5	0.1
Standard-2	5	0.5
Standard-3	10	1
Standard-4	-	5
Standard-5	-	10

Results and discussion

Sensitivity (LOD), linearity, and accuracy

The wavelengths used for the analysis are shown in Table 6. The intelligent Full Range (iFR) analysis mode can measure wavelengths from 167.021 to 852.145 nm in one simultaneous measurement; this allows a significant reduction of the analysis times, this feature is available on iCAP PRO Series ICP-OES instruments. The enhanced eUV analysis mode can be used to further enhance sensitivity for elements that fall in the UV wavelength range. This feature is available on the iCAP PRO XP ICP-OES and ICAP PRO XPS ICP-OES instruments.

Sensitivity and linearity of the target elements were determined from the analysis of the calibration blank and standards. The excellent linearity with coefficient of determination $R^2 > 0.9987$ over the calibration range 0.1 to 10 µg·L^{-1} and limits of detection are shown in Table 7. The LODs were calculated as three times the standard deviation of ten replicate measurements of the calibration blank. The LODs for all the elements of interest are significantly below the expected levels required for environment safety allowance (Table 1). The detection performance of the two- hydride generation sample introduction systems is significantly improved compared to the performance of the standard sample introduction system[3]. The details are given in Table 7.

The subarray plot for arsenic and mercury shows interference-free analysis (Figure 3). The calibration plots (Figure 4) show excellent linearity of the range analyzed. The detection limits obtained for some elements such as arsenic (0.015 µg·L^{-1}) using the integrated hydride generation kit are excellent, where the detection limit achieved for mercury is close to that of ICP-MS performance, with a BEC of 0.004 µg·L^{-1} and an LOD of 0.004 µg·L^{-1}. All measured analytes met the maximum allowance of the environment water criteria (Table 1).

Table 7. Linearity (coefficient of determination, R^2) and sensitivity (LOD as $\mu g \cdot L^{-1}$) data for five hydride-forming elements using three different introduction systems

Analyte	Wavelength (nm)	iCAP PRO ICP-OES and iCAP PRO X ICP-OES equipped with basic hydride kit			iCAP PRO XP ICP-OES and iCAP PRO XPS ICP-OES equipped with integrated hydride kit			Standard sample introduction system[3]	
		Mode	R^2	LOD ($\mu g \cdot L^{-1}$)	Mode	R^2	LOD ($\mu g \cdot L^{-1}$)	Mode	LOD ($\mu g \cdot L^{-1}$)
Hg	184.950	Axial-iFR	0.9987	0.019	Axial-eUV	0.9998	0.004	Axial-eUV	1.1
As	189.042	Axial-iFR	0.9985	0.203	Axial-eUV	1.0000	0.015	Axial-eUV	1.8
Se	196.090	Axial-iFR	0.9999	0.252	Axial-eUV	0.9996	0.035	Axial-eUV	2.4
Sb	206.833	Axial-iFR	0.9989	0.210	Axial-iFR	0.9999	0.036	Axial-iFR	3
Bi	223.061	Axial-iFR	0.9987	0.096	Axial-iFR	0.9998	0.042	Axial-iFR	2.5

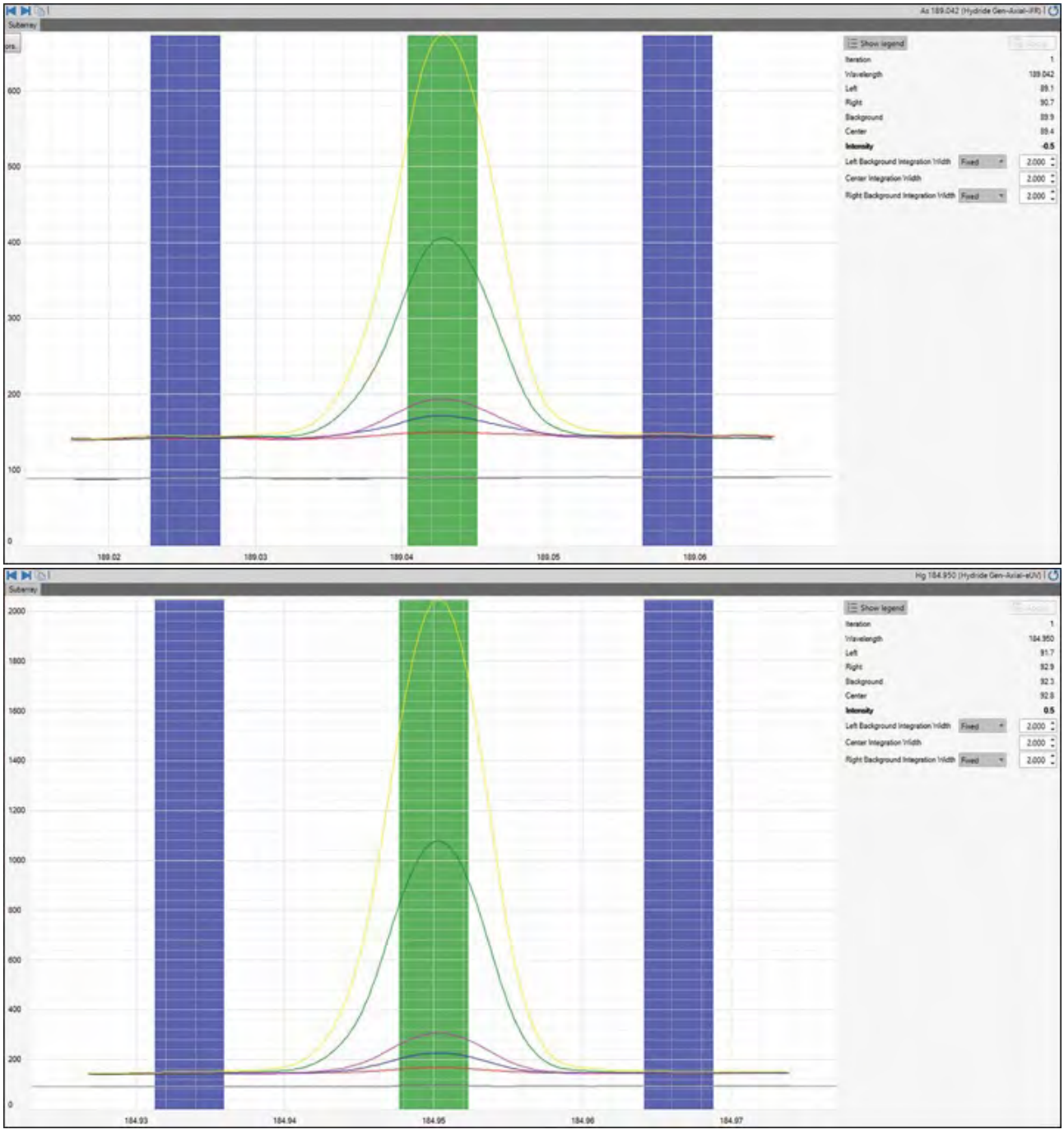

Figure 3. Subarray window for As 189.042 nm and Hg 184.950 nm, indicating the peak (center), right and left background within the Qtegra ISDS Software

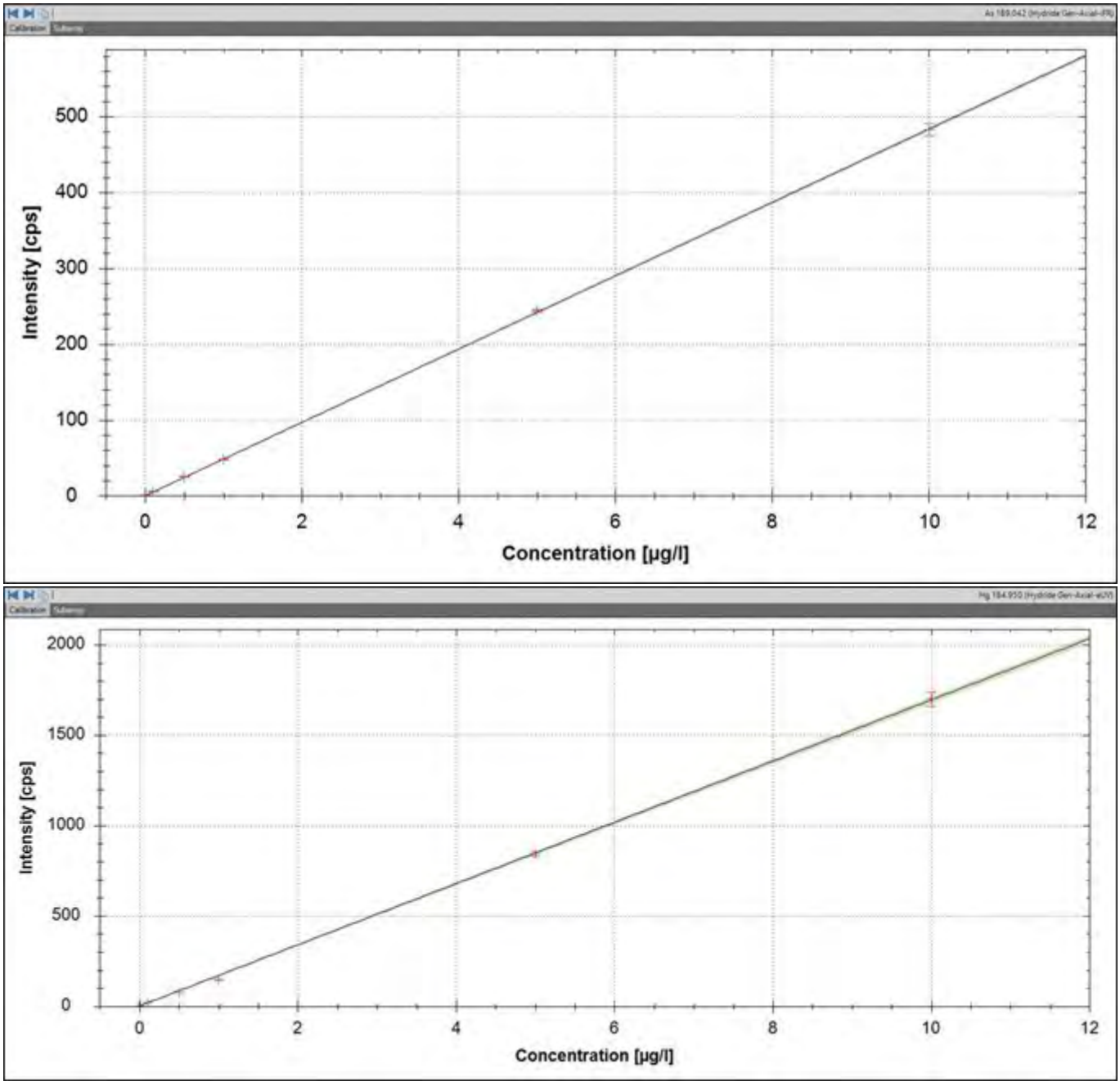

Figure 4. Calibration curve for As 189.042 nm in Axial viewing mode and Hg 184.950 nm in Axial viewing mode assessed over a concentration range of 0.1–10 µg·L^{-1}

Conclusion

The iCAP PRO Series ICP-OES Duo system with basic and integrated hydride generation kits were employed in separate experiments to analyze five hydride-forming elements. These accessories were shown to dramatically improve analysis sensitivity. This analytical method was rigorously tested, and the results obtained clearly demonstrate the following analytical advantages:

- Enhanced sensitivity helps achieve detection limits below 0.05 µg·L^{-1} for hydride-forming elements including arsenic, bismuth, antimony, selenium, and mercury using the integrated hydride generation kit.
- The basic hydride generation kit performed ten times better for the LOD compared to the standard introduction system, allowing the analysis of non-hydride-forming elements simultaneously.
- The performance achieved with the basic hydride kit indicates that achievable detection limits for hydride forming elements are equivalent or better than those with AAS equipped with hydride generation accessory, enabling multi-element determination simultaneously.
- The flexibility of the Qtegra ISDS Software allows creation of a customized analysis method by selecting the eUV analysis mode, which provides enhanced analytical performance.

References

1. EPA homepage: https://www.epa.gov/
2. Thermo Scientific Application Note 43374: Analysis of Hydride Forming Elements with the Thermo Scientific iCAP 7000 Plus Series ICP-OES and the Basic Hydride Generator. https://assets.thermofisher.com/TFS-Assets/CMD/Application-Notes/AN-43374-ICP-OES-Hydride-Forming-Elements-AN43374-EN.pdf
3. Thermo Scientific Technical Note 73763: Thermo Scientific iCAP PRO Series ICP-OES Best Detection Limits Versus Typical Detection Limits in Axial View. https://assets.thermofisher.com/TFS-Assets/CMD/Technical-Notes/tn-73763-icp-oes-icap-pro-detection-limits-tn73763-en.pdf

Learn more at **thermofisher.com/ICP-OES**

thermo scientific

INDUSTRY REPORT

DMA-80 *evo* | ENVIRONMENTAL

MILESTONE

HELPING CHEMISTS

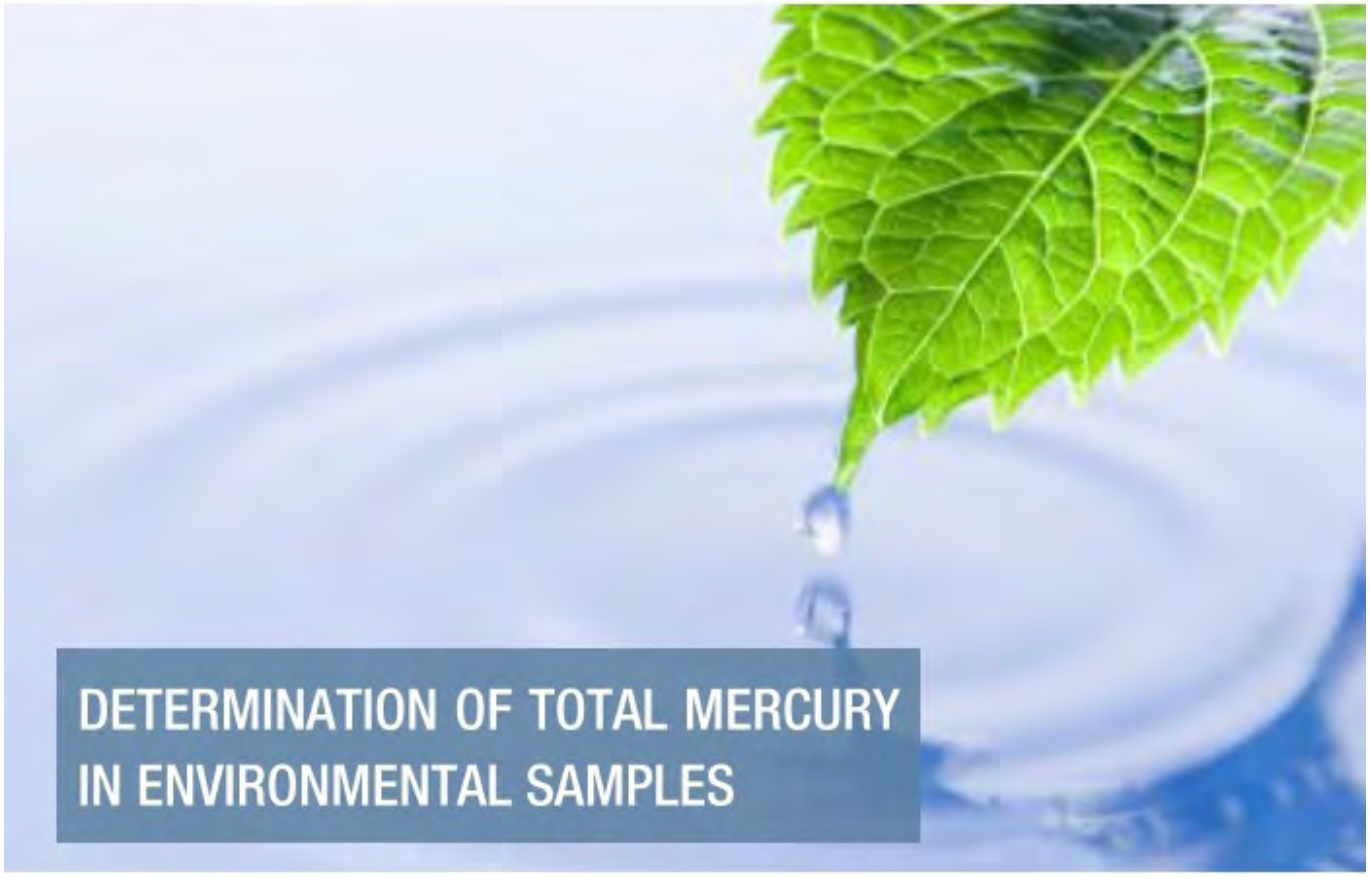

Determination of Total Mercury in Environmental Samples Utilizing Direct Analysis for Mercury Detection in Soil, Sediment, and Waste Water Samples

| SUMMARY

As more emphasis is placed on the monitoring of mercury emissions, both private and public institutions are looking at characterizing soil, sediments and waste water samples. Contaminated soil has to be excavated and remediated, or depending on the level of contamination, disposed of as hazardous waste. Several methods are available for mercury analysis in environmental samples like waste water and soil. Most of these methods however, require elaborate preparation procedures that are labor intensive and subsequently expensive. Direct mercury analysis, as described in EPA Method 7473, is an alternative to these methods and has been used successfully to determine total mercury in environmental samples. This technique requires no sample preparation and delivers results in as little as six (6) minutes per sample making it significantly faster than traditional wet chemistry.

| INTRODUCTION

Mercury is naturally present in the earth and enters the air and water streams through the burning of fossil fuels, discharge of industrial waste and use of pesticides. Companies have also discharged mercury onto their property via production by-products. Now, with more emphasis being placed on the monitoring of this neurotoxin, both private and public institutions are looking at characterizing the soil, sediment and waste water, on their property.

Contaminated soil has to be excavated and remediated, or depending on the level of contamination, disposed of as hazardous waste. Several methods exist for the determination of mercury in environmental samples. Traditional analytical methods such as Cold Vapor Atomic Absorption (CVAA) and ICP MS both require sample preparation prior to analysis. This results in both techniques being costly, labor-intensive and subsequently, having a long turnaround time. Direct

mercury analysis, as described in EPA Method 7473, is a cost-effective, proven alternative to these labor-intensive, wet chemistry techniques.

Direct analysis affords the laboratory many benefits including:

- Reduced Sample Turnaround (6 Minutes)
- No Sample Preparation
- Reduced Hazardous Waste Generation
- Reduction of Analytical Errors
- General Cost Savings (70% versus CVAA)

| EXPERIMENTAL

INSTRUMENT

Figure 1 Milestone's DMA-80 evo

The DMA-80, Direct Mercury Analyzer, as evidenced in EPA Method 7473, from Milestone Srl (www.milestonesrl.com) was used in this study.

The DMA-80 features a circular, stainless steel, interchangeable 40 position autosampler for virtually limitless throughput and can accommodate both nickel (500 mg) and quartz boats (1500 µL) depending on the requirements of the application. It operates from a single phase 110/220V, 50/60 Hz power supply and requires regular grade oxygen as a carrier gas.

As the process does not require the conversion of mercury to mercuric ions, both solid and liquid matrices can be analyzed without the need for acid digestion or other sample preparation. The fact that zero sample preparation is required also eliminates all hazardous waste generation. All results, instrument parameters including furnace temperatures, are controlled and saved with easy export capabilities to Excel or LIMS.

PRINCIPLES OF OPERATION

Direct mercury analysis incorporates the following sequence: Thermal Decomposition, Catalytic Conversion, Amalgamation, and Atomic Absorption Spectrophotometry. Controlled heating stages are implemented to first dry and then thermally decompose sample introduced into a quartz tube.

A continuous flow of oxygen carries the decomposition products through a hot catalyst bed where halogens, nitrogen, and sulphur oxides are trapped. All mercury species are reduced to Hg(0) and are then carried along with reaction gases to a gold amalgamator where the mercury is selectively trapped. All non-mercury vapors and decomposition products are flushed from the system by the continuous flow of gas. The amalgamator is subsequently heated and releases all trapped mercury to the single beam, fixed wavelength atomic absorption spectrophotometer.

Absorbance is measured at 253.7 nm as a function of mercury content.

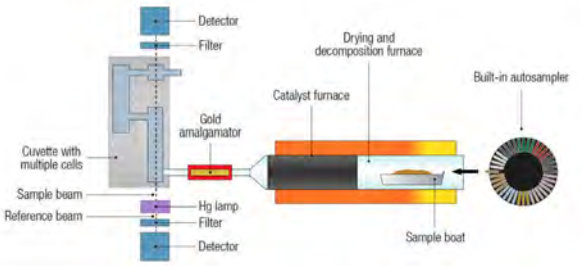

Figure 2 An Internal Schematic of Milestone's DMA-80 evo.

EXPERIMENTAL DISCUSSION

The goal of this study was to evaluate the effectiveness of the DMA-80 to analyse both soil and ground water samples – two vastly different matrices. All soil and water samples were obtained from an independent contract laboratory that had already analysed the samples via CVAA. For this study, the soil and water samples were analysed at various weights in the nickel and quartz sample boats respectively

CALIBRATION

Calibration standards were prepared using a NIST traceable stock solution of 1000 ppm Hg preserved in 5% HNO_3. Working standards of 100 ppb and 1 ppm were prepared and preserved in 37% HCl and stored in amber glass vials.

By injecting increasing sample volumes of standard into the quartz sample boats, calibration graphs of 0 – 20 ng (Figure 3) and 20 – 500 ng (Figure 4) of mercury were created using the 100 ppb and 1 ppm standards respectively.

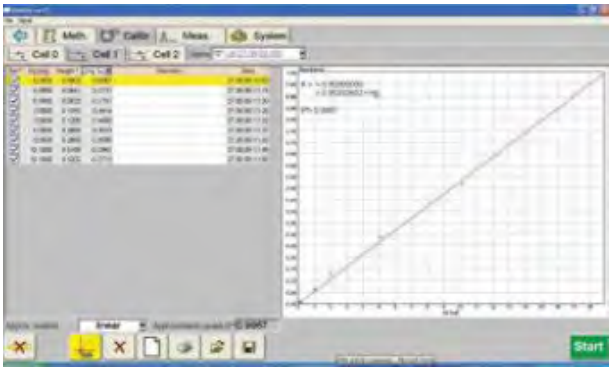

Figure 3 0 ng – 20 ng Calibration Graph for ultra-level

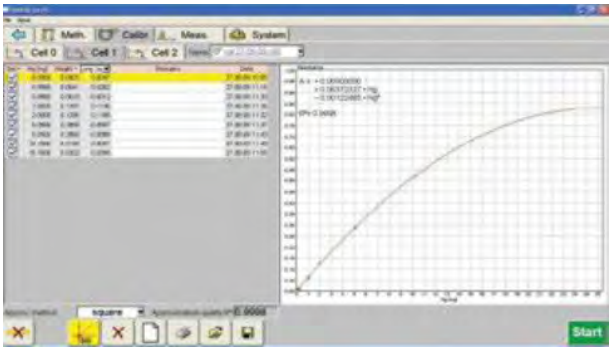

Figure 4 20 ng – 1000 ng Calibration Graph for low to mid-level analysis (ppb, ppm)

| OPERATING CONDITIONS

The DMA-80's operating conditions for all analyses are shown in Table 1.

Parameter	Setting
Drying Temp/Time	90 seconds to 200 °C
Decomposition Ramp	120 seconds to 650 °C
Decomposition Hold	90 seconds at 650 °C
Catalyst Temp	565 °C
Purge Time	60 seconds
Amalgamation Time	12 seconds at 900 °C
Recording Time	30 seconds
Oxygen Flow	120 mL/min

Table 1 Analysis Operating Parameters

| RESULTS

Table 2 shows the results for all samples analysed on the DMA-80. The far column indicates the results previously obtained via CVAA. All sample results were within satisfactory range of previous analyses. The slight discrepancy in the soil sample results can be attributed to using smaller sample sizes which leads to samples being inhomogeneous.

Sample	Concentration (µg/Kg)	Contract Laboratory (µg/Kg)
0,2 (µg/Kg)	0,211	0,205
1 (µg/Kg)	0,915	1,05
5 (µg/Kg)	4,72	5,04
10 (µg/Kg)	9,717	10,3
ICV (5 µg/Kg)	5,446	5,2
blank	0,01	0,03
LCS (5 µg/Kg)	5,773	5,1
soil	0,663	0,9
soil	5,092	5
soil	0,535	0,63
CCV (5 µg/Kg)	5,765	5,5

Table 2 Unknown Environmental Samples on DMA-80 vs Contract Laboratory

In addition to the unknown environmental samples, NIST 2709 San Joaquin Soil, a matrix matched Standard Reference Material (SRM) was periodically analysed.

Sample	Concentration (µg/Kg)	**Certifield** (µg/Kg)
LCS (5 µg/Kg)	5,541	5,9
Soil	398,013	520
Soil	7684,281	6590
Soil	8408,259	7630

Table 2 Unknown Environmental Samples on DMA-80 vs Contract Laboratory (Part II)

Sample	Concentration (mg/Kg)	**Certified** (mg/Kg)
NIST 2709	1,378	1,40 ± 0,08
NIST 2709	1,404	1,40 ± 0,08
NIST 2709	1,406	1,40 ± 0,08
NIST 2709	1,404	1,40 ± 0,08
NIST 2709	1,424	1,40 ± 0,08

Table 3 Summary of results of QA/QC analysis

| CONCLUSION

All results obtained on the DMA-80 were in good agreement with the previous CVAA results. The DMA-80, direct mercury analyser, successfully analysed five replicates of the NIST 2709 SRM. Similar success can be expected when analysing other soil and sludge-type samples. As previously mentioned, a possible reason for the discrepancy in Table 2 can be sample homogeneity. All the liquid standard results were within their expected range. The DMA-80 is a fast, reliable alternative to wet chemistry techniques. No sample preparation enables quick sample turnaround which enable higher throughput for environmental contract laboratories.

Further Reading

Please visit our Hg info center for complete access to application notes, technical papers, as well as links to valuable resources for mercury testing.
Go to http://www.milestonesrl.com

To learn more about mercury and other related topics, feel free to visit these websites.

EPA Method 7473
http://www.epa.gov/waste/hazard/testmethods/sw846/pdfs/7473.pdf

ASTM Method D6722-01
http://www.astm.org/Standards/D6722.htm

Methyl Mercury
http://en.wikipedia.org/wiki/Methylmercury

Mercury in Fish
http://www.epa.gov/waterscience/fish/advice/mercupd.pdf

MILESTONE
HELPING CHEMISTS

MILESTONE Srl - Via Fatebenefratelli, 1/5 - 24010 Sorisole (BG) - Italy Tel: +39 035 573857 - Fax: +39 035 575498
www.milestonesrl.com - email: analytical@milestonesrl.com

SPONSOR RELEASE

ISQ™ 7610 Single Quadrupole GC-MS

Produce results more rapidly and experience unstoppable efficiency in your analysis with the Thermo Scientific™ ISQ™ 7610 Single Quadrupole GC-MS system

To stay ahead, analytical testing laboratories need the ultimate confidence of a GC-MS system that easily and reliably produces trusted results, day after day. For this, you can count on the Thermo Scientific™ ISQ™ 7610 Single Quadrupole GC-MS System.

Simplified operation, automated workflows, and extended dynamic range deliver consistent results from system to system in every laboratory. Thermo Scientific™ NeverVent™ technology, extended-life detector, and intelligent software eliminate unnecessary downtime to maximize sample throughput.

To ensure you are ready for any analytical challenge, the system is upgradeable from entry-level to advanced configurations. Now you can take the lead with rapid return on investment (ROI) for your regulated GC-MS analyses

Increase instrument uptime

Eliminate unnecessary, unplanned instrument downtime and maximize productivity to achieve unprecedented efficiency, day after day. The ISQ 7610 Single Quadrupole GC-MS System combines robustness with the ability to change the GC column and clean the ion source without interrupting your analytical workflows.

Monitor key aspects of your GC-MS system

With Thermo Scientific™ SmartStatus™ instrument tracking within Chromeleon CDS, quickly see whether instruments are ready to run samples, if maintenance is required or if consumables should be replaced. The fully customizable software enables you to make data-driven decisions on when to perform maintenance and avoid unnecessary downtime.

Maximize sample throughput

When high sample throughput is essential, the system delivers results on time and with ease. Automated workflows and simplified instrument operation ensure every user produces consistent results, sample after sample. Extended linear range enables method consolidation so you can analyze more compounds at varying concentrations in a single run.

Realize rapid return on investment

Ensuring your system delivers results as soon as it's installed is necessary to achieve rapid ROI. With built-in intelligence that simplifies instrument setup, analytical methods, and everyday operation, the ISQ 7610 Single Quadrupole GC-MS System is designed for accelerated deployment. Reduced needs for operator training and faster time to full productivity together with maximum sample throughput provide fast return on your instrument investment.

Thermo Fisher Scientific is working to provide more information about our products' environmental impact by stepping up to participate in the ACT Label program with selected products.

Find out more at **thermofisher.com/ISQ7610**

ThermoFisher SCIENTIFIC

Thermo SCIENTIFIC

ISQ™ 7610 Single Quadropole GC-MS

Produce results more rapidly and experience unstoppable efficiency in your analysis with the Thermo Scientific™ ISQ™ 7610 Single Quadrupole GC-MS system.

VIDEO **WEBSITE**

Thermo SCIENTIFIC

SPONSOR RELEASE

iCAP™ PRO XP ICP-OES

Fuel your desire for robust results. Meet data requirements with extending analysis periods. The Thermo Scientific™ iCAP™ PRO XP ICP-OES is rugged on all fronts

Analyze high-matrix trace elemental samples with sensitive multi-element detection and meet your data requirements with the optimal performance of the Thermo Scientific™ iCAP™ PRO XP ICP-OES. Rugged on all fronts, this system needs surprisingly little bench space or user maintenance.

A bench top simultaneous ICP spectrometer with a vertical torch, a purged echelle polychromator and Charge Injection Device (CID) array detector. It includes:

a 4-channel, peristaltic pump to allow for the use of an advance accessories

a solid-state, free-running 27.12 MHz RF generator to ensure robust plasma generation for any sample matrix.

three independent MFCs to precisely control the nebulizer, plasma, and auxiliary gas and to ensure long-term stability.

the option to add an additional gas to the plasma via an integrated MFC with a flow of 0-0.25 L/min. This enables analysis of high-salt samples (up to 30% TDS) or organics.

an interlock drain sensor to shut down the system if a leak in the sample path is detected and to prevent samples from being lost.

an echelle polychromator that is thermostatically controlled to ensure long-term stability and reduce the need for recalibration.

a cross-dispersing prism combined with an echelle to provide a resolution of 7 pm and minimize interferences.

a random-access CID imager that provides full wavelength coverage from 167.021 to 852.145 nm.

an enhanced UV mode to allow better sensitivity and detection limits for elements between 167.021 and 240.063 nm via a second UV focused exposure.

Thermo Scientific™ Qtegra™ Intelligent Scientific Data Solution™ (ISDS) Software, providing an easy-to-navigate platform that allows the analyst to add wavelengths, create methods, analyze samples and post-process the data while the spectrometer is acquiring data.

iCAP PRO Series ICP-OES has ACT label certification

Reduce your lab's environmental impact with the iCAP PRO Series ICP-OES, recipient of the ACT label from My Green Lab. The ACT Environmental Impact Factor Label is the world's premier eco-label for laboratory products. The program ensures Accountability, Consistency, and Transparency in the reporting of environmental impact data to enable sustainable laboratory procurement. It was designed by both scientists and procurement specialists to provide clear, third-party verified information about the sustainability profile of laboratory products. By providing needed transparency around manufacturing, energy and water use, packaging, and end-of-life impacts, ACT makes it easy to choose environmentally preferable products and reduce the carbon impact of laboratory supply chains.

Find out more at **thermofisher.com/iCAP.PRO.XP.ICP-OES**

ThermoFisher SCIENTIFIC

thermo scientific

iCAP PRO Series ICP-OES

Perform like a PRO
Simplicity, robustness and speed

Analyze even the most challenging sample matrices
The Thermo Scientific™ iCAP™ PRO Series ICP-OES combines powerful multi-element capability with flexibility so your lab is ready for any challenge.

Produce consistent, reliable data quickly and easily. Experience enhanced sample throughput, matrix tolerance and flexibility to produce results you can trust.

Achieve precise results first time, every time with the innovative Get Ready feature. This automated technology sets up the instrument for you and checks performance. Manage instrument processes using a logical dashboard interface. Trust in ICP-OES technology driven by Thermo Scientific™ Qtegra™ Intelligent Scientific Data Solution™ (ISDS) Software.

VIDEO **WEBSITE**

ThermoFisher SCIENTIFIC

SPONSOR RELEASE

Save Time. **Go Direct** for Mercury Analysis

The Milestone DMA-80 has been at the forefront of direct total mercury analysis for almost two decades. The challenges in mercury determination are well known to analysts who often face a number of issues connected with tedious sample preparation process or the mercury analysis steps causing memory effect even after long cleaning cycles performed using latest generation of ICP-MS or cold vapor systems.

The DMA-80 mercury determination system can analyze any matrix (solid, liquid or gas) without any pre-treatment or chemical additions in as few as 6 minutes in full compliance with EPA method 7473. With thousands of units installed, Milestone defines the benchmark for direct mercury determination in a wide range of industries: environmental, food energy, cement, cosmetics, agriculture, mining and petrochemical.

- **Improved design** from the outside out for superior performance event at the ppt level.
- **Easy-to-use technology** with a single long-lasting calibration for all matrices.
- **No memory effect** thanks to the revolutionary autoblank feature.
- **Milestone Connect** for 30-years of experience at your fingertips
- **Fully compliant** with US EPA Method 7473, ASTM method D-6722-01 and D-7623-10.
- **Maximize your ROI** with an easy-to-maintain system and reliable components.

Find out more at **milestonesrl.com**

MILESTONE
HELPING CHEMISTS

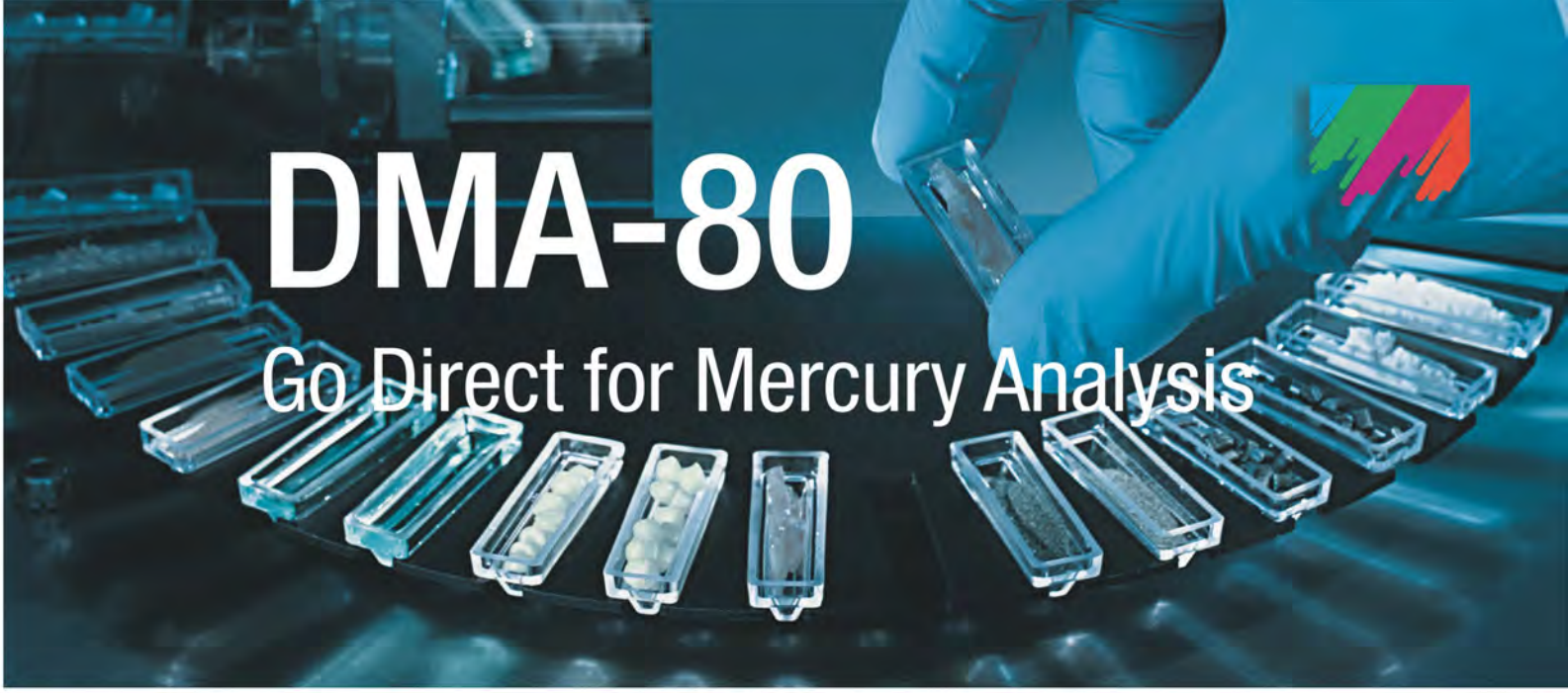

DMA-80

Go Direct for Mercury Analysis

SIX MINUTE, PREP-FREE MERCURY ANALYSIS

If youre looking for unsurpassed processing speed, efficiency and precision for mercury samples, its time for the Milestone DMA-80offering more than double the productivity of traditional cold vapor techniques at a fraction of the cost.

NO SAMPLE PREP REQUIRED

Eliminating the need for any wet chemistry sample treatment prior to analysis.

WIDEST DYNAMIC RANGE

Capable of achieving a detection limit of 0.001 to 30,000 ng of mercury

RESULTS IN JUST 6 MINUTES

Dramatically improves your laboratorys turnaround time and productivity.

UP TO 70% COST REDUCTION

Compared to traditional mercury analysis techniques such as CV-AAS.

Watch Videos, Download Brochures & Application Notes at:

DMA-80

DMA-1

VIDEO

WEBSITE

MILESTONE

MERCURY | MICROWAVE DIGESTION | CLEAN CHEMISTRY | ASHING | EXTRACTION | SYNTHESIS | milestonesrl.com

New Books & Upcoming Events & Trusted Sources for Analytical Chemistry

Notices of Books on Analytical Chemistry

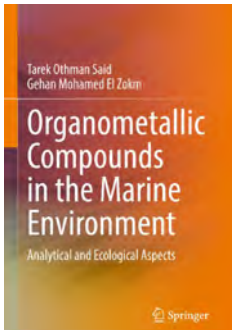

Organometallic Compounds in the Marine Environment

Tarek Othman Said and Gehan Mohamed El Zokm, Authors

August 2025, Springer Cham

This book outlines organometallic compounds (OMCs) in the marine environment, focusing on their analytical and ecological aspects. Divided into 6 chapters, the authors discuss OMCs' occurrence, chemical structure, and environmental impact of OMCs in aquatic systems. In this book, readers will also find critical insights into the sources and effects of OMCs on marine ecosystems, with detailed discussions on extraction methodologies, stability, and speciation analysis. The book highlights advanced analytical techniques such as gas chromatography and atomic absorption spectrometry, providing a thorough understanding of the latest approaches for evaluating OMC levels in marine environments.

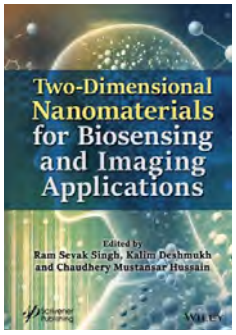

Two-Dimensional Nanomaterials for Biosensing and Imaging Applications

Ram Sevak Singh, Kalim Deshmukh, Chaudhery Mustansar Hussain, Editors

June 2025, Wiley

This book examines the current state and new challenges associated with the development of 2D nanomaterials for biosensing and imaging applications. This volume focuses on the synthesis, processing methods, characterization, properties, and applications of 2D nanomaterials, their nanocomposites or heterostructures for biosensors and imaging devices, and the essential criteria in each specified field. Comparative performance evaluations of various biosensor devices and their advantages and disadvantages for the commercialization of 2D materials-based biosensors are comprehensively covered.

Analytical and Chemometric Tools: Tutorials with Practical Applications to Food Security and Safety

Alessandra Biancolillo, Editor

June 2026, Elsevier

With a generous compilation of practical examples, the book covers a theoretical discussion of chemometric methods, summarizes up-too-date targeted and untargeted analytical methods in the field of forensic science, and presents real-life case studies applied to methods of chemometrics for food and forensic chemistry. This book is a valuable resource for chemists, forensic scientists, food scientists, students, and all those who wish to broaden their knowledge in the allied field. Read more

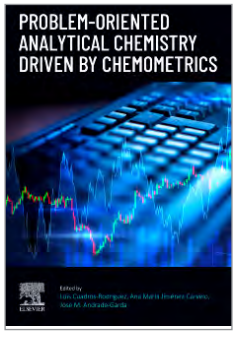

Problem-Oriented Analytical Chemistry Driven by Chemometrics

Luis Cuadros Rodríguez, Ana María Jimenez-Carvelo, Jose M Andrade-Garda, Eds.

January 2026, Elsevier Science

This book covers challenges that are relevant to many fields using analytical techniques, including food quality and safety, environmental studies, product authentication, and petrochemistry using an analytical data science approach. The book's novel approach starts from case studies, allowing analytical chemists to understand how seemingly impenetrable chemometrics techniques can be applied to solve problems. Read more

Events on Analytical Chemistry in 2026

April 06 to 07
XX International Conference on Chemometrics in Analytical Chemistry
Rome, Italy
https://waset.org/chemometrics-in-analytical-chemistry-conference

May 17 to 22
44th International Symposium on Capillary Chromatography and 21st GCXGC Symposium
Congress Centre, Riva del Garda, Italy
Access Info

June 3 to 6
XXIV Brazilian Congress of Toxicology (CBTOX) 2026
WTC Events Center, São Paulo, SP, Brazil
www.cbtox.com.br

June 8 to 9
MassSpecMeet 2026
Lisbon, Portugal
https://scisynopsisconferences.com/mass-spectrometry/

June 15 to 18
49th Annual Meeting of the Brazilian Chemical Society (RASBQ)
Expo Dom Pedro
Campinas, SP, Brazil
https://www.sbq.org.br/49ra/

June 21 to 25
10th International Caparica Conference on Analytical Proteomics
Costa de Caparica, Portugal
www.icap2026.com

July 23 to 24
ANALYTICA ACTA 2026
Paris, France
https://analytical-bioanalytical.pharmaceuticalconferences.com/

August 22 to 28
26th International Mass Spectrometry Conference (IMSC)
Lyon, France
https://imsc26.com/

September 15 to 18
22nd National Meeting on Analytical Chemistry (ENQA) & 10th Ibero-American Congress on Analytical Chemistry (CIAQA)
Ruth Cardoso Cultural and Exhibition Center, Maceió, AL, Brazil
https://enqa2026.com.br/

Pittcon Conference & Expo

Pittcon is a catalyst for the exchange of information, a showcase for the latest advances in laboratory science, and a venue for international connectivity.

Pittcon is a dynamic, transnational conference and exposition on laboratory science, a venue for presenting the latest advances in analytical research and scientific instrumentation, and a platform for continuing education and science-enhancing opportunity. Pittcon is for anyone who develops, buys, or sells laboratory equipment, performs physical or chemical analyses, develops analysis methods, or manages these scientists.

Pittcon Awards

Honoring scientists who have made outstanding contributions to Analytical Chemistry

Each year, Pittcon provides a venue where scientists who have made outstanding contributions to laboratory science, analytical chemistry, and applied spectroscopy are honored.

Among these awards is the **Pittcon Heritage Award** which honors those visionaries whose entrepreneurial careers shaped the instrumentation and laboratory supplies community and by doing so have transformed the scientific community at large.

The award has been presented jointly with Pittcon since 2002 and is given out each year at a special ceremony during the Pittcon Conference and Expo. The recipient's name and achievements are added to the Pittcon Hall of Fame, which conference attendees can visit at the show each year.

Pittcon 2027 – Conference on Analytical Chemistry and Applied Spectroscopy
April 24-28, 2027
David L. Lawrence Convention Center
Pittsburgh, Pennsylvania, USA

Pittcon®
Conference and Exposition

Why Pittsburgh?

From Roots in Steelmaking to Innovative Technology

Meet the New Pittsburgh

- Heavily driven by advanced manufacturing, emerging technologies, healthcare, higher education, and university start-ups
- Over 29 colleges and universities, anchored by highly ranked research institutes like Carnegie Mellon University (CMU), Duquesne University, and the University of Pittsburgh (Pitt).
- Major academic and industrial disciplines include AI, Chemistry, Computer Science, Engineering, Health & Life Sciences, Materials Science, Medical Devices, Nanotechnology, and Robotics
- Corporate R&D headquarters of industrial leaders: Alcoa, Arconic, Calgon Carbon, Covestro, Kraft Heinz, PPG, U.S. Steel, Vitro, and many others
- U.S. Department of Energy (DOE) Government Labs: National Energy Technology Laboratory (NETL) and Bettis Atomic Power Laboratory

Pittcon 2027 Tracks

- AI & Data Analytics
- Bioanalytical & Life Sciences
- Environmental & Energy
- Forensic Science & Toxicology
- Instrumentation Innovations & Applications
- Materials & Nanoscience
- Pharmaceuticals & Biologics
- Professional & Career Development

So What is Pittcon?

Pittcon is a dynamic, international conference and exposition on laboratory science, a venue for presenting the latest advances in analytical research and scientific instrumentation, and a platform for continuing education and science-enhancing opportunity.

WHO SHOULD ATTEND? | EXPLORE PITTCON

Pittcon®
Conference and Exposition

SelectScience® Pioneers online Communication and Promotes Scientific Success

SelectScience®
The Fastest Way to Expert Opinion™

SelectScience® promotes scientists and their work, accelerating the communication of successful science. Through trusted lab product reviews, virtual events, thought-leading webinars, features on hot scientific topics, eBooks and more, independent online publisher SelectScience® provides scientists across the world with vital information about the best products and techniques to use in their work.

Some recent contributions from SelecScience® to the scientific community

News / Life Sciences

Domestic cats may hold the key to understanding breast cancer

An international research team, with participation of the University of Bern, has conducted the world's first comprehensive genetic study of cancer in domestic cats. The study shows that some of the genetic changes in cat tumors closely resemble those found in human cancers, opening up new perspectives for developing targeted cancer therapies, particularly for breast cancer. Access **here**

Webinar

The PFAS measurement crisis: A roundtable discussion

Join this expert roundtable discussion to explore how next-generation analytical standards and Non-Targeted Analysis (NTA) approaches are helping to close the PFAS data gap, improve decision-making, and prepare organizations for the next phase of PFAS regulation. Access **here**

Immersive content

Explore the depths of Raman Spectroscopy

This content hub serves as a comprehensive resource for scientists and professionals looking to harness the full potential of Raman spectroscopy. Explore in-depth applications, technical insights, and expert guidance to advance your research and innovation. Access **here**

SelectScience® is the leading independent online publisher connecting scientists to the best laboratory products and applications.

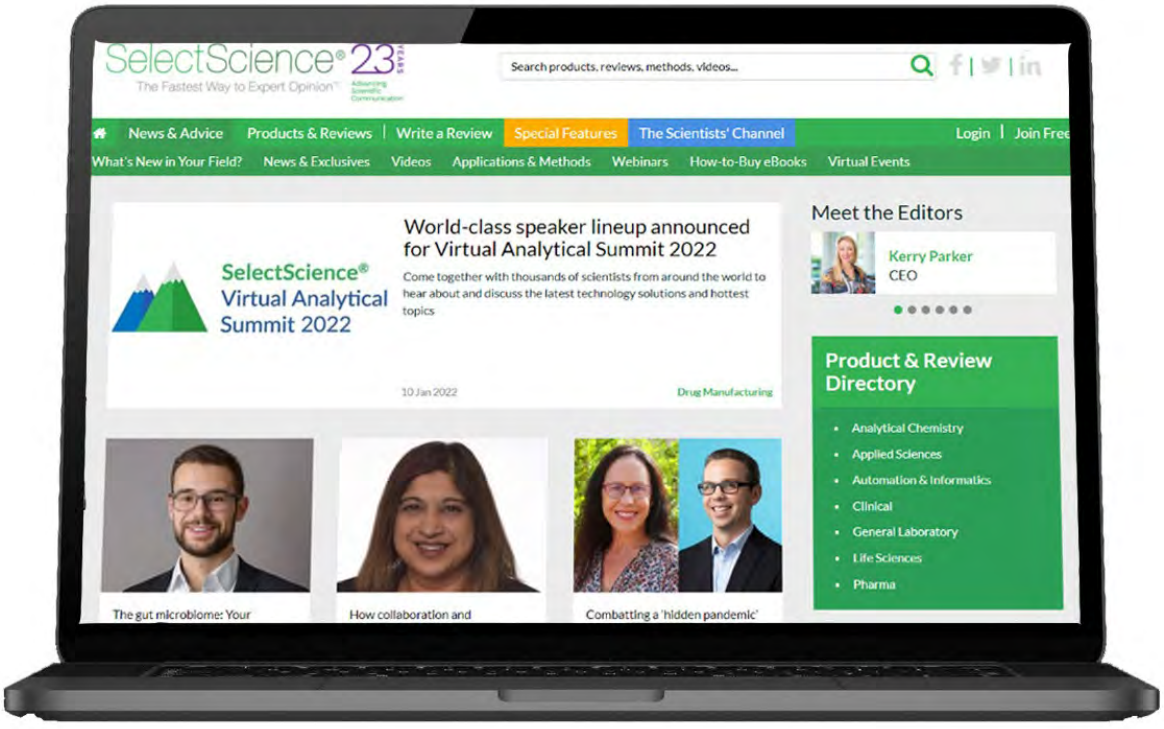

- Working with Scientists to Make the Future Healthier.
- Informing scientists about the best products and applications.
- Connecting manufacturers with their customers to develop, promote and sell technologies.

SelectScience®
The Fastest Way to Expert Opinion

CHROMacademy is the leading provider of eLearning for analytical science

CHROMacademy *helps scientific organizations acquire and maintain excellence in their laboratories*.

For over 10 years, CHROMacademy has increased knowledge, efficiency and productivity across all applications of chromatography. With a comprehensive library of learning resources, members can improve their skills and knowledge at a pace that suits them.

CHROMacademy covers all chromatographic applications – HPLC, GC, mass spec, sample preparation, basic lab skills, and bio chromatography. Each paradigm contains dozens of modules across theory, application, method development, troubleshooting, and more. Invest in analytical eLearning and supercharge your lab.

For more information, please visit www.chromacademy.com/

LC GC's **CHROMacademy**
powered by crawford scientific

CHROMacademy Lite members have access to less than 5% of our content. Premier members get so much more !

Video Training courses

Fundamental HPLC
Fundamental GC
Fundamental LCMS
Fundamental GCMS
HPLC Method Development
GC Method Development

Ask the Expert

We are always on hand to help fix your instrument and chromatographic problems, offer advice on method development, help select a column for your application and more.

To find out more about Premier Membership contact:

Glen Murry: +1 732.346.3056 | Glen.Murry@ubm.com
Peter Romillo: +1 732.346.3074 | Peter.Romillo@ubm.com

www.chromacademy.com

The worlds largest e-Learning website for analytical scientists

PERIODICALS & WEBSITES

American Laboratory® is a platform that addresses basic research, clinical diagnostics, drug discovery, environmental, food and beverage, forensics and other markets, and combines in-depth articles, news, and video to deliver the latest advances in their fields. **Article:** ***Microplastics, Nanoplastics 5x More Present in Atmosphere than Thought.*** A team from the Institute of Earth Environment at the Chinese Academy of Sciences developed a semi-automated microanalytical method to quantify atmospheric plastic particles and their cross-compartmental fluxes in two major Chinese megacities: Guangzhou and Xi'an. **Access here**

LCGC
Chromatographyonline delivers practical, nuts-and-bolts information to help scientists and lab managers become more proficient in the use of chromatographic techniques and instrumentation. **Article:** ***RP-HPLC Fractionation of Tarantula Venom Yields Neuroactive Compounds with Therapeutic Potential.*** By John Chasse. Researchers separated tarantula venom into eleven fractions, revealing neuroactive compounds that mimic FDA-approved drugs, highlighting spider venom's potential for neurological disorder therapeutics through chromatographic purification. **Read more**

Scientia Chromatographica
Scientia Chromatographica is the first and to date the only Latin American scientific journal dedicated exclusively to Chromatographic and Related Techniques. With a highly qualified and internationally recognized Editorial Board, it covers all chromatography topics in all their formats, in addition to discussing related topics such as “The Pillars of Chromatography”, Quality Management, Troubleshooting, Hyphenation (GC-MS, LC-MS, SPE-LC-MS/MS) and others. It also provides columns containing general information, such as: calendar, meeting report, bookstore, etc. **Read more**

Select Science
SelectScience® has transformed global scientific communications and digital marketing. It informs scientists about the best products and applications, connects manufacturers with their customers to develop, promote, and sell technologies, and promotes scientists and their work. This accelerates the communication of successful science. Scientists can make better decisions using independent expert information and easily access manufacturers. SelectScience® informs the global scientific community through editorial, feature, video, and webinar programs. **Read more**

Spectroscopy
With the *Spectroscopy* journal, scientists, technicians, and lab managers gain proficiency through unbiased, peer-reviewed technical articles, trusted troubleshooting advice, and best-practice application solutions. **Article:** ***Artificial Intelligence as the Next Layer of Chemometrics.*** By Jerome Workman, Jr. AI methods can reduce reliance on manual preprocessing while still indicating which spectral regions influence predictions. AI is best viewed as the next developmental layer of chemometrics, not as a competing discipline. **Read more**

BrJAC AUTHOR GUIDELINES

Aims & Scope

Brazilian Journal of Analytical Chemistry is a double-blind peer-reviewed research journal dedicated to the diffusion of significant and original knowledge in all branches of Analytical and Bioanalytical Chemistry. It is addressed to professionals involved in science, technology, and innovation projects at universities, research centers and in industry. **BrJAC welcomes** the submission of research papers reporting studies devoted to new and significant analytical methodologies, putting in evidence the scientific novelty, the impact of the research and demonstrating the analytical or bioanalytical applicability. BrJAC **strongly discourages** those simple applications of routine analytical methodologies, or the extension of these methods to new sample matrices, unless the proposal contains substantial novelty and unpublished data, clearly demonstrating advantages over existing ones.

Additionally, there are other submission categories to BrJAC such as:

Reviews: They should be sufficiently broad in scope, but specific enough to permit an appropriate depth discussion, including critical analyses of the bibliographic references and conclusions. Manuscripts submitted for publication as Reviews must be original and unpublished. Reviews undergo double-blind full peer review and are handled by the Editor of Reviews.

Technical Notes: Concise descriptions of developments in analytical methods, new techniques, procedures, or equipment falling within the scope of the BrJAC. Technical notes also undergo double-blind full peer review.

Letters: Discussions, comments, and suggestions on issues related to Analytical Chemistry or Bioanalytical Chemistry. Letters are welcome and will be published at the discretion of the BrJAC Editor-in-Chief.

Point of View: This category is exclusively invited by the Editor-in-Chief.

See the next items for more information on the journal, the documents preparation, manuscript types, and how to prepare the submission.

Professional Ethics

Originality: manuscripts submitted for publication in BrJAC cannot have been previously published or be currently submitted for publication in another journal.

Preprint: BrJAC does not accept manuscripts that have been posted on preprint servers prior to the submission.

Integrity: the submitted manuscripts are the full responsibility of the authors. Manipulation/invention/omission of data, duplication of publications, the publication of papers under contract and confidentiality agreements, company data, material obtained from non-ethical experiments, publications without consent, the omission of authors, plagiarism, the publication of confidential data and undeclared conflicts of interests are considered serious ethical faults.
BrJAC discourages and restricts the practice of excessive self-citation by the authors.
BrJAC does not practice coercive citation, that is, it does not require authors to include references from BrJAC as a condition for achieving acceptance, purely to increase the number of citations to articles from BrJAC without any scientific justification.

Transparency: The use of artificial intelligence (AI) by authors must comply with the transparency guidelines below:

- Authors are responsible for all content submitted to BrJAC, including the accuracy of AI-generated content.

- The authors must provide a declaration regarding the use of artificial intelligence in preparing the submitted manuscript. A template for this declaration is available for download **here**. Authors must use this template when writing their declaration.
- AI tools should not be listed as authors, as they cannot be held responsible for the published work.
- Any use of AI tools for text or image generation must be declared in the Methods section of the manuscript, with a description of how and for what purpose the AI tools were used.
- If AI is used to create graphics and the cover artwork, the name of the tool(s) used and a brief description of how the image was created should be included in the figure caption. Authors are responsible for ensuring that the terms of use of the tools used state that the result is not the property of the generating site.
- The Editor may, at his/her discretion, determine that the use of AI in a particular submission is too extensive. This determination may result in rejection of the manuscript or a request to remove or reduce the AI-generated portions of the manuscript.
- In the peer review process, the BrJAC states that the opinion of the reviewers consulted is solely that of the reviewer. The use of AI tools in the review of manuscripts is not accepted. This BrJAC standard is intended to protect the confidentiality of the manuscript.

Self-citation: BrJAC discourages and restricts the practice of excessive self-citation by the authors. The maximum percentage of self-citations acceptable by BrJAC is 20%.

Coercive citation: BrJAC does not practice coercive citation. That is, BrJAC does not require authors to include BrJAC references as a condition for acceptance, purely to increase BrJAC articles citations without scientific justification.

Similarities: Manuscripts submitted to BrJAC are analyzed for similarities using specialized software. The maximum total similarity index accepted by the BrJAC is 25%, with a maximum of 3% for each source.

Conflicts of interest: when submitting their manuscript for publication, the authors must include all potential sources of bias such as affiliations, funding sources and financial, management or personal relationships which may affect the work.

Copyright: will become the property of the Brazilian Journal of Analytical Chemistry, if and when a manuscript is accepted for publication. The copyright comprises exclusive rights of reproduction and distribution of the articles, including reprints, photographic reproductions, microfilms or any other reproductions similar in nature, including translations.

Request for permission to reuse figures and tables published in the BrJAC: researchers who want to reuse any document or part of a document published in the BrJAC should request reuse permission from the BrJAC Editor-in-Chief, even if they are the authors of such document. A template for requesting reuse permission can be downloaded **here**.

Misconduct will be treated according to the COPE's recommendations (https://publicationethics.org/) and the Council of Science Editors White Paper on Promoting Integrity in Scientific Journal Publications (https://www.councilscienceeditors.org/).

Manuscript submission

The BrJAC does not charge authors an article processing fee.

Manuscripts must be prepared according to the BrJAC manuscript template. Manuscripts in disagreement with the BrJAC guidelines are not accepted for revision.

The submission of manuscripts is done online by a submitting author through a digital manuscript manager system, which guides the author step by step through the entire submission process.

After the submitting author logs in to the system and enters his/her personal and affiliation details, the submission can be started.

All co-authors must be added to the Authors section.

Five documents are mandatorily uploaded by the submitting author: Cover letter, Title Page, Declaration of AI usage, Novelty Statement and the Manuscript. Templates for these documents are available for download **here**.

The manuscript and the title page must be uploaded as Word files. The cover letter, declaration of AI usage, and novelty statement may be uploaded as PDF files. The manuscript Word file will be converted by the system to a PDF file which will be used in the double-blind peer review process.

All correspondence, including notification of the Editor's decision and requests for revision, is sent by e-mail to the submitting author through the manuscript manager system.

Documents Preparation

It is highly recommended that authors download and use the templates to create their five mandatory documents to avoid the suspension of a submission that does not meet the BrJAC guidelines.

Cover Letter
The cover letter template should be downloaded and filled out carefully.
Any financial conflict of interest or lack thereof and agreement with BrJAC's copyright policy must be declared.
It is the duty of the submitting author to inform his/her collaborators about the submission of the manuscript and its eventual publication.
The Cover Letter must be signed by the corresponding author.

Declaration on the Use of Artificial Intelligence
The Declaration on the AI Use template must be downloaded and filled out carefully.
The corresponding author must sign the Declaration on the AI Use.
In the declaration on the use of artificial intelligence, the corresponding author must indicate whether or not AI tools were used in preparing the manuscript.
If AI tools were used, the author must state which tools were used and for what purpose.

Title Page
The Title Page must contain information for each author: full name, affiliation and full international postal address, and information on the contribution of each author to the work. Acknowledgments must be entered on the Title Page. The submitting author must sign the Title Page.

Novelty Statement
The Novelty Statement must contain clear and succinct information about what is new and innovative in the study in relation to previously related works, including the works of the authors themselves.

Manuscript (all submission categories)

It is highly recommended that authors download the Manuscript template and create their manuscript in this template, keeping the layout of this file.

- **Language**: **English** is the language adopted by BrJAC. The correct use of English is of utmost importance. We highly recommend **Proof-Reading-Service.com**, a professional language editing service that specializes in **journal article proofreading** and **manuscript editing** for submissions to this journal. Upon completion of the proofreading, please provide a certificate confirming that the service has been carried out.
- **Required items**: the manuscript must include a title, abstract, keywords, and the following sections: Introduction, Materials and Methods, Results and Discussion, Conclusion, and References.
- **Identification of authors**: as the BrJAC adopts a double-blind review, the manuscript file must **NOT** contain the authors' names, affiliations nor acknowledgments. Full details of the authors and their acknowledgements should be on the Title Page.

- **Layout**: the lines in the manuscript must be numbered consecutively and double-spaced.
- **Graphics and Tables**: must appear close to the discussion about them in the manuscript. For **figures** use **Arabic** numbers, and for **tables** use **Roman** numbers.
- **Figure files:** when a manuscript is approved for publication, the BrJAC production team will contact the corresponding author to request separate files of each figure and a graphical abstract. These files must have **good resolution** and the extension **PNG or JPG**. The graphical abstract should preferably be created in landscape format. In the article diagrammed in the journal, the graphical abstract will occupy a space of 8 to 9 cm in length and 6 cm in height. Chemical structures must have always the same dimensions.
- **Studies involving biological material**: for studies involving human and animal material for research purposes, authors must state in the manuscript that the research has been approved by the research ethics committee of the institution where the study was conducted.
- **Reuse of previously published material:** Authors must obtain permission from the copyright holder (publisher or scientific society) to reproduce or adapt figures, tables, or other material previously published in the scientific literature, including material originally published by the same authors. Documentation of the permission must be uploaded in the manuscript management system at the time of manuscript submission.
  Material published under Creative Commons licenses: Figures, tables, or other material distributed under a Creative Commons license may be reused or adapted in accordance with the terms of the applicable license. Authors are responsible for ensuring that all license conditions are met.
  Acknowledgment of the original source: The original source must be properly cited in the figure or table caption. When applicable, the type of license (e.g., CC BY 4.0) must also be indicated.
  Credit line: When permission is required, the credit line specified by the copyright holder must be included in the figure or table caption.
- **Chemical nomenclature, units and symbols**: should conform to the rules of the International Union of Pure and Applied Chemistry (IUPAC) and Chemical Abstracts Service. It is recommended that, whenever possible, the authors follow the International System of Units, the International Vocabulary of Metrology (VIM) and the NIST General Table of Units of Measurement. Abbreviations are not recommended except for those recognized by the International Bureau of Weights and Measures or those recorded and established in scientific publications. Use L for liters. Always use superscripts rather than /. For instance: use mg mL^{-1} and NOT mg/mL. Leave a space between numeric values and their units.
- **References throughout the manuscript:** the references must be cited as superscript numbers. It is recommended that references older than 5 (five) years be avoided, except in relevant cases. Include references that are accessible to readers.
- **References item:** This item must be thoroughly checked for errors by the authors before submission. From 2022, BrJAC is adopting the American Chemical Society's Style in the Reference item. Mendeley Reference Manager users will find the Journal of American Chemical Society citation style in the Mendeley View menu. Non-users of the Mendeley Reference Manager may refer to the ACS Reference Style Quick Guide DOI: https://doi.org/10.1021/acsguide.40303

Review process

Manuscripts submitted to the BrJAC undergo an initial check for compliance with all of the journal's guidelines. Submissions that do not meet the journal's guidelines will be suspended and an alert sent to the corresponding author. The authors will be able to resend the submission within 30 days. If the submission according to the journal's guidelines is not made within 30 days, it will be deleted from the BrJAC system on the first subsequent day, and an alert will be sent to the corresponding author.

Manuscripts that are in accordance with the journal's guidelines undergo a similarity analysis using specialized software.

The manuscript is then forwarded to the Editor-in-Chief who will check whether the manuscript is in accordance with the journal's scope and will analyze the similarity report. The maximum total similarity index accepted by the BrJAC is 25%, with a maximum of 3% for each source.

If the manuscript passes the screening described above, it will be forwarded to an Associate Editor who will also analyze the similarity report and invite reviewers.

Manuscripts are reviewed in double-blind mode by at least 2 reviewers. A larger number of reviewers may be used at the discretion of the Editor. As evaluation criteria, the reviewers employ originality, scientific quality, contribution to knowledge in the field of Analytical Chemistry, the theoretical foundation and bibliography, the presentation of relevant and consistent results, compliance with the BrJAC's guidelines, clarity of writing and presentation, and the use of grammatically correct English.

Note: In case the Editors and Reviewers consider the manuscript to require an English revision, the authors will be required to send an English proofreading certificate, by the ProofReading Service or equivalent service, before the final approval of the manuscript by the BrJAC.

The 1st-round review process usually takes around 5-6 weeks. If the manuscript is not rejected but requires corrections, the authors will have one month to submit a corrected version of the manuscript. In another 3-4 weeks, a new decision on the manuscript may be presented to the corresponding author.

The manuscripts accepted for publication are forwarded to the BrJAC production department. Minor changes to the manuscripts may be made, when necessary, to adapt them to BrJAC guidelines or to make them clearer in style, respecting the original content. The articles are sent to the authors for approval before publication. Once published online, a DOI number is assigned to the article.

Final Considerations

Whatever the nature of the submitted manuscript, it must be original in terms of methodology, information, interpretation or criticism.

With regard to the contents of published articles and advertisements, the sole responsibility belongs to the respective authors and advertisers; the BrJAC, its editors, editorial board, editorial office and collaborators are fully exempt from any responsibility for the data, opinions or unfounded statements.

Manuscript submission at www.brjac.com.br